UAB
Universitat Autònoma de Barcelona

INVESTIGATION OF THE INFLUENCE OF THE MEMBRANE LIPID ENVIRONMENT ON G PROTEIN-COUPLED RECEPTOR ACTIVATION BY MOLECULAR DYNAMICS SIMULATIONS

A Thesis presented by Agustín Bruzzese

Submitted to the Institut de Neurociències, Universitat Autònoma de Barcelona
in partial fulfillment
of the requirements for the degree of

DOCTOR in NEUROSCIENCE

2020

Directors:

Dr. Jesús Giraldo & Dr. James Dalton

INc
Institut de
Neurociències

UAB
Universitat Autònoma de Barcelona

Acknowledgements

ACKNOWLEDGEMENTS

ABSTRACT

G protein-coupled receptors (GPCRs) are integral membrane proteins that transmit signals embodied in the chemical structure of endogenous and synthetic ligands from outside to inside the cell. Thus, they are fundamental in physiological and pathological conditions and, consequently, key pharmacological targets. Recently, a number of studies have shown that allosteric interactions exerted by lipids affect the population distribution of active and inactive receptor states, therefore leading to a complex signalling network. As a consequence, the membrane lipid environment has become an important factor in the study of GPCR signal transduction.

The present work takes advantage study of high-throughput molecular dynamics (MD) simulations to elucidate key biological processes in GPCR structure and function. Specifically, this thesis focusses on two main challenging tasks. On the one hand, the molecular understanding of the GPCR activation process. On the other hand, the exploration of the allosteric coupling between the lipids and the receptor protein, thus, aiming at characterizing lipid-modulated protein dynamics. Our approaches have been validated with published experimental results from which we have learnt about the systems and have been a source of ideas and hypotheses for the design of our computational experiments.

The results presented in this thesis show how long-timescale MD simulations can consistently reveal the molecular effects of phospholipids on two pivotal class A GPCRs, the β2-adrenergic and the adenosine A2a receptors. Our computational results are in agreement with published experimental data, and provide complementary information about the ligand-receptor conformational ensembles and the involved protein-lipid interactions. Briefly, our results reveal how GPCRs are sensitive to their lipid environment and, therefore, why lipids are crucial for GPCR dynamics and function.

KEYWORDS: GPCR, β2-adrenergic receptor, adenosine a2a receptor, phospholipid, allosteric modulation, ligand, agonist, orthosteric, molecular dynamics, protein conformation, receptor activation.

CONTENTS

INDEX OF FIGURES

ABBREVIATIONS

Acronym	Meaning
5-HT1AR	Serotonin 1A receptor
5-HT2AR	Serotonin 2A receptor
Å	Ångström = 10^{-10} m
A2aR	Adenosine A2a receptor
AA	All-atoms
ADN	Adenosine
APO	Without ligand
CB1	Cannabinoid 1 receptor
CG	Coarse-grained
CNS	Central nervous system
DMPC	1,2-ditetradecanoyl-sn-glycero-3-phosphocholine
DOPC	1,2-dioleoyl-sn-glycero-3-phosphocholine
DOPE	1,2-dioleoyl-sn-glycero-3-phospho-ethanolamine
DOPG	1,2-dioleoyl-sn-glycero-3-phosphoglycerol
DPPC	1,2-dihexadecanoyl-sn-glycero-3-phosphocholine
ECL	Extracellular loop

FDA	Food and drug administration
FF	Force fields
GPCR	G protein-coupled receptor
GPU	Graphics processing unit
ICL	Intracellular loop
IR	Infrared
M2R	Muscarinic 2 receptor
MD	Molecular dynamics
MOR	μ-opioid receptor
NMR	Nuclear magnetic resonance
OPM	Open protein membrane
PC	Phosphatidylcholine
PDB	Protein Data Bank
PE	Phosphatidylethanolamine
PG	Phosphatidylglycerol
PI	Phosphatidylinositol
POPC	1-palmitoyl-2-oleoyl-sn-glycerol-3-phosphocholine
POPG	1-Hexadecanoyl-2-(9Z-Octadecenoyl)-sn-glycero-3-Phosphoglycerol
PS	Phosphatidylserine

RMSD	Root mean square deviation
RMSF	Root mean square fluctuation
TM	Transmembrane
β2aR	β2-adrenergic receptor

INTRODUCTION

This thesis is organized in nine sections, namely, a background for the work presented, along with its main challenges, a description of the methodology used, the objectives for the study, the results obtained, and, finally, a general discussion and conclusions. The published papers have been added at the end together with the corresponding supplementary material.

Section 1 presents a basic description of biological membranes. This includes a review of the literature involving lipids and GPCRs, in which the characteristics of the membrane and the activation process of the receptor are examined.

Section 2 describes the practical aspects of the application of MD methodology, including MD simulations of proteins, ligands and lipid systems.

Section 3 outlines the research problem that motivated the present work, establishes the hypotheses, the objectives and how to accomplish them during this dissertation.

Section 4 focuses on a review of our results. Particularly, our investigations revolve around the study of two representative class A GPCR prototypes: β2-adrenergic receptor (β2aR) and Adenosine A2a receptor (A2aR). Both have been crystallized in high-resolution structures, and have been described to be greatly influenced by their lipid environment. The goal of our study on β2aR was motivated by published experimental work on this receptor illustrating the lipid influence. We performed several long-timescale MD simulations to map the allosteric modulation and conformational changes in β2aR which occur as a result of interactions with 1,2-dioleoyl-sn-glycero-3-phosphocholine (DOPC), 1,2-dioleoyl-sn-glycero-3-phosphoethanolamine (DOPE), and 1,2-dioleoyl-sn-glycero-3-phosphoglycerol (DOPG) lipids, respectively, without any bound ligand (APO state). Thus, our study may provide a molecular explanation to membrane-dependent receptor constitutive activity. Furthermore, the development of this thesis was coincident with many other studies involving the process of agonist-mediated GPCR activation using theoretical approaches, such as MD simulations. Therefore, we thought that the lipid environment could also aid to explore the molecular mechanisms underlying agonist-mediated GPCR activation. As a result, we carefully examined the agonist-mediated activation of A2aR starting from the inactive conformation with the crystalized-bound endogenous ligand adenosine embedded in two homogenous lipidic environments: DOPG and DOPC. Additional simulations with the synthetic agonist NECA allowed us to retrieve more information on the differen-

tial effects of lipids on agonist function. Thus, our MD simulations provide a basis for the understanding of how the lipid environment may affect the efficacy of agonists.

Section 5 provides a summary of the thesis, together with a general discussion of the results and their conclusions. This section also considers further avenues by which this work could be followed to advance in the GPCR-lipid field.

Section 6 lists the references included in this work.

Section 7 includes the two published papers that constitute the main result of the thesis.

Section 8 is considered as an appendix and includes a third publication, which was obtained once the formalities for the acceptance of the thesis as a compendium of articles were achieved. This third article proposes a classical statistical test (multiple-way ANOVA with repeated measurements on the time factor) for the analysis of agonist-dependent MD simulations of GPCR activation. This statistical analysis allows, in principle, the exploration of agonist efficacy within a statistical framework. The lipid environment, whose contribution is the main element of this thesis was included as a factor of the statistical analysis.

Section 9 includes the supplementary material corresponding to the published articles.

1. BIOLOGICAL MEMBRANES

Biological membranes are one of the most important and complex structures of living cells. The current view on biological membranes is indebted to the pioneering work of Singer and Nicolson, also known as the "fluid mosaic" in 1972(1). In turn, this was influenced by a number of experimental(2) and computational methods(3, 4) that came later. As a result, a growing number of results have been developed so far, complementing and extending the original model. Nowadays, we know biological membranes provide effective diffusion (i.e. enable drugs and metabolites to be transported while keeping waste out of the cell), promote inter-cellular communication, support energy generation, signal transduction, and serve to define different compartments within the cell(5, 6).

Primarily, biological membranes consist of a hydrophobic double layer (known as bilayer) of lipids, with proteins allowed to be bound in different ways(6). New knowledge has been acquired recently, thanks to advances in lipidomics(7) and structural determination(8) and analysis(9) of membrane proteins. Some of them are presented below.

1.1. G-PROTEIN COUPLED RECEPTORS

Membrane proteins such as channels, transporters and pumps help to maintain the structural integrity and organization of the cell and allow selective and controlled traffic of substances, owing to the low permeability of the membrane(10-13). In mammals, the largest and most diverse membrane protein family are the integral membrane GPCRs, encoded by more than 800 different human genes(14, 15). GPCRs mediate the majority of cellular responses. For these reasons, GPCRs are one of the major targets of current market drugs(16).

Recent analyses of the entire superfamily of GPCRs indicate that these receptors can be grouped into the following classes based on their sequences and structural similarity: class A (rhodopsin-like), class B (secretin-like), class C (metabotropic glutamate-like), class D (Fungal), class E (cyclic AMP receptors), and class F (frizzled/taste2)(14-18). This A–F system is designed to cover all GPCRs, in both vertebrates and invertebrates. Some families in the A–F system do not exist in humans. This happens for classes D and E. More recently, an alternative classification system called GRAFS (Glutamate, Rhodopsin, Adhesion, Frizzled/Taste2, Secretin) has been proposed for vertebrate GPCRs(14, 19-21).

In all crystallized proteins to date, GPCRs have been observed to share the following conserved motifs: seven transmembranes (TMs) α-helices, three intracellular loops (ICLs), three extracellular loops (ECLs), a G-protein coupling intracellular site and a ligand-binding extracellular site(22).

1.1.1. GPCR ACTIVATION

Importantly, GPCR structure determination has been accompanied by functional knowledge; and crystallization of these receptors has provided new insights into the features of their activation process(23, 24). GPCRs are flexible proteins that fluctuate between different conformations that can be broadly grouped into inactive, active and intermediate states(25, 26). The transitions between these states, in particular, from the inactive to the active state, can occur during timescales of nanoseconds to milliseconds(27, 28). Most GPCRs exhibit these transitions spontaneously allowing receptor activation to occur, which is known as receptor constitutive activity or basal activity(9, 29-31). Further, the GPCR activation process can be modified both in its magnitude and dynamics by the binding of endogenous or exogenous extracellular ligands(32, 33).

GPCRs can bind a great variety of ligands: neurotransmitters, ions, odorants, tasting molecules, amino acids, nucleotides, peptides and even photons(32, 33). The receptor cavity to which the endogenous ligands responsible for receptor function bind is known as the orthosteric binding site. From a pharmacological perspective, GPCR ligands can be classified according to the efficacy they show for the activation of a particular signalling pathway into agonists, inverse agonists and neutral antagonists (Figure 1 A)(9). Agonists promote the active conformation above the basal level, with full agonists achieving the same maximum functional response as the endogenous agonists. Partial agonists show lower asymptotic maximum activity than full agonists. Inverse agonists display functional response below basal activity and neutral antagonists do not affect the basal response but compete with other ligands for the orthosteric binding site.

Upon agonist binding on the extracellular site, a sequence of conformational changes, which affect mainly the TM domain, is triggered(29). Each class of the GPCR family has its specific mechanism to transmit the ligand-bound extracellular signal. Starting at the orthosteric binding site, the activation process runs along the TM domain reaching the intracellular side, allowing the opening of the cavity for the coupling of the heterotrimeric (Gαβγ) G protein(34). Then,

the G protein undergoes GTP/GDP exchange with subsequent dissociation of Gα and Gβγ sub-units that, in turn, interact with specific downstream intracellular effector systems, including the modulation of the cytoplasmic calcium release(35) and the production of cyclic adenosine monophosphate (cAMP), phosphatidylinositol-4,5-bisphosphate and diacylglycerol(34) (Figure 1 B). In due course, through the process of desensitization, the active conformation of the receptor is prevented and signalling is attenuated by agonist dissociation and/or deactivation through interaction with β-arrestins(36, 37) in response to activation-specific phosphorylation by G protein-coupled receptor kinases and/or internalization(38, 39). This constitutes the G protein-dependent signalling pathway, while GPCRs may also transduce signals through the G protein-independent signalling pathways when other transducers, such as G protein-coupled receptor kinases (GRKs) and arrestins are involved (Figure 1 B).
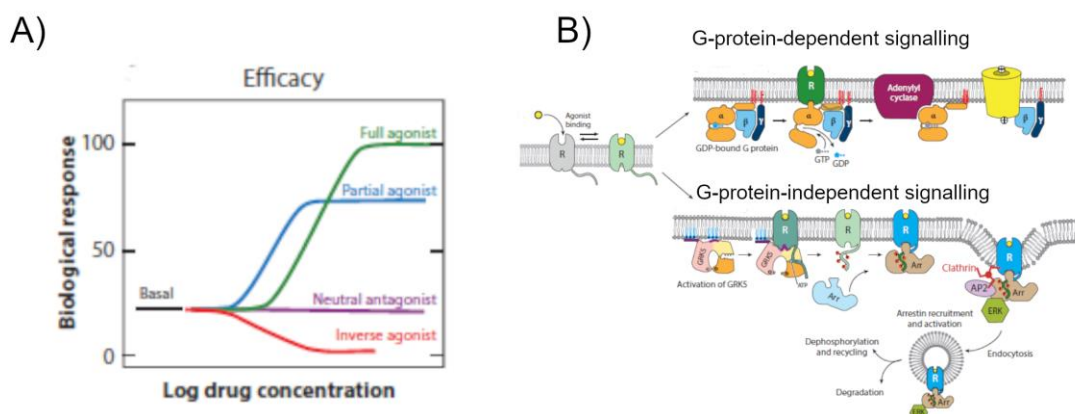
Figure 1. The GPCR functional response: different signaling pathways can be promoted by a single GPCR.

A) Ligand classification based on their asymptotic maximum response (efficacy). B) Agonist binding promotes receptor conformational changes affecting mainly the TM domains (in particular, TM6, blue). A varied array of intracellular signalling proteins, including G-proteins (orange), GRKs (pink) and arrestins (cyan and brown) are bound to the activated receptor leading to different signalling pathways. Taken and adapted from W. I. Weis and B. K. Kobilka, 2018(9).

However, due to the difficulties in crystallizing membrane proteins(40, 41), the crystal structures of most GPCRs are not yet determined.

1.1.2. CLASS A G PROTEIN−COUPLED RECEPTORS

To date, the majority of the available GPCRs crystal structures belong to class A (or rhodopsin-like), which are the largest protein family in humans[42, 43]. As a result, class A members are usually the most studied and represent an important target for therapeutic purposes[44]. At the time of performing this study, 52 class A GPCRs crystal structures had been determined[45, 46].

Of these, there are five receptors for which the structures of both inactive and active (either full active or active-intermediate) states are available: rhodopsin[47], β2aR[48, 49], M2 muscarinic receptor (M2R)[50], A2aR[51, 52], and μ-opioid receptor (MOR)[53]. The crystallization of these class A GPCR active structures has served as an important factor in understanding GPCR activation[9], allowing the characterization of highly conserved amino acid sequence motifs[54], which presumably play important functional roles in the apparently common signalling mechanism shared by all family members[9, 25, 42, 55].

Notably, despite differences among class A GPCRs, inactive- and active-state structure comparisons indicate similar activation-related characteristics concerning conformational changes on the receptor's intracellular side. One of the important rearrangements is the outward movements of TM helices 5 and 6 (including rotation in the latter)[25, 55]. Additionally, TM3 and TM7 also undergo significant conformational changes during activation. Specifically, the intracellular part of TM7 shows an inward movement whereas TM3 translocates vertically[25, 55].

These helix movements during activation are mediated by local microswitches on conserved motifs[54]. Such conserved motifs include the D(E)RY, the CWxP, and the NPxxY, where ''x'' stands for any amino acid residue[55]. To facilitate the comparison of the motifs among the different receptors, we include the Ballesteros−Weinstein numbering scheme as a superscript, which aids in the comparison between homologous class A GPCRs[56]. A particular residue is formatted as X.ZZ, where X represents the helix, 1–7; and ZZ, the residue position relative to the most conserved residue in the named helix (denoted as X.50). For instance, 5.42 indicates a residue in TM5, eight residues before the most conserved residue, Pro$^{5.50}$. In the case where the residue is placed on the loop between two helices, a specific format of X(Y).ZZ is used. In this context, X and Y represent the previous and following helices, and ZZ is the location relative to the most conserved residue in the loop.

The D(E)RY motif is located at the intracellular end of TM3. The electrostatic interaction between $R^{3.50}$ and $E^{6.30}$ on TM6 (known as 'the ionic lock') is supposed to stabilize the inactive conformation(57, 58). The breaking of this interaction facilitates the movement of TMs 3 and 6, and receptor activation(9). The NPxxY motif located at the intracellular end of TM7 is observed to switch inwards in the activated crystal structures. Finally, the CWxP motif is located in the middle section of TM6. In particular, the sidechain rotamer of $W^{6.48}$, in CWxP, was proposed to assume a toggle role in GPCR activation, in recent nuclear magnetic resonance (NMR) studies(59). However, W6.48 does not appear to change its sidechain rotamer in crystal structures of agonist-bound GPCRs reported later(48, 49, 51, 52, 55). These arrangements have got great significance in clarifying several aspects of GPCR activation(9). The importance of water networks in GPCR activation has also been supported by recent crystallographic data(60, 61). Various studies have shown how ordered waters interact with residues that are important in disease states, binding of drugs, receptor activation, and signalling(62-65).

As an additional level of complexity and subtlety in the mechanism of signal transduction, the communication between the orthosteric ligand-binding site and the cytoplasmic region of the receptor responsible for transducer protein binding seems to be loose because they are not rigidly coupled(9, 66). Therefore, the fully molecular processes behind ligand-dependent (de)activation of GPCRs remains scarce, and it is essential to work deeply both at the experimental and computational levels to understand the molecular functioning of these proteins and expectedly perform more efficient drug discovery(9, 25, 42).

1.2. MEMBRANE LIPIDS

Lipids are amphiphilic molecules that spontaneously form a bilayer where the hydrophobic acyl chains are present in the interior and the hydrophilic head groups face outside(67). The main components of the cellular membranes are phospholipids (or also called phosphoglycerides), sphingolipids, glycolipids and sterols (Figure 2)(68).

Phospholipids are the most abundant lipids in eukaryotic membranes. They are named considering firstly their glycerol backbone, and secondly the phosphate-containing moiety. Phospholipids present a polar head group and two hydrophobic fatty acid tails. The two-fatty acid chains may vary in length and saturation state(69). The phosphate group can be esterified with another hydrophilic compound. This allows to classify them into separate classes, based on the nature of the hydrophilic moiety. These classes are named as phosphatidylcholine (PC), phos-

phatidylethanolamine (PE), phosphatidylserine (PS), phosphatidylglycerol (PG) or phosphatidyl-inositol (PI) (Figure 2)(70). Moreover, the different head groups differ in the charge carried by the polar head groups at neutral pH: some phosphoglycerides (e.g., PC and PE) have no net electric charge; others (e.g., PG, PI, and PS) have a net negative charge (Figure 2 A-E). Phospholipids and sphingolipids share a similar structure (Figure 2 F). Sphingolipids are composed by a polar head group and two long non-polar side chains. Sphingolipids are present in all membranes but are particularly abundant in the nervous system, where they are important for proper brain development and functions(71). Sterols are important non-polar components of mammal, plant, and fungal membranes. The basic structure of steroids is the four-ring hydrocarbon. In particular, cholesterol (Figure 2 G) plays a key role in membrane protein in mammals(72). Due to this large structural heterogeneity(68), the lipid composition and distribution varies among bilayers(73-75). PC, sphingomyelin, and glycolipids are preferentially located at the outer layer of the membrane. Meanwhile, PI, PE, and PS are localized in the cytoplasmic half of the bilayer. Some authors have suggested that this diversity could be associated with the differential roles and properties that they perform(76, 77).
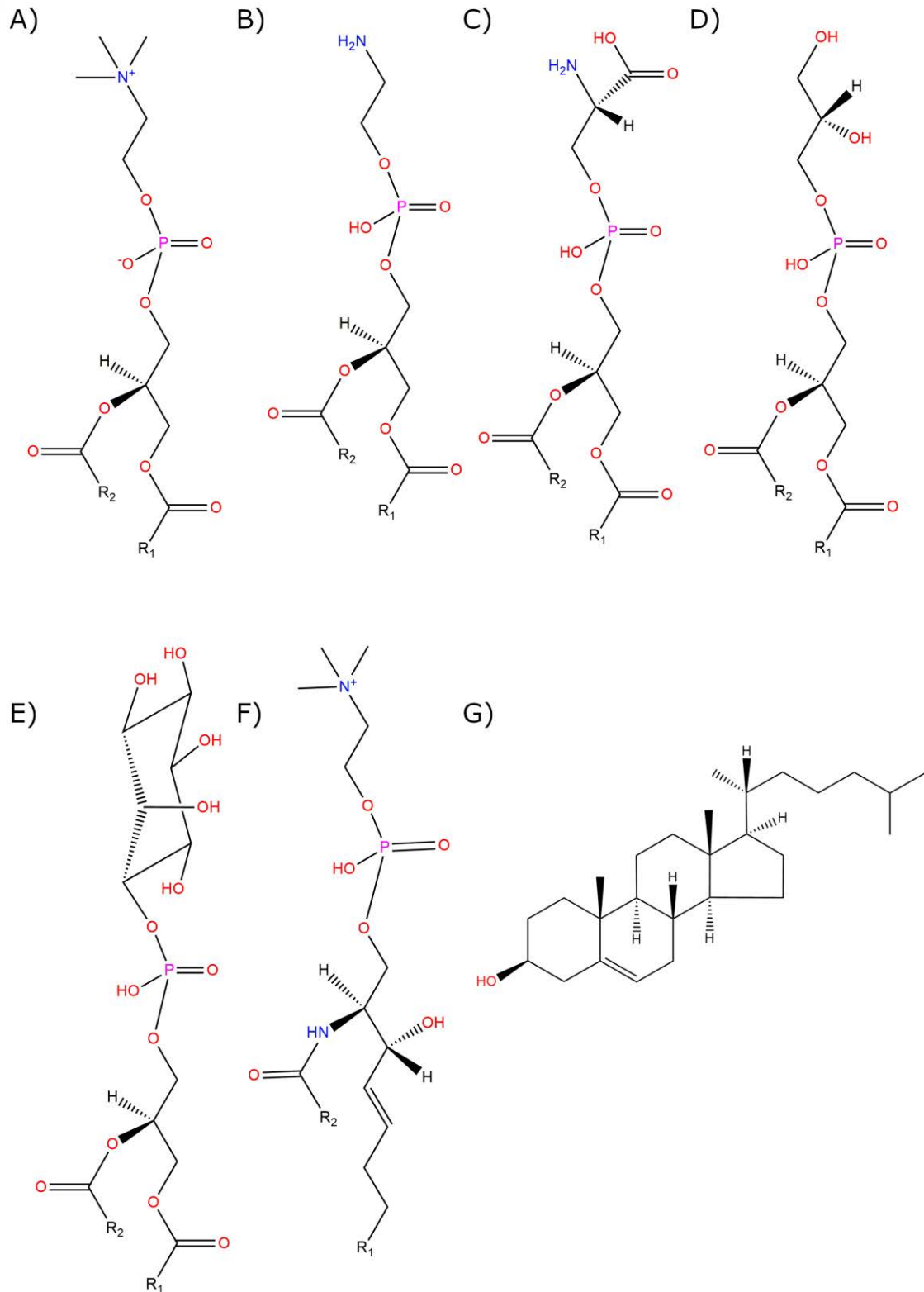
Figure 2. **Molecular structure of the some lipid species in biological membranes.**

Representative structures from each of the most important lipid categories: A) Phosphatidyl-choline (PC) B) Phosphatidylethanolamine (PE) C) Phosphatidylserine (PS) D) Phosphatidylglyc-erol (PG) E) Phosphatidylinositol (PI) F) Sphingolipid (SM) G) Cholesterol. Colour coding of the

atoms is as follows: red for oxygen, magenta for phosphorus, blue for nitrogen and black for carbon.

Indeed, the functional role of lipids is increasingly considered more important. Recent works pointed towards lipids as a cause of some human diseases, including cancer(78) and neuro-degenerative diseases(79), as shown by membrane changes in the brains of Alzheimer's and Parkinson's patients(80-83)

At the same time, lipids have been found to influence GPCR activity(84-87). This matter was introduced after several observations. Firstly, in the absence of ligands, some GPCRs exhibit basal activity, thought to be caused by their surrounding environment, which provides enough energy for the receptor to reach an active state(9, 29-31). Further, lipids facilitate the recruit-ment of heterotrimeric G-proteins(88) and help their crystallization process(41, 89). Moreover, GPCRs are integral membrane proteins with a significant portion of the protein embedded in the membrane. Therefore, portions of protein structures directly interact with the acyl por-tions (hydrophobic) of the lipid membrane. This is accomplished by the hydrophobic matching between the hydrophobic lipid bilayer and the GPCR(85, 86, 90, 91). This means that the thick-ness of the lipid bilayer could adapt to the protein if the width of the protein is not equal to the membrane(92).

Lipids not only determine the biophysical properties of GPCRs in the membrane but also the propensity of these receptors to activate through allosteric protein-lipid interactions.

1.3. MOLECULAR CHARACTERIZATION OF GPCR (DE)ACTIVATION AND LIPID–GPCR IN-TERACTIONS

Given the increasing number of results that point to lipids as important modulators of GPCR structure and function, great interest has formed around the underlying molecular mecha-nisms that govern their interactions, and could potentially be of interest for pharmaceutical research and drug discovery. Nevertheless, the regulation of GPCR function by the allosteric modulation of lipids is not yet well understood.

Importantly, the growing advancements in biophysical techniques allow the gathering of rele-vant information at the molecular level. In particular, MD simulations have proven to be a reli-

able computational approach to explore in detail protein-lipid interactions, receptor-ligand binding, and receptor conformational changes(93).

In this context, the present thesis represents an effort towards the molecular characterization of GPCR-lipid interactions with a special emphasis on their involvement in the activation of these receptors. We have tried to give a computational content to typical pharmacological concepts such as receptor constitutive activity and agonist efficacy with lipids as allosteric modulators.

2. MATERIALS AND METHODS

Experimental methods, such as NMR, infrared (IR) and fluorescence spectroscopies together with X-ray crystallography are some of the techniques that allow obtaining information at the molecular level on GPCRs. However, obtaining data on the molecular mechanisms responsible for the receptor activation process with the inclusion of lipid-protein interactions is challenging. In this regard, computer simulation approaches have proven helpful in opening new avenues in the knowledge of the conformational dynamics and function of these proteins. In particular, MD simulations have been successful in providing accurate molecular features of GPCR conformational space(93).

In the section of the thesis devoted to our published studies, articles have been inserted that summarize the computational work developed during the thesis period. Each of these articles includes its corresponding methods section with a detailed description of the techniques involved. Thus, to avoid redundancy, this chapter offers herein a brief introduction to MD simulations, the key methodology used in our studies.

2.1. INTRODUCTION TO MD SIMULATIONS

MD simulations aim to explore and chemically understand the dynamics of biomolecular systems. Thus, they can be considered relatively close to some experimental techniques such as NMR and complementary to others such as X-ray crystallography or electron microscopy(94). MD is an ideal computational technique for studying GPCR conformational flexibility in a membrane environment and the effects exerted by ligands and lipids(95).

MD simulations are indebted to the pioneering work by Alder and Wainwright during the 1950s(96). Briefly, MD simulations is a deterministic technique that tracks the time fluctuation of the atomic positions or a molecular system with high spatiotemporal resolution(95, 97-100). MD algorithms allow the description of the temporal evolution of atoms according to their potential energy according to Newton's laws.

Newton's second law or the equation of motion ($F_i = m_i a_i$) can be presented for a group of N atoms, where F_i is the force exerted on particle i, m_i is the mass of particle i and a_i is the acceleration of particle i. This force is determined by empirical parameters, also called force fields

(FFs). The FFs are a collection of mathematical equations to model the potential energy, charge polarization and associated constants, designed to accurately reproduce the molecular geometry obtained from X-ray, NMR, IR, etc (101). The most used FFs to study GPCRs using MD simulations are AMBER(102), CHARMM(103, 104), GROMOS(105), and OPLS(106). As a result, the atoms follow a trajectory, calculated by the initial distribution of velocities and their accelerations, which is determined by the gradient of the potential energy function, and the initial positions of the atoms. The potential energy is a function of the atomic positions of all the atoms in the system. To solve the equation for each atom, different algorithms, such as Verlet(107) or leapfrog(108), are applied.

MD simulation techniques have been improved over time to obtain more reliable results. The two most important techniques developed in this area are associated with the control of temperature and pressure. Several thermostats have been developed to keep the system around the desired temperature, such as Langevin (109) and the Nosé-Hoove thermostat (110). Besides, as most experiments are performed under constant pressure, barostats have been developed to keep simulations under constant pressure, such as the Berendsen barostat (111). As a consequence, the calculations can be carried out either at the desired NVT (N: constant particle number, V: constant volume, T: constant temperature), set by inserting the thermostat into the system, or at the desired NPT (P: constant pressure), set by incorporating both thermostat and barostat into the system. The Berendsen barostat and Langevin thermostat are perhaps the most typically used for MD simulations as previously have been reported (112).

2.2. LIMITATIONS OF MD SIMULATIONS

Although MD has proved to be a reliable computational approach, it has limitations. As happens in general with all computer science methods, its application is limited by timescales, algorithms and technical implementations. The main limitation is that some biomolecular processes (such as receptor activation) occur over long-timescales.

To overcome these limitations, the field of MD simulations has developed different approaches involving particle resolution and timescales. I will mention three main types of MD simulations: all-atoms (AA)(113-115), coarse-grained (CG)(116, 117), and intermediate "hybrid" resolution (e.g. PACE)(118-120). The AA MD simulations provide high-resolution information at both time and spatial level (fs and angstrom levels). However, the duration of biomolecular phenomena such as conformational receptor activation and ligand unbinding usually go be-

yond the AA MD capability because of their computational cost(121, 122). Thus, to avoid this problem and, therefore, extend the simulation timescales, CG MD simulations were developed. In the latter simulations, atoms are not treated as individual entities but grouped into bigger objects to simplify the representation of big molecules. However, this often results in a loss of accuracy, particularly concerning the secondary structure of the protein models(123). PACE simulations have been developed to couple lipids and solvents, modelled from MARTINI CG, while proteins are represented by GROMOS AA force field or the PACE UA force field. In this way, it is possible to arrive at long-timescales compared to AA simulations, while at the same time a complete atomic representation of the secondary structure of the protein is preserved.

Apart from advances in methodological approaches, computer architecture developments are of great help to achieve long-timescales, while maintaining the accuracy present in AA MD simulations. An example resides in the graphic processing unit (GPU) hardware, which contains numerous cores with parallel architecture, which is efficient for computational applications such as MD(124, 125).

3. MOTIVATIONS, HYPOTHESES AND AIMS

3.1. THE RESEARCH PROBLEM ADDRESSED IN THE THESIS

GPCRs are involved in numerous human diseases(126-128). This makes them very important targets for drug discovery programs in the pharmaceutical industry in the quest for new medicines.

Although GPCRs have been extensively studied during the past decades, the underlying structural and functional mechanisms responsible for the many critical regulatory processes controlled by this protein superfamily remain unclear, including the first step of signal transduction as receptor activation and lipid allosteric modulation(25). Hence, there is a tendency in recent years to obtain more information at the molecular level(122, 126).

In this section, we highlight some of the most relevant MD findings and limitations that influenced the conception and development of this thesis, namely, GPCR conformational changes and activation, ligands modulation, and lipid allosteric modulation.

MEANINGFUL TIMESCALE MD SIMULATIONS ARE NEEDED

There has lately been a growing interest in developing modelling methods for MD simulations(112, 129). Achieving significant timescales, while maintaining atomistic resolutions and accurately simulate biological processes is a critical step that is conditioned by the capacity of computational resources.

The introduction of strategies that consider recent cost-effective accelerator processors, such as the IBM Cell processor and Nvidia's GPUs, represents a well-positioned innovation that efficiently enhances AA MD. Nowadays, significant timescale MD simulations are possible and easier through ACEMD software(112). Particularly, this software takes advantage of GPUs to achieve relevant timescales (μs) while maintaining atomistic resolution through CHARMM and AMBER FFs.

B2AR AND A2AR WERE SELECTED AS THE RESEARCH SYSTEM

β2aR(27, 28, 85, 130-143) and A2aR(144-148) have been the subject of numerous studies in the context of MD simulations. Thus, there is a rich corpus of literature to which our results can be compared.

To this end, it is essential to utilize crystal structures of good quality to properly run reliable MD simulations, explore GPCR activation and tackle protein-lipid interactions. In this sense, β2aR and A2aR provide the basis presented in this thesis.

INFLUENCE OF THE MEMBRANE LIPID ENVIRONMENT ON G PROTEIN-COUPLED RECEPTOR ACTIVATION

The typical behaviour of class A GPCRs, when they are simulated without a bound G protein, is to fluctuate between inactive and intermediate states without inducing the fully active receptor conformation, even in the presence of an agonist(20, 27, 137, 144, 149-153). Therefore, one of the current challenges when running MD simulations on GPCRs is to understand the molecular basis of their agonist-mediated transition from the inactive state to the active state.

In this regard, several studies have suggested that various factors related with lipids, such as the lipid headgroups, the length of acyl tails, and bilayer thickness may be involved in particular conformational changes in the protein, which may have implications in the activation of GPCRs(3). Hence, the consideration of different lipidic compositions of the membrane and the analysis of the allosteric influences of the selected lipids may be an important element in the exploration of GPCR activation by MD simulations.

3.2.   HYPOTHESES

The following hypotheses have been proposed as the subject of the research for this thesis to take a step forward in the knowledge of GPCR activation in an lipid-dependent membrane environment:

1- The application of ACEMD AA MD simulations can give reliable and achievable molecular details on GPCR conformational ensembles and protein-lipid interactions, which presumably will agree with experimental data.

2- To understand the determinants of membrane-lipid composition on the (de)activation of class A GPCRs, various lipids should be chosen and their allosteric actions analyzed.

3- The distinct lipid headgroups might lead to specific molecular interactions with the receptor, leading to different protein conformations with potentially functional implications. Ultimately, these interactions may induce the (de)activation of class A GPCRs as well as the stability of ligands in the receptor binding site. Thus, the analysis of lipid-

receptor interactions and their allosteric transmission through the protein can provide new insights into the structure-function properties of GPCRs.

To sum up, taking profit of the advanced architecture of intrinsic parallelized GPUs and the implementation of ACEMD software, it is expected that AA MD simulations of some selected GPCRs in membranes of different lipid compositons will provide relevant information on the receptor activation process and lipid allosteric modulation, in achievable timescales.

3.3.   AIMS AND OBJECTIVES

The general aims of this thesis are:

1. To better understand at the molecular level the pharmacological properties of constitutive receptor activity and agonist efficacy by MD simulations.

2. To identify the lipid-receptor interactions allosterically contributing to receptor activation.

3. To provide a methodology that can be transferable to different receptor systems and that can set the basis for a new structure-based drug design.

To accomplish these general aims, two class A GPCRs were selected: β2AR and adenosine A2aR. For each of these systems the following specific objectives were proposed.

FIRST ARTICLE OF THIS THESIS: "STRUCTURAL INSIGHTS INTO POSITIVE AND NEGATIVE ALLOSTERIC REGULATION OF A G PROTEIN-COUPLED RECEPTOR THROUGH PROTEIN-LIPID INTERACTIONS".

New experimental data on β2aR coming at the beginning of the present thesis pointed to phospholipids as essential allosteric modulators of GPCR activity(84). However, how lipids exert their effects on GPCR conformations at the atomic level was unclear.

Therefore, the specific objectives of this study were:

i.   To map at the atomic level the allosteric modulation that DOPE, DOPC and DOPG phospholipids exert on apo β2aR in an active receptor state.

ii.   To extract general mechanistic conclusions on phospholipid-GPCR interactions.

SECOND ARTICLE OF THIS THESIS: "INSIGHTS INTO ADENOSINE A2A RECEPTOR ACTIVATION THROUGH COOPERATIVE MODULATION OF AGONIST AND ALLOSTERIC LIPID INTERACTIONS".

The understanding of the molecular interactions involved in agonist binding and ensuing receptor activation is essential for rational drug design in GPCRs. In particular, agonist binding to A2aR does not guarantee that the active state is reached during MD simulations(150). Thus, to our knowledge, previously to the publication of this study, the full transition of A2aR from the inactive to the active state had not yet been described with unbiased MD simulations. Thus it remained unclear how the agonist-mediated activation of A2aR occurs.

Therefore, by using as a starting point the inactive crystal structure of A2aR, the specific objectives of this study were:

i. To identify the molecular determinants of A2AR activation by adenosine under different lipid environments.

ii. To identify the differential allosteric effects of lipids on adenosine-mediated A2aR activation.

iii. To validate adenosine results with NECA, a more potent A2aR agonist.

3.4. PROTOCOL TO ACCOMPLISH THE OBJECTIVES

To develop an investigation that allows us to fulfil the stated objectives, all MD simulations were performed with ACEMD software(112) on specialized GPU-computer hardware. As a general approach, the receptor complexes were embedded in a containing lipid bilayer and solvated with TIP3P water molecules above and below the membrane, with a concentration of 0.3 M KCl for zero system net charge. Membrane, water and protein parameters were generated according to the CHARMM36 force-field(104) and adenosine/NECA parameters were generated according to CGenFF v1.0.0(154). The exact size of the system and type of lipid varied depending on the specific system (see each published study for particular details). Each receptor-membrane system was equilibrated for 28 ns at 300 K (Langevin thermostat) and 1 atmosphere (Berendsen barostat). During the initial 8 ns of equilibration, protein and ligand heavy atoms were harmonically restrained and progressively released over 2 ns. During the final 20 ns of equilibration, no restraints were applied. Unrestrained production MD trajecto-

ries were yielded under the same conditions with varying total time length depending on each study, but always using 4 fs time step.

4. RESULTS

The purpose of this thesis has the ultimate objective of gaining insight into the impact of the membrane lipid environment on the (de)activations of GPCRs by MD simulations. This has been done to better understand the regulatory processes behind Class A GPCRs, which, hopefully, would allow in a later step the design of more effective drugs. To this end, two prototypical class A GPCRs, β2aR and A2aR, embedded in different lipid environments, were selected.

The work presented in this section belongs to the following published studies, which are referred in the text by the chapter's numbers:

4.1. *Structural insights into positive and negative allosteric regulation of a G protein-coupled receptor through protein-lipid interactions.* Bruzzese A, Gil C, Dalton JAR, Giraldo J. *Sci Rep*. 2018;8(1):4456. Published 2018 Mar 13.

4.2. *Insights into Adenosine A2a receptor activation through cooperative modulation of agonist and allosteric lipid interactions.* Bruzzese A, Dalton JAR, Giraldo J. *PLoS Comput Biol*. 2020;16(4):e1007818. Published 2020 Apr 16.

Agustín Bruzzese (AB) performed the corresponding MD simulations and analysis under the supervision of James Dalton (JD). Also, AB was involved in the writing of the first versions of the manuscripts, whereas the subsequent versions were co-supervised by Jesús Giraldo and JD. The central findings of these studies are provided in this section regarding the original premises and specified objectives.

4.1. STRUCTURAL INSIGHTS INTO POSITIVE AND NEGATIVE ALLOSTERIC REGULATION OF A G PROTEIN-COUPLED RECEPTOR THROUGH PROTEIN-LIPID INTERACTIONS

Long-timescale MD simulations revealed the molecular effects of three lipids on β2aR activity via different protein-lipid interactions. In agreement with published experimental results, we show that net negatively charged lipids (such as DOPG) stabilize an active-like β2aR state that is capable of docking Gsα protein. Net-neutral zwitterionic lipids (DOPE and DOPC), on the other hand, inactivate the receptor, generating either fully inactive or intermediate states with kinetics depending on the distribution of lipid headgroup charge and hydrophobicity. Such

chemical variations among lipid head groups change the thickness and density of the membrane, which, by lateral compression effects, destabilizes the active state of β2aR differently. This reveals how and why β2aR is sensitive to its cell membrane environment.

4.2. INSIGHTS INTO ADENOSINE A$_{2A}$ RECEPTOR ACTIVATION THROUGH COOPERATIVE MODULATION OF AGONIST AND ALLOSTERIC LIPID INTERACTIONS

The results gathered on β2aR were used to uncover the underlying molecular mechanism behind A2aR activation. In this regard, long-timescale MD simulations consistently showed the activation process of A2aR in different lipid environments. In DOPC with bound adenosine, we observe the transition to an intermediate receptor conformation consistent with the known adenosine-bound crystal state. Two different intermediate conformations were obtained in a DOPG lipid membrane. One is similar to that observed in DOPC with bound adenosine, while the other is closer to, although not fully reached, the active state. Exclusively with DOPG and the adenosine-bound receptor, we consistently reproduced the fully active receptor characteristics. The presence/absence of agonist and phospholipid-mediated allosteric effects on the intracellular side of the receptor are factors responsible for these singular receptor conformations. These results suggest that cooperative effects between receptor-bound ligand and lipids play a key role in GPCR activation. Finally, the results exhibit how and why A2aR, similarly to β2aR, is sensitive to its cell membrane environment.

Overall, we believe our results have contributed to understanding the receptor allosteric modulation through protein-lipid interactions. These results on A2aR and β2aR are in good agreement with experimentally reported data(84, 155). The obtained results show the modulatory effect of membrane lipid composition on GPCR conformational ensembles. In addition, it may be speculated that such modulation may be important for other GPCRs.

To some extent, these findings may also be meaningful in the design of drug discovery programs and might explain how membrane impairment in some diseases (e.g. Alzheimer's and Parkinson's) could affect GPCR-mediated cell signalling. This suggests the relevance that the membrane lipid composition and the methodologies that include this factor may have in GPCR-based therapeutics.

Therefore, in this thesis, a detailed analysis of lipid effects on GPCR function and ligand efficacy is presented, which is consistent with current experimental data.

5.   CONCLUSIONS

The research herein presented was aimed to examine the effect of the lipid composition of the cell membrane on GPCR (de)activation. Importantly, the allosteric interactions exerted by lipids affect the population distribution of active and inactive receptor states, thus leading to a complex signalling network. This is the reason why there is increasing interest in exploring methodologies and techniques to increase the current knowledge on the molecular mechanisms by which lipids modulate the activity of GPCRs, as this could have a direct impact on drug discovery. This work offers new insights into this field by selecting two prototypical class A GPCRs and applying AA MD simulations. The following general conclusions were reached:

1.   The first hypothesis of this thesis states that the high computational performance of ACEMD software could facilitate the description of the molecular mechanisms that govern protein-lipid interactions and their involvement in GPCR (de)activation by making long-timescale MD simulations computationally accessible. This hypothesis has been accomplished in our two published studies in which computational results seem to be in good agreement with experimental data.

2.   The selection of two crystal structures, one in an active state (β2aR) and the other in an inactive state (A2aR), has allowed us to analyze different aspects related with receptor (de)activation. Comparison between the stabilization of an active state, in the case of β2aR, with the induction of an active state from a starting inactive state, in the case of A2aR, allows to identify the conmmonalities and differences between conformational selection and conformational induction mechanisms, using MD simulations. On the other hand, we consistently have described similar positive and negative allosteric modulation on these GPCRs through the differential effect of various phospholipids. These modulatory effects depend on the formation/lack of electrostatic interaction between the lipid headgroups and the protein. As a result, a molecular view on how lipids modulate GPCR function is provided.

3.   Finally, this work can be relevant for other research groups either from the private or public sectors involved in the GPCR field. We believe this methodology can be extended to

other GPCRs following similar premises.

5.1. FURTHER DIRECTIONS

The work presented in this thesis can be further extended to cover other aspects in the complex GPCR field:

1- To study the effect of lipids on GPCR dimerization. There is a significant amount of experimental data pointing to receptor oligomerization for new therapeutic approaches (bivalent drugs)(156, 157). In this context, membrane lipids seem to be tightly involved in the regulation of GPCR oligomerization.

2- To explore the effect of lipid-GPCR modulation using MD simulations with varying complexity scale. The accuracy of AA FF calculations comes with a high computational cost if it is required to perform them at biologically relevant timescales (microseconds). At the beginning of the study, we expected that the CG MARTINI FF would be a useful alternative for studying lipid-protein interactions and receptor activation due to its reductionist nature, which would allow for a significant speed-up in computational performance. However, the resulting protein behaviour and protein-lipid interactions were not consistent with experimental results and we left this approach. Thanks to the continuous advances in the field of MD simulations, it could be that today, CG MARTINI FF is sufficiently accurate, and therefore could become a great asset for the study of protein-lipid interactions.

3- To develop a close-physiological membrane. Although this current research presents two prototype class A GPCRs in the context of different membranes, it remains to be studied how a more physiological membrane (both in disease and healthy contexts) might affect GPCR functional behavior in a more physiological-like setting.

6.   REFERENCES

1.   Singer SJ, Nicolson GL. The fluid mosaic model of the structure of cell membranes. Science. 1972;175(4023):720-31.

2.   Bolla JR, Agasid MT, Mehmood S, Robinson CV. Membrane Protein-Lipid Interactions Probed Using Mass Spectrometry. Annu Rev Biochem. 2019;88:85-111.

3.   Muller MP, Jiang T, Sun C, Lihan M, Pant S, Mahinthichaichan P, et al. Characterization of Lipid-Protein Interactions and Lipid-Mediated Modulation of Membrane Protein Function through Molecular Simulation. Chem Rev. 2019;119(9):6086-161.

4.   Enkavi G, Javanainen M, Kulig W, Rog T, Vattulainen I. Multiscale Simulations of Biological Membranes: The Challenge To Understand Biological Phenomena in a Living Substance. Chem Rev. 2019;119(9):5607-774.

5.   Edidin M. Lipids on the frontier: a century of cell-membrane bilayers. Nat Rev Mol Cell Biol. 2003;4(5):414-8.

6.   Jain MK. Biomembranes: Molecular structure and function. Cell. 1989;58(5):813-4.

7.   Sethi S, Brietzke E. Recent advances in lipidomics: Analytical and clinical perspectives. Prostaglandins Other Lipid Mediat. 2017;128-129:8-16.

8.   Opella SJ. Solid-state NMR and membrane proteins. J Magn Reson. 2015;253:129-37.

9.   Weis WI, Kobilka BK. The Molecular Basis of G Protein-Coupled Receptor Activation. Annual review of biochemistry. 2018;87:897-919.

10.   Cuello LG, Jogini V, Cortes DM, Pan AC, Gagnon DG, Dalmas O, et al. Structural basis for the coupling between activation and inactivation gates in K(+) channels. Nature. 2010;466(7303):272-5.

11.   Pletneva NV, Pletnev VZ, Sarkisyan KS, Gorbachev DA, Egorov ES, Mishin AS, et al. Crystal Structure of Phototoxic Orange Fluorescent Proteins with a Tryptophan-Based Chromophore. PLoS One. 2015;10(12):e0145740.

12.   Xu Y, Tao Y, Cheung LS, Fan C, Chen LQ, Xu S, et al. Structures of bacterial homologues of SWEET transporters in two distinct conformations. Nature. 2014;515(7527):448-52.

13.   Kanai R, Ogawa H, Vilsen B, Cornelius F, Toyoshima C. Crystal structure of a Na+-bound Na+,K+-ATPase preceding the E1P state. Nature. 2013;502(7470):201-6.

14.   Fredriksson R, Lagerstrom MC, Lundin LG, Schioth HB. The G-protein-coupled receptors in the human genome form five main families. Phylogenetic analysis, paralogon groups, and fingerprints. Mol Pharmacol. 2003;63(6):1256-72.

15.   Rosenbaum DM, Rasmussen SG, Kobilka BK. The structure and function of G-protein-coupled receptors. Nature. 2009;459(7245):356-63.

16.   Santos R, Ursu O, Gaulton A, Bento AP, Donadi RS, Bologa CG, et al. A comprehensive map of molecular drug targets. Nat Rev Drug Discov. 2017;16(1):19-34.

17.   Lagerstrom MC, Schioth HB. Structural diversity of G protein-coupled receptors and significance for drug discovery. Nat Rev Drug Discov. 2008;7(4):339-57.

18.   Foord SM, Bonner TI, Neubig RR, Rosser EM, Pin JP, Davenport AP, et al. International Union of Pharmacology. XLVI. G protein-coupled receptor list. Pharmacol Rev. 2005;57(2):279-88.

19.   Lindsley CW. The top prescription drugs of 2012 globally: biologics dominate, but small molecule CNS drugs hold on to top spots. ACS Chem Neurosci. 2013;4(6):905-7.

20.   Kobilka BK, Deupi X. Conformational complexity of G-protein-coupled receptors. Trends Pharmacol Sci. 2007;28(8):397-406.

21.   Nordstrom KJ, Sallman Almen M, Edstam MM, Fredriksson R, Schioth HB. Independent HHsearch, Needleman--Wunsch-based, and motif analyses reveal the overall hierarchy for most of the G protein-coupled receptor families. Mol Biol Evol. 2011;28(9):2471-80.

22.   Katritch V, Cherezov V, Stevens RC. Structure-function of the G protein-coupled receptor superfamily. Annu Rev Pharmacol Toxicol. 2013;53:531-56.

23.   Jacobson KA, Costanzi S. New insights for drug design from the X-ray crystallographic structures of G-protein-coupled receptors. Mol Pharmacol. 2012;82(3):361-71.

24.   Xiang J, Chun E, Liu C, Jing L, Al-Sahouri Z, Zhu L, et al. Successful Strategies to Determine High-Resolution Structures of GPCRs. Trends Pharmacol Sci. 2016;37(12):1055-69.

25.   Latorraca NR, Venkatakrishnan AJ, Dror RO. GPCR Dynamics: Structures in Motion. Chem Rev. 2017;117(1):139-55.

26.   Hilger D, Masureel M, Kobilka BK. Structure and dynamics of GPCR signaling complexes. Nature structural & molecular biology. 2018;25(1):4-12.

27.   Dror RO, Arlow DH, Maragakis P, Mildorf TJ, Pan AC, Xu H, et al. Activation mechanism of the beta2-adrenergic receptor. Proc Natl Acad Sci U S A. 2011;108(46):18684-9.

28.   Nygaard R, Zou Y, Dror RO, Mildorf TJ, Arlow DH, Manglik A, et al. The dynamic process of beta(2)-adrenergic receptor activation. Cell. 2013;152(3):532-42.

29.   Manglik A, Kruse AC. Structural Basis for G Protein-Coupled Receptor Activation. Biochemistry. 2017;56(42):5628-34.

30.   Thal DM, Glukhova A, Sexton PM, Christopoulos A. Structural insights into G-protein-coupled receptor allostery. Nature. 2018;559(7712):45-53.

31.   Seifert R, Wenzel-Seifert K. Constitutive activity of G-protein-coupled receptors: cause of disease and common property of wild-type receptors. Naunyn Schmiedebergs Arch Pharmacol. 2002;366(5):381-416.

32.   McCorvy JD, Butler KV, Kelly B, Rechsteiner K, Karpiak J, Betz RM, et al. Structure-inspired design of beta-arrestin-biased ligands for aminergic GPCRs. Nat Chem Biol. 2018;14(2):126-34.

33.   Wingler LM, Elgeti M, Hilger D, Latorraca NR, Lerch MT, Staus DP, et al. Angiotensin Analogs with Divergent Bias Stabilize Distinct Receptor Conformations. Cell. 2019;176(3):468-78.e11.

34.   Oldham WM, Hamm HE. Heterotrimeric G protein activation by G-protein-coupled receptors. Nat Rev Mol Cell Biol. 2008;9(1):60-71.

35.   Kiselyov K, Shin DM, Muallem S. Signalling specificity in GPCR-dependent Ca2+ signalling. Cell Signal. 2003;15(3):243-53.

36.   Shenoy SK, Lefkowitz RJ. beta-Arrestin-mediated receptor trafficking and signal transduction. Trends Pharmacol Sci. 2011;32(9):521-33.

37.   Scheerer P, Sommer ME. Structural mechanism of arrestin activation. Curr Opin Struct Biol. 2017;45:160-9.

38.   Tesmer JJ. Hitchhiking on the heptahelical highway: structure and function of 7TM receptor complexes. Nat Rev Mol Cell Biol. 2016;17(7):439-50.

39.   Bockaert J, Marin P, Dumuis A, Fagni L. The 'magic tail' of G protein-coupled receptors: an anchorage for functional protein networks. FEBS Lett. 2003;546(1):65-72.

40.   Ostermeier C, Michel H. Crystallization of membrane proteins. Curr Opin Struct Biol. 1997;7(5):697-701.

41.   Caffrey M. A lipid's eye view of membrane protein crystallization in mesophases. Curr Opin Struct Biol. 2000;10(4):486-97.

42.   Tehan BG, Bortolato A, Blaney FE, Weir MP, Mason JS. Unifying family A GPCR theories of activation. Pharmacol Ther. 2014;143(1):51-60.

43.   Lee Y, Basith S, Choi S. Recent Advances in Structure-Based Drug Design Targeting Class A G Protein-Coupled Receptors Utilizing Crystal Structures and Computational Simulations. J Med Chem. 2018;61(1):1-46.

44.   Overington JP, Al-Lazikani B, Hopkins AL. How many drug targets are there? Nat Rev Drug Discov. 2006;5(12):993-6.

45.   Pandy-Szekeres G, Munk C, Tsonkov TM, Mordalski S, Harpsoe K, Hauser AS, et al. GPCRdb in 2018: adding GPCR structure models and ligands. Nucleic Acids Res. 2018;46(D1):D440-D6.

46.   Isberg V, Mordalski S, Munk C, Rataj K, Harpsoe K, Hauser AS, et al. GPCRdb: an information system for G protein-coupled receptors. Nucleic Acids Res. 2016;44(D1):D356-64.

47.   Choe HW, Kim YJ, Park JH, Morizumi T, Pai EF, Krauss N, et al. Crystal structure of metarhodopsin II. Nature. 2011;471(7340):651-5.

48.   Rasmussen SG, DeVree BT, Zou Y, Kruse AC, Chung KY, Kobilka TS, et al. Crystal structure of the beta2 adrenergic receptor-Gs protein complex. Nature. 2011;477(7366):549-55.

49.   Rasmussen SG, Choi HJ, Fung JJ, Pardon E, Casarosa P, Chae PS, et al. Structure of a nanobody-stabilized active state of the beta(2) adrenoceptor. Nature. 2011;469(7329):175-80.

50.   Kruse AC, Ring AM, Manglik A, Hu J, Hu K, Eitel K, et al. Activation and allosteric modulation of a muscarinic acetylcholine receptor. Nature. 2013;504(7478):101-6.

51.   Lebon G, Warne T, Edwards PC, Bennett K, Langmead CJ, Leslie AG, et al. Agonist-bound adenosine A2A receptor structures reveal common features of GPCR activation. Nature. 2011;474(7352):521-5.

52.   Garcia-Nafria J, Lee Y, Bai X, Carpenter B, Tate CG. Cryo-EM structure of the adenosine A2A receptor coupled to an engineered heterotrimeric G protein. Elife. 2018;7.

53.   Huang W, Manglik A, Venkatakrishnan AJ, Laeremans T, Feinberg EN, Sanborn AL, et al. Structural insights into μ-opioid receptor activation. Nature. 2015;524(7565):315-21.

54.   Bockaert J, Pin JP. Molecular tinkering of G protein-coupled receptors: an evolutionary success. EMBO J. 1999;18(7):1723-9.

55.   Nygaard R, Frimurer TM, Holst B, Rosenkilde MM, Schwartz TW. Ligand binding and micro-switches in 7TM receptor structures. Trends Pharmacol Sci. 2009;30(5):249-59.

56.   Ballesteros JA, Weinstein H. Integrated methods for the construction of three-dimensional models and computational probing of structure-function relations in G protein-coupled receptors. Methods in Neurosciences. 1995;25:366-428.

57.   Ballesteros JA, Jensen AD, Liapakis G, Rasmussen SG, Shi L, Gether U, et al. Activation of the beta 2-adrenergic receptor involves disruption of an ionic lock between the cytoplasmic ends of transmembrane segments 3 and 6. J Biol Chem. 2001;276(31):29171-7.

58.   Vogel R, Mahalingam M, Ludeke S, Huber T, Siebert F, Sakmar TP. Functional role of the "ionic lock"--an interhelical hydrogen-bond network in family A heptahelical receptors. J Mol Biol. 2008;380(4):648-55.

59.   Eddy MT, Lee MY, Gao ZG, White KL, Didenko T, Horst R, et al. Allosteric Coupling of Drug Binding and Intracellular Signaling in the A2A Adenosine Receptor. Cell. 2018;172(1-2):68-80.e12.

60.   Liu W, Chun E, Thompson AA, Chubukov P, Xu F, Katritch V, et al. Structural basis for allosteric regulation of GPCRs by sodium ions. Science. 2012;337(6091):232-6.

61.   Haga K, Kruse AC, Asada H, Yurugi-Kobayashi T, Shiroishi M, Zhang C, et al. Structure of the human M2 muscarinic acetylcholine receptor bound to an antagonist. Nature. 2012;482(7386):547-51.

62.   Congreve M, Langmead CJ, Mason JS, Marshall FH. Progress in structure based drug design for G protein-coupled receptors. Journal of medicinal chemistry. 2011;54(13):4283-311.

63.   Angel TE, Gupta S, Jastrzebska B, Palczewski K, Chance MR. Structural waters define a functional channel mediating activation of the GPCR, rhodopsin. Proceedings of the National Academy of Sciences of the United States of America. 2009;106(34):14367-72.

64.   Venkatakrishnan AJ, Ma AK, Fonseca R, Latorraca NR, Kelly B, Betz RM, et al. Diverse GPCRs exhibit conserved water networks for stabilization and activation. Proceedings of the National Academy of Sciences of the United States of America. 2019;116(8):3288-93.

65.   Mason JS, Bortolato A, Congreve M, Marshall FH. New insights from structural biology into the druggability of G protein-coupled receptors. Trends Pharmacol Sci. 2012;33(5):249-60.

66.   Yao X, Parnot C, Deupi X, Ratnala VR, Swaminath G, Farrens D, et al. Coupling ligand structure to specific conformational switches in the beta2-adrenoceptor. Nat Chem Biol. 2006;2(8):417-22.

67.   Nagle JF, Tristram-Nagle S. Lipid bilayer structure. Curr Opin Struct Biol. 2000;10(4):474-80.

68.   Shevchenko A, Simons K. Lipidomics: coming to grips with lipid diversity. Nat Rev Mol Cell Biol. 2010;11(8):593-8.

69.   Gitler C. Plasticity of biological membranes. Annu Rev Biophys Bioeng. 1972;1:51-92.

70.   Fahy E, Subramaniam S, Brown HA, Glass CK, Merrill AH, Jr., Murphy RC, et al. A comprehensive classification system for lipids. J Lipid Res. 2005;46(5):839-61.

71.   Olsen ASB, Faergeman NJ. Sphingolipids: membrane microdomains in brain development, function and neurological diseases. Open Biol. 2017;7(5).

72.   Grouleff J, Irudayam SJ, Skeby KK, Schiott B. The influence of cholesterol on membrane protein structure, function, and dynamics studied by molecular dynamics simulations. Biochim Biophys Acta. 2015;1848(9):1783-95.

73.   van Meer G, Voelker DR, Feigenson GW. Membrane lipids: where they are and how they behave. Nat Rev Mol Cell Biol. 2008;9(2):112-24.

74.   van Meer G. Dynamic transbilayer lipid asymmetry. Cold Spring Harb Perspect Biol. 2011;3(5).

75.   Marquardt D, Geier B, Pabst G. Asymmetric lipid membranes: towards more realistic model systems. Membranes (Basel). 2015;5(2):180-96.

76.   Nicolson GL. The Fluid-Mosaic Model of Membrane Structure: still relevant to understanding the structure, function and dynamics of biological membranes after more than 40 years. Biochim Biophys Acta. 2014;1838(6):1451-66.

77.   Nguyen MHL, Rickeard BW, DiPasquale M, Marquardt D. Asymmetric Model Membranes: Frontiers and Challenges.   Biomimetic Lipid Membranes: Fundamentals, Applications, and Commercialization2019. p. 47-71.

78.   Freeman MR, Di Vizio D, Solomon KR. The Rafts of the Medusa: cholesterol targeting in cancer therapy. Oncogene. 2010;29(26):3745-7.

79.   Yao J, Ho D, Calingasan NY, Pipalia NH, Lin MT, Beal MF. Neuroprotection by cyclodextrin in cell and mouse models of Alzheimer disease. J Exp Med. 2012;209(13):2501-13.

80.   Mendis LH, Grey AC, Faull RL, Curtis MA. Hippocampal lipid differences in Alzheimer's disease: a human brain study using matrix-assisted laser desorption/ionization-imaging mass spectrometry. Brain Behav. 2016;6(10):e00517.

81.   Martín V, Fabelo N, Santpere G, Puig B, Marín R, Ferrer I, et al. Lipid alterations in lipid rafts from Alzheimer's disease human brain cortex. J Alzheimers Dis. 2010;19(2):489-502.

82.   Fabelo N, Martin V, Santpere G, Marin R, Torrent L, Ferrer I, et al. Severe alterations in lipid composition of frontal cortex lipid rafts from Parkinson's disease and incidental Parkinson's disease. Mol Med. 2011;17(9-10):1107-18.

83.   Fabelo N, Martin V, Marin R, Moreno D, Ferrer I, Diaz M. Altered lipid composition in cortical lipid rafts occurs at early stages of sporadic Alzheimer's disease and facilitates APP/BACE1 interactions. Neurobiol Aging. 2014;35(8):1801-12.

84.   Dawaliby R, Trubbia C, Delporte C, Masureel M, Van Antwerpen P, Kobilka BK, et al. Allosteric regulation of G protein-coupled receptor activity by phospholipids. Nat Chem Biol. 2016;12(1):35-9.

85.   Mahmood I, Liu X, Neya S, Hoshino T. Influence of lipid composition on the structural stability of g-protein coupled receptor. Chem Pharm Bull (Tokyo). 2013;61(4):426-37.

86.   Oates J, Watts A. Uncovering the intimate relationship between lipids, cholesterol and GPCR activation. Curr Opin Struct Biol. 2011;21(6):802-7.

87.   Morra G, Razavi AM, Pandey K, Weinstein H, Menon AK, Khelashvili G. Mechanisms of Lipid Scrambling by the G Protein-Coupled Receptor Opsin. Structure. 2018;26(2):356-67 e3.

88.   Hamm HE. How activated receptors couple to G proteins. Proc Natl Acad Sci U S A. 2001;98(9):4819-21.

89.   Rasmussen SG, Choi HJ, Rosenbaum DM, Kobilka TS, Thian FS, Edwards PC, et al. Crystal structure of the human beta2 adrenergic G-protein-coupled receptor. Nature. 2007;450(7168):383-7.

90.   Stansfeld PJ, Jefferys EE, Sansom MS. Multiscale simulations reveal conserved patterns of lipid interactions with aquaporins. Structure. 2013;21(5):810-9.

91.   Zhang D, Zhao Q, Wu B. Structural Studies of G Protein-Coupled Receptors. Mol Cells. 2015;38(10):836-42.

92.   Andersen OS, Koeppe RE, 2nd. Bilayer thickness and membrane protein function: an energetic perspective. Annu Rev Biophys Biomol Struct. 2007;36:107-30.

93.   Hollingsworth SA, Dror RO. Molecular Dynamics Simulation for All. Neuron. 2018;99(6):1129-43.

94.   Karplus M, McCammon JA. Molecular dynamics simulations of biomolecules. Nat Struct Biol. 2002;9(9):646-52.

95.   Lee EH, Hsin J, Sotomayor M, Comellas G, Schulten K. Discovery through the computational microscope. Structure. 2009;17(10):1295-306.

96.   Alder BJ, Wainwright TE. Phase Transition for a Hard Sphere System. The Journal of Chemical Physics. 1957;27(5):1208-9.

97.   Mori T, Miyashita N, Im W, Feig M, Sugita Y. Molecular dynamics simulations of biological membranes and membrane proteins using enhanced conformational sampling algorithms. Biochim Biophys Acta. 2016;1858(7 Pt B):1635-51.

98.   Stansfeld PJ, Sansom MS. Molecular simulation approaches to membrane proteins. Structure. 2011;19(11):1562-72.

99.   Dror RO, Dirks RM, Grossman JP, Xu H, Shaw DE. Biomolecular simulation: a computational microscope for molecular biology. Annu Rev Biophys. 2012;41(1):429-52.

100.   Cournia Z, Allen TW, Andricioaei I, Antonny B, Baum D, Brannigan G, et al. Membrane Protein Structure, Function, and Dynamics: a Perspective from Experiments and Theory. J Membr Biol. 2015;248(4):611-40.

101.   Monticelli L, Tieleman DP. Force fields for classical molecular dynamics. Methods Mol Biol. 2013;924:197-213.

102.   Cornell WD, Cieplak P, Bayly CI, Gould IR, Merz KM, Ferguson DM, et al. A Second Generation Force Field for the Simulation of Proteins, Nucleic Acids, and Organic Molecules. J Am Chem Soc. 1995;117(19):5179-97.

103.   MacKerell AD, Bashford D, Bellott M, Dunbrack RL, Evanseck JD, Field MJ, et al. All-atom empirical potential for molecular modeling and dynamics studies of proteins. J Phys Chem B. 1998;102(18):3586-616.

104.   Huang J, MacKerell AD, Jr. CHARMM36 all-atom additive protein force field: validation based on comparison to NMR data. J Comput Chem. 2013;34(25):2135-45.

105.   Oostenbrink C, Villa A, Mark AE, van Gunsteren WF. A biomolecular force field based on the free enthalpy of hydration and solvation: the GROMOS force-field parameter sets 53A5 and 53A6. J Comput Chem. 2004;25(13):1656-76.

106.   Jorgensen WL, Tirado-Rives J. The OPLS [optimized potentials for liquid simulations] potential functions for proteins, energy minimizations for crystals of cyclic peptides and crambin. J Am Chem Soc. 1988;110(6):1657-66.

107.   Verlet L. Computer "Experiments" on Classical Fluids. I. Thermodynamical Properties of Lennard-Jones Molecules. Physical Review. 1967;159(1):98-103.

108.   Mazur AK. Common Molecular Dynamics Algorithms Revisited: Accuracy and Optimal Time Steps of Störmer–Leapfrog Integrators. Journal of Computational Physics. 1997;136(2):354-65.

109.   Grest GS, Kremer K. Molecular dynamics simulation for polymers in the presence of a heat bath. Phys Rev A Gen Phys. 1986;33(5):3628-31.

110.   Hoover WG. Canonical dynamics: Equilibrium phase-space distributions. Phys Rev A Gen Phys. 1985;31(3):1695-7.

111.   Berendsen HJC, Postma JPM, van Gunsteren WF, DiNola A, Haak JR. Molecular dynamics with coupling to an external bath. The Journal of Chemical Physics. 1984;81(8):3684-90.

112.   Harvey MJ, Giupponi G, Fabritiis GD. ACEMD: Accelerating Biomolecular Dynamics in the Microsecond Time Scale. J Chem Theory Comput. 2009;5(6):1632-9.

113.   Klauda JB, Venable RM, Freites JA, O'Connor JW, Tobias DJ, Mondragon-Ramirez C, et al. Update of the CHARMM all-atom additive force field for lipids: validation on six lipid types. J Phys Chem B. 2010;114(23):7830-43.

114.   Jambeck JP, Lyubartsev AP. An Extension and Further Validation of an All-Atomistic Force Field for Biological Membranes. J Chem Theory Comput. 2012;8(8):2938-48.

115.   Dickson CJ, Madej BD, Skjevik AA, Betz RM, Teigen K, Gould IR, et al. Lipid14: The Amber Lipid Force Field. J Chem Theory Comput. 2014;10(2):865-79.

116.   Saiz L, Klein ML. Computer simulation studies of model biological membranes. Acc Chem Res. 2002;35(6):482-9.

117.   Marrink SJ, Risselada HJ, Yefimov S, Tieleman DP, de Vries AH. The MARTINI force field: coarse grained model for biomolecular simulations. J Phys Chem B. 2007;111(27):7812-24.

118.   Shi Q, Izvekov S, Voth GA. Mixed atomistic and coarse-grained molecular dynamics: simulation of a membrane-bound ion channel. J Phys Chem B. 2006;110(31):15045-8.

119.   Wan C-K, Han W, Wu Y-D. Parameterization of PACE Force Field for Membrane Environment and Simulation of Helical Peptides and Helix–Helix Association. J Chem Theory Comput. 2011;8(1):300-13.

120.   Kar P, Gopal SM, Cheng Y-M, Panahi A, Feig M. Transferring the PRIMO Coarse-Grained Force Field to the Membrane Environment: Simulations of Membrane Proteins and Helix–Helix Association. J Chem Theory Comput. 2014;10(8):3459-72.

121.   Deupi X, Kobilka BK. Energy landscapes as a tool to integrate GPCR structure, dynamics, and function. Physiology (Bethesda). 2010;25(5):293-303.

122.   Deganutti G, Moro S, Reynolds CA. Peeking at G-protein-coupled receptors through the molecular dynamics keyhole. Future Med Chem. 2019;11(6):599-615.

123.   Ward MD, Nangia S, May ER. Evaluation of the hybrid resolution PACE model for the study of folding, insertion, and pore formation of membrane associated peptides. J Comput Chem. 2017;38(16):1462-71.

124.   Buch I, Harvey MJ, Giorgino T, Anderson DP, De Fabritiis G. High-throughput all-atom molecular dynamics simulations using distributed computing. J Chem Inf Model. 2010;50(3):397-403.

125.   Harvey MJ, De Fabritiis G. High-throughput molecular dynamics: the powerful new tool for drug discovery. Drug Discov Today. 2012;17(19-20):1059-62.

126.   Sengupta D, Prasanna X, Mohole M, Chattopadhyay A. Exploring GPCR-Lipid Interactions by Molecular Dynamics Simulations: Excitements, Challenges, and the Way Forward. J Phys Chem B. 2018;122(22):5727-37.

127.   Hauser AS, Attwood MM, Rask-Andersen M, Schioth HB, Gloriam DE. Trends in GPCR drug discovery: new agents, targets and indications. Nature reviews Drug discovery. 2017;16(12):829-42.

128. Candia M, Kratzer B, Pickl WF. On Peptides and Altered Peptide Ligands: From Origin, Mode of Action and Design to Clinical Application (Immunotherapy). Int Arch Allergy Immunol. 2016;170(4):211-33.

129. Giupponi G, Harvey MJ, De Fabritiis G. The impact of accelerator processors for high-throughput molecular modeling and simulation. Drug Discov Today. 2008;13(23-24):1052-8.

130. Bai Q, Perez-Sanchez H, Zhang Y, Shao Y, Shi D, Liu H, et al. Ligand induced change of beta2 adrenergic receptor from active to inactive conformation and its implication for the closed/open state of the water channel: insight from molecular dynamics simulation, free energy calculation and Markov state model analysis. Phys Chem Chem Phys. 2014;16(30):15874-85.

131. Ranganathan A, Dror RO, Carlsson J. Insights into the role of Asp79(2.50) in beta2 adrenergic receptor activation from molecular dynamics simulations. Biochemistry. 2014;53(46):7283-96.

132. Ozcan O, Uyar A, Doruker P, Akten ED. Effect of intracellular loop 3 on intrinsic dynamics of human beta2-adrenergic receptor. BMC Struct Biol. 2013;13:29.

133. Bai Q, Zhang Y, Ban Y, Liu H, Yao X. Computational study on the different ligands induced conformation change of beta2 adrenergic receptor-Gs protein complex. PLoS One. 2013;8(7):e68138.

134. Ozgur C, Doruker P, Akten ED. Investigation of allosteric coupling in human beta2-adrenergic receptor in the presence of intracellular loop 3. BMC Struct Biol. 2016;16(1):9.

135. Dickson CJ, Hornak V, Velez-Vega C, McKay DJ, Reilly J, Sandham DA, et al. Uncoupling the Structure-Activity Relationships of beta2 Adrenergic Receptor Ligands from Membrane Binding. Journal of medicinal chemistry. 2016;59(12):5780-9.

136. Plazinska A, Plazinski W, Jozwiak K. Agonist binding by the beta2-adrenergic receptor: an effect of receptor conformation on ligand association-dissociation characteristics. Eur Biophys J. 2015;44(3):149-63.

137. Dror RO, Pan AC, Arlow DH, Borhani DW, Maragakis P, Shan Y, et al. Pathway and mechanism of drug binding to G-protein-coupled receptors. Proc Natl Acad Sci U S A. 2011;108(32):13118-23.

138. Manna M, Niemela M, Tynkkynen J, Javanainen M, Kulig W, Muller DJ, et al. Mechanism of allosteric regulation of beta2-adrenergic receptor by cholesterol. Elife. 2016;5:e18432.

139. Chan HC, Filipek S, Yuan S. The Principles of Ligand Specificity on beta-2-adrenergic receptor. Sci Rep. 2016;6:34736.

140. Tikhonova IG, Selvam B, Ivetac A, Wereszczynski J, McCammon JA. Simulations of biased agonists in the beta(2) adrenergic receptor with accelerated molecular dynamics. Biochemistry. 2013;52(33):5593-603.

141. Sun X, Agren H, Tu Y. Microsecond Molecular Dynamics Simulations Provide Insight into the Allosteric Mechanism of the Gs Protein Uncoupling from the beta2 Adrenergic Receptor. J Phys Chem B. 2014;118(51):14737-44.

142. Dror RO, Arlow DH, Borhani DW, Jensen MO, Piana S, Shaw DE. Identification of two distinct inactive conformations of the beta2-adrenergic receptor reconciles structural and biochemical observations. Proc Natl Acad Sci U S A. 2009;106(12):4689-94.

143. Neale C, Herce HD, Pomes R, Garcia AE. Can Specific Protein-Lipid Interactions Stabilize an Active State of the Beta 2 Adrenergic Receptor? Biophys J. 2015;109(8):1652-62.

144. Li J, Jonsson AL, Beuming T, Shelley JC, Voth GA. Ligand-dependent activation and deactivation of the human adenosine A(2A) receptor. J Am Chem Soc. 2013;135(23):8749-59.

145. Rodriguez D, Pineiro A, Gutierrez-De-Teran H. Molecular dynamics simulations reveal insights into key structural elements of adenosine receptors. Biochemistry. 2011;50(19):4194-208.

146. Lyman E, Higgs C, Kim B, Lupyan D, Shelley JC, Farid R, et al. A role for a specific cholesterol interaction in stabilizing the Apo configuration of the human A(2A) adenosine receptor. Structure. 2009;17(12):1660-8.

147. Lee JY, Lyman E. Agonist dynamics and conformational selection during microsecond simulations of the A(2A) adenosine receptor. Biophys J. 2012;102(9):2114-20.

148.   Lovera S, Cuzzolin A, Kelm S, De Fabritiis G, Sands ZA. Reconstruction of apo A2A receptor activation pathways reveal ligand-competent intermediates and state-dependent cholesterol hotspots. Sci Rep. 2019;9(1):14199.

149.   Manglik A, Kim Tae H, Masureel M, Altenbach C, Yang Z, Hilger D, et al. Structural Insights into the Dynamic Process of β2-Adrenergic Receptor Signaling. Cell. 2015;162(6):1431.

150.   Prosser RS, Ye L, Pandey A, Orazietti A. Activation processes in ligand-activated G protein-coupled receptors: A case study of the adenosine A2A receptor. Bioessays. 2017;39(9).

151.   Ye L, Van Eps N, Zimmer M, Ernst OP, Prosser RS. Activation of the A2A adenosine G-protein-coupled receptor by conformational selection. Nature. 2016;533(7602):265-8.

152.   Miao Y, Nichols SE, Gasper PM, Metzger VT, McCammon JA. Activation and dynamic network of the M2 muscarinic receptor. Proceedings of the National Academy of Sciences of the United States of America. 2013;110(27):10982-7.

153.   Kim TH, Chung KY, Manglik A, Hansen AL, Dror RO, Mildorf TJ, et al. The role of ligands on the equilibria between functional states of a G protein-coupled receptor. J Am Chem Soc. 2013;135(25):9465-74.

154.   Vanommeslaeghe K, Hatcher E, Acharya C, Kundu S, Zhong S, Shim J, et al. CHARMM general force field: A force field for drug-like molecules compatible with the CHARMM all-atom additive biological force fields. J Comput Chem. 2010;31(4):671-90.

155.   Mizumura T, Kondo K, Kurita M, Kofuku Y, Natsume M, Imai S, et al. Activation of adenosine A(2A) receptor by lipids from docosahexaenoic acid revealed by NMR. Sci Adv. 2020;6(12):eaay8544.

156.   Mancia F, Assur Z, Herman AG, Siegel R, Hendrickson WA. Ligand sensitivity in dimeric associations of the serotonin 5HT2c receptor. EMBO Rep. 2008;9(4):363-9.

157.   Dix AV, Moss SM, Phan K, Hoppe T, Paoletta S, Kozma E, et al. Programmable nanoscaffolds that control ligand display to a G-protein-coupled receptor in membranes to allow dissection of multivalent effects. J Am Chem Soc. 2014;136(35):12296-303.

7.   PUBLICATIONS

7.1. STRUCTURAL INSIGHTS INTO POSITIVE AND NEGATIVE ALLOSTERIC REGULATION OF A G PROTEIN-COUPLED RECEPTOR THROUGH PROTEIN-LIPID INTERACTIONS

SCIENTIFIC REP⚙RTS

OPEN

Structural insights into positive and negative allosteric regulation of a G protein-coupled receptor through protein-lipid interactions

Agustín Bruzzese[1,2], Carles Gil[3], James A. R. Dalton [1,2] & Jesús Giraldo[1,2]

Lipids are becoming known as essential allosteric modulators of G protein-coupled receptor (GPCRs). However, how they exert their effects on GPCR conformation at the atomic level is still unclear. In light of recent experimental data, we have performed several long-timescale molecular dynamics (MD) simulations, totalling 24 μs, to rigorously map allosteric modulation and conformational changes in the β_2 adrenergic receptor (β2AR) that occur as a result of interactions with three different phospholipids. In particular, we identify different sequential mechanisms behind receptor activation and deactivation, respectively, mediated by specific lipid interactions with key receptor regions. We show that net negatively charged lipids stabilize an active-like state of β2AR that is able to dock $G_s\alpha$ protein. Clustering of anionic lipids around the receptor with local distortion of membrane thickness is also apparent. On the other hand, net-neutral zwitterionic lipids inactivate the receptor, generating either fully inactive or intermediate states, with kinetics depending on lipid headgroup charge distribution and hydrophobicity. These chemical differences alter membrane thickness and density, which differentially destabilize the β2AR active state through lateral compression effects.

G protein-coupled receptors (GPCRs) are implicated in the regulation of many physiological and pathological processes[1]. For this reason, GPCRs are a major target of current marketed drugs[2]. GPCRs are seven-helix trans-membrane domain (7TM) receptors that reside in and signal through the lipid membrane of the cell[1]. From an atomistic perspective, GPCRs are flexible proteins that fluctuate between several conformations that can be broadly grouped into inactive, active and intermediate states, and which can be modulated by ligands[3]. The transitions between different conformations, for instance from active to inactive state, can occur along time scales of nanoseconds to milliseconds[4,5]. However, it is still unclear how exactly ligand binding induces (or selects for) receptor activation and elicits efficient signal transduction[3,4,6,7]. In addition to modulation by ligands, phospholipids have been shown to alter the activity of certain proteins by interacting with transmembrane helices, for example in sarcoplasmic reticulum Ca^{2+}-ATPase, large-conductance mechanosensitive channel MscL, multidrug transporter LmrP, and rhodopsin[8,9]. These effects have typically been shown to be mediated by H-bond formation (or lack thereof) between the protein and phospholipid headgroups[8]. In addition, interactions with cholesterol have been shown to be important for GPCRs, e.g. influencing ionic-lock formation in A2A adenosine receptor[10] and thermal stability of β_2 adrenergic receptor (β2AR)[11].

Molecular dynamics (MD) is a suitable computational technique for studying GPCR flexibility in its membrane environment. MD simulations at atomic resolution can give information on specific molecular processes, including interactions of proteins with lipids, receptor-ligand binding, and receptor conformational change[12]. Recent X-ray crystal structures of β2AR have provided high-resolution insights into two major conformations associated with GPCR function: an inactive inverse agonist-bound state[13] and an active state in complex with an agonist and G_s protein[14]. These crystal structures constitute a reference point for comparison between active and inactive states (see SI Figs 1 and 2). Moreover, the β2AR is widely expressed throughout the body and can adopt

[1]Laboratory of Molecular Neuropharmacology and Bioinformatics, Institut de Neurociències and Unitat de Bioestadística, Universitat Autònoma de Barcelona, 08193 Bellaterra, Spain. [2]Network Biomedical Research Centre on Mental Health (CIBERSAM), 08193 Bellaterra, Spain. [3]Department of Biochemistry and Molecular Biology, Institut de Neurociències, Universitat Autònoma de Barcelona, 08193 Bellaterra, Spain. Correspondence and requests for materials should be addressed to J.A.R.D. (email: james.dalton@uab.es) or J.G. (email: jesus.giraldo@uab.es)
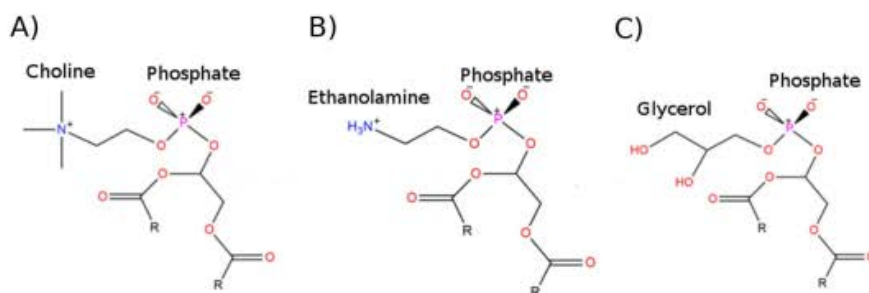
50

Figure 1. Structural comparison of DOPC, DOPE and DOPG unsaturated lipids. DOPC (**A**) contains two fatty-acid chains of 18 carbons each (R) and its headgroup, which is composed of a positively-charged choline group bound to the phosphate group. DOPE (**B**) contains identical fatty-acid chains but its headgroup is composed of a positively-charged ethanolamine group bound to the phosphate group. DOPG (**C**) contains identical fatty-acid chains but its headgroup is composed of a neutral glycerol group bound to the phosphate group.

highly diverse conformations with each of them having particular signalling patterns[15]. As such, this receptor constitutes an ideal paradigmatic system for the structural exploration of its (in)activation, both by theoretical and experimental approaches[4,16–19]. From a structure-function perspective, by comparing the active and inactive crystal structures, some authors have emphasized the importance of the rearrangement of transmembrane (TM) helices 5, 6 and 7 in transmitting the signal through the membrane[3–5,20,21]. Further research in this area may include the mechanisms underlying the transitions and fluctuations of β2AR amongst its many conformational states.

Several MD simulation studies of β2AR, initialized from its various crystal structures, have been performed before e.g.[4,5,15,16,18,22–33]. Although precise methodological protocols differ, most of these MD simulations share a common theme. By way of summary, the majority do not include intracellular loop 3 (ICL3) of β2AR[4,5,16,18,22,26–28,30–33], which is missing in β2AR crystal structures[11,13,14,34–41] and therefore requires explicit modelling. When the active receptor state(s) is simulated, co-crystallized molecules such as G_s protein or nanobody are usually first removed[4,22,29,31,32]. In addition, most simulations of β2AR are performed within a homogeneous membrane consisting of 1-palmitoyl-2-oleoyl-sn-glycero-3-phosphocholine (POPC) lipids[4,5,16,18,22–28,30–33]. This is due to the relative abundance of this particular phospholipid in healthy mammalian membranes[42]. Noteworthy, MD simulations of β2AR carried out from the inactive state crystal structure suggest that within this state exist two conformations that are in equilibrium: an inactive (broken ionic-lock) and a very-inactive (closed ionic-lock)[15]. On the other hand, MD simulations starting from the active crystal structure in a POPC membrane (without bound G protein or nanobody) usually result in the spontaneous deactivation of the receptor, even with an agonist bound[4]. This suggests that the preferred state of β2AR under normal conditions is the inactive, with TM6 fluctuating between a set of inward orientations (representing very inactive, inactive or intermediate), and only adopting an active state with an outward TM6 when a G protein is bound[3,5,17]. However, these observations may be influenced by the absence of ICL3 (which connects TM5 and TM6) in some of these MD simulations. Indeed, in recent MD studies which did include ICL3, receptor behaviour was found to be altered because of noticeable allosteric effects[23,25]. Likewise, experimental data suggests ICL3 is important for the spontaneous activation of β2AR[43]. Interestingly, recent data gathered in a β2AR ligand binding study suggests that protein and membrane interplay improves the interaction between protein and ligand and could be important for drug development[26].

In a related experimental study using artificial nanodiscs, the phospholipids 1,2-dioleoyl-sn-glycero-3-phosphoglycerol (DOPG) and 1,2-dioleoyl-sn-glycero-3-phospho-ethanolamine (DOPE) were shown to be strong allosteric modulators of β2AR, stabilizing and destabilizing the active receptor state, respectively[44]. Furthermore, 1,2-dioleoyl-sn-glycero-3-phosphocholine (DOPC), a close relative of POPC, does not favour either active or inactive states and instead allows the receptor to explore different conformations without particular preference[44]. The differences between these three phospholipids lie in the electrostatic charges of their headgroups as all contain the same unsaturated fatty acid chains (two chains of 18 carbons each). Both DOPC (Fig. 1A) and DOPE (Fig. 1B) contain a positively charged headgroup which, in combination with the negatively charged phosphate group, yields a dipole with net neutral charge. The main difference between them is that DOPC has three methyl groups connected to its headgroup nitrogen atom while DOPE has three hydrogens. This makes the DOPC headgroup more hydrophobic, while the corresponding hydrogens in DOPE are free to make ionic/H-bond interactions with other molecules. Other authors have suggested that DOPE and DOPC have different orientations in the membrane due to different intermolecular interactions between P-N groups[45–47]. Unlike the other two, DOPG (Fig. 1C) has a neutral headgroup with two polar hydroxyls which, in combination with the negatively charged phosphate group, yields a net negatively charged phospholipid.

Lipid characterizations of human tissue show that dioleoyl (DO) fatty acid chains are abundant in membranes[48]. Although DOPG lipids specifically have low biological expression (<2%[44]), it represents over >7% of all β2AR-bound phospholipids (>16% for PG lipids in general)[44], which possibly indicates enrichment in the vicinity of β2AR. As lipid composition can be affected by disease, as shown by membrane changes in the brains of Alzheimer's and Parkinson's patients[49–52], these effects could have a bearing on the activity of GPCRs

51

such as β2AR. Along this line of research, recently published MD simulations of β2AR inserted in a homogenous 1-palmitoyl-2-oleoyl-sn-glycero-3-phosphoglycerol (POPG) membrane has shown that a single anionic lipid is able to disrupt the receptor ionic lock[16], a typical feature of the inactive (or very-inactive) receptor state[15,16]. This occurs through formation of a salt-bridge between the lipid phosphate group and residue $R^{3.50}$ (Ballesteros-Weinstein numbering[53]) of the ionic-lock[16]. Thus, it suggests a possible mechanism by which net negatively charged phospholipids can potentially interact with positively charged residues located at the intracellular side of β2AR, thereby possibly contributing to the (de)stabilization of the (in)active receptor state.

Despite these findings, a structural explanation of both positive and negative allosteric regulation by phospholipids on β2AR activity remains unclear. To this aim, we focus on the allosteric effects of DOPG, DOPE, and DOPC phospholipids on the conformational changes of the active state of β2AR, including modelled ICL3, in unbiased atomistic long-timescale MD simulations. Specifically, we investigate from a structural point-of-view whether these different phospholipids can allosterically modulate β2AR in a reproducible fashion, either positively or negatively as suggested in analogous experiments[44], by acting on specific intracellular residues. From a more general perspective, our results potentially open new insights into how phospholipids might influence GPCR behaviour and signalling at a molecular level. In addition, the present study suggests that the choice of membrane lipid composition in computational MD simulations of GPCRs can significantly affect outcome.

Materials and Methods

β2AR modelling. The crystal structure of the active state of β2AR (PDB entry: 3SN6)[14] was selected. The G_s protein complex, nanobody, lysozyme-fusion protein, and co-crystallized agonist were removed from the structure. Mutated residues (T96, T98 and E187) were substituted by native ones (M96, M98 and N187) in order to obtain a *wt* receptor sequence. The crystallographic-missing extracellular loop 2 (ECL2) was completed by homology modelling to the corresponding region of the inactive crystal structure of β2AR (PDB entry: 2RH1)[15] using MODELLER v9.14[54]. Intracellular loop 3 (ICL3) was confirmed using secondary structure prediction tools, Jpred[55] and PSIpred[56] (residues 238 to 262) and then modelled using MODELLER. The complete receptor was then energy-minimized in the AMBER-14SB force-field[57] with CHIMERA[58].

Molecular dynamics (MD) simulations. Three all-atom MD systems were constructed, consisting of β2AR in active state (as described above) in three homogeneous membranes: DOPG, DOPE and DOPC (Fig. 1), respectively, using CHARMM-GUI[59]. Each receptor-membrane system was solvated with TIP3P water molecules above and below the membrane, with a concentration of 0.3 M KCl for zero system net charge. On the protein, six residues were protonated according to previously published MD simulation protocols specific for β2AR, as well as being consistent with protocols used for other homologous Class A GPCRs[4,22,60]: $D79^{2.50}$, $E122^{3.41}$, $D130^{3.49}$, $D234^{5.73}$, $E237^{5.76}$ and $E268^{6.30}$ (Ballesteros-Weinstein numbering[53] as superscript). MD simulations were performed using the CHARMM36 force field[61] and ACEMD software[62]. Briefly, each receptor-membrane system was equilibrated for 28 ns at 300 K and 1 atmosphere. During the initial 8 ns of equilibration, the protein was harmonically restrained and progressively released over 2 ns steps. During the final 20 ns of equilibration, no restraints were applied. For each receptor-membrane system a production run of 4 μs was performed without restraints under the same conditions, with a second replicate simulation executed in each case to verify observations. This constitutes a total production simulation time of 24 μs.

MD simulation analysis. For each MD simulation trajectory, root mean square deviation (RMSD) measurements of the transmembrane (TM) domain (TM helices 1–7 plus helix 8), as well as TM6 or ICL3 by itself, were made with VMD software[63] v1.9.2 in order to evaluate protein conformational changes and stability of receptor state. The distance between the Cα atoms of ionic-lock residues $R131^{3.50}$ on TM3 and $E268^{6.30}$ on TM6 was used as an indication of proximity between these two helices. RMSD of the "triad core", named by Huang *et al.*[64], (all heavy atoms of residues: $I121^{3.40}$, $P211^{5.50}$ and $F282^{6.44}$) was used as an indicator of receptor state[4,65]. In order to assess membrane characteristics and protein-membrane interactions: i) the distance(s) between ionic-lock residue $R131^{3.50}$ (terminal nitrogen atoms) and closest lipid phosphate group (centre-of-mass) was measured with PLUMED[66]; (ii) membrane thickness calculated as average distance from lower to upper-leaflet phosphorus atoms, implementing default settings of MEMBPLUGIN[67] within VMD[63] over total simulation time; (iii) membrane density calculated across bilayer Z-axis using default settings of MEMBPLUGIN[67], analyzing mean mass of fatty acid chains and phosphate groups across whole membrane over total simulation time; (iv) area per lipid calculated by dividing total membrane area by total number of upper leaflet lipids (membrane area defined by its maximum X,Y dimensions minus cross-sectional area of protein in the same plane); (v) number of protein-lipid electrostatic interactions calculated every 4 ns between charged lipid atoms of inner-leaflet and charged protein TM6 atoms (counting all charged atom-atom pairs with distance <4.5 Å) using a custom-made script executed within VMD[63]; (vi) radial distribution function implemented twice with the Radial Pair Distribution plugin[68] within VMD[63]: firstly, *g(r)* of whole TM6 with respect to lower-leaflet lipid phosphate groups and secondly, *g(r)* of positively charged atoms of four lysine sidechains on intracellular side of TM6 ($K263^{6.25}$, $K267^{6.29}$, $K270^{6.32}$, $K273^{6.35}$, Ballesteros-Weinstein numbering[53] as superscript) and negatively charged oxygen atoms of lower-leaflet lipid phosphate groups. As a further validation of receptor state, the co-crystallized $G_s\alpha$ protein (PDB entry: 3SN6) was docked to the intracellular side of relevant MD-generated β2AR structures (as well as re-docked into the original active β2AR crystal structure, PDB entry: 3SN6, as a control). The Rosetta online server (ROSIE) was used for protein-protein docking[69] with the following protocol: (i) receptor conformation taken from the end of its respective 4 μs MD simulation and superimposed over the active crystal structure of β2AR containing its $G_s\alpha$ protein (PDB entry: 3SN6)[14] (ii) the original crystallized receptor removed from the complex, (iii) the structure of $G_s\alpha$ moved 3 Å away from the MD-generated receptor structure so that there are no steric clashes and clear space is apparent between both proteins, (iv) protein-protein docking is initiated. As ICL3 is long and potentially highly

flexible, it was removed prior to protein-protein docking (during step iii) so as not to create steric conflicts with $G_s\alpha$ during docking (ROSIE is not able to move backbone of loops during docking). However, all other loops and receptor structural elements were maintained. All analytical plots were generated using GNUplot[70] version 4.449.

Results

β2AR is one of the most studied and frequently crystallized Class A GPCRs. However, the structure of intracellular loop 3 (ICL3) that connects TM5 and TM6 is unknown because it is missing in all β2AR crystal structures. ICL3 has recently been shown to be potentially important in β2AR activity[23,25]. On this basis, we *ab initio* modelled ICL3 prior to performing MD simulations. As a result, β2AR contains 13 positively charged residues located at the intracellular ends of TM5, TM6, and ICL3 (SI Fig. 1), which have been suggested as important for G protein interaction[71]. β2AR has been crystallized in both active (G_s protein-bound, PDB entry: 3SN6)[14] and inactive (carazolol-bound, PDB entry: 2RH1)[13] states. Briefly, one of the most remarkable differences between them is the orientation of TM6. In the active state, an outward movement of ~14 Å is observed (SI Fig. 2). As a result, the ionic-lock ($R^{3.50}$ and $E^{6.30}$, with Ballesteros-Weinstein numbering[53] as superscript, which indicates relative residue position along each TM helix) reaches a distance of 18.9 Å in the active state but only 11.1 Å in the inactive (SI Fig. 2)[13,14]. Other features of the active state include a shortening of TM7 (below the conserved NPxxY motif[1]) where it connects with H8, and an ordered helical second intracellular loop (ICL2), which is disordered in the inactive state (SI Fig. 2)[13]. Mechanistically, the motion of three residues in the core of β2AR has been shown to be important in the receptor (de)activation process. These residues constitute the triad core: $I^{3.40}$, $P^{5.50}$ and $F^{6.44}$ (Ballesteros-Weinstein numbering[53] as superscript), with its packing rearrangement (SI Fig. 2) involved in the relative motions of TM3, TM5 and TM6, serving as a connector between extracellular and intracellular receptor regions[4,65]. In light of observations of relevant β2AR crystal structures, proposed ICL3 functionality[23], and experimental data that shows β2AR is strongly allosterically modulated by different phospholipids[44], we have investigated the sum of these effects by employing long-timescale MD simulations of the active state of apo β2AR (PDB entry: 3SN6)[14] in three different homogenous membranes consisting of lipids: DOPC, DOPE and DOPG, respectively. In order to quantify the respective modulation of receptor state by each lipid, six metrics were utilised: conformational re-arrangement of the triad core, ionic-lock distance changes, RMSD of total protein, ICL3, and TM6, as well as radial distribution $g(r)$ of TM6 with respect to lipids.

Lipid DOPC partially inactivates β2-adrenergic receptor. In a 4 µs MD simulation of β2AR in a homogenous membrane of DOPC, ICL3 shows high flexibility and transiently adopts different conformations during the first microsecond (SI Fig. 3). During this time, the loop does not interact with the membrane but gradually moves to an inward position, interacting with ICL2 on the intracellular side of the receptor, as well as intermittently with H8 (SI Fig. 3). From 1 µs onwards, β2AR maintains ICL3 in this inward conformation (SI Fig. 3). The conformational changes of ICL3 precede a change in the conformation of TM6, which occurs from 2 µs onwards. In an RMSD profile of TM6 with respect to the inactive-state crystal structure of β2AR (PDB entry: 2RH1), TM6 begins at 7.0 Å but decreases to 3.5–5.5 Å from 2 µs onwards, finishing at 4.7 Å (SI Fig. 4). This suggests that the receptor is gradually being deactivated (closer in conformation to the inactive state). However, over 4 µs, TM6 does not fully reach the conformation of the inactive crystal structure (PDB id: 2RH1) and ICL2 remains in its helical state (Fig. 2). This is despite the receptor containing certain features of the inactive crystal structure such as helical extension at the intracellular end of TM7 (Fig. 2). Likewise, conformational changes are also observed in the triad core, which maintains an active-like conformation of $I^{3.40}$, $P^{5.50}$ and $F^{6.44}$ until 3.5 µs (Fig. 3), at which point, the RMSD of $F^{6.44}$ increases to 4.6 Å, which resembles an inactive-like conformation. Supporting the partial inactivation of β2AR into an intermediate state, the ionic-lock distance gradually decreases to 11.1 Å over 4 µs (SI Fig. 5) and the TM domain reaches an RMSD of 3.4 Å compared to the inactive crystal structure (SI Fig. 6). In general terms, this tallies with the experimental results of Dawaliby *et al.*[44], which show that DOPC neither favours the active or inactive state of β2AR, but in effect here weakly destabilises the active[44]. Likewise, these results are supported by the computational results of Dror *et al.*[4] whose long-timescale MD simulations of β2AR in a POPC membrane also exhibited gradual inactivation. Although POPC is not the same as DOPC (POPC contains fatty-acid chains of 18 and 16 carbons, respectively), they both contain the same lipid headgroup and therefore at a chemical level the inter-lipid, water-lipid and protein-lipid interactions would be expected to be similar, which allows for comparison.

Lipid DOPE fully deactivates β2-adrenergic receptor. In a 4 µs MD simulation of β2AR in a homogenous DOPE membrane, like in DOPC, ICL3 shows high flexibility and adopts different conformations during the first 2 µs (SI Fig. 3). During this time, ICL3 does not interact with the membrane but does not reach a stable conformation either. Interestingly, the RMSD profile of TM6 shows faster conformational changes than in DOPC, decreasing from 7.0 Å to 1.9 Å within 1 µs, when comparing with the inactive crystal structure (SI Fig. 4). This suggests an almost instant destabilization of the active state and fast receptor deactivation. Indeed, at 1 µs, TM6 is observed to be in the full inactive conformation (Fig. 4, SI Fig. 4), which does not occur in the DOPC membrane and indicates that DOPE induces greater conformational change, particularly on TM6. In accordance with this inward movement of TM6, the ionic-lock distance also decreases, reaching 7.6 Å between $R^{3.50}$ and $E^{6.30}$ at 1 µs (SI Fig. 5). This is less than the distance of the "open" ionic-lock in the inactive crystal structure (PDB id: 2RH1) and is indicative of a "closed" ionic-lock, a common feature of fully inactive GPCR crystal structures[15]. Regarding the triad core, its RMSD profile reveals an initial perturbation of $P^{5.50}$ and $F^{6.44}$ in the first 0.5 µs and then a rapid packing rearrangement of these residues towards an inactive-like conformation at 1 µs (Fig. 5). Nevertheless, during this time, the receptor continues to have some active-like features on its intracellular side, such as helical ICL2 and shortened TM7. These continue until 2 µs, at which point they also transition into their inactive configurations (Fig. 4, SI Fig. 6). Like in DOPC, ICL3 adopts an inward orientation after 2 µs, interacting with ICL2
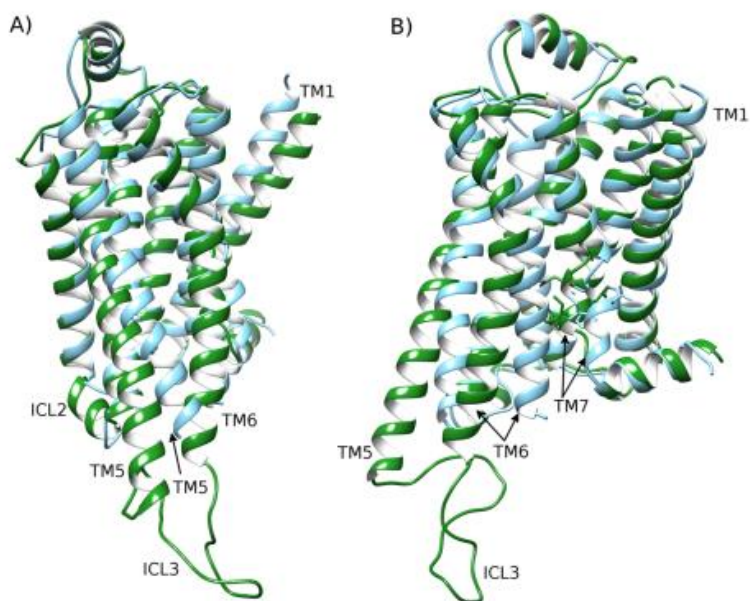
Figure 2. Partial inactivation of β_2AR in a DOPC membrane. Superposition of the inactive-state crystal structure of β_2AR (PDB id: 2RH1, blue) and an MD-generated conformation achieved after 4 μs within a DOPC membrane (green), showing a 90° rotation between (**A**) and (**B**) around the membrane plane. At the beginning of the MD simulation, β_2AR starts in its active crystal state (PDB id: 3SN6). Intracellular loops (ICL) 2 and 3, and transmembrane (TM) helices 5, 6 and 7 are labelled. Residues of the NPxxY motif on TM7 are displayed.
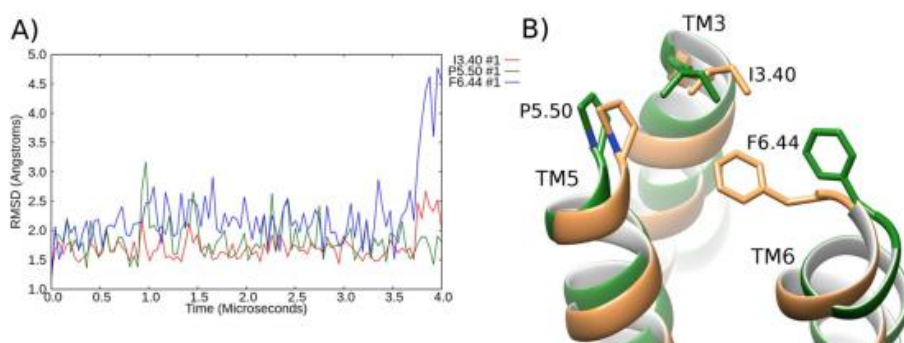

Figure 3. Partial inactivation of the triad core of $\beta2AR$ in a DOPC membrane. (**A**) RMSD profile of the conformational changes of the triad core: $I^{3.40}$ (red), $P^{5.50}$ (green) and $F^{6.44}$ (blue) over a 4 μs MD simulation in a DOPC membrane, compared to the active crystal structure (PDB id: 3SN6). (**B**) Superposition of the triad core observed at 4 μs compared to the active crystal structure triad core (orange, PDB id: 3SN6). Relevant residues are labelled: proline (P), isoleucine (I), phenylalanine (F) on transmembrane (TM) helices 3, 5, 6.

(Fig. 4, SI Fig. 3). However, its exact conformation is a little different as it is even more inward than in DOPC, corresponding with what has been previously described as a "very inactive" conformation[15] and remains mostly stable until the end of the simulation (SI Fig. 3). The receptor finally obtains a full complement of inactive-state features from 2.5 μs onwards, including a stable triad core (Fig. 5), closed ionic-lock (SI Fig. 5), inward TM6 (SI Fig. 4), disordered ICL2 and extended TM7 (Fig. 4), each of which is in agreement with the inactive-state crystal structure (PDB entry: 2RH1)[15]. In addition, each of these features is maintained until the end of the simulation. This suggests that DOPE membranes can induce and maintain deactivation of $\beta2AR$. Furthermore, this result has been duplicated in a second MD simulation, revealing the reproducibility of this DOPE-mediated deactivation of $\beta2AR$ (SI Figs 4–6). Overall, the TM domain transitions from the active state to fully inactive state, including disordered ICL2 and extended TM7 at the NYxxP motif, with an RMSD of 2.5 Å compared to the inactive crystal
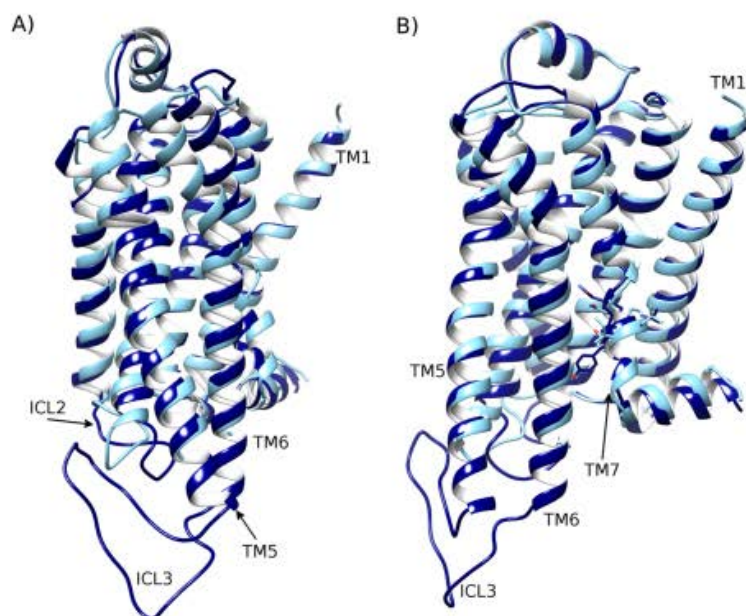
Figure 4. Full deactivation of β_2AR in a DOPE membrane. Superposition of the inactive crystal structure of β_2AR (PDB id: 2RH1, light blue) and the conformation of β_2AR (dark blue) achieved after a 4 μs MD simulation within a DOPE membrane, showing a 90° rotation between (**A**) and (**B**) around the membrane plane (extracellular-side: top, intracellular-side: bottom). Beginning from the active crystal structure (PDB id: 3SN6), the receptor reaches an inactive conformation (dark blue), with an almost identical arrangement with respect to the inactive crystal structure (light blue) of helices TM5, TM6, TM7 (residues of the NPxxY motif are displayed), and disordered intracellular loop 2 (ICL2).
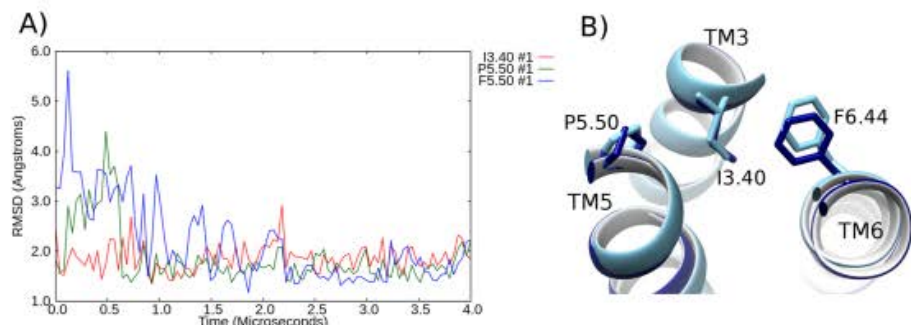

Figure 5. Full deactivation of the triad core of β_2AR in a DOPE membrane. (**A**) RMSD profile of the conformational changes of the triad core: $I^{3.40}$ (red), $P^{5.50}$ (green) and $F^{6.44}$ (blue) over a 4 μs MD simulation, compared to the inactive crystal structure of β_2AR (PDB id: 2RH1). In this instance, the MD simulation trajectory, which begins from the active state, is aligned to the inactive crystal structure of β_2AR (PDB id: 2RH1). (**B**) Superposition of the final triad core conformation achieved after 4 μs (dark blue) against the inactive crystal structure of β_2AR (light blue). Relevant residues are labelled: proline (P), isoleucine (I), phenylalanine (F) on transmembrane (TM) helices 3, 5, 6.

structure (SI Fig. 6). These observations are in general agreement with the experimental results of Dawaliby et al.[44], who show that DOPE strongly favours the inactive state of β2AR and destabilises the active[44].

Lipid DOPG stabilizes active-like state of β2-adrenergic receptor. In a 4 μs MD simulation of β2AR in a DOPG membrane, there is an initial rapid change in the conformation of ICL3, whose RMSD increases by 15 Å compared to its initial modelled state (in the active crystal structure of β2AR) within the first 0.1 μs (SI Fig. 8A). This is due to ICL3 adopting a more outward orientation (SI Fig. 8B), which begins to see it interacts with the DOPG membrane inner layer (Fig. 6, SI Fig. 7). After 0.3 μs, positively charged residues on ICL3 make
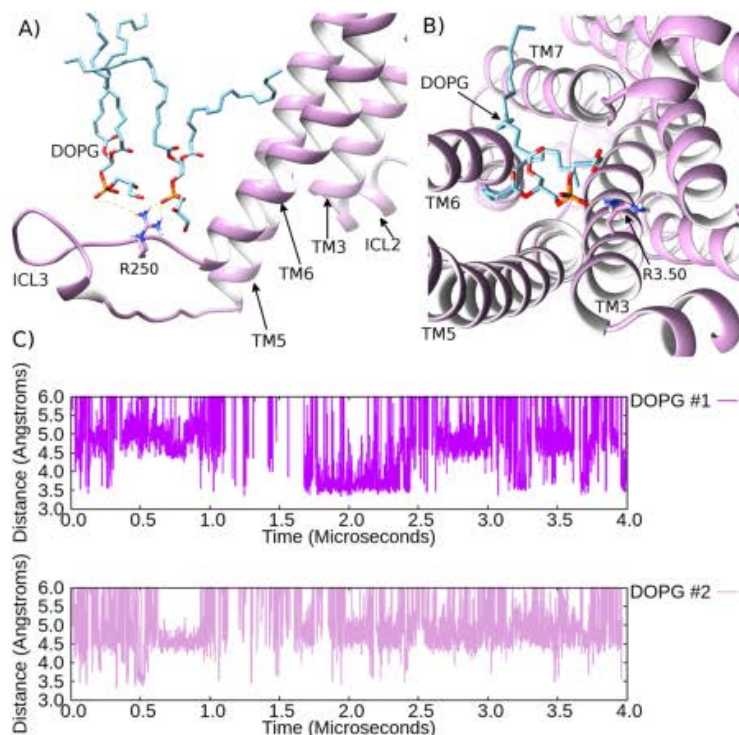
55

Figure 6. Stabilization of an active-like state of β_2AR by protein-lipid allosteric interactions. (**A**) An example of DOPG-ICL3/R250 ionic interaction at 4 μs in an MD simulation of β_2AR (light magenta) within a DOPG (light blue) membrane. (**B**) Intracellular view of β_2AR (light magenta) where ionic-lock residue $R^{3.50}$ interacts with a DOPG lipid, which protrudes between TM6 and TM7. (**C**) Protein-lipid interactions over time between $R^{3.50}$ and lipid phosphate groups in two MD simulations of β_2AR embedded in a DOPG membrane (DOPG #1 and DOPG #2, respectively).

close interactions with the neutral headgroups and negatively charged phosphate groups of DOPG lipids (for example, Fig. 6A and SI Fig. 7). These protein-lipid interactions are primarily mediated by R250, and to a lesser extent R253 and H256 (SI Fig. 7). This set of ICL3-DOPG interactions is observed throughout the entirety of 4 μs, exclusively maintaining ICL3 in an outward orientation (with an RMSD of 15–20 Å, SI Fig. 8A). In addition to the influences of ICL3, TM6 appears to be stabilized in its outward conformation by residues located near its N-terminus, such as $H269^{6.31}$, $K270^{6.32}$ and $K273^{6.35}$ (Ballesteros-Weinstein numbering[53] as superscript, SI Fig. 7), which are observed to interact with phosphate groups of DOPG lipids, presumably providing an outward pull on the helix. Over 4 μs of the simulation, the RMSD of TM6 is 2.0–5.0 Å (compared to the active crystal structure, SI Fig. 9), finishing at 4.3 Å, which is similar to its starting conformation, although slightly more outward (Fig. 7). This may be a consequence of the numerous interactions between ICL3 and TM6 with the membrane, as well as no bound agonist. However, during 1–2 μs, TM6 adopts an almost identical conformation to the active crystal structure with an RMSD of 2.0–3.4 Å (SI Fig. 9), which shows this conformation is also relatively stable. As a result of TM6 and ICL3 maintaining outward orientations, the ionic-lock remains open with a distance of 15–21 Å (SI Fig. 5). This is in agreement with the active-state crystal structure of β2AR[14]. Interestingly, in a previous study, the intrusion of a POPG lipid (a chemically close relative of DOPG, containing an identical lipid headgroup) was observed to occur between TM6 and TM7 of β2AR in its active state[16]. This POPG lipid was specifically observed to interact with $R^{3.50}$ on TM3 (an ionic-lock residue) via a protein-lipid salt-bridge[16]. We can confirm that in addition to the ionic interactions we observe between DOPG lipids and residues on ICL3/TM6, we also observe this extra interaction between $R^{3.50}$ and a DOPG lipid in our MD simulations. Specifically, this interaction is formed between $R^{3.50}$ and the headgroup/phosphate group of a single DOPG lipid bound between TM6 and TM7 at the intracellular side of β2AR (Fig. 6), and appears to assist in maintaining TM6 in an outward orientation. Furthermore, this interaction forms very quickly (within the first few hundred nanoseconds of the simulation) and remains mostly stable over 4 μs, albeit with some fluctuations (Fig. 6). It is also only observed here in a DOPG membrane. Regarding the triad core of β2AR in DOPG, residues $I^{3.40}$, $P^{5.50}$, and $F^{6.44}$ maintain their same rotameric states as observed in the active crystal structure, exhibiting RMSDs of 1.5, 1.0, and 2.4 Å, respectively (Fig. 8).

As a consequence of the previously mentioned protein-lipid interactions and subsequent stabilization of the triad core in an active-like state, the TM domain is observed to remain in an active-like state over 4 μs, including
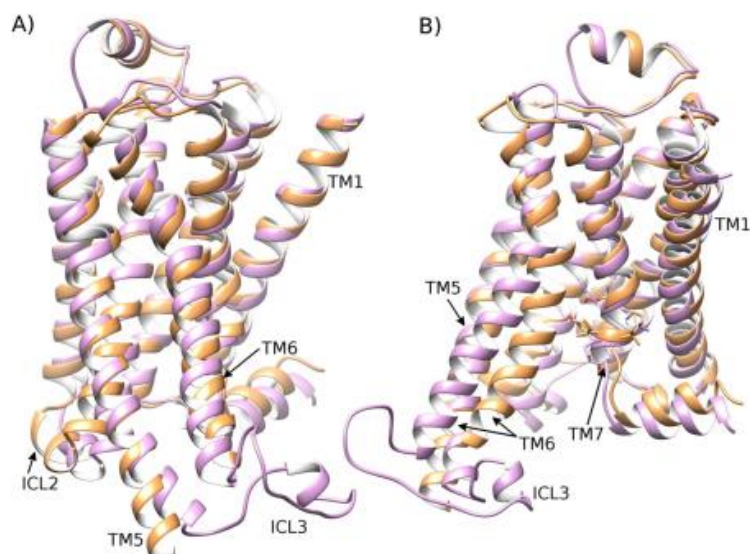
56

Figure 7. Stabilization of an active-like state of β_2AR in a DOPG membrane. Comparison of the active-state crystal structure (PDB id: 3SN6) of β_2AR (orange) and a receptor conformation (light magenta) achieved after $4\,\mu s$ of an MD simulation within a DOPG membrane, showing 90° rotation between (**A**) and (**B**) around the membrane plane (extracellular-side: top, intracellular-side: bottom). Residues of the NPxxY motif on TM7 are displayed. Due to electrostatic interactions between ICL3/TM6 and the membrane, an active-like state of β_2AR is stabilized.
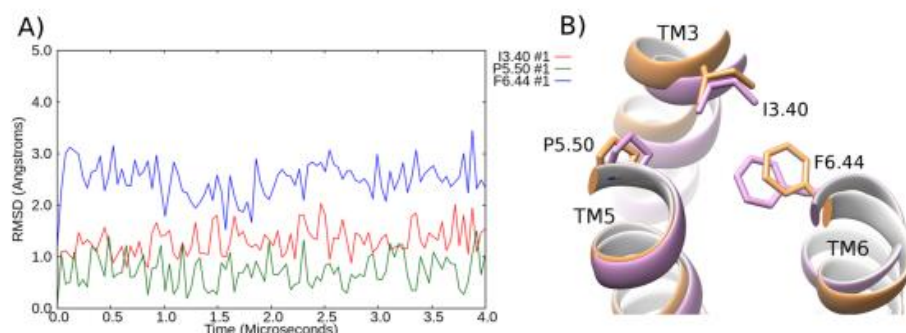

Figure 8. Stabilization of the triad core in an active-like state of β_2AR in DOPG. (**A**) RMSD profile of the conformational changes of the triad core: $I^{3.40}$ (red), $P^{5.50}$ (green) and $F^{6.44}$ (blue) over a $4\,\mu s$ MD simulation, compared to the active crystal structure of β_2AR (PDB id: 3SN6). (**B**) Superposition of the final MD-generated triad core conformation (light magenta) compared to the active crystal structure (PDB id: 3SN6, orange).

helical ICL2 and shortened TM7 at the NYxxP motif (Fig. 7). This is supported by the overall RMSD of the receptor remaining at 2.0–3.4 Å compared to the initial active crystal structure and finishing at 2.3 Å (SI Fig. 10). Taken together, these results indicate that DOPG lipids are able to stabilize an active-like state of $\beta 2AR$, even without a bound G protein or bound agonist. These observations are in general agreement with the experimental results of Dawaliby *et al.*[44], who show that DOPG strongly favours the active state of $\beta 2AR$ compared to DOPE and DOPC lipids. Intriguingly, our results may also offer an explanation of basal activity in $\beta 2AR$[72], especially if the lipid environment is chemically similar to that of DOPG.

In order to validate that the DOPG-stabilized receptor conformation was indeed active at a functional level, we re-docked the co-crystallized $G_s\alpha$ protein (PDB entry: 3SN6) back into the active crystal structure (as a control) and into the MD-generated conformation of $\beta 2AR$ obtained after $4\,\mu s$ in a DOPG membrane. In both cases, $G_s\alpha$ is able to adopt an almost identical interaction with the receptor as originally observed in the crystal structure complex without any steric clashes with intracellular loops 1 or 2 (SI Fig. 11). The re-docking of the active crystal structure of $\beta 2AR$ with $G_s\alpha$ generates an I_sc score of −8.0 (ROSIE Interface score from 0 to −10; more
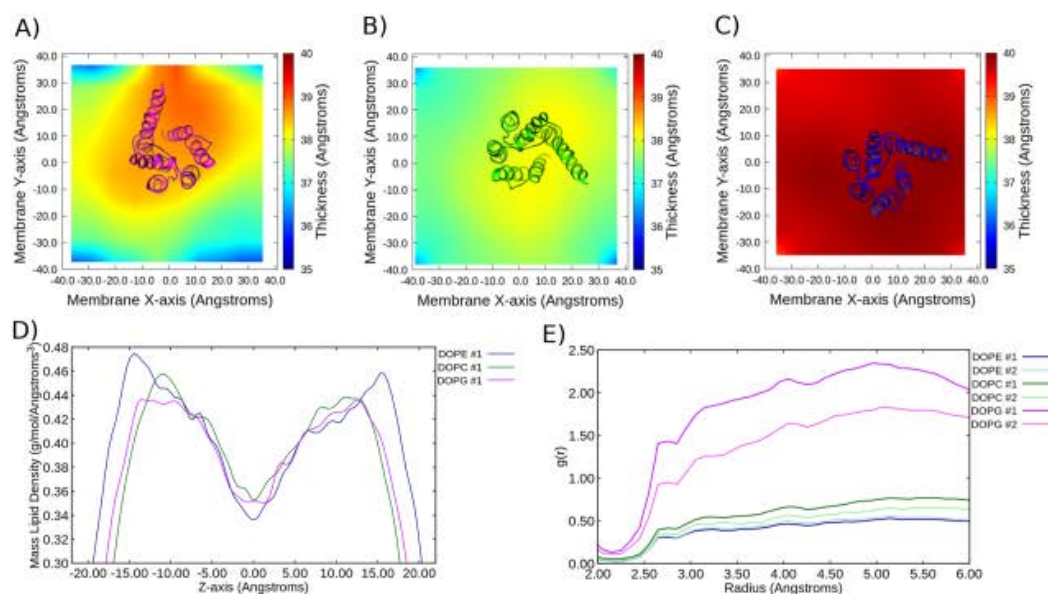
Figure 9. Membrane physical characteristics and effect on β₂AR conformation. Membrane thickness measurements from 4 μs MD simulations of β₂AR in (**A**) DOPG, (**B**) DOPC and (**C**) DOPE, respectively. (**D**) Average membrane density measurements from same MD simulations. (**E**) Radial distribution $g(r)$ of TM6 with respect to lower leaflet lipids from MD simulations of β₂AR in three different membranes.

negative is better with −5 a threshold for respectable interaction) while the resulting conformation of β2AR in DOPG with G$_s$α has an I_sc of −7.5. This suggests a similar mode of interaction between G$_s$α and β2AR embedded in a DOPG membrane as observed in the original active crystal structure. As an additional comparison, we also attempted to dock G$_s$α into β2AR conformations generated at the end of respective MD simulations in DOPC and DOPE membranes. In the case of DOPC, a partial interaction between G$_s$α and β2AR was possible resulting in an I_sc of −5.8, although G$_s$α is positioned at a different angle to the active crystal structure and not fully inserted into the receptor. In the case of DOPE, docking is poor with an I_sc of −4.7 and G$_s$α is unable to insert into the receptor, making only superficial contacts (SI Fig. 11).

Membrane characteristics and lipid headgroups facilitate allosteric modulation of β2AR. In an effort to explain the different effects that DOPC, DOPE and DOPG membranes have on β2AR conformational change, we sought to quantify the physical characteristics of each membrane and their specific effects on protein-lipid interaction, specifically with regard to the intracellular conformation of TM6 (key for GPCR activation[3–5,20,21]). Time-averaged membrane thickness measurements reveal that DOPG possesses the greatest degree of intra-membrane variation, with >3.0 Å thickness difference between its periphery and core (i.e. thicker around the protein). This compares with an internal variation of <2 Å for DOPC and <1 Å for DOPE (Fig. 9A–C). This suggests that DOPG lipids preferentially cluster around the protein, whilst less so for DOPC lipids and even less for DOPE whose membrane is nearly uniform. In addition, DOPE constitutes the thickest membrane (some 1.5–2.5 Å thicker than DOPC and 0.5–4.0 Å thicker than DOPG). Likewise, time-averaged membrane density measurements show that the DOPE membrane is most dense, particularly at the level of its headgroups (both upper and lower leaflets, Fig. 9D) whilst DOPG and DOPC membranes are less dense. This translates into an average area per lipid of 61 Å² for DOPE, 68 Å² for DOPC and 71 Å² for DOPG, which are consistent with previously calculated theoretical and experimental measurements[73,74]. As intracellular interactions between phospholipids and the receptor appear to facilitate allosteric modulation in DOPG, we calculated the time-averaged radial distribution $g(r)$ of TM6 with respect to surrounding lipid phosphate groups in the lower leaflet of each membrane, respectively. This analysis shows that TM6 as a whole in a DOPG membrane has far greater propensity for approaching lipid phosphate groups than in DOPC or DOPE (Fig. 9E). In addition, this propensity is even lower in DOPE than in DOPC, suggesting a different TM6 conformational landscape in each. In order to probe further, we calculated $g(r)$ a second time, now for just positively charged sidechains located at the intracellular end of TM6 (four lysine residues: K263$^{6.25}$, K267$^{6.29}$, K270$^{6.32}$, K273$^{6.35}$, see SI Fig. 12). This analysis reveals peaks in $g(r)$ at 4.5–5.0 Å in all three membrane types (DOPG > DOPC > DOPE), which likely reflects electrostatic interactions between positive charges on TM6 and negative charges on lipid phosphate groups. To confirm this hypothesis, we calculated the mean number of electrostatic interactions between charged protein and lipid atoms (distance cut-off <4.5 Å) in the lower leaflet of each membrane (SI Fig. 12). Results show that in DOPG, TM6 makes more protein-lipid electrostatic interactions (2.8 atom-pairs ± 1.5 SD) than in either DOPC (1.1 atom-pairs ± 1.0 SD) or

58

DOPE (0.7 atom-pairs $\pm$ 0.8 SD). Although these differences may not appear marked, over the course of respective MD simulations their effects are cumulative, leading to considerable differences in TM6-lipid attraction. Taken together, the differences in protein-lipid interactions, TM6 conformational landscapes and physical membrane characteristics, a picture of two sets of forces becomes clear. Firstly, attractive protein-lipid interactions, particularly with respect to TM6, maintain the protein in an active-like state in a DOPG membrane, with these same interactions considerably weaker in DOPC and DOPE membranes, respectively. Secondly, different membrane thickness and densities, particularly between DOPC and DOPE, appear to exert different effects on protein conformation. In the case of a DOPE membrane, its greater density and thickness laterally compresses the protein into an inactive state at a faster rate than in DOPC. On the other hand, in a thinner and less dense DOPC membrane, the protein appears to have greater conformational freedom and inactivates slower. At the heart of these differences lie different lipid headgroups. For example, the positively charged headgroup of DOPE lipids create unfavourable interactions with positively charged residues located on TM6, as well as enabling inter-lipid H-bonds between the headgroup of one lipid with the phosphate group of its neighbour (for example, see SI Fig. 13). These charged inter-lipid interactions contribute to the greater density of a DOPE membrane. On the other hand, the more hydrophobic headgroup of DOPC lipids facilitates moderate interaction with TM6, and an absence of inter-lipid H-bonds contributes to lower membrane density.

Discussion

Taking profit of recent experimental data, which shows phospholipid-mediated allosteric modulation of β2AR activity[44], we decided to study the molecular basis behind these effects by simulating β2AR in three different homogeneous membranes of DOPC, DOPE and DOPG using atomistic molecular dynamics. In remarkable agreement with the experimental data[44], we have been able to identify how DOPC, DOPE and DOPG differentially modulate β2AR activity. This receptor modulation consists of either: partial inactivation, full deactivation or stable activation, respectively, and is seemingly governed by the chemistry of protein-interacting lipid headgroups, as no agonists, antagonists, G proteins or nanobodies are included in any of our MD simulations.

DOPG, with its neutral headgroup and negatively charged phosphate group, appears to play a critical role in the stabilization of the active state of β2AR by making several electrostatic protein-lipid interactions. Firstly, ICL3, through its positively charged residues R250, K253, and R259, interacts with the negatively charged DOPG phosphate groups. Once ICL3 has interacted with the membrane, it is able to maintain a continuous interaction. Secondly, TM6 is able to maintain its outward active conformation through the influences of ICL3, as well as by its own specific attractive interactions between H269$^{6.31}$, K270$^{6.32}$ and K273$^{6.35}$ with DOPG phosphate groups. In addition, the ionic-lock residue R$^{3.50}$ on TM3 is able to interact with the phosphate group of a single DOPG lipid, which is able to protrude between TM6 and TM7 on the intracellular side of the receptor. This appears to assist in the stabilization of the active-like conformation of TM6, although is perhaps less significant than the more direct protein-lipid interactions involving TM6 and ICL3. Consistent with these multiple electrostatic protein-lipid interactions, the radial distribution $g(r)$ of TM6 with respect to lower-leaflet DOPG lipids is much more pronounced than in other membranes. These results are notable because it has been suggested previously that the active state of GPCRs, including β2AR, could only be stabilized in MD simulations by bound G proteins or mimetics[3–5,33]. However, our results instead support a pivotal role of lipids in the stable activation of β2AR, even in the absence of a bound agonist or G protein, ensuring the receptor remains in a conformation that is suitable for G protein binding. Although speculative, this might be the case for other homologous GPCRs too. On the contrary, in a DOPC homogeneous membrane, we observe a slow gradual inactivation of β2AR, which reaches an intermediate-like state after 4 µs. This is an expected result because it is in general agreement with other published MD simulations regarding β2AR in phosphatidylcholine (PC) lipid membranes, with POPC being the most commonly employed[4,5,16,18,22–28,30–33]. This supports the notion that the active state of β2AR is inherently unstable and will gradually inactivate without strongly favourable electrostatic protein-lipid interactions (or bound G protein). By analysing the chemical structure and dynamic behaviour observed in DOPC, it is clear why this lipid is unable to make ionic interactions with β2AR. Although DOPC contains a dipole consisting of PO_4^- and N^+ groups, it has three methyl groups bonded to N^+, meaning its headgroup is bulky, hydrophobic and tilted parallel to the surface of the membrane as it seeks to minimize contact with water[45]. As a consequence, its headgroup partially obstructs electrostatic interactions between its phosphate group and positively charged residues on the intracellular side of the receptor. Thus, on average we observe fewer TM6-lipid electrostatic interactions and lower TM6 radial distribution $g(r)$ in a DOPC membrane compared to DOPG. Finally, the DOPE membrane elicits a similar effect to that of DOPC as it also promotes destabilization of the β2AR active state. However, the kinetics of this process is notably quicker. In this case, β2AR undergoes full deactivation to its inactive state within 1.0–2.5 µs (depending on simulation analysed). As DOPE does not contain methyl groups on N^+, its headgroup is more hydrophilic than DOPC, therefore not as tilted, and instead orientated towards the water phase[45–47]. The exposed N^+ of DOPE may also have a repulsive effect on positively charged residues located at the intracellular side of TM5, TM6, and ICL3. In particular, this contributes to accelerated deactivation of β2AR by restricting TM6-lipid electrostatic interactions. In addition, as the DOPE membrane has higher density and thickness compared to DOPC, receptor conformation is more restricted with lower TM6 radial distribution $g(r)$.

An additional feature of β2AR-lipid interaction involves the distortion or thickening of the membrane in the vicinity of the receptor. This is particularly noticeable in DOPG, where membrane thickness increases up to 3 Å or more within a radius of ~10 Å around the protein. Interestingly, this effect is also noticeable in DOPC, although to a lesser extent but seems absent in a DOPE membrane. These observations are similar to membrane distortions observed around rhodopsin, where the active state (Meta II) creates local bilayer thickening, not apparent with the inactive state (Meta I)[75]. This can be explained by an increase in the hydrophobic thickness of rhodopsin observed during its activation process, which should then be matched by lipids that are in close proximity[75,76]. Likewise, a similar effect can be seen with sarcoplasmic reticulum Ca^{2+}-ATPase, where conformational change
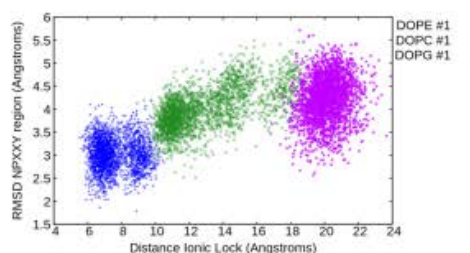
59

Figure 10. Conformational sampling of β₂AR in apo state within DOPC, DOPE and DOPG membranes over respective 4 μs MD simulations. Conformational change (RMSD compared to inactive crystal structure, PDB id: 2RH1) of TM7 motif NPxxY against distance between ionic-lock residues (R$^{3.50}$ and E$^{6.30}$). Data is extracted from 2 to 4 μs of each respective MD simulation.

between E1 and E2 states alters the hydrophobic mismatch between protein and membrane, resulting in local bulging or pinching of the bilayer[77,78]. Being homologous to rhodopsin, it is consistent that the active state of β2AR creates local thickening of the membrane, such as that observed here in a DOPG membrane, in particular. Also, as the active state of β2AR is destabilized in a DOPC membrane (or fully deactivated in DOPE), it follows that local thickening is less apparent (or absent). Extrapolating from these observations, it would also appear that it is not so much the greater thickness of a DOPE membrane that enhances β2AR deactivation, but rather its pattern of lipid headgroup charges and associated higher membrane density.

As has been described previously, the active and inactive crystal structures of β2AR contain different packing arrangements of their triad core[4,65]. In DOPE membranes, we observe the conformational transition of this triad core from active to inactive. This occurs due to the inward movement and rotation of TM6 towards the core of the receptor. This allows F$^{6.44}$ to move away from P$^{5.50}$ and relocate onto the other side of I$^{3.40}$. However, in DOPC membranes, β2AR does not reach the full inactive state within the simulated time period. As a result, the triad core fluctuates between inactive and active conformations, with F$^{6.44}$ able to adopt both inactive-like and active-like orientations due to an intermediate conformation of TM6, which is neither fully inward nor outward. In addition, I$^{3.40}$ experiences fluctuations in its rotameric state reflecting both inactive-like and active-like conformations. Finally, in DOPG membranes, the triad core of β2AR is seen to maintain an active-like state, albeit with some minor fluctuations in F$^{6.44}$, which is mainly a consequence of initial fluctuations in TM6 (interactions with the membrane are dynamic). Some of these fluctuations in TM6 may also be enhanced by the lack of a bound agonist, which might otherwise help to further stabilize the active state.

A key factor in our observations of lipid-mediated allosteric modulation of β2AR is the action of ICL3. This non-crystallized region is often neglected in computational studies[4,5,16,18,22,26-28,30-33] but has been shown to be important by experiments[43]. In our experience, it is critical that this highly flexible loop is included as it provides one of the earliest sources of protein conformational change in our MD simulations, making electrostatic interactions with the DOPG membrane (or indeed not making them in the case of DOPC or DOPE). Although we have not directly tested it, we do not believe the active state of β2AR would be as readily stabilized in DOPG membranes without ICL3, as interactions between this loop and the membrane are so prominent. On this basis, we conclude that ICL3 should ideally be included in all MD simulations of β2AR, as well as that of other GPCRs, regardless of membrane composition. Despite these observations, other conformational changes besides ICL3 are also important. In particular, TM6 is highly influential in the conformational selection of β2AR, and provides a connection between ICL3 and the triad core at the centre of the receptor. In addition, the conformation of TM7, which although not directly connected to the triad core or ICL3, is also important, particularly in defining the state of the intracellular G protein binding-site of β2AR, which displays differences depending on membrane environment. In particular, the conformation of the NPxxY motif[4] located on TM7 (in terms of RMSD) can be used to precisely define receptor state when combined with ionic-lock distance information between TM3 and TM6 (Fig. 10 and SI Fig. 14). In this schematic, the stabilized active-like state of β2AR in DOPG is clearly distinguishable from that of β2AR in DOPC (intermediate) or DOPE (inactive). As a consequence, a G$_s$α protein can be docked into the DOPG-modulated receptor conformation, obtaining an almost identical fit to that observed in the G$_s$ protein-bound crystal structure of β2AR[14]. Another intriguing aspect of β2AR (and other GPCRs in general) is its known ability to activate G proteins, albeit at a low level, even without the presence of agonists[72]. This is referred to as basal activity[72]. It is also known that the inactive state of β2AR resides at a lower energy level than the active state[72]. Therefore, in order for the receptor to access and/or remain in the active state, compensating energetic interactions are needed. Our results suggest that in addition to a bound agonist (which is not explicitly simulated here) anionic lipids may provide this additional energy through interactions with the protein, allowing β2AR to reach its active state. Indeed, this suggests a role of lipids in the regulation of β2AR basal activity. Likewise, the role of cationic lipids, especially those with an exposed ammonium group, may be to assist in the deactivation of β2AR, thereby reducing basal activity.

Although beyond the scope of this study, rather than stabilizing or destabilizing the active state of β2AR, it is interesting to speculate if the reverse process of activating the inactive state of β2AR could also be induced by lipids during MD simulations. To our knowledge this has not yet been achieved. However, we believe it could be theoretically possible, although longer simulation times than those performed here may be required. In addition,

a bound agonist may also be required to accelerate the kinetics of the process. It is certainly an interesting prospect, and if obtainable, could confirm the hypothesis that lipids have a stronger effect on GPCRs than previously thought. It may also be possible to directly demonstrate basal GPCR activity, for which MD simulations have not yet been able to satisfactorily model. Intriguingly, it has yet to be determined experimentally whether other GPCRs are sensitive to phospholipids in the same way as β2AR. From our computational results, we observe that electronegative lipids strongly act on β2AR to stabilize its active conformation(s), while lipids with positively charged headgroups may act to deactivate it. This may hold true for other homologous GPCRs that possess similar patterns of positively charged residues on TM6 and ICL3. Another interesting question concerns how heterogeneous membranes, which likely reflect mammalian physiology more accurately than homogenous membranes, might affect GPCR behaviour through different blends of phospholipids containing a variety of headgroups and fatty acid chains. This is a complex problem requiring further studies but could reveal how specific cellular environments might differentially regulate GPCR-mediated signalling at the molecular level.

Associated Content. *Supporting Information.* Comparison of inactive and active β2AR crystal structures; RMSD plots of ICL3, TM6, and whole protein in DOPG, DOPE, DOPC membranes; plot of ionic-lock distances in DOPG, DOPE, DOPC membranes; visual of selected protein-lipid interactions in DOPG membrane; visual of G protein dockings, plots of electrostatic TM6-lipid interactions and radial distribution *g(r)*.

References

1. Katritch, V., Cherezov, V. & Stevens, R. C. Structure-function of the G protein-coupled receptor superfamily. *Annu Rev Pharmacol Toxicol* **53**, 531–556 (2013).
2. Santos, R. *et al.* A comprehensive map of molecular drug targets. *Nat Rev Drug Discov* **16**, 19–34 (2017).
3. Latorraca, N. R., Venkatakrishnan, A. J. & Dror, R. O. GPCR Dynamics: Structures in Motion. *Chem Rev* **117**, 139–155 (2017).
4. Dror, R. O. *et al.* Activation mechanism of the beta2-adrenergic receptor. *Proc Natl Acad Sci USA* **108**, 18684–18689 (2011).
5. Nygaard, R. *et al.* The dynamic process of beta(2)-adrenergic receptor activation. *Cell* **152**, 532–542 (2013).
6. Staus, D. P. *et al.* Allosteric nanobodies reveal the dynamic range and diverse mechanisms of G-protein-coupled receptor activation. *Nature* **535**, 448–452 (2016).
7. Gregorio, G. G. *et al.* Single-molecule analysis of ligand efficacy in β2AR–G-protein activation. *Nature* **547**, 68–73 (2017).
8. Lee, A. G. Biological membranes: the importance of molecular detail. *Trends Biochem Sci* **36**, 493–500 (2011).
9. Stansfeld, P. J. & Sansom, M. S. Molecular simulation approaches to membrane proteins. *Structure* **19**, 1562–1572 (2011).
10. Lyman, E. *et al.* A role for a specific cholesterol interaction in stabilizing the Apo configuration of the human A(2A) adenosine receptor. *Structure* **17**, 1660–1668 (2009).
11. Hanson, M. A. *et al.* A specific cholesterol binding site is established by the 2.8 A structure of the human beta2-adrenergic receptor. *Structure* **16**, 897–905 (2008).
12. Lee, E. H., Hsin, J., Sotomayor, M., Comellas, G. & Schulten, K. Discovery through the computational microscope. *Structure* **17**, 1295–1306 (2009).
13. Cherezov, V. *et al.* High-resolution crystal structure of an engineered human beta2-adrenergic G protein-coupled receptor. *Science* **318**, 1258–1265 (2007).
14. Rasmussen, S. G. F. *et al.* Crystal structure of the β2 adrenergic receptor-Gs protein complex. *Nature* **477**, 549–555 (2011).
15. Dror, R. O. *et al.* Identification of two distinct inactive conformations of the beta2-adrenergic receptor reconciles structural and biochemical observations. *Proc Natl Acad Sci USA* **106**, 4689–4694 (2009).
16. Neale, C., Herce, H. D., Pomes, R. & Garcia, A. E. Can Specific Protein-Lipid Interactions Stabilize an Active State of the Beta 2 Adrenergic Receptor? *Biophys J* **109**, 1652–1662 (2015).
17. Manglik, A. *et al.* Brian K. Structural Insights into the Dynamic Process of β2-Adrenergic Receptor Signaling. *Cell* **162**, 1431 (2015).
18. Bai, Q. *et al.* Ligand induced change of beta2 adrenergic receptor from active to inactive conformation and its implication for the closed/open state of the water channel: insight from molecular dynamics simulation, free energy calculation and Markov state model analysis. *Phys Chem Chem Phys* **16**, 15874–15885 (2014).
19. Chung, K. Y. *et al.* Conformational changes in the G protein Gs induced by the β2 adrenergic receptor. *Nature* **477**, 611–615 (2011).
20. Bang, I. & Choi, H. J. Structural features of beta2 adrenergic receptor: crystal structures and beyond. *Mol Cells* **38**, 105–111 (2015).
21. Dalton, J. A., Lans, I. & Giraldo, J. Quantifying conformational changes in GPCRs: glimpse of a common functional mechanism. *BMC Bioinformatics* **16**, 124 (2015).
22. Ranganathan, A., Dror, R. O. & Carlsson, J. Insights into the role of Asp79(2.50) in beta2 adrenergic receptor activation from molecular dynamics simulations. *Biochemistry* **53**, 7283–7296 (2014).
23. Ozcan, O., Uyar, A., Doruker, P. & Akten, E. D. Effect of intracellular loop 3 on intrinsic dynamics of human beta2-adrenergic receptor. *BMC Struct Biol* **13**, 29 (2013).
24. Bai, Q., Zhang, Y., Ban, Y., Liu, H. & Yao, X. Computational study on the different ligands induced conformation change of beta2 adrenergic receptor-Gs protein complex. *PLoS One* **8**, e68138 (2013).
25. Ozgur, C., Doruker, P. & Akten, E. D. Investigation of allosteric coupling in human beta2-adrenergic receptor in the presence of intracellular loop 3. *BMC Struct Biol* **16**, 9 (2016).
26. Dickson, C. J. *et al.* Uncoupling the Structure-Activity Relationships of beta2 Adrenergic Receptor Ligands from Membrane Binding. *J Med Chem* **59**, 5780–5789 (2016).
27. Plazinska, A., Plazinski, W. & Jozwiak, K. Agonist binding by the beta2-adrenergic receptor: an effect of receptor conformation on ligand association-dissociation characteristics. *Eur Biophys J* **44**, 149–163 (2015).
28. Dror, R. O. *et al.* Pathway and mechanism of drug binding to G-protein-coupled receptors. *Proc Natl Acad Sci USA* **108**, 13118–13123 (2011).
29. Manna, M. *et al.* Mechanism of allosteric regulation of beta2-adrenergic receptor by cholesterol. *Elife* **5**, e18432 (2016).
30. Mahmood, I., Liu, X., Neya, S. & Hoshino, T. Influence of lipid composition on the structural stability of g-protein coupled receptor. *Chem Pharm Bull (Tokyo)* **61**, 426–437 (2013).
31. Chan, H. C., Filipek, S. & Yuan, S. The Principles of Ligand Specificity on beta-2-adrenergic receptor. *Sci Rep* **6**, 34736 (2016).
32. Tikhonova, I. G., Selvam, B., Ivetac, A., Wereszczynski, J. & McCammon, J. A. Simulations of biased agonists in the beta(2) adrenergic receptor with accelerated molecular dynamics. *Biochemistry* **52**, 5593–5603 (2013).
33. Sun, X., Agren, H. & Tu, Y. Microsecond Molecular Dynamics Simulations Provide Insight into the Allosteric Mechanism of the Gs Protein Uncoupling from the beta2 Adrenergic Receptor. *J Phys Chem B* **118**, 14737–14744 (2014).
34. Ring, A. M. *et al.* Adrenaline-activated structure of β2-adrenoceptor stabilized by an engineered nanobody. *Nature* **502**, 575–579 (2013).
35. Weichert, D. *et al.* Covalent agonists for studying G protein-coupled receptor activation. *Proc Natl Acad Sci USA* **111**, 10744–10748 (2014).

36. Zou, Y., Weis, W. I. & Kobilka, B. K. N-terminal T4 lysozyme fusion facilitates crystallization of a G protein coupled receptor. *PLoS One* **7**, e46039 (2012).

37. Wacker, D. *et al.* Conserved binding mode of human beta2 adrenergic receptor inverse agonists and antagonist revealed by X-ray crystallography. *J Am Chem Soc* **132**, 11443–11445 (2010).

38. Bokoch, M. P. *et al.* Ligand-specific regulation of the extracellular surface of a G-protein-coupled receptor. *Nature* **463**, 108–112 (2010).

39. Rasmussen, S. G. F. *et al.* Crystal structure of the human β2 adrenergic G-protein-coupled receptor. *Nature* **450**, 383–387 (2007).

40. Rasmussen, S. G. *et al.* Structure of a nanobody-stabilized active state of the beta(2) adrenoceptor. *Nature* **469**, 175–180 (2011).

41. Rosenbaum, D. M. *et al.* Structure and function of an irreversible agonist-beta(2) adrenoceptor complex. *Nature* **469**, 236–240 (2011).

42. Ackerman, D. G. & Feigenson, G. W. Lipid bilayers: clusters, domains and phases. *Essays Biochem* **57**, 33–42 (2015).

43. Chakir, K. *et al.* The third intracellular loop and the carboxyl terminus of beta2-adrenergic receptor confer spontaneous activity of the receptor. *Molecular pharmacology* **64**, 1048–1058 (2003).

44. Dawaliby, R. *et al.* Allosteric regulation of G protein-coupled receptor activity by phospholipids. *Nat Chem Biol* **12**, 35–39 (2016).

45. Dill, K. A. & Stigter, D. Lateral interactions among phosphatidylcholine and phosphatidylethanolamine head groups in phospholipid monolayers and bilayers. *Biochemistry* **27**, 3446–3453 (1988).

46. Mingins, J., Stigter, D. & Dill, K. A. Phospholipid interactions in model membrane systems. I. Experiments on monolayers. *Biophys J* **61**, 1603–1615 (1992).

47. Stigter, D., Mingins, J. & Dill, K. A. Phospholipid interactions in model membrane systems. II. Theory. *Biophys J* **61**, 1616–1629 (1992).

48. Stillwell, W. In *An Introduction to Biological Membranes* 57–83 (Elsevier, 2013).

49. Mendis, L. H., Grey, A. C., Faull, R. L. & Curtis, M. A. Hippocampal lipid differences in Alzheimer's disease: a human brain study using matrix-assisted laser desorption/ionization-imaging mass spectrometry. *Brain Behav* **6**, e00517 (2016).

50. Martin, V. *et al Lipid Alterations in Lipid Rafts from Alzheimer's Disease Human Brain Cortex*. Vol. 19 (2010).

51. Fabelo, N. *et al.* Severe alterations in lipid composition of frontal cortex lipid rafts from Parkinson's disease and incidental Parkinson's disease. *Mol Med* **17**, 1107–1118 (2011).

52. Fabelo, N. *et al.* Altered lipid composition in cortical lipid rafts occurs at early stages of sporadic Alzheimer's disease and facilitates APP/BACE1 interactions. *Neurobiol Aging* **35**, 1801–1812 (2014).

53. Ballesteros, J. A. & Weinstein, H. Integrated methods for the construction of three-dimensional models and computational probing of structure-function relations in G protein-coupled receptors. *Methods in Neurosciences* **25**, 366–428 (1995).

54. Eswar, N., Eramian, D., Webb, B., Shen, M.-Y. & Sali, A. in *Structural Proteomics: High-Throughput Methods* (eds Bostjan Kobe, Mitchell Guss, & Thomas Huber) 145–159 (Humana Press, 2008).

55. Drozdetskiy, A., Cole, C., Procter, J. & Barton, G. J. JPred4: a protein secondary structure prediction server. *Nucleic Acids Res* **43**, W389–394 (2015).

56. Buchan, D. W., Minneci, F., Nugent, T. C., Bryson, K. & Jones, D. T. Scalable web services for the PSIPRED Protein Analysis Workbench. *Nucleic Acids Res* **41**, W349–357 (2013).

57. Case, D. A. *et al.* The Amber biomolecular simulation programs. *J Comput Chem* **26**, 1668–1688 (2005).

58. Pettersen, E. F. *et al.* UCSF Chimera–a visualization system for exploratory research and analysis. *J Comput Chem* **25**, 1605–1612 (2004).

59. Jo, S., Kim, T., Iyer, V. G. & Im, W. CHARMM-GUI: a web-based graphical user interface for CHARMM. *J Comput Chem* **29**, 1859–1865 (2008).

60. Lans, I., Dalton, J. A. & Giraldo, J. Selective Protonation of Acidic Residues Triggers Opsin Activation. *J Phys Chem B* **119**, 9510–9519 (2015).

61. Huang, J. & MacKerell, A. D. Jr. CHARMM36 all-atom additive protein force field: validation based on comparison to NMR data. *J Comput Chem* **34**, 2135–2145 (2013).

62. Harvey, M. J., Giupponi, G. & Fabritiis, G. D. ACEMD: Accelerating Biomolecular Dynamics in the Microsecond Time Scale. *J Chem Theory Comput* **5**, 1632–1639 (2009).

63. Humphrey, W., Dalke, A. & Schulten, K. VMD: visual molecular dynamics. *J Mol Graph* **14**(33-38), 27–38 (1996).

64. Huang, W. *et al.* Structural insights into μ-opioid receptor activation. *Nature* **524**, 315–321 (2015).

65. Valentin-Hansen, L., Holst, B., Frimurer, T. M. & Schwartz, T. W. PheVI:09 (Phe6.44) as a sliding microswitch in seven-transmembrane (7TM) G protein-coupled receptor activation. *J Biol Chem* **287**, 43516–43526 (2012).

66. Bonomi, M. *et al.* PLUMED: A portable plugin for free-energy calculations with molecular dynamics. *Computer Physics Communications* **180**, 1961–1972 (2009).

67. Guixà-González, R. *et al.* MEMBPLUGIN: studying membrane complexity in VMD. *Bioinformatics* **30**, 1478–1480 (2014).

68. Levine, B. G., Stone, J. E. & Kohlmeyer, A. Fast Analysis of Molecular Dynamics Trajectories with Graphics Processing Units–Radial Distribution Function Histogramming. *J Comput Phys* **230**, 3556–3569 (2011).

69. Lyskov, S. *et al.* Serverification of molecular modeling applications: the Rosetta Online Server that Includes Everyone (ROSIE). *PLoS One* **8**, e63906 (2013).

70. Williams, T., Kelley, C. & Others. Gnuplot 4.4: an interactive plotting program. 81–87 (2010).

71. Muramatsu, T. & Suwa, M. Statistical analysis and prediction of functional residues effective for GPCR-G-protein coupling selectivity. *Protein Eng Des Sel* **19**, 277–283 (2006).

72. Lamichhane, R. *et al.* Single-molecule view of basal activity and activation mechanisms of the G protein-coupled receptor beta2AR. *Proc Natl Acad Sci USA* **112**, 14254–14259 (2015).

73. Ding, W., Palaiokostas, M., Wang, W. & Orsi, M. Effects of Lipid Composition on Bilayer Membranes Quantified by All-Atom MolecularDynamics. *The journal of physical chemistry. B* **119**, 15263–15274 (2015).

74. Pan, J. *et al.* Molecular structures of fluid phase phosphatidylglycerol bilayers as determined by small angle neutron and X-ray scattering. *Biochimica et biophysica acta* **1818**, 2135–2148 (2012).

75. Brown, M. F. Modulation of rhodopsin function by properties of the membrane bilayer. *Chemistry and physics of lipids* **73**, 159–180 (1994).

76. Mondal, S., Khelashvili, G., Shan, J., Andersen, O. S. & Weinstein, H. Quantitative modeling of membrane deformations by multihelical membrane proteins: application to G-protein coupled receptors. *Biophysical journal* **101**, 2092–2101 (2011).

77. Lee, A. G. How lipids affect the activities of integral membrane proteins. *Biochimica et biophysica acta* **1666**, 62–87 (2004).

78. Andersen, O. S. & Koeppe, R. E. 2nd Bilayer thickness and membrane protein function: an energetic perspective. *Annual review of biophysics and biomolecular structure* **36**, 107–130 (2007).

Acknowledgements

Author Contributions

A.B. performed modelling, simulations and analysis. All authors contributed to writing and reviewing of the manuscript. J.G. and J.A.R.D. co-supervised study.

Additional Information

7.2. INSIGHTS INTO ADENOSINE A$_{2A}$ RECEPTOR ACTIVATION THROUGH COOPERATIVE MODULATION OF AGONIST AND ALLOSTERIC LIPID INTERACTIONS
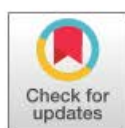
PLOS COMPUTATIONAL BIOLOGY

RESEARCH ARTICLE

Insights into adenosine A₂A receptor activation through cooperative modulation of agonist and allosteric lipid interactions

Agustín Bruzzese[1,2,3], James A. R. Dalton[1,2,3]*, Jesús Giraldo[1,2,3]*

1 Laboratory of Molecular Neuropharmacology and Bioinformatics, Unitat de Bioestadística and Institut de Neurociències, Universitat Autònoma de Barcelona, Bellaterra, Spain, 2 Unitat de Neurociència Traslacional, Parc Taulí Hospital Universitari, Institut d'Investigació i Innovació Parc Taulí (I3PT), Institut de Neurociències, Universitat Autònoma de Barcelona, Bellaterra, Spain, 3 Instituto de Salud Carlos III, Centro de Investigación Biomédica en Red de Salud Mental, CIBERSAM, Spain

* James.Dalton@uab.es (JARD); Jesus.Giraldo@uab.es (JG)

Abstract

The activation process of G protein-coupled receptors (GPCRs) has been extensively studied, both experimentally and computationally. In particular, Molecular Dynamics (MD) simulations have proven useful in exploring GPCR conformational space. The typical behaviour of class A GPCRs, when subjected to unbiased MD simulations from their crystallized inactive state, is to fluctuate between inactive and intermediate(s) conformations, even with bound agonist. Fully active conformation(s) are rarely stabilized unless a G protein is also bound. Despite several crystal structures of the adenosine A2a receptor (A2aR) having been resolved in complex with co-crystallized agonists and Gₛ protein, its agonist-mediated activation process is still not completely understood. In order to thoroughly examine the conformational landscape of A2aR activation, we performed unbiased microsecond-length MD simulations in quadruplicate, starting from the inactive conformation either in apo or with bound agonists: endogenous adenosine or synthetic NECA, embedded in two homogeneous phospholipid membranes: 1,2-dioleoyl-sn-glycerol-3-phosphoglycerol (DOPG) or 1,2-dioleoyl-sn-glycerol-3-phosphocholine (DOPC). In DOPC with bound adenosine or NECA, we observe transition to an intermediate receptor conformation consistent with the known adenosine-bound crystal state. In apo state in DOPG, two different intermediate conformations are obtained. One is similar to that observed with bound adenosine in DOPC, while the other is closer to the active state but not yet fully active. Exclusively, in DOPG with bound adenosine or NECA, we reproducibly identify receptor conformations with fully active features, which are able to dock Gₛ protein. These different receptor conformations can be attributed to the action/absence of agonist and phospholipid-mediated allosteric effects on the intracellular side of the receptor.

65

Author summary

Unbiased microsecond-length MD simulations of the adenosine A2a receptor (A2aR) were performed in quadruplicate, starting from the inactive conformation either in apo or with bound agonists: adenosine or NECA, each of them embedded in two different homogeneous phospholipid membranes. Different intermediate or active receptor conformations were found depending on the presence/absence of bound agonist and type of lipid environment. Exclusively, in DOPG with bound agonist, we reproducibly identify receptor conformations with fully active features, which are able to dock G_s protein. These different receptor conformations can be attributed to the action/absence of agonist and phospholipid-mediated allosteric effects on the intracellular side of the receptor. Dynamic structural data are key for the understanding of agonist-mediated GPCR activation simulated in realistic membrane environments.

Introduction

G protein-coupled receptors (GPCRs) are heptahelical transmembrane proteins [1, 2]. In the simplest scheme, they mediate many physiological and pathological processes by transduction of signals across cellular membranes and exist in a conformational equilibrium between active and inactive forms [3, 4]. In the absence of ligands, some GPCRs exhibit basal activity, thought to be caused by their surrounding environment, which provides enough energy for the receptor to obtain an active state [5–8]. Only in the active state are GPCRs able to bind cytosolic proteins, such as G protein or β-arrestin, mediating different downstream signalling pathways from the same receptor [9, 10]. Moreover, GPCR signalling effects can be modified by the binding of endogenous or exogenous extracellular ligands [11, 12]. Ligand binding triggers conformational changes in the orthosteric site that are amplified into larger conformational rearrangements [6]. For these reasons, GPCRs are one of the major targets of current market drugs [13]. Thus, it is essential to deeply understand ligand-dependent (de)activation of GPCRs in order to suitably understand human physiology and expectedly perform more efficient drug discovery.

Advancements in the crystallization process of GPCRs (and membrane proteins in general) have enabled several studies to gain important insight into features of their activation process [14, 15]. Most GPCR crystal structures belong to the class A (or rhodopsin-like) family, which represents the majority (approximately 85%) of the total superfamily [16, 17], and are important pharmaceutical drug targets [17]. As a result, class A family members are typically the most studied and possess a number of highly conserved sequence motifs [18], which presumably play important functional roles in common signalling mechanisms shared by all family members [16, 19]. In particular, the crystallization of class A GPCR active structures has served as an important factor in their proposed activation mechanism, such as: rhodopsin [20], β2 adrenergic receptor (B2aR) [21, 22], M2 muscarinic receptor (M2R) [23], adenosine A2a receptor (A2aR) [24, 25], and μ-opioid receptor (μOR) [26]. From this structural data, the common and simplest activation mechanism for class A GPCRs involves the movement of transmembrane helix (TM) 3, TM5, TM6 and TM7 with respect to each other [5, 6, 16, 27, 28]. The importance of water for G protein-coupled receptors (GPCRs) has also been supported by recent crystallographic data [29, 30] and from different studies showing how ordered waters interact with residues that are important in disease states, binding of drugs, receptor activation, and signalling [31–34]. However, as it has been pointed out [5, 35], the communication between the orthosteric ligand binding-site and the cytoplasmic region of the receptor

66

Publications

responsible for transducer protein binding is loose because they are not rigidly coupled. This includes an additional difficulty to the molecular understanding of ligand-dependent GPCR (de)activation. Molecular dynamics (MD) is a suitable computational technique for studying GPCR flexibility in a membrane environment. MD simulations at atomic resolution can give information on specific molecular processes, including interactions of proteins with lipids, receptor-ligand binding, and receptor conformational change [36]. There have been numerous studies on how GPCRs activate and transmit their signals from the extracellular side through to G protein binding on the intracellular side [5, 6, 18, 37–39]. In particular, MD simulations have been successful in providing accurate molecular features of GPCR conformational space [36]. In general, the typical behaviour of class A GPCRs, when they are observed without bound G protein, is to fluctuate between inactive and intermediate(s) states without inducing the fully active conformation, even in the presence of an agonist [40–48]. Therefore, one of the current challenges with GPCRs is to understand the molecular basis for their agonist-mediated transition into the active state. In a recently published experimental study, two different phospholipids proved to act as negative and positive allosteric modulators of the β2-adrenergic receptor (β2AR): 1,2-dioleoyl-sn-glycerol-3-phosphoethyl (DOPE) and 1,2-dioleoyl-sn-glycerol-3-phosphoglycerol (DOPG), respectively, while 1,2-dioleoyl-sn-glycerol-3-phosphocholine (DOPC) acted as neutral [49]. Consequently, we previously performed a computational study that supported these results by stabilizing the active conformation of apo β2AR in MD simulations for several microseconds using a DOPG membrane. This supports the notion that phospholipids may be involved in the activation process of class A GPCRs [50]. In particular, anionic DOPG (Fig 1A) appears to play a critical role in the stabilization of the active state of β2AR by making several electrostatic protein-lipid interactions [49, 50]. Meanwhile, DOPC (Fig 1B) (a close relative of POPC and a net neutral lipid) allows slow destabilization of the β2AR active state [49, 50]. These effects have been shown to be mediated by H-bond formation (or lack thereof) between the protein and phospholipid headgroups [51]. Moreover, data gathered in a β2AR ligand binding study suggests that protein and membrane interplay improves interaction between protein and ligand and could be important for drug development [49, 52]. Likewise, our recent computational study on homologous cannabinoid receptor 1 (CB1) found compelling evidence for positive allosteric communication between bound CB1 agonists and DOPG membrane phospholipids, which appears to enhance the speed of receptor activation [53]. Still, an interesting question is how much different membranes might affect the activation process of other class A GPCRs and the functional effect of their agonists.

A2aR is a prototypical GPCR class A member, ubiquitously expressed in the body [54]. On the one hand, it binds endogenous adenosine, which regulates vasodilation, inflammation [55] and affects the central nervous system (CNS), inhibiting dopaminergic activity [56]. On the other hand, the inhibition of A2aR by molecules like caffeine leads to an increase in dopaminergic activity, which makes antagonists of A2aR an important target for treating Parkinson's [57] and Alzheimer's diseases [58, 59]. Despite current knowledge, to date, only one selective A2aR agonist (Regadenoson) has gained FDA approval, as well as an antagonist (Istradefylline), which in combination with levodopa is used for the treatment of Parkinson's disease in Japan [58, 59]. A2aR is an ideal system to study GPCR activation processes because it has a high propensity for binding lipid allosteric modulators [60], is a well-known drug target for several agonists and antagonists, and has been the focus of recent NMR studies [42, 61–64]. These studies show that, upon the addition of a full agonist, A2aR activation follows outward movements of TM5 and TM6 (including rotation in the latter), an inward shift of the intracellular part of TM7, and a vertical translation of TM3 [42, 61–64]. Also, A2aR has received a lot of attention regarding ligand binding, lipid allosteric modulation and its activation process in MD simulations [44, 65–78] partly because it is a receptor that has been crystallized in three
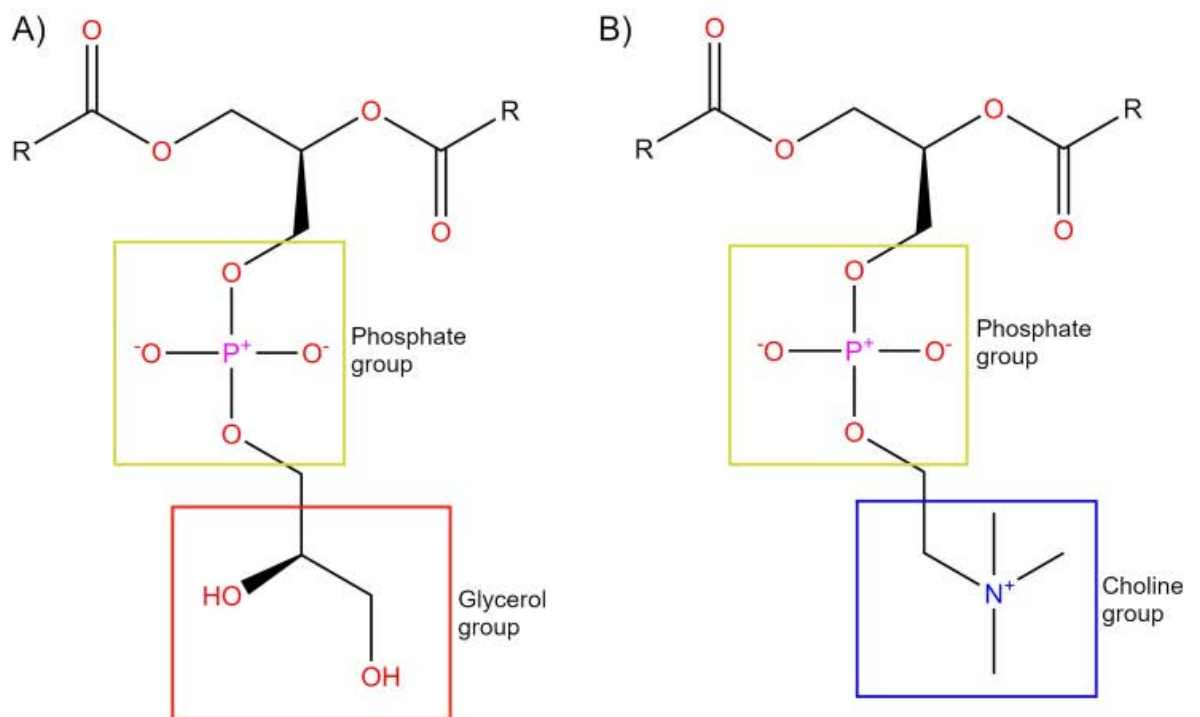
67

Fig 1. Structural comparison of DOPG and DOPC lipid headgroups. DOPG (A) headgroup is composed of a neutral glycerol group (red box) bound to the phosphate group (yellow box). DOPC (B) headgroup is composed of a positively-charged choline group bound (blue box) to the phosphate group (yellow box). DOPC and DOPG contain identical 18:1 fatty-acid chains (R).

https://doi.org/10.1371/journal.pcbi.1007818.g001

distinct conformational states: inactive (in the presence of an antagonist or inverse agonist) [29, 63, 79–91], intermediate (in the presence of an agonist) [92–95], and active (in the presence of an agonist plus modified or native stimulatory G proteins) [24, 25] (S1 Table).

These crystal structures can constitute a reference point for comparison between active, intermediate, and inactive states of A2aR during MD simulations. Such published MD simulations usually share a common protocol. For example, intracellular co-crystallized molecules such as G_s protein and activating nanobody are first removed (e.g. [44, 68, 71, 76]) and then performed within a homogeneous membrane consisting of 1-palmitoyl-2-oleoyl-sn-glycerol-3-phosphocholine (POPC) lipids (e.g. [65–76, 78]). This is due to the relative abundance of this particular phospholipid in healthy mammalian membranes [96, 97]. In this context, previous MD simulation data has shown that the structural motions of A2aR may depend on its phospholipid environment [65] as well as on cholesterol, which has been shown to enhance A2aR activation and signalling [77, 78]. On the other hand, recent MD studies have obtained results on the important role of ligand binding in A2aR activation [44, 67, 69, 70]. In addition, A2aR has been described as a weakly coupled system, due to the fact that binding of an agonist does not guarantee that the active state is reached under experimental conditions [41] and ligand binding may not be an exclusive driving force for achieving full receptor activation [44, 67, 69, 70, 78]. Thus, to our knowledge, the full agonist-mediated transition of A2aR from the

inactive form towards the active state has not yet been described with unbiased MD simulations and it remains unclear how agonists select or induce the active form of A2aR [41].

Thus, previously mentioned data indicates that ligand binding together with lipid membrane allosteric effects are important components of signal transduction that when systematically studied can lead to a deeper understanding of class A GPCR function, which could potentially lead to the development of more effective drugs [70]. To this aim, we have chosen to study the agonist-mediated activation process of A2aR by performing quadruplicated unbiased microsecond-length MD simulations with bound agonists: adenosine or 5'-N-ethylcarboxamidoadenosine (NECA) in two different homogeneous lipid environments: DOPC or DOPG (Fig 1). These two phospholipids contain the same 18:1 fatty-acid chains so are ideally suited for determining the allosteric effect of different lipid head groups on the receptor. Our results suggest that anionic phospholipids with a neutral head group such as DOPG play an important positive allosteric role in the activation of A2aR, similarly to β2AR and CB1, and work in a synergistic fashion with bound agonist. These observations might open new lines of ligand-lipid cooperativity in GPCR behavioural modulation and signalling at a molecular level.

Results

NECA is a highly potent synthetic agonist of A2aR [98], while adenosine is a weaker endogenous agonist. Instead of the 5'-hydroxymethylene group positioned at C4' of the ribose moiety in adenosine (Fig 2A), NECA contains an N-ethylcarboxamido group (S1 Fig). Upon docking adenosine (Fig 2A) or NECA (S1 Fig) into the inactive human A2aR crystal structure [29], both ligands re-form their observed crystal interactions, which include an H-bond with E169$^{45.53}$ and aromatic π−π stacking with F168$^{45.52}$, both of which are located in the second extracellular loop (ECL2) (residues appended with Ballesteros X(Y).ZZ numbering [99] as superscript, which indicates relative position ZZ along TM helix X or loop between helices X and Y) (Fig 2B and 2C, S1 Fig). In addition, both adenosine and NECA make H-bonds with N253$^{6.55}$, S277$^{7.42}$ and H278$^{7.43}$ located on TM6 and TM7, respectively. This process yields an inactive receptor structure [29], crystallized at high resolution, with bound adenosine or NECA in a binding pose consistent with that previously crystallized in the thermostabilized A2aR intermediate state [93] (Fig 2B and 2C, S1 Fig).

In order to prepare for studying the dynamics of the A2aR activation mechanism at a molecular level, we initially compared the following crystal structures: agonist-bound, G$_s$ protein-bound active state [25], the inactive state bound to inverse agonist ZM241385 [29], and the intermediate state bound to adenosine or NECA [93]. In brief, the most remarkable conformational differences between them are located in: i) TM3, TM5, TM6, and TM7 helices, and ii) hydrophobic receptor core (Fig 2) (S1 Fig). Both the intermediate and active crystals share common structural differences with respect to the inactive crystal structure. Firstly, TM3 is rotated and moved upwards (from intracellular to extracellular) in the intermediate and active crystals. On this basis, a shift of residue L95$^{3.43}$ correlates with TM3 upward axial movement (S2 Fig, S3 Fig) [16]. In conjunction, W246$^{6.48}$ located on TM6 also changes orientation. This residue is known as the "toggle switch" in class A GPCRs because it can differentially rotate between alternative receptor conformational states [18, 100, 101], including A2aR [44], in particular. However, in the respective crystal structures of A2aR (S2 Fig, S3 Fig), dynamic rotation of W246$^{6.48}$ (sidechain dihedral angle χ1: 285˚) is not observed but instead shows a vertical displacement of 1.7 Å. Moreover, the distance between TM3 and TM7 is decreased, most noticeably between intracellular residues R102$^{3.50}$ and Y288$^{7.53}$, which are 5.0 Å closer in the active state, while the distance between TM3 and TM5 is increased, exemplified by residues
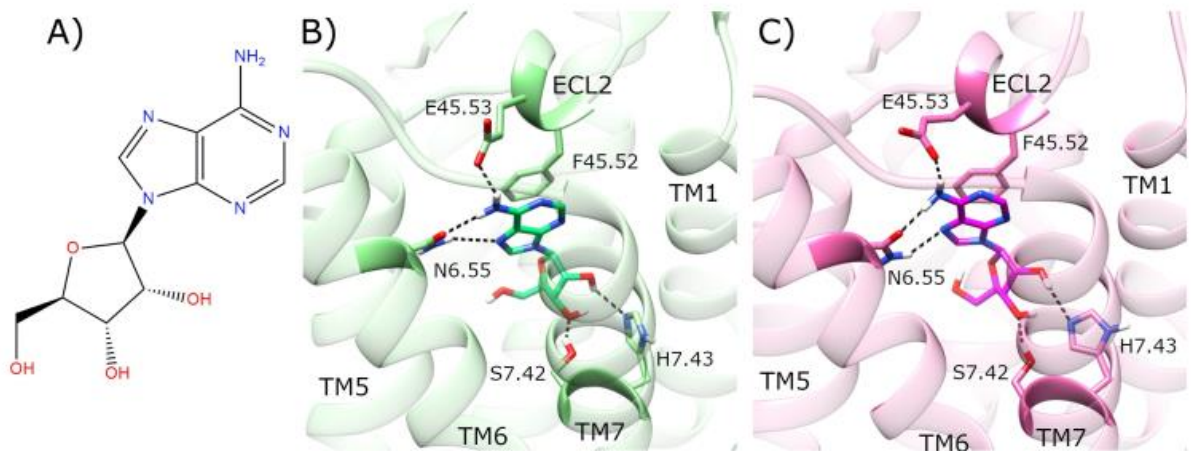
69

Fig 2. Docking of adenosine in the inactive crystal structure of adenosine A2a receptor (A2aR). A) Molecular structure of adenosine. Comparison of B) co-crystallized adenosine (lime) in agonist-bound A2aR crystal structure (PDB entry: 2YDO, light green), and C) docked adenosine (magenta) in the inactive crystal structure of A2aR (PDB entry: 4EIY, pink). Selected residues participating in ligand binding are displayed. ECL2 and TM helices 1, 5–7 are labelled.

https://doi.org/10.1371/journal.pcbi.1007818.g002

R102$^{3.50}$ and Q207$^{5.68}$, which are 2.7 Å further away in the intermediate state (S2 Fig, S3 Fig) (S2 Table). The main difference between intermediate and active crystal structures can be observed in the intracellular distance between TM3 and TM6, and ionic-lock residues R102$^{3.50}$ and E228$^{6.30}$, in particular. Both crystals have TM6 oriented outwards compared with the inactive crystal structure. However, TM3-TM6 distance reaches 18.6 Å in the active, but only 9.9 Å in the intermediate crystal structure (S2 Fig, S3 Fig) (S2 Table).

In agreement with NMR studies [42, 61–64] and previous MD simulation data [44, 65–78], comparison of A2aR crystal structures points to TM3, TM5, TM6 and TM7 as key receptor-activating helices. Therefore, we base our quantitative MD analysis of A2aR activation/modulation on the following metrics: TM3-TM5, TM3-TM6, TM3-TM7 distances; W246$^{6.48}$ χ1 dihedral angle change; TM3 and ECL2 vertical (Z-axial) movement; root mean square deviation (RMSD) of transmembrane domain (TMD), ECL2, TM6 and L95$^{3.43}$. In addition, experimentally verified protein-agonist H-bonds involving residues N253$^{6.55}$, E169$^{45.53}$, H278$^{7.43}$, S277$^{7.42}$, as well as π-π stacking with F168$^{45.52}$, are monitored. In addition, in order to characterize the role of internal water networks in receptor activation, water-mediated interactions in the receptor core between residues pairs are also quantified.

Apo A2aR embedded in DOPC membrane remains in inactive state

Over four independent MD simulations of 2.0 µs each of apo A2aR embedded in a DOPC membrane, ECL2 displays noticeable variable behaviour. In replicas #2 and #3, a conformational change occurs (at 400 ns and 1000 ns, respectively) where ECL2 moves downwards by 2–4 Å to form a lid over the orthosteric pocket (Fig 3A–3F). Over the course of this process, ECL2 reaches a maximum of 8.6 Å and 10.9 Å RMSD, respectively (S4 Fig). However, in replica #3, the loop moves back towards its original position, away from the orthosteric pocket. This shows alternative conformations of ECL2 are possible but not necessarily physically stable. Nevertheless, in replica #2, the loop remains in a downwards position partially covering the top of the orthosteric pocket (Fig 3A), albeit with conformational fluctuations (S4 Fig). This conformational change of ECL2 is possible in the apo state due to the lack of bound

70

UAB
Universitat Autònoma
de Barcelona

Publications

INc
Institut de
Neurociències
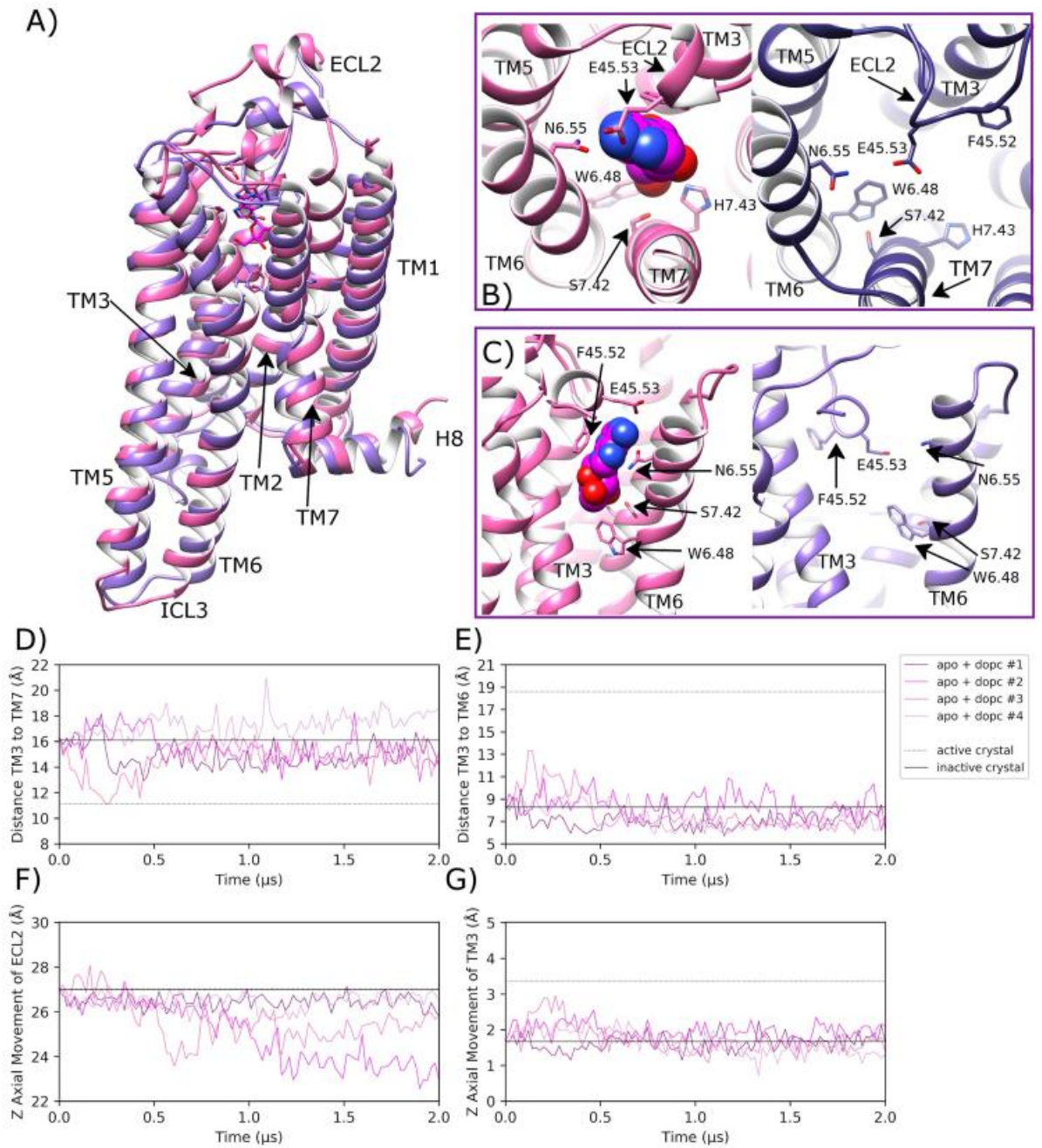
Fig 3. Stabilization of the inactive conformation of apo A2aR in DOPC membrane. A) Superposition of the inactive-state crystal structure of A2aR (PDB entry: 4EIY, pink) with docked adenosine and an MD-generated apo conformation achieved within a DOPC membrane (magenta, belonging to replica #2 from 1.7 µs) showing B) and C) selected residues delineating the orthosteric pocket. ECL2 and TM helices are labelled where applicable. D) Fluctuation of the distance between TM3-TM7 (from Cα atoms of R102$^{3.50}$ and Y288$^{7.53}$, respectively) during MD simulations, starting from the inactive crystal structure (PDB entry: 4EIY). E) Fluctuation of the distance

between TM3-TM6 (from Cα atoms of R102$^{3.50}$ and E228$^{6.30}$, respectively). F) and G) Vertical movement of ECL2 and TM3, respectively. MD simulations are performed in quadruplicate. Corresponding flat-lines are included to show the observed distance in the active (PDB entry: 6GDG) and inactive (PDB entry: 4EIY) A2aR crystal structures.

agonist and because the receptor remains inactive, thus generally maintaining the TM3-TM7 starting distance of 16.1 Å (Fig 3D). This allows the latter section of ECL2 to adopt a lower position between the extracellular ends of TM3 and TM7. However, in the other two replicas, ECL2 broadly maintains its original crystal structure position (average RMSD across replicas #1 and #4 of 2.4 Å (0.7 SD) (S4 Fig), which demonstrates ECL2 variability as previously discussed in class A GPCRs, especially in the apo state [102]. Despite the differences in observed ECL2 dynamics across replicas, little conformational change is observed in the receptor as a whole with an average RMSD of 2.2 Å (0.5 SD) (S5 Fig) or in key helices such as TM3 (average Z-axis displacement of 0.2 Å (0.6 SD), Fig 3G) and TM6 (average RMSD of 2.0 Å (0.7 SD), S6 Fig). Likewise, important residues such as L95$^{3.43}$ on TM3 and W246$^{6.48}$ on TM6 show no sustained conformational change across all four replicas (S7 Fig, S8 Fig). Likewise, the average distance between TM3 and TM6 (measured between ionic lock residues R102$^{3.50}$ and E228$^{6.30}$) is 7.8 Å (1.3 SD across all four replicas, which is similar to the inactive crystal structure distance of 8.2 Å (Fig 3E). In addition, the average distance between TM3 and TM5 is 14.9 Å (1.5 SD), which is indicative of a stabilized inactive receptor state across all four replicas (S9 Fig). Interestingly, TM7 appears to be one of the more flexible regions of the apo receptor as the distance between TM3 and TM7 (measured between R102$^{3.50}$ and Y288$^{7.53}$) is seen to vary more than other measured distances (Fig 3D, average distance of 15.8 Å (1.5 SD). For example, in replica #4, TM7 is seen to move outwards, increasing TM3-TM7 distance relative to the inactive crystal state, while in replica #3, TM7 temporarily moves inwards towards TM3 before reverting to its original state. Despite some of these observed differences, TM7 regularly revisits its inactive crystal conformation across all four replicas, suggesting this state is at least meta-stable and in line with the receptor remaining inactive (Fig 3D).

Adenosine-bound A2aR in DOPC membrane reaches intermediate conformation

During quadruplicate MD simulations of inactive A2aR with bound adenosine embedded in a DOPC membrane, the ligand displays variable behaviour (Fig 4B). In replicas #3 and #4, adenosine achieves a stable binding mode in the orthosteric pocket between helices TM3, TM6 and TM7 (Fig 4), which is consistent with its crystallized pose in the A2aR intermediate crystal structure [93]. As a result, ligand RMSD does not exceed 4.5 Å over the course of either replica, finishing at 1.7 Å in replica #3 and 3.8 Å in replica #4 (Fig 4D). However, in replicas #1 and #2, adenosine changes its binding pose frequently without finding stability, in some cases moving up to a maximum of 8.9 Å. This is because adenosine is relatively small and is able to occupy an alternative space in the orthosteric pocket in between helices TM1, TM2 and TM7 (S10 Fig). However, this alternative binding pose is not stable as reflected by the high conformational fluctuation observed in these respective replicas (Fig 4E). As a result, in the replicas where adenosine achieves a stable binding pose (#3 and #4), residue E169$^{45.53}$ located on ECL2 makes a protein-ligand H-bond with an average occupancy of 5.4% (6.3 SD), while F168$^{45.52}$ makes a protein-ligand ring-stacking interaction with adenosine 12.3% (7.7 SD) of the time (S11 Fig). However, in replicas #1 and #2 where adenosine is less stable, the frequency of these interactions decreases to 2.9% (1.4 SD) and 8.4% (6.7 SD), respectively. Despite this difference across replicas, ECL2-ligand interactions assist in the maintenance of ECL2 near its original crystal conformation (average RMSD of 2.8 Å (0.8 SD), especially relative to apo A2aR in
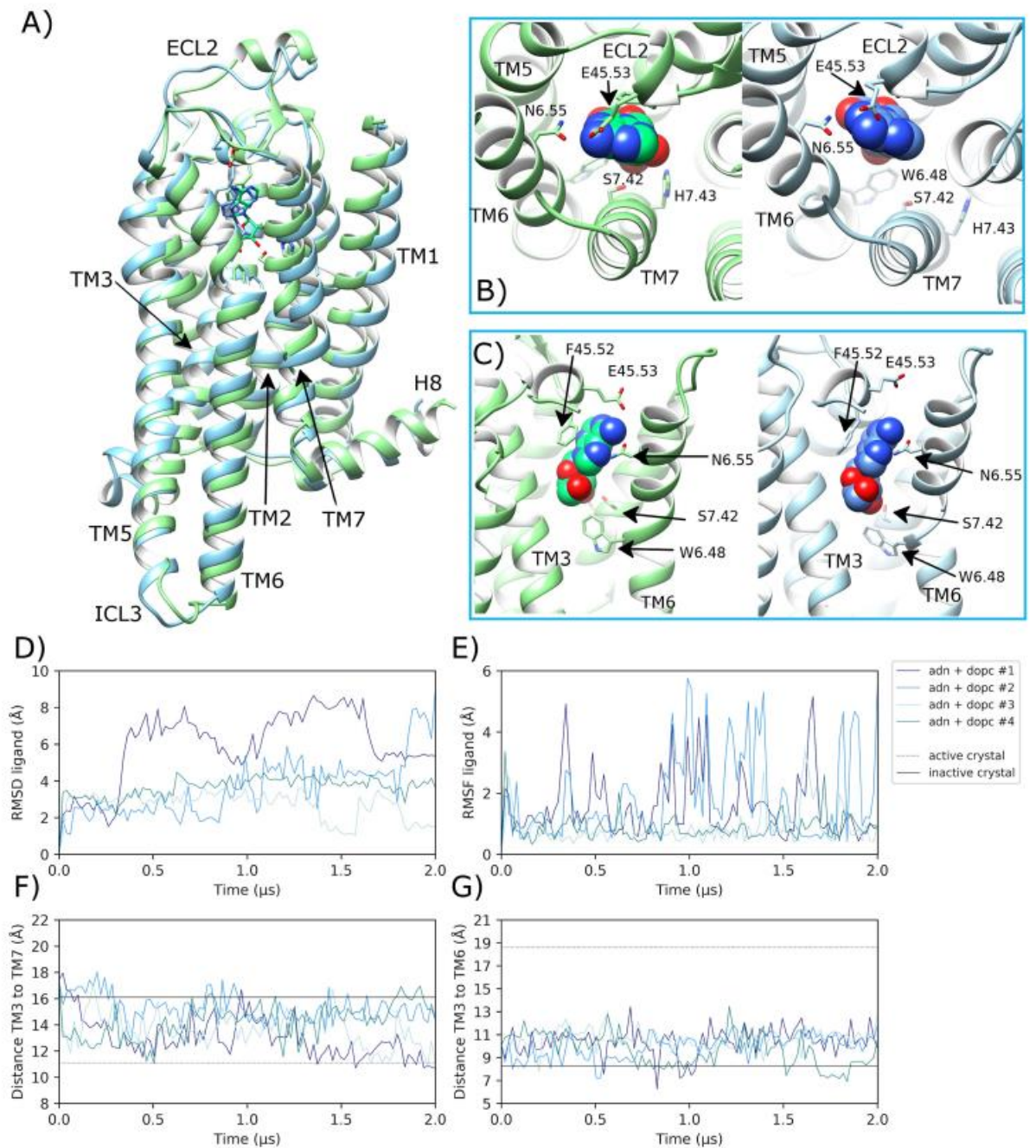
Fig 4. Transition towards an intermediate conformation of adenosine-bound A2aR in DOPC membrane. A) Superposition of the intermediate state crystal structure of A2aR (PDB entry: 2YDO, light green) and an MD-generated conformation achieved within a DOPC membrane (blue, belonging to replica #3 from 1.5 µs) bound to adenosine, showing B) and C) protein-agonist interactions in the orthosteric pocket with adenosine atoms displayed as spheres. ECL2 and TM helices are

73

labelled where applicable. D) RMSD of bound adenosine (ADN) (calculated with respect to initial docking pose). E) Conformational fluctuation (RMSF) of adenosine. F) Distance between TM3-TM7 (from Cα atoms of R102$^{3.50}$ and Y288$^{7.53}$, respectively) during MD simulations starting from the inactive crystal structure (PDB entry: 4EIY). G) Distance between TM3-TM6 (from Cα atoms of R102$^{3.50}$ and E228$^{6.30}$, respectively). MD simulations are performed in quadruplicate. Corresponding flat-lines show the observed distance in the active (PDB entry: 6GDG) and inactive (PDB entry: 4EIY) A2aR crystal structures.

DOPC (S4 Fig). This may also play a role in encouraging TM3 to move upwards into a more active conformation (ECL2 and TM3 are connected by a disulphide bridge) in replicas #3 and #4, where TM3 moves upwards (according to Z-axis) by an average of 0.8 Å (0.2 SD (S7 Fig)).

Regarding key protein-agonist interactions, N253$^{6.55}$ located on TM6 and S277$^{7.42}$ and H278$^{7.43}$ located on TM7 make H-bonds with adenosine with average occupancies of 92.1% (7.0 SD), 49.5% (25.2 SD) and 62.9% (16.1 SD) (S11 Fig), respectively, in replicas #3 and #4 where the ligand is more stable (conversely only 37.1%, 11.4% and 17.3%, respectively, for replicas #1 and #2). These interactions can be correlated with conformational changes in helices TM6 and TM7. For example, the distance between TM3 and TM7 decreases as TM7 moves inwards in all four simulations before 0.5 μs (Fig 4F). Although this conformational change is maintained until the end in only two replicas (#1 and #3, Fig 4F). On TM6, the rotameric state of W246$^{6.48}$ changes from g+ to trans in three out of four replicas after 0.25 μs (S8 Fig). This precedes the gradual separation of the intracellular end of TM6 away from TM3 by a maximum of 5.1 Å, which starts at a distance of 8.2 Å and increases up to 13.4 Å within 0.7 μs across these same three replicas (Fig 4G). However, as this conformational change of TM6 occurs mainly at its intracellular end, RMSD of TM6 shows only moderate change, reaching 4.0 Å in replica #4 (S6 Fig). Finally, conformational change is also observed in TM5 (3 out of 4 replicas) as it adopts a more outward orientation, up to 7.0 Å further away from TM3 (S9 Fig), mirroring changes in TM6. However, these changes in TM5 appear to be relatively unstable and fluctuate over time (S9 Fig) with an average distance from TM3 of 17.0 Å (1.9 SD) across all four replicas.

Taking these observed conformational changes together, the receptor achieves a full complement of intermediate-like crystal structure [93] features in three out of four replicas (#1, #3 and #4). This suggests partial receptor activation from the inactive state into a consistent intermediate conformation is readily achievable on microsecond timescales with bound agonist and membrane consisting of neutral phospholipids, although generation of a fully active receptor state is not. This is in general agreement with previous studies [44, 67, 69, 70]. Collectively, observed intermediate receptor features include a partial upwards translation of TM3 (i.e. not at the active crystal level), outward movement of TM5 and TM6 (only partial in case of TM6), and inward movement of TM7, resulting in closer interaction with TM3 (Fig 4). However, these conformational changes are only maintained consistently over 2.0 μs in replica #3, while in replicas #1 and #4 such intermediate-like features are more transient and coincide only briefly (specifically at 1.9 μs and 1.2 μs, respectively). This is likely due to the stable ligand binding-mode achieved in replica #3, including high H-bond occupancy with S277$^{7.42}$ compared to the other replicas (S11 Fig). The importance of this H-bond has been highlighted previously [103]. On the other hand, replica #2 fails to obtain an intermediate-like conformation of TM7, although some minor conformational changes are noted in TM3, TM5 and TM6, similar to other replicas. This lack of effect is likely due to a particularly unstable ligand binding-mode where the more frequent protein-ligand interactions occur with residues located on ECL2 (F168$^{45.52}$) and TM6 (N253$^{6.55}$), rather than TM7, which results in low H-bond occupancy with S277$^{7.42}$ in particular (S11 Fig).

As an extra control, additional MD simulations were performed in duplicate in a POPC membrane with or without bound adenosine (summarized in S12 Fig). Like in DOPC,

74

adenosine displays a similar level of positional instability when bound to the receptor in POPC (S12 Fig). Nevertheless, in both replicas the receptor is observed to reach an intermediate conformation similar to that observed in DOPC with bound adenosine (S12 Fig). This can be contrasted with the apo state in POPC where the receptor is observed to remain in an inactive conformation in both replicas and ECL2 is observed to move towards the empty orthosteric pocket by up to 2.0 Å (S12 Fig) in a similar manner to that observed with the apo state in DOPC. This suggests that DOPC and POPC membranes have similar effect (or lack of it) on A2aR with or without bound agonist, as might be expected.

Apo A2aR fluctuates between inactive and intermediate states in DOPG membrane

Over quadruplicate MD simulations with apo A2aR in a DOPG membrane, ECL2 is broadly maintained in its initial crystal conformation (average final RMSD of 2.8 Å (0.9 SD), Fig 5) in similar fashion to the adenosine-bound receptor in DOPC (S4 Fig). This is different to that of apo A2aR in DOPC where ECL2 is observed to change conformation by approaching the open orthosteric pocket (Fig 3). This suggests that the extracellular side of the receptor behaves differently in an anionic membrane environment, which is related to conformational changes in the TM domain that contribute to conformational restriction of ECL2. In particular, this involves inward movement of TM7 (see below) that narrows the orthosteric pocket, which has previously been described in agonist-bound A2aR crystal structures [27]. In more detail, within 500 ns, similar to the behaviour of A2aR with bound adenosine, there is an initial change of conformation in TM3, TM5, TM6, and TM7. In particular, in two of four replicas (#1 and #2), TM3 shows noticeable upward movement by an average of 2.1 Å (0.3 SD) (Fig 5G), which is most sustained in replica #1. Likewise, in three of four replicas (#1, #2, #4), TM5 (S9 Fig) and TM6 move outward, while TM7 shifts inwards (Fig 5D and 5E) as their respective distances from TM3 change (mean (SD): 11.2 Å (1.1) and 12.1 Å (0.9), respectively). These respective outward and inward helical movements are synchronized, occurring at 250 ns in replicas #1 and #4, and after 1.4 μs in replica #2. However, it is noticeable that TM7 movement occurs shortly after those in TM6 take place first (Fig 5D and 5E). Therefore, without bound ligand acting on TM7, TM6 conformational changes need to be triggered first by protein-lipid intracellular interactions, such as those provided by anionic DOPG phospholipids. As has been previously shown with homologous β2-adrenergic and CB1 receptors, protein-DOPG H-bonds and electrostatic interactions are able to exert an outward pull on TM6 [50, 53]. These initial intracellular conformational changes in TM6 leave a space next to TM3, which TM7 can occupy by spontaneously moving inwards, creating intracellular and extracellular conformational changes that affect other receptor regions such as the G protein binding-site or ECL2.

In similar fashion to β2-adrenergic and CB1 [50, 53], DOPG is able to make specific protein-lipid interactions with A2aR through its negatively charged phosphate or polar head groups with positively charged or polar residues on the intracellular side of the receptor (Fig 6). As a result, time-averaged membrane thickness profiles across DOPG-containing MD simulations reveal that DOPG phospholipids cluster more strongly around A2aR than DOPC (Fig 6A–6C). In particular, four high occupancy DOPG interaction sites at specific intracellular receptor regions can be identified (Fig 6B and 6C). These correspond to areas between TM1 and H8, between TM3-TM4 and intracellular loop 2 (ICL2), and on the respective intracellular surfaces of TM5 and TM6 (Fig 6D–6G). In these sites, specific protein-lipid H-bonds and electrostatic interactions can be identified, including DOPG interaction with: i) a pair of tryptophan residues at the intracellular side of TM1 (W29$^{1.55}$ and W32$^{1.58}$), ii) neighbouring arginines on TM4 and ICL2 (R111$^{34.52}$, R120$^{4.41}$), iii) a pair of arginines on TM5 (R199$^{5.60}$,

75

Publications
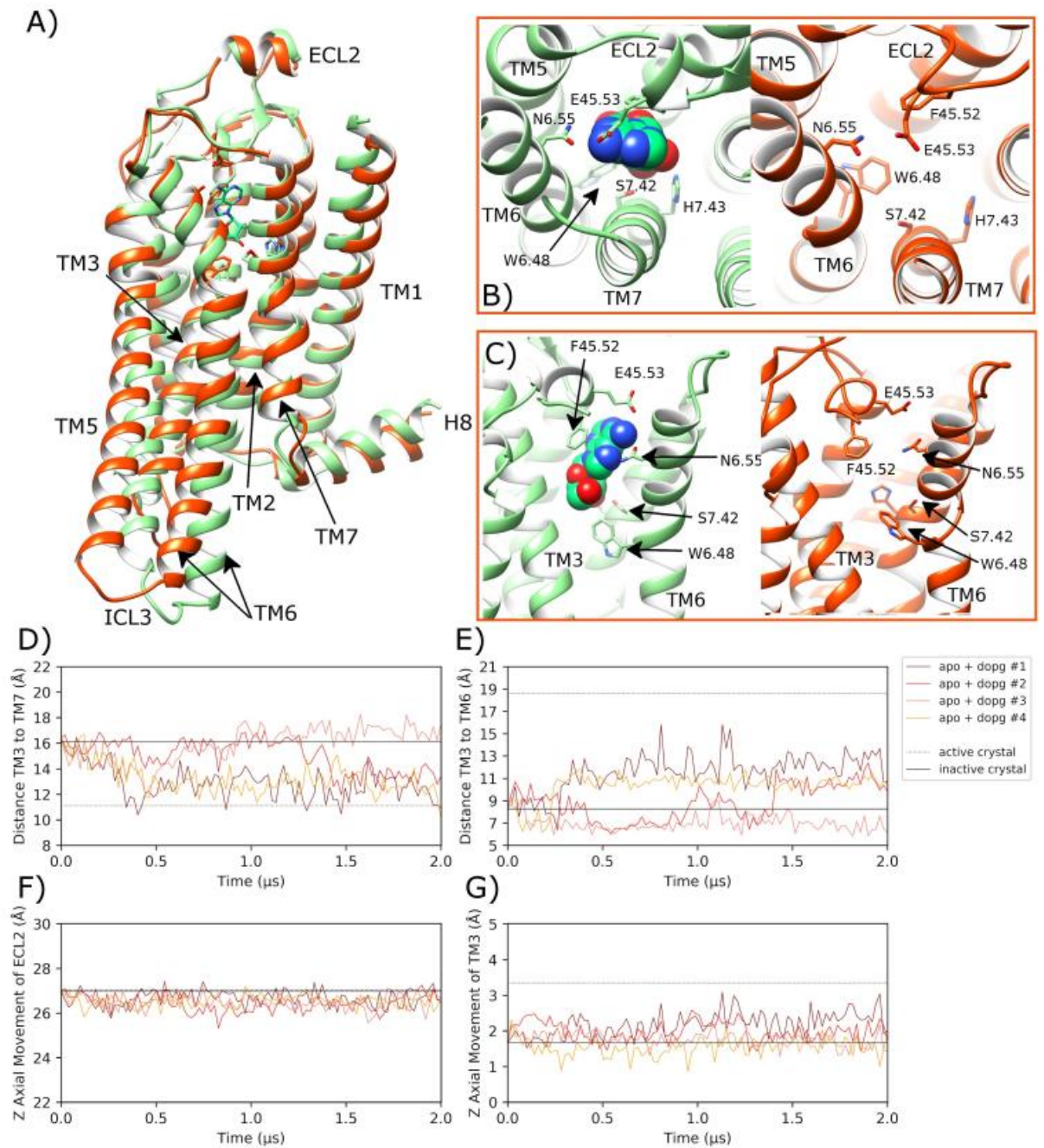
Fig 5. Transition towards an alternative intermediate conformation of apo A2aR in a DOPG membrane. A) Comparison of the intermediate state crystal structure of A2aR (PDB entry: 2YDO, light green) with bound adenosine and an MD-generated apo conformation achieved within a DOPG membrane (orange, belonging to replica #1 from 1.6 μs), showing B) and C) selected residues delineating the orthosteric pocket. ECL2 and TM helices are labelled where applicable. D) Distance between

PLOS COMPUTATIONAL BIOLOGY

TM3-TM7 (from Cα atoms of R102$^{3.50}$ and Y288$^{7.53}$, respectively) during MD simulations, starting from the inactive crystal structure (PDB entry: 4EIY). E) Distance between TM3-TM6 (from Cα atoms of R102$^{3.50}$ and E228$^{6.30}$, respectively). F) and G) Vertical movement of ECL2 and TM3, respectively. MD simulations are performed in quadruplicate. Corresponding flat-lines show the observed distance in the active (PDB entry: 6GDG) and inactive (PDB entry: 4EIY) A2aR crystal structures.

https://doi.org/10.1371/journal.pcbi.1007818.g005

R206$^{5.67}$), iv) a lysine-histidine couple on TM6 (H230$^{6.32}$, K233$^{6.35}$). Each of these protein-lipid interactions is observed across all replicas in a DOPG membrane and marked by particularly stable lipid binding modes. For example, in several trajectories, a single DOPG molecule closely interacts with residue H230$^{6.32}$ continuously for 2 μs or, in others, one lipid is exchanged for another after 500–1000 ns and the interaction is re-established (S13 Fig).

By way of comparison, only two high occupancy protein-lipid interaction sites are observed in DOPC membranes: between TM1-TM2 and TM4 and, to a lesser extent, between TM3 and TM4 on the other side of the receptor (Fig 6A). It is particularly noticeable that DOPC phospholipids are not seen to cluster around TM5 or TM6 like with DOPG (Fig 6B and 6C). Interestingly, the TM1-TM2-TM4 external cavity is recognized as containing the cholesterol consensus motif or CCM, which in active A2aR appears to favourably bind membrane cholesterol and could account for its experimentally observed enhancement of receptor signalling [69, 77]. Interestingly, in our MD simulations, this cavity instead sequesters DOPC phospholipids, which might provide an opposite effect to cholesterol, potentially suggesting competition between these two molecules. In terms of comparison between DOPG and cholesterol, the binding of phospholipids to the intracellular surfaces of TM5 and TM6 may potentially share similarities with a reported second binding-site of cholesterol in a hydrophobic external crevice between TM5 and TM6 [104]. As cholesterol is an uncharged molecule, its precise mode of interaction is likely different to the electrostatic nature of anionic DOPG, meaning these two molecular species might theoretically be able to co-bind the receptor in this area. However, the exact function of cholesterol binding in this location in terms of receptor activation is difficult to verify as it was observed within MD simulations of the antagonist-bound inactive receptor (which remains inactive) and because crystal structures of active A2aR lack co-crystallized cholesterol [104].

Of the three replicas in a DOPG membrane where TM6 conformational change is observed (#1, #2, #4), concomitant rotameric changes in the sidechain of W246$^{6.48}$ are seen as it moves from g+ to trans (S8 Fig). This feature is similar to that observed with bound adenosine in a DOPC membrane and suggests that W246$^{6.48}$ acts as an activation switch (or at least facilitator to an intermediate receptor state) even if no agonist is bound. Also noteworthy, different degrees of TM6 conformational change appear to correlate with the duration W246$^{6.48}$ maintains a continuous trans conformation. For example, in replicas #2 and #4, where W246$^{6.48}$ adopts a trans conformation for ~250 ns and ~800 ns, respectively, the distance between ionic lock residues located on TM3 and TM6 (R102$^{3.50}$ and E228$^{6.30}$) increases up to a maximum of 12.4 Å and 11.9 Å, respectively, as TM6 moves outwards (Fig 5E). This level of conformational change in TM6 is comparable to that which occurs in a DOPC membrane when adenosine is bound and suggests formation of a similar intermediate receptor state (S14 Fig). However, in replica #1, W246$^{6.48}$ maintains a trans conformation for 1.5 μs after an initial rapid switch and TM6 is seen to undergo a more considerable conformational change, establishing a distance from TM3 of up to 15.8 Å (Fig 5E). Although only transient in nature, this degree of TM6 conformational change is close to that observed in the active G protein-bound A2aR crystal structure [25]. This suggests formation of an intermediate receptor conformation that is "enhanced" and different from the others (Fig 5A). Indeed, this is further supported by TM6 RMSD, which increases up to 6.0 Å (S6 Fig) while RMSD of the TM domain temporarily reaches 2.2 Å compared to the active crystal state before regressing (S5 Fig). Together these
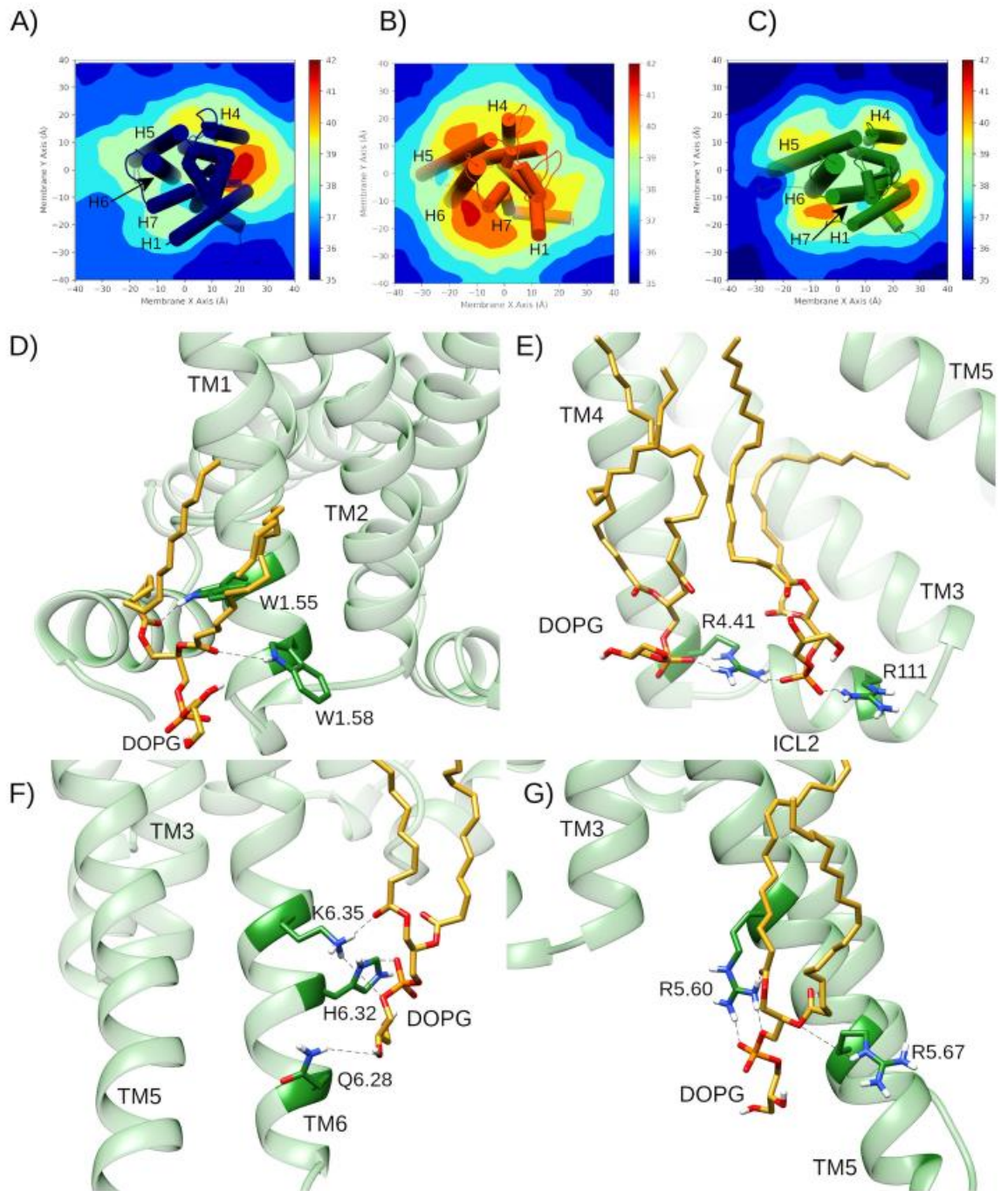
77

78

Fig 6. Membrane thickness and allosteric protein-lipid interactions during MD simulations of A2aR. Average membrane thickness measurements across 2 µs MD simulations of A2aR in A) DOPC with bound adenosine (replica #1), B) DOPG in apo (replica #2), and C) DOPG with bound adenosine (replica #1). D-G) Specific intracellular protein-lipid interactions of adenosine-bound A2aR in a DOPG membrane during 2.0 µs MD simulation (replica #1). D) Allosteric interaction between polar residues on TM1 (W29$^{1.55}$ and W32$^{1.58}$) in A2aR (green) with a DOPG lipid (gold). Electrostatic and H-bond interactions between charged/polar residues on: E) TM4 and ICL2 (R111$^{34.52}$, R120$^{4.41}$), F) TM6 (Q226$^{6.28}$, H230$^{6.32}$, K233$^{6.35}$) and G) TM5 (R199$^{5.60}$, R206$^{5.67}$) with DOPG lipids (gold).

data suggest the receptor reaches a transient conformation close to the active state before returning to a less-active, more conventional intermediate state. On the other hand, replica #3 shows that A2aR in a DOPG membrane can remain in an inactive-like state throughout. This demonstrates that the physical effect of a DOPG membrane on apo A2aR is variable over a two-microsecond time-period.

Finally, in addition to allosteric protein-lipid interactions formed at the receptor surface, the outward orientation of TM6 in a DOPG membrane can be further assisted by formation of a specific protein-lipid salt-bridge at the intracellular side of the receptor interior, which has previously been observed to occur in homologous β2-adrenergic and CB1 receptors [50, 53, 105]. This particular allosteric interaction is possible because of the internalization of a single DOPG lipid from the lower leaflet into the G protein binding-site between TM6 and TM7 (Fig 7A). Specifically, it is stabilized by an electrostatic interaction between DOPG phosphate group and R102$^{3.50}$ sidechain on TM3 (Fig 7A), which normally forms part of the TM3-TM6 ionic-lock in the inactive receptor state. This protein-lipid interaction is found to occur on a consistent basis in all four replicas in DOPG and is stable in three, persisting for more than 1.5 µs in each case (Fig 7C). Furthermore, it appears to be especially suited to DOPG lipids as it is not observed in any of the simulations performed in DOPC. This is likely due to the bulky hydrophobic head-group of phosphatidylcholine (PC) lipids, which are seemingly unable to penetrate the TM6-TM7 gap to the same extent as the smaller hydrophilic head-group of phosphatidylglycerol (PG) lipids [105]. However, despite the prominence and eye-catching nature of this allosteric interaction, it does not by itself guarantee receptor activation or transition to an intermediate receptor conformation as demonstrated by lack of receptor activation in replica #3 (Fig 5). In this particular replica, allosteric interaction between a DOPG lipid and lysine-histidine couple on the exterior of TM6 (H230$^{6.32}$, K233$^{6.35}$) is less stable compared to other replicas. Therefore, lipid interaction with TM6 appears more important than penetration of a lipid into the G protein binding-site between TM6 and TM7.

Adenosine-bound A2aR in DOPG membrane reaches active conformation

In MD simulations of adenosine-bound A2aR in DOPG, unlike in DOPC, the agonist displays higher positional stability across all four replicas and remains in a binding pose that is consistent with the adenosine-bound crystal [93], as well as the NECA-bound active crystal state [25] (Fig 8B). This is confirmed by an average ligand RMSD of 1.4 Å (0.6 SD) (Fig 8D) and average ligand conformational fluctuation (RMSF) of 1.1 Å (0.6 SD) (Fig 8E) across all four replicas. As a result, bound adenosine sustains key protein-ligand interactions for longer compared to corresponding simulations in a DOPC membrane. For example, regarding ECL2, aromatic stacking between F168$^{45.52}$ and the bicyclic ligand core is observed for 55.2% (11.9 SD) of the time on average, while H-bonding with E169$^{45.53}$ shows an average occupancy of 29.2% (9.5 SD) (S15 Fig). These interactions appear to consistently shift ECL2 upwards by an average of 1.2 Å (0.4 SD) (S4 Fig) with an average loop RMSD of 3.1 Å (1.1 SD) across all replicas. This conformational change is not observed as consistently with bound adenosine in a DOPC membrane (S4 Fig), which suggests protein-DOPG allosteric interactions also have an effect in agonist-bound receptor states. Furthermore, in a DOPG membrane, the ribose hydroxyl
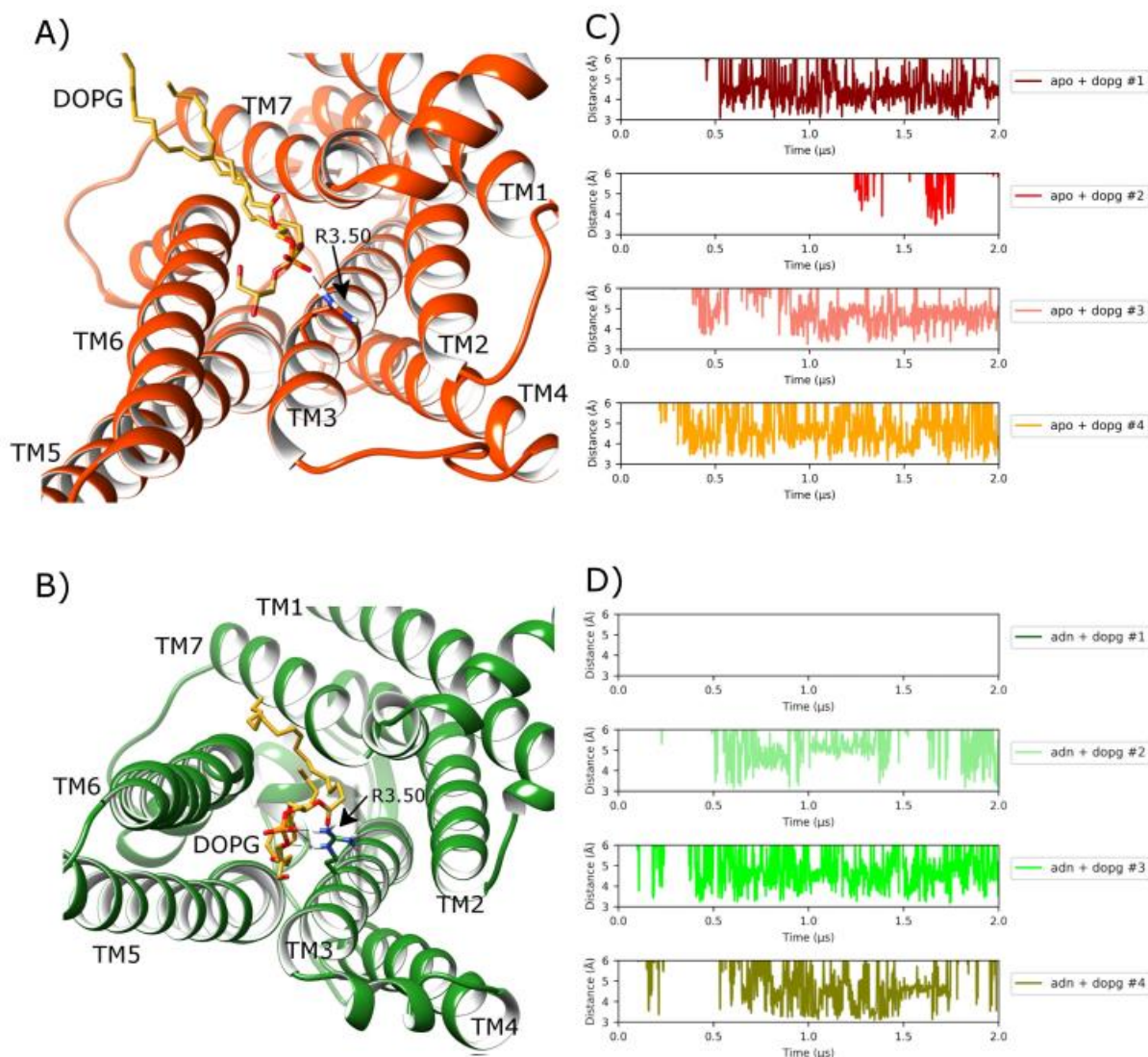
Fig 7. Protein-lipid allosteric interaction with the ionic-lock in MD simulations of A2aR in a DOPG membrane. A) Intracellular view of A2aR where ionic-lock residue R102$^{3.50}$ electrostatically interacts with a DOPG lipid, which intrudes between TM6 and TM7 into the G protein binding-site in apo state (orange) (belonging to replica #4 from 1.8 μs), and B) with bound adenosine (green) (belonging to replica #2 from 1.6 μs). Protein-lipid interaction distance over time between R102$^{3.50}$ sidechain and lipid phosphate group in four replicas of A2aR in DOPG membrane in C) apo state and D) adenosine-bound (ADN), respectively.

groups of adenosine make stronger H-bonds with S277$^{7.52}$ and H278$^{7.53}$ on TM7 with average occupancies of 59.3% (13.8 SD) and 41.8% (19.4 SD), respectively (S15 Fig). At the same time, N253$^{6.55}$ forms a stable protein-ligand H-bond with average occupancy of 95.0% (5.4 SD) across all replicas in DOPG (S15 Fig). In light of these effects on ligand stability and extracellular conformational changes, adenosine-bound A2aR displays the same four protein-DOPG
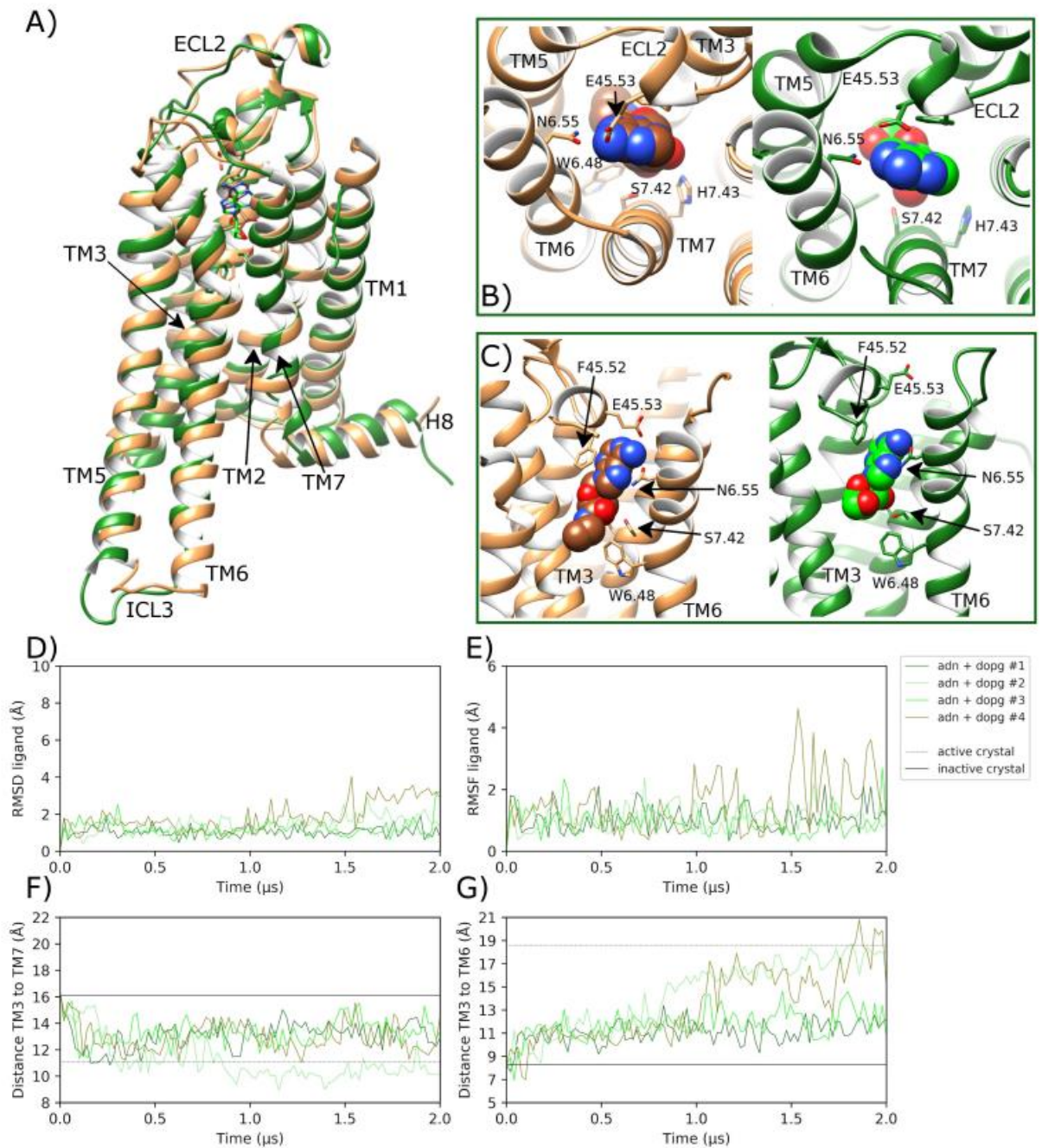
Fig 8. Transition towards an active-like state of A2aR in MD simulations with bound adenosine in a DOPG membrane. A) Comparison of the MD-generated conformation of A2aR bound to adenosine (ADN) within a DOPG membrane (green, belonging to replica #2 from 0.7 μs) with the active crystal structure of A2aR with bound NECA (brown, PDB entry: 6GDG), showing B) and C) protein-agonist interactions in the orthosteric pocket with adenosine and NECA atoms displayed as

UAB
Universitat Autònoma
de Barcelona

Publications

INc
Institut de
Neurociències

spheres. ECL2 and TM helices labelled where applicable. D) RMSD of bound adenosine (calculated with respect to initial docking pose). E) Conformational fluctuation (RMSF) of adenosine. F) Distance between TM3-TM7 (from Cα atoms of R102$^{3.50}$ and Y288$^{7.53}$, respectively) during MD simulations starting from the inactive crystal structure (PDB entry: 4EIY). G) Distance between TM3-TM6 (from Cα atoms of R102$^{3.50}$ and E228$^{6.30}$, respectively). MD simulations are performed in quadruplicate. Corresponding flat-lines show the observed distance in the active (PDB entry: 6GDG) and inactive (PDB entry: 4EIY) A2aR crystal structures.

allosteric interaction hot-spots as seen with the apo state in DOPG: TM1-H8, TM3-4-ICL2, TM5, and TM6 (Fig 6B and 6C). Closer inspection reveals the same specific intracellular protein-lipid interactions as observed in the apo state (Fig 6D–6G) but with increased stability of interaction between the lysine-histidine couple on the intracellular surface of TM6 (H230$^{6.32}$, K233$^{6.35}$) and a DOPG molecule (S13 Fig). This is suggestive of an allosteric pathway acting through TM6 for two-way communication between bound agonist in the orthosteric pocket and bound intracellular lipids.

As a consequence of protein-lipid electrostatic interactions at the intracellular side of the receptor (Fig 6D–6G) and stable adenosine binding, profound receptor conformational changes are observed in TM helices. Firstly, in replicas #1 and #3, TM3 moves upwards by a maximum of 1.9 and 1.6 Å, respectively, and by an average of 0.8 Å (0.4 SD) across all replicas (S7 Fig). This vertical shift matches that observed in the fully active crystal structure of A2aR and results in an average L95$^{3.43}$ RMSD from the inactive state of 3.1 Å (0.8 SD) (S7 Fig), as TM3 undergoes axial rotation. Likewise, across all replicas, respective TM3-TM5 (S9 Fig) and TM3-TM7 (Fig 8F) distances rapidly reach and even surpass those seen in the fully active crystal structure (mean (SD) distances: 22.1 Å (2.6) and 12.5 Å (1.5), respectively). This suggests the receptor is activating across all replicas with inward movement of TM7, upwards movement of TM3 and outward movement of TM5 all occurring within 100 ns.

Meanwhile, the sidechain of W246$^{6.48}$ rapidly moves from g+ to trans within 200 ns in three out of four replicas (S8 Fig), which assists more consistent conformational change in TM6 (Fig 8G). However, only in replicas #2 and #4, does TM6 continue to move outwards enough to establish a TM3-TM6 distance that matches the active crystal state (maximum values of 18.6 Å and 20.4 Å, respectively) within the final 400 ns of each replica (Fig 8G). This degree of conformational change corresponds to a maximum TM6 RMSD of 7.8 Å and 8.4 Å, and a minimum of 2.3 Å compared to TM6 in the active crystal (S6 Fig). This degree of movement can be directly correlated with particularly stable DOPG binding to the intracellular surface of TM6 via positively charged residues: H230$^{6.32}$ and K233$^{6.35}$ (S13 Fig). Likewise, following a similar trend to TM6, receptor RMSD exceeds 4.9 Å in replicas #2 and #4, and reaches a minimum of 2.2 and 2.3 Å compared to the active crystal (S5 Fig), respectively. These conformational changes allow water molecules to penetrate the core of the receptor, forming a continuous channel from the bottom of the orthosteric pocket to the intracellular space, unlike in the apo state in DOPC where the core is mostly desolvated (Fig 9A and 9B). In addition, the adenosine-bound state shows less water density in its orthosteric pocket compared to the apo state, which is fully hydrated. This is because the agonist displaces several water molecules as well as creating a narrower binding pocket, which tends to eliminate even more waters, as has been previously proposed in GPCR activation [27]. Interestingly, the observed movement of W246$^{6.48}$ disrupts its water-mediated interaction with D52$^{2.50}$ seen in the apo state in DOPC (Fig 9C and 9D). Indeed, recent NMR studies have suggested that W246$^{6.48}$ is involved in the same receptor micro-switch as D52$^{2.50}$ [63]. This could mean that in order for TM6 to move outwards and for TM3 to move upwards, the water network that connects W246$^{6.48}$ and D52$^{2.50}$ needs to be broken. As such, when W246$^{6.48}$ toggles into its trans position, it makes a new water-mediated H-bond with bound adenosine via a pair of water molecules (Fig 9D). This exact interaction is not observed in the adenosine-bound

Publications
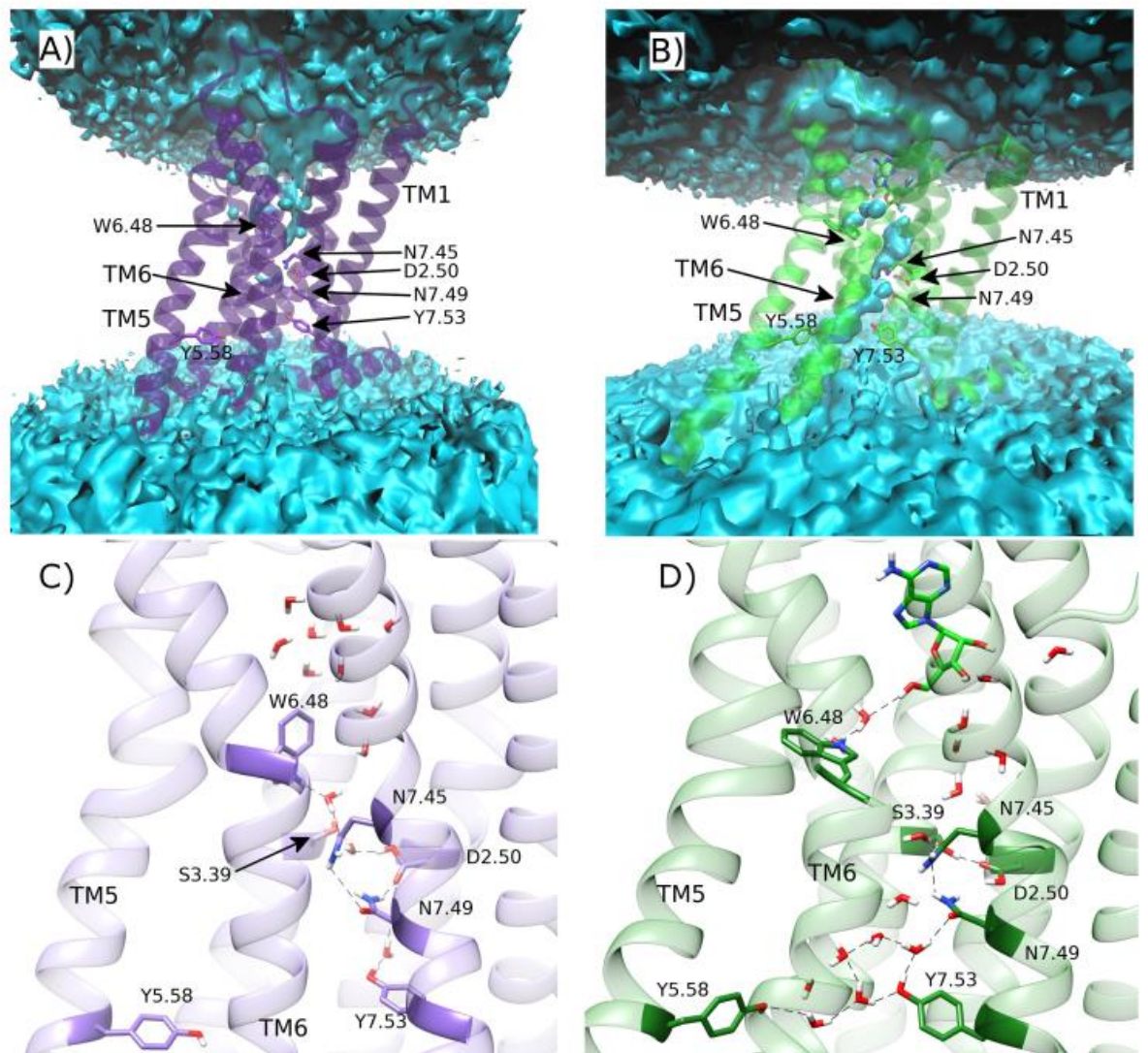
Fig 9. Comparison of water-mediated polar networks in the core of A2aR during MD simulations. Average water density of A) apo A2aR in DOPC membrane, and B) A2aR bound to adenosine within a DOPG membrane (green) over respective replica #1 trajectories. Respective water molecule distribution snapshots at C) 1.5 µs and D) 1.3 µs. Water-mediated hydrogen bonds are represented as dotted lines.

intermediate A2aR crystal structure even though the same pair of water molecules are co-crystallized (S16 Fig). Nevertheless, our MD simulations suggest it may play a role in the transition to a fully active receptor state. In addition, a direct interaction is formed between D52$^{2.50}$ and S91$^{3.39}$ in the core of the receptor, which can be observed in the adenosine-bound crystal structure (S16 Fig). These residues are connected to N280$^{7.45}$, N284$^{7.49}$ and Y288$^{7.53}$ on the NPxxY motif of TM7, as well as Y197$^{5.58}$ on TM5, via numerous water-mediated interactions (Fig

9D). Perhaps most notably, waters also play a role in the reorientation of Y197$^{5.58}$ and Y288$^{7.53}$ side-chains towards each other, which form a stabilizing residue-residue interaction in G protein-bound active crystal structures [24, 25, 106]. Interestingly, some of these waters have also been co-crystallized in the high-resolution inactive and medium-resolution adenosine-bound A2aR crystal structures [29, 93] (S16 Fig), supporting their involvement in A2aR activation as observed in our MD simulations and in other GPCRs [33].

It should be noted however that, although A2aR obtains a full set of active-like conformational features in replicas #2 and #4 (Fig 8), no one single receptor conformation is consistently stabilized. This is likely due to the absence of a bound G protein, which if present would presumably stabilize the precise receptor conformation observed in the G protein-bound A2aR crystal [25]. Instead, in our system, the activated free receptor appears to explore a wider landscape of active-like metastable conformations, especially in replica #4 where TM5 and TM6 obtain orientations more outward than the active crystal structure (S17 Fig). Indeed, recent NMR data has identified two different and distinct active conformational states of A2aR [61]. This appears to fit with our data as we are able to identify at least two distinct active-like receptor conformations, which have appreciable difference in TM5, TM6 and TM7 (S18 Fig). Conformational fluctuation observed in active-like states of A2aR may also be a consequence of allosteric intrusion of a single DOPG lipid between TM6 and TM7 into the G protein binding-site of the receptor (Fig 7). This protein-lipid allosteric interaction was previously observed with the apo state in DOPG and reoccurs here in replicas #1, #3 and #4, although not in replica #2. Interestingly, this seems to exert a destabilizing effect on the active-like receptor conformation obtained in replica #4, which sees TM6 moves further outwards in the process. On the contrary, in replica #2, with no internalized lipid molecule, receptor conformational change appears more gradual and stable. Therefore, this particular protein-lipid interaction may lead to alternative active-like receptor conformations or may simply be detrimental to sustained receptor activation in general. On the contrary, in replica #1 and 3, TM6 does not reach the fully active conformation and instead the receptor remains in an intermediate-like state, which is mostly consistent with the adenosine-bound A2aR crystal structure [93]. This demonstrates that even in conducive conditions, with bound adenosine and anionic phospholipid membrane, full receptor activation is not guaranteed within a time period of two microseconds.

NECA is a more potent agonist than adenosine

In order to contrast the endogenous agonist (adenosine) with the effects of a potent synthetic agonist, quadruplicated MD simulations were performed from the inactive state with bound NECA in DOPC and DOPG membranes. These MD simulations reveal several similarities but key differences between the biological effect of the two agonists. Firstly, bound NECA is comparatively more stable in the orthosteric pocket in both membrane types than adenosine (S19 Fig, S20 Fig). However, NECA stability is enhanced by a DOPG membrane (S20 Fig), like that observed with adenosine. In particular, in a DOPG membrane relative to DOPC, NECA makes a closer and more stable H-bond with residue S207$^{7.42}$ on TM7 (mean (SD) H-bond occupancies of 67.8% (18.8) and 55.2% (16.3), respectively; S21 Fig, S22 Fig). Likewise, when comparing both agonists in a DOPC membrane, NECA makes a stronger and more stable H-bond with S207$^{7.42}$ than adenosine (mean (SD) occupancies of 55.2% (16.3) and 30.4% (23.6), respectively; S11 Fig, S21 Fig). This difference may explain the extra potency of NECA, which in DOPC results in the receptor reaching an intermediate conformation in 4/4 replicas, and in DOPG results in the receptor obtaining an active-like conformation in 3/4 replicas and at least partial activation in the fourth (S20 Fig, S21 Fig). This shows, like with bound adenosine, that a DOPG membrane enhances the effectiveness of NECA through positive allosteric

84

modulation of bound phospholipids on the intracellular side of the receptor, which interact in the same way as observed previously e.g. with residue R102[3.50] (S23 Fig). The cumulative effects of bound phospholipids and agonist are observed to have profound consequences on the overall population of receptor conformations, which can be defined according to key inter-helical TM3-TM6 and TM3-TM7 distances (Fig 10, S24 Fig, S25 Fig). Furthermore, MD simulations with the more potent NECA agonist clearly reveal that agonist-mediated receptor activation results in approximately equal formation of two distinct active-like receptor conformations, as previously proposed by NMR experiments [41]. One of these conformations has a comparatively wider separation between TM3, TM6, and TM7 helices and resembles the G protein-bound active crystal structure, while the other has relatively closer TM helices but is still active-like (Fig 10).

Protein-protein docking reproduces the G protein-bound A2aR crystal interaction

In order to validate that A2aR bound to adenosine or NECA in a DOPG membrane is indeed able to reach an active receptor conformation at a functional level, we docked the co-crystallized $G_s\alpha$ protein[25] into MD-generated active-like conformations of A2aR obtained during each replica (as well as re-docking back into the active A2aR crystal structure as a control). In the two replicas with bound adenosine or three replicas with bound NECA where A2aR reaches the fully active conformation, $G_s\alpha$ is able to dock into the intracellular G protein binding-site without any steric clashes with TM helices or ICL1 and 2 (Fig 11). Mainly, adequate docking is achieved due to proper separation of TM5/TM6 from TM3. The re-docking of the active crystal structure of A2aR with $G_s\alpha$ generates an interface docking score of -7.9 (no units, I_sc range from 0.0 to -10.0; more negative is better with -5.0 representing a threshold for respectable interaction [107]) (Fig 11A, S3 Table), while an MD-generated conformation with bound adenosine in DOPG from replica #2 with $G_s\alpha$ gives a score of -7.7 and an RMSD for $G_s\alpha$ of 0.8 Å (Fig 11B, S3 Table). Likewise, with bound NECA in DOPG, replica #3 with $G_s\alpha$ also gives a score of -7.7 and an RMSD for $G_s\alpha$ of 1.1 Å (S3 Table). This supports a proper mode of interaction between $G_s\alpha$ and A2aR bound to adenosine or NECA in a DOPG membrane. On the contrary, MD-generated receptor conformations in an intermediate or inactive state (in DOPG without bound agonist or in DOPC with or without bound agonist) only obtain I_sc docking scores from -3.3 to -6.1 and $G_s\alpha$ RMSD of 4.9–8.3 Å (S3 Table).

Discussion

The relatively recent availability of high-resolution crystal and cryo-EM structures of GPCRs in different states has facilitated understanding of factors governing their process of activation. These structures have been informative in elucidating the molecular basis for A2aR activation and ligand binding in particular, and have also opened up avenues for studying the role of receptor dynamics and receptor conformation ensembles [42, 61–64]. Interestingly, A2aR has also been crystallized with different interacting lipids [29, 80, 81, 88, 92, 94], which highlights the importance of phospholipids in the process of stabilizing different receptor conformations [69, 77]. Here we have performed unbiased high-throughput MD simulations of A2aR, starting from the inactive crystal structure [29] with or without bound agonists: adenosine or NECA, in PC or PG homogeneous lipid environments to give a deeper understanding of the receptor activation process and cooperative forces between agonist and phospholipids.

From our results, when A2aR is embedded in different phospholipid membranes, anionic PG lipids preferentially cluster around four intracellular areas of the protein: TM1-H8, TM3-TM4-ICL2, TM5, and TM6. On the other hand, neutral PC lipids cluster around just
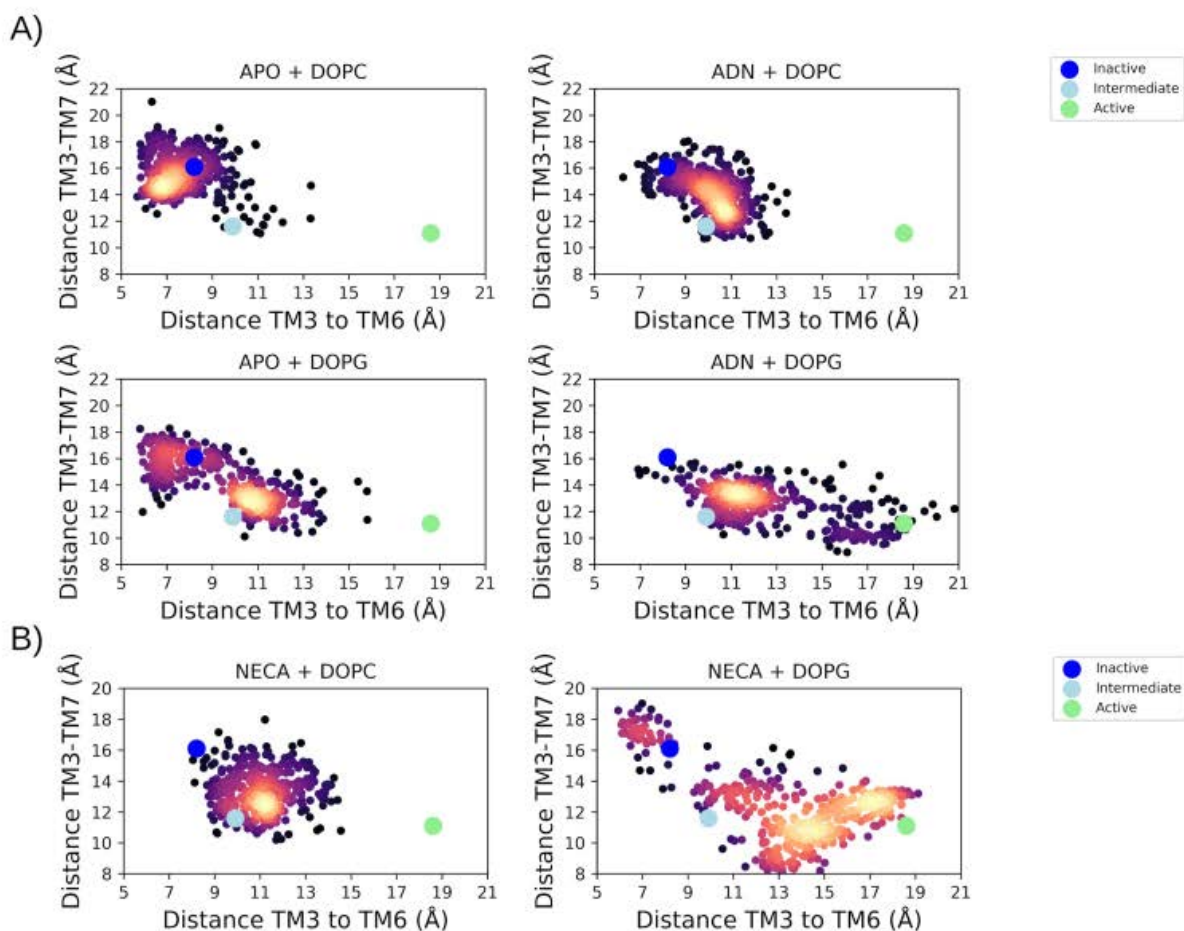
85

Fig 10. The two-dimensional collective variable (CV) space of A2aR activation and receptor conformations during respective MD simulations: A) apo or with bound adenosine (ADN); B) with bound NECA. CVs correspond to distances between ionic lock residues R3.50 and E6.30 (TM3-TM6), and residues R3.50 and Y7.53 (TM3-TM7). The reference distances from inactive, intermediate and active crystal structures are shown as blue, cyan, and green dots, respectively. Frequency of receptor conformation is represented by a "heat" scale (low: black, high: yellow).

two intracellular areas: a cavity formed by TM1-TM2-TM4 and to a lesser extent TM3-TM4. The primary interaction site for PC is consistent with a previously described intracellular interaction site for cholesterol, which is also a neutral and mostly hydrophobic molecule. Through its binding, cholesterol has been reported to stabilize the active receptor conformation [69, 77]. This poses the possibility of PC lipids and cholesterol competing at the same location and exerting different influences over receptor activity. Likewise, cholesterol has been suggested to also bind between TM5 and TM6, which could conceivably potentiate allosteric effects of PG lipids in this area. Although an intriguing question, cholesterol binding is beyond the scope of this study, which as a relatively weak and slow process (compared to phospholipids) would necessitate much longer MD simulations and preclude execution of quadruplicates [108]. In terms of protein-phospholipid interactions on the extracellular side of the receptor, we also
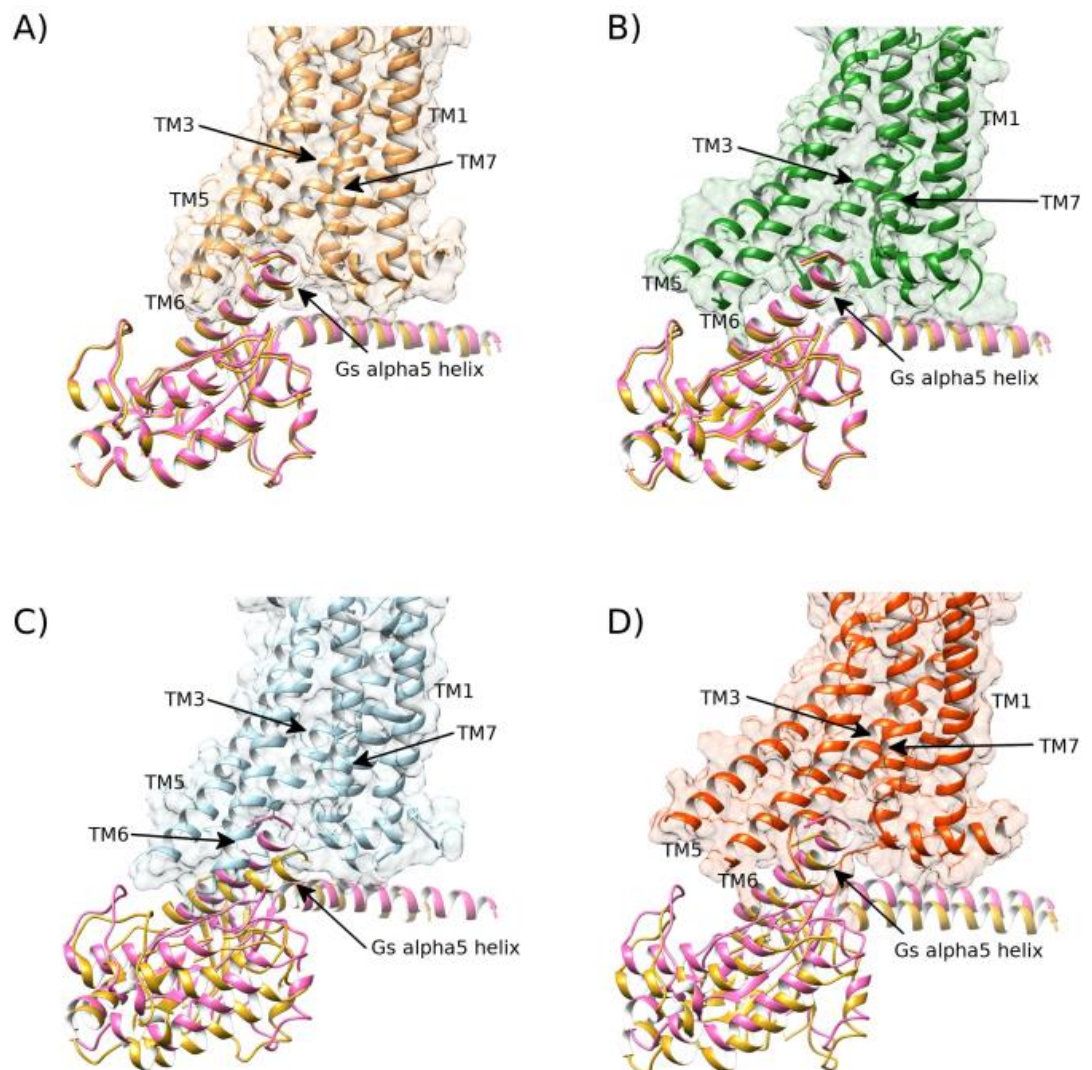
Fig 11. The MD-generated receptor conformation of A2aR bound to adenosine in DOPG membrane is able to bind co-crystallized G$_s$-alpha protein in the same way as the active-state crystal structure (PDB id: 6GDG). A) The crystal structure of the active state of A2aR (brown) bound to its co-crystallized G$_s$-alpha protein (pink, PDB id: 6GDG) and its re-docked G$_s$-alpha subunit superimposed (gold). B) MD-generated active-like conformation of A2aR bound to adenosine in a DOPG membrane (green, belonging to replica #2 from 1.6 µs) docks G$_s$-alpha protein (gold) in similar fashion to the active crystal (pink). C) Intermediate conformation of A2aR, bound to adenosine in DOPC membrane (blue, belonging to replica #4 from 1.3 µs) fails to properly dock G$_s$-alpha protein (gold) compared to its active crystal position (pink). D) Intermediate conformation of apo A2aR in DOPG membrane (red, belonging to replica #1 from 1.6 µs) partially docks G$_s$-alpha protein (gold) compared to its active crystal position (pink).

observe some binding of phospholipids in the hydrophobic interface between TM1 and TM7 as has been previously proposed in some GPCRs [109]. However, in our MD simulations these are not as physically stable as interactions at the intracellular side (hence, relative lack of clustering intensity in Fig 6) and are seemingly not specific to either PC or PG lipids. One potential

functional outcome of having several high occupancy intracellular allosteric sites for anionic PG lipids means that they may regulate multiple local conformational dynamics of the receptor. In particular, three of four PG-interaction hot spots correlate with positions of TM3, TM5 and TM6, which are key helices in the activation process of class A GPCRs, including A2aR [16, 27]. These specific protein-lipid interactions are mainly mediated by electrostatic contacts between positively charged sidechains and negatively charged lipid phosphate groups and tend to favour the outward movement of the cytoplasmic halves of TM5 and TM6, thus aiding intracellular conformational change. As such, there is a correlation between sustained binding of PG lipids to intracellular regions of TM6 and enhanced TM6 conformational change, resulting in more efficient G protein docking, rearrangement of the internal water-mediated polar network, tryptophan sidechain toggling, more stable protein-agonist H-bonding, and increased stabilization of ECL2. This creates a multidirectional allosteric network where different entities affect the action of others. ECL2 is thought to play an important role in receptor signalling, controlling access to the orthosteric pocket and recognition of agonists [110]. Indeed, disruption of the conserved disulphide bridge between ECL2 and TM3 largely diminishes receptor function [110, 111]. In DOPG, ECL2 tends to be stabilized in a higher position above the orthosteric pocket than in PC membranes (S26 Fig), which appears to assist TM3 conformational change and vice versa, as well as enhancing the stability of bound agonist. This indirect relationship between membrane phospholipids and ECL2 may provide a structural explanation for how GPCRs exhibit different ligand efficacies in different cell lines [110, 112]. On the contrary, PC lipids, which have a more bulky and hydrophobic head group than DOPG, are less suited for forming electrostatic or H-bond protein-lipid interactions with the receptor [50]. Thus, this absence of sustained protein-lipid interaction triggers fewer intracellular conformational changes in the receptor, preferentially favouring an inactive conformation, which, in turn, destabilizes agonist binding and promotes ECL2 flexibility.

As a result, the apo state of A2aR in PC membranes remains inactive, which prevents adequate G protein docking. This is expected and in agreement with previously published MD simulations [65, 72]. In contrast, two distinct intermediate receptor conformations can be identified in the apo state in a DOPG membrane, which depend partly on the stability of key allosteric protein-lipid interactions. One of these conformations is consistent with the intermediate state observed with bound agonist in PC membranes, as well as the agonist-bound A2aR crystal structure [93], whilst the other is "enhanced" with a more outwards TM6 conformation that is closer to an active-like state, albeit not physically stable. This is a striking result, because A2aR has been reported to signal across cellular membranes in the absence of agonists [42, 113], which our MD simulations suggest may be dependent on phospholipid content. Moreover, these two different intermediate receptor conformations are notable because NMR experiments have identified two distinct intermediates of A2aR, which were resolved in apo and agonist-stabilized states, respectively [41]. Taken together, this demonstrates that like other homologous GPCRs [50, 53], A2aR can be positively modulated by PG lipids even without bound agonist. On the other hand, neutral PC lipids induce little or no conformational change over a microsecond time-window and instead depend on agonist binding for reaching an intermediate receptor state. Indeed, it may be the case that a millisecond time period is required, or concomitant G protein binding, for the receptor to reach a fully active state in this type of membrane. These findings also raise the classical debate on induction vs selection in receptor activation [114]. Our results are compatible with both views because if an agonist is able to induce similar receptor conformational changes as the receptor is able to achieve by itself (in an appropriate membrane environment) then it would also be able to stabilize (select) an active receptor conformation if the orthosteric pocket is not obstructed [114–116].

Interestingly, the possibility that A2aR activation includes both induced fit and conformational selection mechanisms has been proposed by others on the basis of NMR experiments [61].

In agreement with previously published data [70], adenosine displays high mobility in the pocket of A2aR when embedded in a neutral PC membrane, while NECA shows noticeably greater stability. This translates into more consistent receptor activation by NECA, which is a more potent agonist. However, when adenosine is reasonably stable, the receptor transitions towards an intermediate conformation with TM3 moving partially upwards due to steric influences on this helix, as well as protein-ligand interactions with ECL2, which connects with TM3 via a disulphide bridge [110, 111]. This is interesting because such TM3 transitions occur less consistently in the apo state in DOPG despite favourable intracellular protein-lipid allosteric interactions. This suggests that agonist binding drives conformational change that favours a particular pathway of receptor activation, which leads to a more consistent intermediate conformation. Conversely, the pattern of receptor activation mediated by DOPG lipids directs the apo receptor to more diverse conformational changes, which potentially involve various intermediate conformations or different activation pathways, as has been recently proposed by MD simulations in a cholesterol-rich membrane [78]. Indeed, here in the apo state, the predominant activation pathway proceeds through TM6 first, while with bound agonist, a faster pathway proceeds through TM3 and TM7, and later TM6. Likewise, the existence of different receptor intermediate conformations suggest natural variation in the A2aR activation process, which could perhaps offer opportunities in drug design if a pathway through one intermediate conformation was deemed therapeutically more advantageous than another [106].

Agonist-bound A2aR in DOPG is able to activate via a two-step activation mechanism, starting from inactive to intermediate and then to an active-like state. Receptor activation begins with conformational changes in the orthosteric pocket and the triggering of micro-switches in the receptor core followed by the inward shift of TM7, upwards axial tilt of TM3 and outward movement of TM5. This is combined with a partial outward displacement and rotation of TM6, which brings together the intracellular ends of TM5 and TM6, which gradually adjust their inter-helical contacts, consistent with the intermediate agonist-bound crystal structure [93]. As a result, this modifies water-mediated hydrogen-bond networks in the core of the receptor, ultimately leading to the formation of a continuous water column extending from the orthosteric pocket to the intracellular side of the receptor and connecting residues Y288$^{7.53}$ and Y197$^{5.58}$, which have previously been shown to be an activation-associated micro-switch [93, 106]. Secondly, TM6 moves even further out, achieving the fully outward conformation of the G protein-bound active crystal structure [24, 25]. This extra conformational change in TM6 appears to be facilitated by the membrane and not agonist, at least according to our observations in a microsecond timescale. As a consequence, G$_s\alpha$ protein can be docked into agonist-bound DOPG-modulated receptor conformations, obtaining similar fits to that observed in the G$_s$ protein-bound crystal structure [25]. In all aspects, these MD-generated active-like receptor states are remarkably consistent with the crystallized NECA-bound active state [24, 25]. Furthermore, these results are reproducible across different MD simulations with different agonists, revealing consistent cooperativity between agonist and DOPG lipids in the A2aR activation process. It also supports the notion that anionic phospholipids are crucial for activation of class A GPCRs in general [49, 50, 53]. Intriguingly, it is possible to differentiate between two distinct active-like receptor conformations, which are dependent on slightly different TM6 and TM7 orientations. These observations are supported by recent NMR studies where A2aR appeared able to have more than one active state, although their precise conformational details were not revealed [61]. Most notably across our MD simulations, protein-DOPG interactions assist receptor activation through enhanced stabilization of bound agonist in the orthosteric pocket. This effect is strongest for the endogenous agonist

89

adenosine, which is able to form more stable protein-ligand H-bonds as a result but it is also apparent with NECA, thus providing an explanation of how ligand efficacy might be dependent on lipid environment [65, 77]. Achieving a stable binding pose of agonist appears a precondition for obtaining the fully active receptor state and is a likely consequence of more stable protein-ligand interactions with TM6, TM7, as well as ECL2. These observations are similar to experimental data reported in β2AR, where DOPG lipids improve the binding of agonists and activation of the receptor [49]. In this context, it is logical that DOPG lipids stabilize the binding of agonists in A2aR.

The cooperative effects between ligands and lipids are the underlying principle of the present study. The cooperativity described in this work corresponds to allosteric interactions in the broad sense, i.e. specific protein-lipid interactions affecting the binding stability of the agonist and binding of the agonist focusing the functional effect of protein-lipid interactions, inducing specific conformational changes in the receptor. Most notably, DOPG lipids accelerate the activation process of an agonist-bound receptor, which in a microsecond timeframe enables full receptor activation to occur more consistently but does not always guarantee it. Interestingly, when comparing A2aR activation with that of CB1 [53], it is striking that activation of the former only proceeds with PG lipids while activation of the latter proceeds in both PG and PC lipid environments, albeit faster and more reliably with PG. This may be because these two receptors show different levels of activity. In particular, CB1 is known to have high constitutive activity and may be easier to activate relative to other GPCRs [8]. For example, as previously noted in the core of CB1, the semi-conserved residue L$^{6.44}$ may confer higher TM6 flexibility, which may allow for easier receptor conformational change [53]. The equivalent residue in A2aR is F242$^{6.44}$, which as a bulkier amino acid may enhance hydrophobic interactions in the receptor core that help to stabilize the inactive state. This could be one reason why activation of A2aR is observed more scarcely in the microsecond timescale relative to CB1 and why protein-lipid interactions appear to be so important for A2aR [77]. Presumably, if our MD simulations were extended into the millisecond time range, then we might observe full A2aR activation in PC membranes. However, this is currently an untestable hypothesis. Irrespective of this, we consider our findings to be sufficiently compelling and potentially enable a better understanding of receptor activation, agonist efficacy, and protein-lipid positive allosteric modulation in A2aR, especially as its observed dynamics broadly mirror those of other class A GPCRs, such as muscarinic M2, CB1 and opsin [43, 53, 117].

Methods

A2aR modelling

The high-resolution crystal structure of the antagonist-bound inactive state of human adenosine A2a receptor (A2aR) (PDB entry: 4EIY) [29] was selected and co-crystallized ligands, waters and ions were removed. By using CHIMERA software [118], crystallographic missing atoms were added (on residues Q148, E161, R220, R293) and non-native residues were removed or converted to native (at N-terminus: G-1 and A0 deleted, P1 substituted for M) in order to obtain a *wt* receptor sequence. In addition, the non-native fusion protein located between L208 (on TM5) and E219 (on TM6) was excised and the crystallographic missing intracellular loop 3 (ICL3) was modelled (residues 209 to 218) by basing it upon the equivalent region of thermostabilized A2aR crystal structure (PDB entry: 3PWH) [79] using MODELLER v9.14 [119].

In order to validate MD generated conformations, the intermediate adenosine-bound (PDB entry: 2YDO), intermediate NECA-bound (PDB entry: 2YDV) [93] and NECA-bound fully active (PDB entry: 6GDG) [25] A2aR crystal structures were utilized. Non-native residues

90

were converted to wt in both structures and crystallographic missing ICL3 and extracellular loop 2 (ECL2) were completed in each respective structure using relevant A2aR crystal structures: PDB entries 3PWH [79] or 5G53 [24] as templates with MODELLER software [119].

The structures of adenosine and NECA were retrieved from their respective crystal structures of thermostabilized adenosine/NECA-bound A2aR (PDB entry: 2YDO/2YDV) [93]. As these thermostabilized receptor states are in a similar conformation to our utilized inactive state (PDB entry: 4EIY) [29], docking of adenosine and NECA was performed by firstly superimposing receptor structures (PDB entries: 2YDO or 2YDV onto 4EIY) with CHIMERA [118] and then, secondly, by transferring the coordinates of the agonist from one to the other whilst avoiding steric conflicts where possible. Finally, in order to optimize protein-ligand contacts, the resulting complexes were energy-minimized in the AMBER-14SB force-field [120] with CHIMERA [118].

Molecular dynamics (MD) simulations

Eight all-atom MD systems were constructed using CHARMM-GUI [121], consisting of A2aR in an inactive state (as described above) with or without bound adenosine or NECA embedded in DOPG, DOPC or POPC homogeneous lipid bilayers (80 Å x 80 Å), respectively. The position of the receptor in the membrane(s) is as reported by the OPM database for A2aR PDB entry: 4EIY [29]. Each receptor-membrane system was solvated with TIP3P water molecules above and below the membrane, and an overall concentration of 0.3 M K$^+$Cl$^-$ with ratio of positive/negative ions adjusted accordingly (automatically during CHARMM-GUI system setup) in order to maintain net zero charge in each system. On the protein, eight residues were protonated according to previously published MD simulation protocols specific for A2aR [44, 72, 74, 78, 122], as well as being consistent with protocols used for other homologous class A GPCRs [47, 53, 95, 117, 123]: E13$^{1.39}$, D52$^{2.50}$ (both receptor core), D101$^{3.49}$, E212$^{5.73}$, E219$^{6.21}$, E228$^{6.30}$, H230$^{6.32}$, E294$^{8.49}$ (all intracellular) (with Ballesteros numbering [99] as superscript, which indicates relative residue position along each TM helix). Membrane, water and protein parameters were generated according to the CHARMM36 force-field [124] and adenosine parameters were generated according to CGenFF v1.0.0 [125]. MD simulations were performed with ACEMD software [126] on specialized GPU-computer hardware. Briefly, each receptor-membrane system was equilibrated for 28 ns at 300 K (Langevin thermostat) and 1 atmosphere (Berendsen barostat) using a 4 fs time-step and electrostatics cut-off of 9.0 Å. During the initial 8 ns of equilibration, protein (and ligand) heavy atoms were harmonically restrained and progressively released over 2 ns steps. During the final 20 ns of equilibration, no restraints were applied. For each receptor-membrane system, a production run of 2 μs was performed without restraints under the same conditions, with second, third and fourth replicate simulations executed in each case to verify observations (in case of POPC systems, only a second replicate was executed). This constitutes a total production simulation time of 56 μs across the eight systems.

MD simulation analysis

Structural comparison was carried out for receptor conformations sampled from MD simulations against A2aR crystal structures: fully active (PDB entry: 6GDG) [25], intermediate (PDB entries: 2YDO and 2YDV) [93], or inactive state (PDB entry: 4EIY) [29]. In each MD simulation trajectory, in order to assess membrane effects on receptor conformation, root mean square deviation (RMSD) of Cα atoms of TM domain (TM helices 1–7), as well as TM6 and ECL2 by themselves, were calculated with VMD software [127] v1.9.2. To further validate receptor state, multiple internal measurements were made including: χ1 dihedral angle of

W246$^{6.48}$, vertical movement of TM3 and ECL2 according to distance offset in the Z axis (perpendicular to the membrane) from centre of mass of each to centre of mass of TM domain, distance between Cα atoms of residue pairs: R102$^{3.50}$ and E228$^{6.30}$, R102$^{3.50}$ and Q207$^{5.68}$, and R102$^{3.50}$ and Y288$^{7.53}$, representing proximity between helices: TM3-TM6, TM3-TM5 and TM3-TM7, respectively. The following lipid measurements were calculated: i) protein-lipid distance between residues R102$^{3.50}$ (sidechain terminal nitrogen atoms) or H230$^{6.32}$ (sidechain centre-of-mass) and closest lipid phosphate group (centre-of-mass) using PLUMED v2.4 [128]; (ii) membrane thickness as average distance from lower to upper-leaflet phosphorus atoms as per default settings of MEMBPLUGIN [129] within VMD [127]. For the ligand: (i) protein-ligand π–π stacking was calculated as function of distance between centre of mass of aromatic ring of F$^{45.52}$ and adenine ring of adenosine or NECA (applied criteria for interaction: 3.5 Å); ii) "Hydrogen Bonds" function within VMD was used to analyse protein-ligand H-bond occupancies (applied criteria of donor-acceptor distance: 3.5 Å and 60° angle); (iii) ligand conformational change in terms of RMSD with respect to initial position; and (iv) ligand positional stability expressed in terms of root mean square fluctuation (RMSF) were made within VMD. Internal water molecule density was measured by the function "Volmap" within VMD using default options. Criteria for water-mediated interactions in the receptor were defined by two residues forming hydrogen bonds with the same water molecule or a pair of hydrogen bonded water molecules. All analytical plots were generated using Matplotlib version 3.0.0 [130].

Protein-Protein docking

As validation of receptor state, co-crystallized G$_s$α protein (PDB entry: 6GDG) [25] was docked to the intracellular side of selected MD-generated A2aR conformations (as well as redocked into the original fully active A2aR crystal structure as a control). The Rosetta online server (ROSIE) was used for protein-protein docking [107] with the following protocol: (i) receptor conformation taken from simulation of its respective MD simulation and superimposed over the active crystal structure of A2aR containing its G$_s$α protein (PDB entry: 6GDG) [25], (ii) the original crystallized receptor removed from the complex, (iii) the structure of G$_s$α moved 3.0 Å away from the MD-generated receptor conformation so that there are no steric clashes and clear space is apparent between both proteins, (iv) protein-protein docking is initiated. As ICL3 is long and potentially highly flexible, it was removed prior to protein-protein docking (during step iii) so as not to create unavoidable steric conflicts with G$_s$α during docking (ROSIE is not able to move backbone of loops). However, all other loops and receptor structural elements were maintained.

Supporting information

S1 File. Details of the simulations. This zip file contains a README document with data and software description as well as topology, scripts and input files within the corresponding generated folders.
(ZIP)

S1 Fig. Docking of NECA in the inactive crystal structure of adenosine A2a receptor (A2aR). A) Molecular structure of NECA. Comparison of B) co-crystallized NECA (lime) in agonist-bound A2aR crystal structure (PDB entry: 2YDV, light green), and C) docked NECA (magenta) in the inactive crystal structure of A2aR (PDB entry: 4EIY, pink). Selected residues participating in ligand binding are displayed. Extracellular loop (ECL) 2 and transmembrane

92

(TM) helices 5–7 are labelled.
(TIF)

S2 Fig. Structural comparison between A2aR intermediate and inactive crystal structures.
A) structural superposition of the intermediate adenosine-bound crystal structure (PDB entry: 2YDO, light green) on the inactive-state crystal structure (PDB entry: 4EIY, pink). B) Comparative positioning of residue L$^{3.43}$ located on TM3 and rotameric state of W$^{6.48}$ on TM6. C) Intracellular distance between residues R$^{3.50}$ and Y$^{7.53}$ on TM3 and TM7 (indicated by dashed lines) before/after receptor conformational change. D) Distance between residues R$^{3.50}$ and Q$^{5.68}$ (indicated by dashed lines). E) Partial separation of ionic-lock residues R$^{3.50}$ and E$^{6.30}$ on TM3 and TM6 (indicated by dashed lines). Relevant structural features are labelled: extracellular loops (ECL) 1, 2 and 3, and transmembrane (TM) helices 1–3, 5–7.
(TIF)

S3 Fig. Structural comparison between A2aR active and inactive crystal structures. A) structural superposition of the active-state crystal structure (PDB entry: 6GDG, brown) on the inactive-state crystal structure (PDB entry: 4EIY, pink). B) Proposed scheme of activation for A2aR, including rotation and upwards axial movement of TM3, outwards movement of TM5, rotation plus outward movement of TM6, and inwards movement of TM7. C) Comparative positioning of residue L$^{3.43}$ located on TM3 and rotameric state of W$^{6.48}$ on TM6. D) Intracellular conformational change of TM5 with increased separation (indicated by dashed lines) between residues R$^{3.50}$ and Q$^{5.68}$ after receptor activation. E) Intracellular comparison of distance between residues R$^{3.50}$ and Y$^{7.53}$ after receptor activation (indicated by dashed lines). F) Intracellular conformational change of TM6 and separation (indicated by dashed lines) of ionic-lock residues R$^{3.50}$ and E$^{6.30}$ after receptor activation. Relevant structural features are labelled: intracellular loop (ICL) 2, extracellular loops (ECL) 1, 2 and 3, and transmembrane (TM) helices 1–3, 5–7.
(TIF)

S4 Fig. Comparison of conformational change of extracellular loop 2 (ECL2) in MD simulations of A2aR. A) RMSD of ECL2 from the starting inactive A2aR crystal structure (PDB entry: 4EIY). B) Vertical movement of ECL2 along Z-axis (containing residues: G142-A173). MD simulations are performed in quadruplicate, with or without bound adenosine (ADN) in DOPC or DOPG homogeneous membranes.
(TIF)

S5 Fig. Conformational change of helix bundle of A2aR in MD simulations. A) RMSD of helices 1–7 from the inactive crystal structure (PDB entry: 4EIY) and B) with respect to the active crystal structure of A2aR (PDB entry: 6GDG). MD simulations are performed in quadruplicate, with or without bound adenosine (ADN) in DOPC or DOPG homogeneous membranes.
(TIF)

S6 Fig. TM6 conformational change of A2aR in MD simulations. A) RMSD from the starting inactive A2aR crystal structure (PDB entry: 4EIY) and B) with respect to the active A2aR crystal structure (PDB entry: 6GDG). MD simulations are performed in quadruplicate, with or without bound adenosine (ADN) and in DOPC or DOPG homogeneous membranes.
(TIF)

S7 Fig. Assessment of conformational change along TM3 during MD simulations of A2aR. A) RMSD of residue L3.43 on TM3 compared to the inactive crystal structure (PDB entry: 4EIY) and B) assessment of vertical movement of TM3 along Z-axis. MD simulations are

93

performed in quadruplicate with or without bound adenosine (ADN) and in DOPC or DOPG homogeneous membranes.
(TIF)

S8 Fig. Assessment of rotameric conformational change of residue W6.48 on TM6. A) W246$^{6.48}$ rotameric switch starting from *gauche*(-) (285°) (belonging to replica #2 from 1.7 μs in APO embedded in DOPC, in magenta) to trans (180°) during MD simulation replica #4 from 1.8 μs in DOPG with bound adenosine (in green). B) χ1 dihedral angle of residue W246$^{6.48}$ over time. MD simulations are performed in quadruplicate, with or without bound adenosine (ADN) in DOPC or DOPG homogeneous membranes.
(TIF)

S9 Fig. Comparison of TM3-TM5 inter-helical distance in MD simulations of A2aR. Distance between TM3-TM5 is measured between Cα atoms of R102$^{3.50}$ and Q207$^{5.68}$. MD simulations are performed in quadruplicate, with or without bound adenosine (ADN) in DOPC or DOPG homogeneous membranes.
(TIF)

S10 Fig. Alternative binding pose of adenosine in A2aR in DOPC membrane. A) Superposition of the intermediate crystal structure of A2aR (PDB entry: 2YDO, light green) and an MD-generated conformation achieved within a DOPC membrane bound to adenosine (in blue, belonging to replica #1 at 1.9 μs) showing B) and C) ligand atoms as spheres and selected residues making protein-ligand interactions as sticks. Intracellular loop (ICL) 3, extracellular loop (ECL) 2, and transmembrane (TM) helices 1–3 and 5–7 are labelled.
(TIF)

S11 Fig. Assessment of key protein-ligand interactions in MD simulations of adenosine-bound A2aR embedded in DOPC membrane. A) Left: distance of F$^{45.52}$ with respect to ribose moiety of adenosine (ADN). Right: frequency (%) of protein-ligand π-π stacking (within range of 0.0 to 4.0 Å) over 2 μs. B) Evaluation of protein-ligand H-bond distances formed by residues: N253$^{6.55}$, E169$^{45.53}$, H278$^{7.43}$, S277$^{7.42}$ (N—O or O—O). C) Mean protein-ligand interactions (%) and protein-ligand H-bond occupancies per replica (%) for selected residues.
(TIF)

S12 Fig. MD simulation data of adenosine A2a receptor (A2aR) with or without bound adenosine (ADN) starting from the inactive receptor crystal structure (PDB id: 4EIY) in a POPC membrane. Top row: RMSD and conformational fluctuation (RMSF) of bound adenosine ligand; second row: TM3-TM7 and ionic lock (TM3-TM6) inter-helical distances; third row: RMSD of whole TMD (TMs 1–7) or only TM6; fourth row: RMSD compared to active crystal structure (PDB id: 6GDG) of whole TMD (TMs 1–7) or only TM6; fifth row: χ1 dihedral angle of W246$^{6.48}$ on TM6 starting from *gauche*(-) crystal position (285°), and vertical movement of extracellular loop 2 (ECL2); bottom row: vertical movement of TM3 and RMSD of ECL2. MD simulations are performed in duplicate in POPC homogeneous membranes.
(TIF)

S13 Fig. Protein-lipid interaction between closest DOPG molecule and residue H2306.32 in MD simulations of A2aR with or without bound adenosine. A) Residues H230$^{6.32}$ and K233$^{6.35}$ on TM6 of A2aR in apo state (orange) and B) A2aR with bound adenosine (green) interacting with DOPG lipid (gold). Histidine-lipid interaction distances over time in four replicas of A2aR in DOPG membrane in C) apo state and D) adenosine-bound (ADN), respectively.
(TIF)

94

S14 Fig. Intermediate conformation of the apo state of A2aR in a DOPG membrane. A) Comparison of the intermediate crystal structure of A2aR (PDB entry: 2YDO, light green) and an MD-generated apo conformation achieved within a DOPG membrane (in red, belonging to replica #2 at 1.6 μs) showing B) and C) selected residues delineating the orthosteric pocket. Intracellular loop (ICL) 3, extracellular loop (ECL) 2, and transmembrane (TM) helices 1–3, 5–7 are labelled.
(TIF)

S15 Fig. Assessment of key protein-ligand interactions in MD simulations of adenosine-bound A2aR embedded in DOPG membrane. A) Left: distance of $F^{45.52}$ with respect to ribose moiety of adenosine (ADN). Right: frequency (%) of protein-ligand π-π stacking (within range of 0.0 to 4.0 Å) over 2 μs. B) Evaluation of protein-ligand H-bond distances formed by residues: $N253^{6.55}$, $E169^{45.53}$, $H278^{7.43}$, $S277^{7.42}$ (N—O or O—O). C) Mean protein-ligand interactions (%) and protein-ligand H-bond occupancies per replica (%) for selected residues.
(TIF)

S16 Fig. State-dependent water-mediated polar network across the ZM241385-bound and adenosine-bound A2aR crystal structures. The water network retrieved from: A) the inactive crystal structure (PDB entry: 4EIY, pink) and B) the intermediate crystal structure (PDB entry: 2YDO, light green). Residues and ligands are shown as sticks and water molecules are shown as red spheres.
(TIF)

S17 Fig. Alternative active-like conformational state of A2aR generated in an MD simulation with bound adenosine in a DOPG membrane. A) Comparison of an MD-generated conformation of A2aR bound to adenosine within a DOPG membrane (in green, belonging to replica #4 at 1.8 μs) with the active crystal structure of A2aR (brown, PDB entry: 6GDG) showing B) and C) ligand atoms as spheres and residues making protein-ligand interactions as sticks. Intracellular loop (ICL) 3, extracellular loop (ECL) 2, and transmembrane (TM) helices 1–3, 5–7 are labelled.
(TIF)

S18 Fig. Comparison of two active-like receptor conformations generated in MD simulations of A2aR with bound adenosine in a DOPG membrane. A) Comparison of an MD-generated conformation of A2aR bound to adenosine within DOPG belonging to replica #2 (at 1.6 μs, green) with respect to replica #4 (at 1.8 μs, olive green) showing B) and C) ligand atoms as spheres and residues making protein-ligand interactions as sticks. Intracellular loop (ICL) 3, extracellular loop (ECL) 2, and transmembrane (TM) helices 1–3, 5–7 are labelled.
(TIF)

S19 Fig. MD simulation data of adenosine A2a receptor (A2aR) with bound NECA starting from the inactive receptor crystal structure (PDB id: 4EIY) in a DOPC membrane. Top row: RMSD and conformational fluctuation (RMSF) of bound NECA ligand; second row: TM3-TM7 and ionic lock (TM3-TM6) inter-helical distances; third row: RMSD of whole TMD (TMs 1–7) or only TM6; fourth row: RMSD compared to active crystal structure (PDB id: 6GDG) of whole TMD (TMs 1–7) or only TM6; fifth row: χ1 dihedral angle of $W246^{6.48}$ on TM6 starting from *gauche*(-) crystal position (285˚), and vertical movement of extracellular loop 2 (ECL2); bottom row: vertical movement of TM3 and RMSD of ECL2. MD simulations are performed in quadruplicate in DOPC homogeneous membranes.
(TIF)

Publications

S20 Fig. MD simulation data of adenosine A2a receptor (A2aR) with bound NECA starting from the inactive receptor crystal structure (PDB id: 4EIY) in a DOPG membrane. Top row: RMSD and conformational fluctuation (RMSF) of bound NECA ligand; second row: TM3-TM7 and ionic lock (TM3-TM6) inter-helical distances; third row: RMSD of whole TMD (TMs 1–7) or only TM6; fourth row: RMSD compared to active crystal structure (PDB id: 6GDG) of whole TMD (TMs 1–7) or only TM6; fifth row: $\chi 1$ dihedral angle of W246$^{6.48}$ on TM6 starting from *gauche*(-) crystal position (285˚), and vertical movement of extracellular loop 2 (ECL2); bottom row: vertical movement of TM3 and RMSD of ECL2. MD simulations are performed in quadruplicate in DOPG homogeneous membranes.
(TIF)

S21 Fig. Assessment of key protein-ligand interactions in MD simulations of NECA-bound A2aR embedded in DOPC membrane. A) Left: distance of F$^{45.52}$ with respect to ribose moiety of NECA. Right: frequency (%) of protein-ligand π-π stacking (within range of 0.0 to 4.0 Å) over 2 μs. B) Evaluation of protein-ligand H-bond distances formed by residues: N253$^{6.55}$, E169$^{45.53}$, H278$^{7.43}$, S277$^{7.42}$ (N—O or O—O). C) Mean protein-ligand interactions (%) and protein-ligand H-bond occupancies per replica (%) for selected residues.
(TIF)

S22 Fig. Assessment of key protein-ligand interactions in MD simulations of NECA-bound A2aR embedded in DOPG membrane. A) Left: Distance of F$^{45.52}$ with respect to ribose moiety of NECA. Right: frequency (%) of protein-ligand π-π stacking (within range of 0.0 to 4.0 Å) interaction over 2 μs. B) Evaluation of protein-ligand H-bond distances formed by residues: N253$^{6.55}$, E169$^{45.53}$, H278$^{7.43}$, S277$^{7.42}$ (N—O or O—O). C) Mean protein-ligand interactions (%) and protein-ligand H-bond occupancies per replica (%) for selected residues.
(TIF)

S23 Fig. Protein-lipid allosteric interaction with the ionic-lock in MD simulations of NECA-bound A2aR in DOPG membrane. A) Electrostatic interaction between ionic-lock residue R102$^{3.50}$ of A2aR (green) from an intracellular viewpoint and a DOPG lipid, which intrudes between TM6 and TM7 (snapshot belonging to replica #1 at 1.7 μs). B) Protein-lipid interaction distance over time between R102$^{3.50}$ sidechain and lipid phosphate group in four replicas of NECA-bound A2aR in DOPG membrane.
(TIF)

S24 Fig. Frequency distribution of receptor conformations formed during different MD simulations with and without bound adenosine in two different membranes (DOPC or DOPG) according to two different inter-helical distances. A) Population of receptor conformations according to distance between residues R$^{3.50}$ and Y$^{7.53}$ (TM3-TM7), and (B) between ionic lock residues R$^{3.50}$ and E$^{6.30}$ (TM3-TM6). Vertical black lines indicate values of inactive (PDB entry: 4EIY), intermediate (PDB entry: 2YDO) and active (PDB entry: 6GDG) crystal structures.
(TIF)

S25 Fig. Frequency distribution of receptor conformations (according to two inter-helical distances) formed during MD simulations with bound NECA in two different membranes (DOPC or DOPG) or with/without bound adenosine in a POPC membrane. First and second rows: population of receptor conformations according to distance between $^{R3.50}$ and $^{Y7.53}$ (TM3-TM7); third and fourth rows: according to distance between ionic lock residues $^{R3.50}$ and E$^{6.30}$ (TM3-TM6). Vertical black lines indicate values of inactive (PDB entry: 4EIY),

96

intermediate (PDB entry: 2YDO) and active (PDB entry: 6GDG) crystal structures.
(TIF)

S26 Fig. Boxplots of receptor characteristics from MD simulations of adenosine A2a receptor (A2aR) in apo or with bound adenosine (ADN) or NECA in three different membranes. Top row: inter-helical distances between: residues R$^{3.50}$ and Y$^{7.53}$ (TM3-TM7), and ionic lock residues R$^{3.50}$ and E$^{6.30}$ (TM3-TM6); bottom row: vertical movements of extracellular loop 2 (ECL2) and TM3, respectively. MD simulations in DOPG or DOPC were performed in quadruplicate. MD simulations in POPC were performed in duplicate.
(TIF)

S1 Table. Adenosine A2a receptor crystal structures.
(TIF)

S2 Table. Comparison of A2aR crystal structure distances. Comparison of TM3-TM6, TM3-TM5 and TM3-TM7 inter-helical distances in active, intermediate and inactive crystal states.
(TIF)

S3 Table. Evaluation of Gαs protein docking. Comparison of best docking quality of Gα$_s$ protein into inactive, intermediate and active crystals structures, and different MD-generated conformations of A2aR achieved under different conditions and performed in quadruplicate.
(TIF)

Author Contributions

Conceptualization: James A. R. Dalton, Jesús Giraldo.

Formal analysis: Agustín Bruzzese, James A. R. Dalton, Jesús Giraldo.

Funding acquisition: Jesús Giraldo.

Investigation: Agustín Bruzzese, James A. R. Dalton, Jesús Giraldo.

Methodology: Agustín Bruzzese, James A. R. Dalton, Jesús Giraldo.

Resources: Jesús Giraldo.

Supervision: James A. R. Dalton, Jesús Giraldo.

Writing – original draft: Agustín Bruzzese, James A. R. Dalton.

Writing – review & editing: James A. R. Dalton, Jesús Giraldo.

References

1. Fredriksson R, Lagerstrom MC, Lundin LG, Schioth HB. The G-protein-coupled receptors in the human genome form five main families. Phylogenetic analysis, paralogon groups, and fingerprints. Mol Pharmacol. 2003; 63(6):1256–72. https://doi.org/10.1124/mol.63.6.1256 PMID: 12761335

2. Rosenbaum DM, Rasmussen SG, Kobilka BK. The structure and function of G-protein-coupled receptors. Nature. 2009; 459(7245):356–63. https://doi.org/10.1038/nature08144 PMID: 19458711

3. Latorraca NR, Venkatakrishnan AJ, Dror RO. GPCR Dynamics: Structures in Motion. Chem Rev. 2017; 117(1):139–55. https://doi.org/10.1021/acs.chemrev.6b00177 PMID: 27622975

4. Hilger D, Masureel M, Kobilka BK. Structure and dynamics of GPCR signaling complexes. Nat Struct Mol Biol. 2018; 25(1):4–12. https://doi.org/10.1038/s41594-017-0011-7 PMID: 29323277

5. Weis WI, Kobilka BK. The Molecular Basis of G Protein-Coupled Receptor Activation. Annu Rev Biochem. 2018; 87:897–919. https://doi.org/10.1146/annurev-biochem-060614-033910 PMID: 29925258

97

UAB
Universitat Autònoma
de Barcelona

Publications

INc
Institut de
Neurociències

6. Manglik A, Kruse AC. Structural Basis for G Protein-Coupled Receptor Activation. Biochemistry. 2017; 56(42):5628–34. https://doi.org/10.1021/acs.biochem.7b00747 PMID: 28967738

7. Thal DM, Glukhova A, Sexton PM, Christopoulos A. Structural insights into G-protein-coupled receptor allostery. Nature. 2018; 559(7712):45–53. https://doi.org/10.1038/s41586-018-0259-z PMID: 29973731

8. Seifert R, Wenzel-Seifert K. Constitutive activity of G-protein-coupled receptors: cause of disease and common property of wild-type receptors. Naunyn Schmiedebergs Arch Pharmacol. 2002; 366(5):381–416. https://doi.org/10.1007/s00210-002-0588-0 PMID: 12382069

9. Wang W, Qiao Y, Li Z. New Insights into Modes of GPCR Activation. Trends Pharmacol Sci. 2018; 39 (4):367–86. https://doi.org/10.1016/j.tips.2018.01.001 PMID: 29395118

10. Zhou XE, Melcher K, Xu HE. Understanding the GPCR biased signaling through G protein and arrestin complex structures. Curr Opin Struct Biol. 2017; 45:150–9. https://doi.org/10.1016/j.sbi.2017.05.004 PMID: 28558341

11. McCorvy JD, Butler KV, Kelly B, Rechsteiner K, Karpiak J, Betz RM, et al. Structure-inspired design of beta-arrestin-biased ligands for aminergic GPCRs. Nat Chem Biol. 2018; 14(2):126–34. https://doi.org/10.1038/nchembio.2527 PMID: 29227473

12. Wingler LM, Elgeti M, Hilger D, Latorraca NR, Lerch MT, Staus DP, et al. Angiotensin Analogs with Divergent Bias Stabilize Distinct Receptor Conformations. Cell. 2019; 176(3):468–78 e11. https://doi.org/10.1016/j.cell.2018.12.005 PMID: 30639099

13. Santos R, Ursu O, Gaulton A, Bento AP, Donadi RS, Bologa CG, et al. A comprehensive map of molecular drug targets. Nat Rev Drug Discov. 2017; 16(1):19–34. https://doi.org/10.1038/nrd.2016.230 PMID: 27910877

14. Jacobson KA, Costanzi S. New insights for drug design from the X-ray crystallographic structures of G-protein-coupled receptors. Mol Pharmacol. 2012; 82(3):361–71. https://doi.org/10.1124/mol.112.079335 PMID: 22695719

15. Xiang J, Chun E, Liu C, Jing L, Al-Sahouri Z, Zhu L, et al. Successful Strategies to Determine High-Resolution Structures of GPCRs. Trends Pharmacol Sci. 2016; 37(12):1055–69. https://doi.org/10.1016/j.tips.2016.09.009 PMID: 27726881

16. Tehan BG, Bortolato A, Blaney FE, Weir MP, Mason JS. Unifying Family A GPCR Theories of Activation. Pharmacol Ther. 2014; 143:51–60. https://doi.org/10.1016/j.pharmthera.2014.02.004 PMID: 24561131

17. Lee Y, Basith S, Choi S. Recent Advances in Structure-Based Drug Design Targeting Class A G Protein-Coupled Receptors Utilizing Crystal Structures and Computational Simulations. J Med Chem. 2018; 61(1):1–46. https://doi.org/10.1021/acs.jmedchem.6b01453 PMID: 28657745

18. Trzaskowski B, Latek D, Yuan S, Ghoshdastider U, Debinski A, Filipek S. Action of molecular switches in GPCRs—theoretical and experimental studies. Curr Med Chem. 2012; 19(8):1090–109. https://doi.org/10.2174/092986712799320556 PMID: 22300046

19. Cong X, Topin J, Golebiowski J. Class A GPCRs: Structure, Function, Modeling and Structure-based Ligand Design. Curr Pharm Des. 2017; 23(29):4390–409. https://doi.org/10.2174/1381612823666170710151255 PMID: 28699533

20. Choe HW, Kim YJ, Park JH, Morizumi T, Pai EF, Krauss N, et al. Crystal structure of metarhodopsin II. Nature. 2011; 471(7340):651–5. https://doi.org/10.1038/nature09789 PMID: 21389988

21. Rasmussen SG, DeVree BT, Zou Y, Kruse AC, Chung KY, Kobilka TS, et al. Crystal structure of the beta(2) adrenergic receptor-Gs protein complex. Nature. 2011; 477:549–57. https://doi.org/10.1038/nature10361 PMID: 21772288

22. Rasmussen SG, Choi HJ, Fung JJ, Pardon E, Casarosa P, Chae PS, et al. Structure of a nanobody-stabilized active state of the beta(2) adrenoceptor. Nature. 2011; 469(7329):175–80. https://doi.org/10.1038/nature09648 PMID: 21228869

23. Kruse AC, Ring AM, Manglik A, Hu J, Hu K, Eitel K, et al. Activation and allosteric modulation of a muscarinic acetylcholine receptor. Nature. 2013; 504(7478):101–6. https://doi.org/10.1038/nature12735 PMID: 24256733

24. Carpenter B, Nehme R, Warne T, Leslie AG, Tate CG. Structure of the adenosine A(2A) receptor bound to an engineered G protein. Nature. 2016; 536(7614):104–7. https://doi.org/10.1038/nature18966 PMID: 27462812

25. Garcia-Nafria J, Lee Y, Bai X, Carpenter B, Tate CG. Cryo-EM structure of the adenosine A2A receptor coupled to an engineered heterotrimeric G protein. Elife. 2018; 7.

26. Huang W, Manglik A, Venkatakrishnan AJ, Laeremans T, Feinberg EN, Sanborn AL, et al. Structural insights into m-opioid receptor activation. Nature. 2015; 524(7565):315–21. https://doi.org/10.1038/nature14886 PMID: 26245379

98

27. Dalton JA, Lans I, Giraldo J. Quantifying conformational changes in GPCRs: glimpse of a common functional mechanism. BMC Bioinformatics. 2015; 16(1):124.

28. Lans I, Dalton JA, Giraldo J. Helix 3 acts as a conformational hinge in Class A GPCR activation: An analysis of interhelical interaction energies in crystal structures. J Struct Biol. 2015; 192(3):545–53. https://doi.org/10.1016/j.jsb.2015.10.019 PMID: 26522273

29. Liu W, Chun E, Thompson AA, Chubukov P, Xu F, Katritch V, et al. Structural basis for allosteric regulation of GPCRs by sodium ions. Science. 2012; 337(6091):232–6. https://doi.org/10.1126/science.1219218 PMID: 22798613

30. Haga K, Kruse AC, Asada H, Yurugi-Kobayashi T, Shiroishi M, Zhang C, et al. Structure of the human M2 muscarinic acetylcholine receptor bound to an antagonist. Nature. 2012; 482(7386):547–51. https://doi.org/10.1038/nature10753 PMID: 22278061

31. Congreve M, Langmead CJ, Mason JS, Marshall FH. Progress in structure based drug design for G protein-coupled receptors. J Med Chem. 2011; 54(13):4283–311. https://doi.org/10.1021/jm200371q PMID: 21615150

32. Angel TE, Gupta S, Jastrzebska B, Palczewski K, Chance MR. Structural waters define a functional channel mediating activation of the GPCR, rhodopsin. Proc Natl Acad Sci U S A. 2009; 106 (34):14367–72. https://doi.org/10.1073/pnas.0901074106 PMID: 19706523

33. Venkatakrishnan AJ, Ma AK, Fonseca R, Latorraca NR, Kelly B, Betz RM, et al. Diverse GPCRs exhibit conserved water networks for stabilization and activation. Proc Natl Acad Sci U S A. 2019; 116 (8):3288–93. https://doi.org/10.1073/pnas.1809251116 PMID: 30728297

34. Mason JS, Bortolato A, Congreve M, Marshall FH. New insights from structural biology into the druggability of G protein-coupled receptors. Trends Pharmacol Sci. 2012; 33(5):249–60. https://doi.org/10.1016/j.tips.2012.02.005 PMID: 22465153

35. Yao X, Parnot C, Deupi X, Ratnala VR, Swaminath G, Farrens D, et al. Coupling ligand structure to specific conformational switches in the b$_2$-adrenoceptor. Nat Chem Biol. 2006; 2(8):417–22. https://doi.org/10.1038/nchembio801 PMID: 16799554

36. Hollingsworth SA, Dror RO. Molecular Dynamics Simulation for All. Neuron. 2018; 99(6):1129–43. https://doi.org/10.1016/j.neuron.2018.08.011 PMID: 30236283

37. Standfuss J, Edwards PC, D'Antona A, Fransen M, Xie G, Oprian DD, et al. The structural basis of agonist-induced activation in constitutively active rhodopsin. Nature. 2011; 471(7340):656–60. https://doi.org/10.1038/nature09795 PMID: 21389983

38. Lee Y, Choi S, Hyeon C. Communication over the Network of Binary Switches Regulates the Activation of A2A Adenosine Receptor. PLoS Comput Biol. 2015; 11(2):e1004044. https://doi.org/10.1371/journal.pcbi.1004044 PMID: 25664580

39. Miao Y, McCammon JA. Graded activation and free energy landscapes of a muscarinic G-protein-coupled receptor. Proc Natl Acad Sci U S A. 2016; 113(43):12162–7. https://doi.org/10.1073/pnas.1614538113 PMID: 27791003

40. Manglik A, Kim TH, Masureel M, Altenbach C, Yang Z, Hilger D, et al. Structural Insights into the Dynamic Process of beta-Adrenergic Receptor Signaling. Cell. 2015; 161(5):1101–11. https://doi.org/10.1016/j.cell.2015.04.043 PMID: 25981665

41. Prosser RS, Ye L, Pandey A, Orazietti A. Activation processes in ligand-activated G protein-coupled receptors: A case study of the adenosine A2A receptor. Bioessays. 2017; 39(9).

42. Ye L, Van Eps N, Zimmer M, Ernst OP, Prosser RS. Activation of the A2A adenosine G-protein-coupled receptor by conformational selection. Nature. 2016; 533(7602):265–8. https://doi.org/10.1038/nature17668 PMID: 27144352

43. Miao Y, Nichols SE, Gasper PM, Metzger VT, McCammon JA. Activation and dynamic network of the M2 muscarinic receptor. Proc Natl Acad Sci U S A. 2013; 110(27):10982–7. https://doi.org/10.1073/pnas.1309755110 PMID: 23781107

44. Li J, Jonsson AL, Beuming T, Shelley JC, Voth GA. Ligand-dependent activation and deactivation of the human adenosine A(2A) receptor. J Am Chem Soc. 2013; 135(23):8749–59. https://doi.org/10.1021/ja404391q PMID: 23678995

45. Kobilka BK, Deupi X. Conformational complexity of G-protein-coupled receptors. Trends Pharmacol Sci. 2007; 28(8):397–406. https://doi.org/10.1016/j.tips.2007.06.003 PMID: 17629961

46. Kim TH, Chung KY, Manglik A, Hansen AL, Dror RO, Mildorf TJ, et al. The role of ligands on the equilibria between functional states of a G protein-coupled receptor. J Am Chem Soc. 2013; 135 (25):9465–74. https://doi.org/10.1021/ja404305k PMID: 23721409

47. Dror RO, Arlow DH, Maragakis P, Mildorf TJ, Pan AC, Xu H, et al. Activation mechanism of the beta2-adrenergic receptor. Proc Natl Acad Sci U S A. 2011; 108(46):18684–9. https://doi.org/10.1073/pnas.1110499108 PMID: 22031696

99

48. Dror RO, Pan AC, Arlow DH, Borhani DW, Maragakis P, Shan Y, et al. Pathway and mechanism of drug binding to G-protein-coupled receptors. Proc Natl Acad Sci U S A. 2011; 108(32):13118–23. https://doi.org/10.1073/pnas.1104614108 PMID: 21778406

49. Dawaliby R, Trubbia C, Delporte C, Masureel M, Van Antwerpen P, Kobilka BK, et al. Allosteric regulation of G protein-coupled receptor activity by phospholipids. Nat Chem Biol. 2016; 12(1):35–9. https://doi.org/10.1038/nchembio.1960 PMID: 26571351

50. Bruzzese A, Gil C, Dalton JAR, Giraldo J. Structural insights into positive and negative allosteric regulation of a G protein-coupled receptor through protein-lipid interactions. Sci Rep. 2018; 8(1):4456. https://doi.org/10.1038/s41598-018-22735-6 PMID: 29535353

51. Lee AG. Biological membranes: the importance of molecular detail. Trends Biochem Sci. 2011; 36 (9):493–500. https://doi.org/10.1016/j.tibs.2011.06.007 PMID: 21855348

52. Dickson CJ, Hornak V, Velez-Vega C, McKay DJ, Reilly J, Sandham DA, et al. Uncoupling the Structure-Activity Relationships of beta2 Adrenergic Receptor Ligands from Membrane Binding. J Med Chem. 2016; 59(12):5780–9. https://doi.org/10.1021/acs.jmedchem.6b00358 PMID: 27239696

53. Diaz O, Dalton JAR, Giraldo J. Revealing the Mechanism of Agonist-Mediated Cannabinoid Receptor 1 (CB1) Activation and Phospholipid-Mediated Allosteric Modulation. J Med Chem. 2019; 62 (11):5638–54. https://doi.org/10.1021/acs.jmedchem.9b00612 PMID: 31095906

54. de Lera Ruiz M, Lim YH, Zheng J. Adenosine A2A receptor as a drug discovery target. J Med Chem. 2014; 57(9):3623–50. https://doi.org/10.1021/jm4011669 PMID: 24164628

55. Ohta A, Sitkovsky M. Role of G-protein-coupled adenosine receptors in downregulation of inflammation and protection from tissue damage. Nature. 2001; 414(6866):916–20. https://doi.org/10.1038/414916a PMID: 11780065

56. Dunwiddie TV, Masino SA. The role and regulation of adenosine in the central nervous system. Annu Rev Neurosci. 2001; 24:31–55. https://doi.org/10.1146/annurev.neuro.24.1.31 PMID: 11283304

57. Morelli M, Carta AR, Jenner P. Adenosine A2A receptors and Parkinson's disease. Handb Exp Pharmacol. 2009(193):589–615. https://doi.org/10.1007/978-3-540-89615-9_18 PMID: 19639294

58. Jespers W, Schiedel AC, Heitman LH, Cooke RM, Kleene L, van Westen GJP, et al. Structural Mapping of Adenosine Receptor Mutations: Ligand Binding and Signaling Mechanisms. Trends Pharmacol Sci. 2018; 39(1):75–89. https://doi.org/10.1016/j.tips.2017.11.001 PMID: 29203139

59. Chen JF, Eltzschig HK, Fredholm BB. Adenosine receptors as drug targets—what are the challenges? Nat Rev Drug Discov. 2013; 12(4):265–86. https://doi.org/10.1038/nrd3955 PMID: 23535933

60. Song W, Yen HY, Robinson CV, Sansom MSP. State-dependent Lipid Interactions with the A2a Receptor Revealed by MD Simulations Using In Vivo-Mimetic Membranes. Structure. 2019; 27 (2):392–403 e3. https://doi.org/10.1016/j.str.2018.10.024 PMID: 30581046

61. Susac L, Eddy MT, Didenko T, Stevens RC, Wuthrich K. A2A adenosine receptor functional states characterized by (19)F-NMR. Proc Natl Acad Sci U S A. 2018; 115(50):12733–8. https://doi.org/10.1073/pnas.1813649115 PMID: 30463958

62. Eddy MT, Gao ZG, Mannes P, Patel N, Jacobson KA, Katritch V, et al. Extrinsic Tryptophans as NMR Probes of Allosteric Coupling in Membrane Proteins: Application to the A2A Adenosine Receptor. J Am Chem Soc. 2018; 140(26):8228–35. https://doi.org/10.1021/jacs.8b03805 PMID: 29874058

63. Eddy MT, Lee MY, Gao ZG, White KL, Didenko T, Horst R, et al. Allosteric Coupling of Drug Binding and Intracellular Signaling in the A2A Adenosine Receptor. Cell. 2018; 172(1–2):68–80 e12. https://doi.org/10.1016/j.cell.2017.12.004 PMID: 29290469

64. Ye L, Neale C, Sljoka A, Lyda B, Pichugin D, Tsuchimura N, et al. Mechanistic insights into allosteric regulation of the A2A adenosine G protein-coupled receptor by physiological cations. Nat Commun. 2018; 9(1):1372. https://doi.org/10.1038/s41467-018-03314-9 PMID: 29636462

65. Ng HW, Laughton CA, Doughty SW. Molecular dynamics simulations of the adenosine A2a receptor in POPC and POPE lipid bilayers: effects of membrane on protein behavior. J Chem Inf Model. 2014; 54 (2):573–81. https://doi.org/10.1021/ci400463z PMID: 24460123

66. Ng HW, Laughton CA, Doughty SW. Molecular dynamics simulations of the adenosine A2a receptor: structural stability, sampling, and convergence. J Chem Inf Model. 2013; 53(5):1168–78. https://doi.org/10.1021/ci300610w PMID: 23514445

67. Rodriguez D, Pineiro A, Gutierrez-de-Teran H. Molecular dynamics simulations reveal insights into key structural elements of adenosine receptors. Biochemistry. 2011; 50(19):4194–208. https://doi.org/10.1021/bi200100t PMID: 21480628

68. Sabbadin D, Ciancetta A, Moro S. Bridging molecular docking to membrane molecular dynamics to investigate GPCR-ligand recognition: the human A(2)A adenosine receptor as a key study. J Chem Inf Model. 2014; 54(1):169–83. https://doi.org/10.1021/ci400532b PMID: 24359090

100

69. Lyman E, Higgs C, Kim B, Lupyan D, Shelley JC, Farid R, et al. A role for a specific cholesterol interaction in stabilizing the Apo configuration of the human A(2A) adenosine receptor. Structure. 2009; 17 (12):1660–8. https://doi.org/10.1016/j.str.2009.10.010 PMID: 20004169

70. Lee JY, Lyman E. Agonist Dynamics and Conformational Selection during Microsecond Simulations of the A(2A) Adenosine Receptor. Biophys J. 2012; 102(9):2114–20. https://doi.org/10.1016/j.bpj.2012.03.061 PMID: 22824275

71. Deganutti G, Moro S. Supporting the Identification of Novel Fragment-Based Positive Allosteric Modulators Using a Supervised Molecular Dynamics Approach: A Retrospective Analysis Considering the Human A2A Adenosine Receptor as a Key Example. Molecules. 2017; 22(5).

72. Caliman AD, Swift SE, Wang Y, Miao Y, McCammon JA. Investigation of the conformational dynamics of the apo A2A adenosine receptor. Protein Sci. 2015; 24(6):1004–12. https://doi.org/10.1002/pro.2681 PMID: 25761901

73. Liu Y, Burger SK, Ayers PW, Vohringer-Martinez E. Computational study of the binding modes of caffeine to the adenosine A2A receptor. J Phys Chem B. 2011; 115(47):13880–90. https://doi.org/10.1021/jp2022049 PMID: 21970461

74. Keranen H, Gutierrez-de-Teran H, Aqvist J. Structural and energetic effects of A2A adenosine receptor mutations on agonist and antagonist binding. PLoS One. 2014; 9(10):e108492. https://doi.org/10.1371/journal.pone.0108492 PMID: 25285959

75. Massink A, Gutierrez-de-Teran H, Lenselink EB, Ortiz Zacarias NV, Xia L, Heitman LH, et al. Sodium ion binding pocket mutations and adenosine A2A receptor function. Mol Pharmacol. 2015; 87(2):305–13. https://doi.org/10.1124/mol.114.095737 PMID: 25473121

76. Deganutti G, Welihinda A, Moro S. Comparison of the Human A2A Adenosine Receptor Recognition by Adenosine and Inosine: New Insight from Supervised Molecular Dynamics Simulations. Chemmedchem. 2017; 12(16):1319–26. https://doi.org/10.1002/cmdc.201700200 PMID: 28517175

77. McGraw C, Yang L, Levental I, Lyman E, Robinson AS. Membrane cholesterol depletion reduces downstream signaling activity of the adenosine A2A receptor. Biochim Biophys Acta Biomembr. 2019; 1861(4):760–7. https://doi.org/10.1016/j.bbamem.2019.01.001 PMID: 30629951

78. Lovera S, Cuzzolin A, Kelm S, De Fabritiis G, Sands ZA. Reconstruction of apo A2A receptor activation pathways reveal ligand-competent intermediates and state-dependent cholesterol hotspots. Sci Rep. 2019; 9(1):14199. https://doi.org/10.1038/s41598-019-50752-6 PMID: 31578448

79. Dore AS, Robertson N, Errey JC, Ng I, Hollenstein K, Tehan B, et al. Structure of the Adenosine A(2A) Receptor in Complex with ZM241385 and the Xanthines XAC and Caffeine. Structure. 2011; 19 (9):1283–93. https://doi.org/10.1016/j.str.2011.06.014 PMID: 21885291

80. Jaakola VP, Griffith MT, Hanson MA, Cherezov V, Chien EY, Lane JR, et al. The 2.6 angstrom crystal structure of a human A2A adenosine receptor bound to an antagonist. Science. 2008; 322 (5905):1211–7. https://doi.org/10.1126/science.1164772 PMID: 18832607

81. Hino T, Arakawa T, Iwanari H, Yurugi-Kobayashi T, Ikeda-Suno C, Nakada-Nakura Y, et al. G-protein-coupled receptor inactivation by an allosteric inverse-agonist antibody. Nature. 2012; 482:237–40. https://doi.org/10.1038/nature10750 PMID: 22286059

82. Batyuk A, Galli L, Ishchenko A, Han GW, Gati C, Popov PA, et al. Native phasing of x-ray free-electron laser data for a G protein-coupled receptor. Sci Adv. 2016; 2(9):e1600292. https://doi.org/10.1126/sciadv.1600292 PMID: 27679816

83. Melnikov I, Polovinkin V, Kovalev K, Gushchin I, Shevtsov M, Shevchenko V, et al. Fast iodide-SAD phasing for high-throughput membrane protein structure determination. Sci Adv. 2017; 3(5): e1602952. https://doi.org/10.1126/sciadv.1602952 PMID: 28508075

84. Martin-Garcia JM, Conrad CE, Nelson G, Stander N, Zatsepin NA, Zook J, et al. Serial millisecond crystallography of membrane and soluble protein microcrystals using synchrotron radiation. IUCrJ. 2017; 4(Pt 4):439–54. https://doi.org/10.1107/S205225251700570X PMID: 28875031

85. Weinert T, Olieric N, Cheng R, Brunle S, James D, Ozerov D, et al. Serial millisecond crystallography for routine room-temperature structure determination at synchrotrons. Nat Commun. 2017; 8(1):542. https://doi.org/10.1038/s41467-017-00630-4 PMID: 28912485

86. Cheng RKY, Segala E, Robertson N, Deflorian F, Dore AS, Errey JC, et al. Structures of Human A1 and A2A Adenosine Receptors with Xanthines Reveal Determinants of Selectivity. Structure. 2017; 25 (8):1275–85 e4. https://doi.org/10.1016/j.str.2017.06.012 PMID: 28712806

87. Congreve M, Andrews SP, Dore AS, Hollenstein K, Hurrell E, Langmead CJ, et al. Discovery of 1,2,4-triazine derivatives as adenosine A(2A) antagonists using structure based drug design. J Med Chem. 2012; 55(5):1898–903. https://doi.org/10.1021/jm201376w PMID: 22220592

101

88. Segala E, Guo D, Cheng RK, Bortolato A, Deflorian F, Dore AS, et al. Controlling the Dissociation of Ligands from the Adenosine A2A Receptor through Modulation of Salt Bridge Strength. J Med Chem. 2016; 59(13):6470–9. https://doi.org/10.1021/acs.jmedchem.6b00653 PMID: 27312113

89. Sun B, Bachhawat P, Chu ML, Wood M, Ceska T, Sands ZA, et al. Crystal structure of the adenosine A2A receptor bound to an antagonist reveals a potential allosteric pocket. Proc Natl Acad Sci U S A. 2017; 114(8):2066–71. https://doi.org/10.1073/pnas.1621423114 PMID: 28167788

90. Broecker J, Morizumi T, Ou WL, Klingel V, Kuo A, Kissick DJ, et al. High-throughput in situ X-ray screening of and data collection from protein crystals at room temperature and under cryogenic conditions. Nat Protoc. 2018; 13(2):260–92. https://doi.org/10.1038/nprot.2017.135 PMID: 29300389

91. Rucktooa P, Cheng RKY, Segala E, Geng T, Errey JC, Brown GA, et al. Towards high throughput GPCR crystallography: In Meso soaking of Adenosine A2A Receptor crystals. Sci Rep. 2018; 8(1):41. https://doi.org/10.1038/s41598-017-18570-w PMID: 29311713

92. Xu F, Wu H, Katritch V, Han GW, Jacobson KA, Gao ZG, et al. Structure of an agonist-bound human A2A adenosine receptor. Science. 2011; 332(6027):322–7. https://doi.org/10.1126/science.1202793 PMID: 21393508

93. Lebon G, Warne T, Edwards PC, Bennett K, Langmead CJ, Leslie AG, et al. Agonist-bound adenosine A2A receptor structures reveal common features of GPCR activation. Nature. 2011; 474(7352):521–5. https://doi.org/10.1038/nature10136 PMID: 21593763

94. Lebon G, Edwards PC, Leslie AG, Tate CG. Molecular Determinants of CGS21680 Binding to the Human Adenosine A2A Receptor. Mol Pharmacol. 2015; 87(6):907–15. https://doi.org/10.1124/mol.114.097360 PMID: 25762024

95. White KL, Eddy MT, Gao ZG, Han GW, Lian T, Deary A, et al. Structural Connection between Activation Microswitch and Allosteric Sodium Site in GPCR Signaling. Structure. 2018; 26(2):259–69 e5. https://doi.org/10.1016/j.str.2017.12.013 PMID: 29395784

96. Ackerman DG, Feigenson GW. Lipid bilayers: clusters, domains and phases. Essays Biochem. 2015; 57:33–42. https://doi.org/10.1042/bse0570033 PMID: 25658342

97. Leekumjorn S, Sum AK. Molecular characterization of gel and liquid-crystalline structures of fully hydrated POPC and POPE bilayers. J Phys Chem B. 2007; 111(21):6026–33. https://doi.org/10.1021/jp0686339 PMID: 17488110

98. Cusack NJ, Hourani SM. 5'-N-ethylcarboxamidoadenosine: a potent inhibitor of human platelet aggregation. Br J Pharmacol. 1981; 72(3):443–7. https://doi.org/10.1111/j.1476-5381.1981.tb10995.x PMID: 7260485

99. Ballesteros JA, Weinstein H. Integrated methods for the construction of three-dimensional models and computational probing of structure-function relations in G protein-coupled receptors. Methods in Neurosciences. 1995; 25:366–428.

100. Kobilka BK. G protein coupled receptor structure and activation. Biochim Biophys Acta. 2007; 1768 (4):794–807. https://doi.org/10.1016/j.bbamem.2006.10.021 PMID: 17188232

101. Shi L, Liapakis G, Xu R, Guarnieri F, Ballesteros JA, Javitch JA. Beta2 adrenergic receptor activation. Modulation of the proline kink in transmembrane 6 by a rotamer toggle switch. J Biol Chem. 2002; 277:40989–96. https://doi.org/10.1074/jbc.M206801200 PMID: 12167654

102. Woolley MJ, Conner AC. Understanding the common themes and diverse roles of the second extracellular loop (ECL2) of the GPCR super-family. Mol Cell Endocrinol. 2017; 449:3–11. https://doi.org/10.1016/j.mce.2016.11.023 PMID: 27899324

103. Kim J, Wess J, van Rhee AM, Schoneberg T, Jacobson KA. Site-directed mutagenesis identifies residues involved in ligand recognition in the human A2a adenosine receptor. J Biol Chem. 1995; 270 (23):13987–97. https://doi.org/10.1074/jbc.270.23.13987 PMID: 7775460

104. Rouviere E, Arnarez C, Yang L, Lyman E. Identification of Two New Cholesterol Interaction Sites on the A2A Adenosine Receptor. Biophys J. 2017; 113(11):2415–24. https://doi.org/10.1016/j.bpj.2017.09.027 PMID: 29211995

105. Neale C, Herce HD, Pomes R, Garcia AE. Can Specific Protein-Lipid Interactions Stabilize an Active State of the Beta 2 Adrenergic Receptor? Biophys J. 2015; 109(8):1652–62. https://doi.org/10.1016/j.bpj.2015.08.028 PMID: 26488656

106. Carpenter B, Tate CG. Active state structures of G protein-coupled receptors highlight the similarities and differences in the G protein and arrestin coupling interfaces. Curr Opin Struct Biol. 2017; 45:124–32. https://doi.org/10.1016/j.sbi.2017.04.010 PMID: 28482214

107. Lyskov S, Chou FC, Conchuir SO, Der BS, Drew K, Kuroda D, et al. Serverification of molecular modeling applications: the Rosetta Online Server that Includes Everyone (ROSIE). PLoS ONE. 2013; 8(5):e63906. https://doi.org/10.1371/journal.pone.0063906 PMID: 23717507

102

108. Cang X, Du Y, Mao Y, Wang Y, Yang H, Jiang H. Mapping the functional binding sites of cholesterol in beta2-adrenergic receptor by long-time molecular dynamics simulations. J Phys Chem B. 2013; 117 (4):1085–94. https://doi.org/10.1021/jp3118192 PMID: 23298417

109. Sengupta D, Prasanna X, Mohole M, Chattopadhyay A. Exploring GPCR-Lipid Interactions by Molecular Dynamics Simulations: Excitements, Challenges, and the Way Forward. J Phys Chem B. 2018; 122(22):5727–37. https://doi.org/10.1021/acs.jpcb.8b01657 PMID: 29685028

110. Cao R, Giorgetti A, Bauer A, Neumaier B, Rossetti G, Carloni P. Role of Extracellular Loops and Membrane Lipids for Ligand Recognition in the Neuronal Adenosine Receptor Type 2A: An Enhanced Sampling Simulation Study. Molecules. 2018; 23(10).

111. Peeters MC, van Westen GJ, Li Q, AP IJ. Importance of the extracellular loops in G protein-coupled receptors for ligand recognition and receptor activation. Trends Pharmacol Sci. 2011; 32(1):35–42. https://doi.org/10.1016/j.tips.2010.10.001 PMID: 21075459

112. Kenakin T. Drug efficacy at G protein-coupled receptors. Annu Rev Pharmacol Toxicol. 2002; 42:349–79. https://doi.org/10.1146/annurev.pharmtox.42.091401.113012 PMID: 11807176

113. Ibrisimovic E, Drobny H, Yang Q, Hofer T, Boehm S, Nanoff C, et al. Constitutive activity of the A2A adenosine receptor and compartmentalised cyclic AMP signalling fine-tune noradrenaline release. Purinergic Signal. 2012; 8(4):677–92. https://doi.org/10.1007/s11302-012-9298-3 PMID: 22476939

114. Giraldo J. Agonist induction, conformational selection, and mutant receptors. FEBS Lett. 2004; 556(1–3):13–8. https://doi.org/10.1016/s0014-5793(03)01404-2 PMID: 14706818

115. Changeux JP, Edelstein S. Conformational selection or induced fit? 50 years of debate resolved. F1000 Biol Rep. 2011; 3:19. https://doi.org/10.3410/B3-19 PMID: 21941598

116. Deupi X, Kobilka BK. Energy landscapes as a tool to integrate GPCR structure, dynamics, and function. Physiology (Bethesda). 2010; 25(5):293–303.

117. Lans I, Dalton JA, Giraldo J. Selective Protonation of Acidic Residues Triggers Opsin Activation. J Phys Chem B. 2015; 119(30):9510–9. https://doi.org/10.1021/acs.jpcb.5b01908 PMID: 26140747

118. Pettersen EF, Goddard TD, Huang CC, Couch GS, Greenblatt DM, Meng EC, et al. UCSF Chimera—a visualization system for exploratory research and analysis. J Comput Chem. 2004; 25(13):1605–12. https://doi.org/10.1002/jcc.20084 PMID: 15264254

119. Eswar N, Eramian D, Webb B, Shen MY, Sali A. Protein structure modeling with MODELLER. Methods Mol Biol. 2008; 426:145–59. https://doi.org/10.1007/978-1-60327-058-8_8 PMID: 18542861

120. Case DA, Cheatham TE 3rd, Darden T, Gohlke H, Luo R, Merz KM Jr., et al. The Amber biomolecular simulation programs. J Comput Chem. 2005; 26(16):1668–88. https://doi.org/10.1002/jcc.20290 PMID: 16200636

121. Jo S, Kim T, Iyer VG, Im W. CHARMM-GUI: a web-based graphical user interface for CHARMM. J Comput Chem. 2008; 29(11):1859–65. https://doi.org/10.1002/jcc.20945 PMID: 18351591

122. Caliman AD, Miao Y, McCammon JA. Mapping the allosteric sites of the A2A adenosine receptor. Chem Biol Drug Des. 2018; 91(1):5–16. https://doi.org/10.1111/cbdd.13053 PMID: 28639411

123. Zhang XC, Sun K, Zhang L, Li X, Cao C. GPCR activation: protonation and membrane potential. Protein Cell. 2013; 4(10):747–60. https://doi.org/10.1007/s13238-013-3073-2 PMID: 24057762

124. Huang J, MacKerell AD Jr. CHARMM36 all-atom additive protein force field: validation based on comparison to NMR data. J Comput Chem. 2013; 34(25):2135–45. https://doi.org/10.1002/jcc.23354 PMID: 23832629

125. Vanommeslaeghe K, Hatcher E, Acharya C, Kundu S, Zhong S, Shim J, et al. CHARMM general force field: A force field for drug-like molecules compatible with the CHARMM all-atom additive biological force fields. J Comput Chem. 2010; 31(4):671–90. https://doi.org/10.1002/jcc.21367 PMID: 19575467

126. Harvey MJ, Giupponi G, De Fabritiis G. ACEMD: Accelerating Biomolecular Dynamics in the Microsecond Time Scale. J Chem Theory Comput. 2009; 5(6):1632–9. https://doi.org/10.1021/ct9000685 PMID: 26609855

127. Humphrey W, Dalke A, Schulten K. VMD: visual molecular dynamics. J Mol Graph. 1996; 14(1):33–8. https://doi.org/10.1016/0263-7855(96)00018-5 PMID: 8744570

128. Bonomi M, Branduardi D, Bussi G, Camilloni C, Provasi D, Raiteri P, et al. PLUMED: A portable plugin for free-energy calculations with molecular dynamics. Comput Phys Commun. 2009; 180(10):1961–72.

129. Guixa-Gonzalez R, Rodriguez-Espigares I, Ramirez-Anguita JM, Carrio-Gaspar P, Martinez-Seara H, Giorgino T, et al. MEMBPLUGIN: studying membrane complexity in VMD. Bioinformatics. 2014; 30 (10):1478–80. https://doi.org/10.1093/bioinformatics/btu037 PMID: 24451625

130. Hunter JD. Matplotlib: A 2D Graphics Environment. Comput Sci Eng. 2007; 9(3):90–5.

103

8.   APPENDIX

8.1. STATISTICS FOR THE ANALYSIS OF MOLECULAR DYNAMICS SIMULATIONS: PROVID-ING P VALUES FOR AGONIST-DEPENDENT GPCR ACTIVATION

scientific reports

Check for updates

OPEN Statistics for the analysis of molecular dynamics simulations: providing *P* values for agonist-dependent GPCR activation

Agustín Bruzzese[1,2,3], James A. R. Dalton[1,2,3] & Jesús Giraldo[1,2,3✉]

Molecular dynamics (MD) is the common computational technique for assessing efficacy of GPCR-bound ligands. Agonist efficacy measures the capability of the ligand-bound receptor of reaching the active state in comparison with the free receptor. In this respect, agonists, neutral antagonists and inverse agonists can be considered. A collection of MD simulations of both the ligand-bound and the free receptor are needed to provide reliable conclusions. Variability in the trajectories needs quantification and proper statistical tools for meaningful and non-subjective conclusions. Multiple-factor (time, ligand, lipid) ANOVA with repeated measurements on the time factor is proposed as a suitable statistical method for the analysis of agonist-dependent GPCR activation MD simulations. Inclusion of time factor in the ANOVA model is consistent with the time-dependent nature of MD. Ligand and lipid factors measure agonist and lipid influence on receptor activation. Previously reported MD simulations of adenosine A2a receptor (A2aR) are reanalyzed with this statistical method. TM6–TM3 and TM7–TM3 distances are selected as dependent variables in the ANOVA model. The ligand factor includes the presence or absence of adenosine whereas the lipid factor considers DOPC or DOPG lipids. Statistical analysis of MD simulations shows the efficacy of adenosine and the effect of the membrane lipid composition. Subsequent application of the statistical methodology to NECA A2aR agonist, with resulting *P* values in consistency with its pharmacological profile, suggests that the method is useful for ligand comparison and potentially for dynamic structure-based virtual screening.

Molecular dynamics (MD) simulations is an established computational tool for the examination of the conformational flexibility of molecules, in particular proteins[1]. G protein-coupled receptors (GPCRs) are membrane proteins responsible for signal transduction from outside to inside the cell. Thus, the healthy or pathologic state of living organisms greatly depends on the correct or anomalous functional molecular state of GPCRs. This is translated into the fact that GPCRs are the target for about one third of current marketed medicines[2].

GPCRs, also known as 7-transmembrane (7-TM) receptors, have in common that they all bear seven transmembrane helices which are connected by three extra- and three intracellular loops. A number of biophysical approaches amongst them crystallography and different spectroscopic techniques have studied the conformational changes associated to the activation of GPCRs[3]. Particularly in Class A GPCRs, receptor activation involves a large outward movement of TM helix 6 (TM6) from the central TM3 and a smaller inward movement of TM7 as relevant mechanistic conformational features[4].

To reveal GPCR activation conformational features, MD simulations need at least µs-length trajectories and the use of several replicas to provide sufficient confidence to computational results. It is worth noting that, although starting from the same conformational arrangement and applying identical experimental conditions,

[1]Laboratory of Molecular Neuropharmacology and Bioinformatics, Unitat de Bioestadística and Institut de Neurociències, Universitat Autònoma de Barcelona, 08193 Bellaterra, Spain. [2]Unitat de Neurociència Traslacional, Parc Taulí Hospital Universitari, Institut d'Investigació i Innovació Parc Taulí (I3PT), Institut de Neurociències, Universitat Autònoma de Barcelona, Bellaterra, Spain. [3]Centro de Investigación Biomédica en Red de Salud Mental, CIBERSAM, Instituto de Salud Carlos III, Madrid, Spain. ✉email: Jesus.Giraldo@uab.es

two independent trajectories can evolve differently leading to dissimilar results. Also importantly is that MD simulations are inherently time-dependent and, consequently, the time factor should be present in their statistical analysis.

Despite the wide use of MD simulations there is not a unified approach for their analyses. Different multivariate statistical analyses such as cluster and principal component analysis and, more recently, machine learning approaches are being applied[5,6]. Here we present a multiple-factor analysis of variance (ANOVA) with repeated measurements on the time factor, a classical statistical approach which makes use of the time-dependent nature of MD simulations and quantifies the statistical effect that several experimental conditions may have on the activation capability of a receptor. The main advantages of the approach are (1) its general practicality, as it is included in most statistical packages, and (2) the computational production of P values, which removes subjectivity from conclusions.

Results and discussion

In the present article we reanalyze a recent study of ours in which the activation of the adenosine A2a Class A GPCR (A2aR) was examined[7]. In this study, 2 μs-length MD simulations of A2aR under 2 experimental conditions: absence/presence of endogenous adenosine and DOPC (1,2-dioleoyl-sn-glycerol-3-phosphocholine)/DOPG (1,2-dioleoyl-sn-glycerol-3-phosphoglycerol) lipid environment were performed[7]. To provide sufficient variability, 4 replicas were run in each condition value. Figure 1 shows the trajectories of each of the replicas in each of the experimental conditions for the two main variables reflecting the receptor activation process, namely, the distances between TM3 and TM6 (TM3–TM6) and between TM3 and TM7 (TM3–TM7). Values were collected every 0.02 μs, totalizing 100 time-points for each replica. Visual inspection of Fig. 1A shows the effect of both the ligand (agonist, in this case) and lipid factors on TM3–TM6: adenosine increases the magnitude of this variable over the apo receptor and, similarly, does DOPG with respect to DOPC. The same overall effects, though in an opposite direction and lower degree, happen for TM3–TM7 (Fig. 1B): adenosine decreases the TM3–TM7 distance over the apo receptor and, seemingly, does DOPG with respect to DOPC. However, there are differences between the 4 replicas within each of the (lipid, ligand) experimental conditions. We may all agree that the visual variability observed between and within curves in Fig. 1 needs quantification and proper statistical analysis to provide meaningful conclusions.

Figure 2 depicts means and standard errors of the mean (SEM) along time for the 4 replicas included in each of the (ligand, lipid) experimental conditions of the MD simulations for TM3–TM6 and TM3–TM7 variables. To statistically assess the variability between and within replicas a three-factor (time, ligand, lipid) ANOVA with repeated measurements on the time factor was performed. Table 1 shows the P values for the tested effects on the selected variables, where an MD simulation trajectory or replica takes the sense of subject or experimental unit in the common statistical language.

On the analysis of TM3–TM6, Table 1 shows that both Lipid and Ligand variables have significant effects ($P = 0.0062$ and $P = 0.0008$, respectively). On the contrary, the Lipid × Ligand interaction is not significant ($P = 0.5669$), meaning that the effect of the ligand is similar in both lipid environments. When analyzing the within-trajectory effects, we see that Time is significant ($P < 0.0001$) and also both Time × Lipid ($P < 0.0001$) and Time × Ligand ($P < 0.0001$) interactions, meaning that there is an increase in average of TM3–TM6 with time and that this increase depends on the lipid and the ligand compositions. Finally, the absence of statistical significance of the Lipid × Ligand interaction maintains this value when time is also included in the interaction ($P = 0.9473$). Translating probability values into pharmacological concepts, we can say that DOPG environment facilitates receptor activation more than DOPC and that adenosine is more efficacious than the free receptor in inducing an active conformation, irrespective of the membrane lipid composition. The activation of the receptor occurs progressively along time and the effect along time is not the same for each of the lipids and also for adenosine in comparison to the free receptor. Finally, the effect of the lipid along time happens for both adenosine-bound and the free receptor.

On the analysis of TM3–TM7, we see that, similarly to the TM3–TM6 evaluation, both Lipid and Ligand variables have significant effects ($P = 0.0411$ and $P = 0.0201$, respectively). Analogously also to TM3–TM6, the Lipid × Ligand interaction is not significant ($P = 0.9288$). It is worth noting that the P values for the Lipid and Ligand effects are lower in TM3–TM7 than in TM3–TM6, which is in agreement with depicted curve profiles and the general consensus that TM6 outward movement is the principal structural feature characterizing Class A GPCR activation. When analyzing the within-trajectory effects, we see that Time is significant ($P = 0.0021$) but, contrary to TM3–TM6, neither Time × Lipid ($P = 0.9912$) nor Time × Ligand ($P = 0.9984$) interactions are significant. Or in other words, neither the effect of lipid nor the effect of ligand significantly increase with time. Finally, the absence of statistical significance of the Lipid × Ligand interaction maintains this value when time is also included in the interaction ($P = 0.2869$). We may attribute the differences in statistical significance between TM3–TM6 and TM3–TM7 variables in the Time interaction effects to the observed large effects on the TM3–TM6 variable of the inclusion of both Ligand = adenosine and Lipid = DOPG conditions (compare Fig. 2A,B).

Interestingly, the Ligand factor provides a statistical comparison between the free receptor and an agonist-bound receptor; in the present case, adenosine. Thus, a correspondence can be made between the P value and the concept of intrinsic efficacy[8]; in the present case, for two different structural features: TM3–TM6 and TM3–TM7, with the former as the most indicative of receptor activation.

To investigate whether the proposed statistical methodology can be useful for drug comparison, we selected a set of trajectories of NECA (5'-N-ethylcarboxamidoadenosine) A2aR agonist which were run under the same conditions of trajectory-length, lipid composition and number of replicas as those of adenosine (Figs. 3 and 4). As in the case of adenosine, these trajectories are described individually in Ref.[7]. Considering that NECA is a
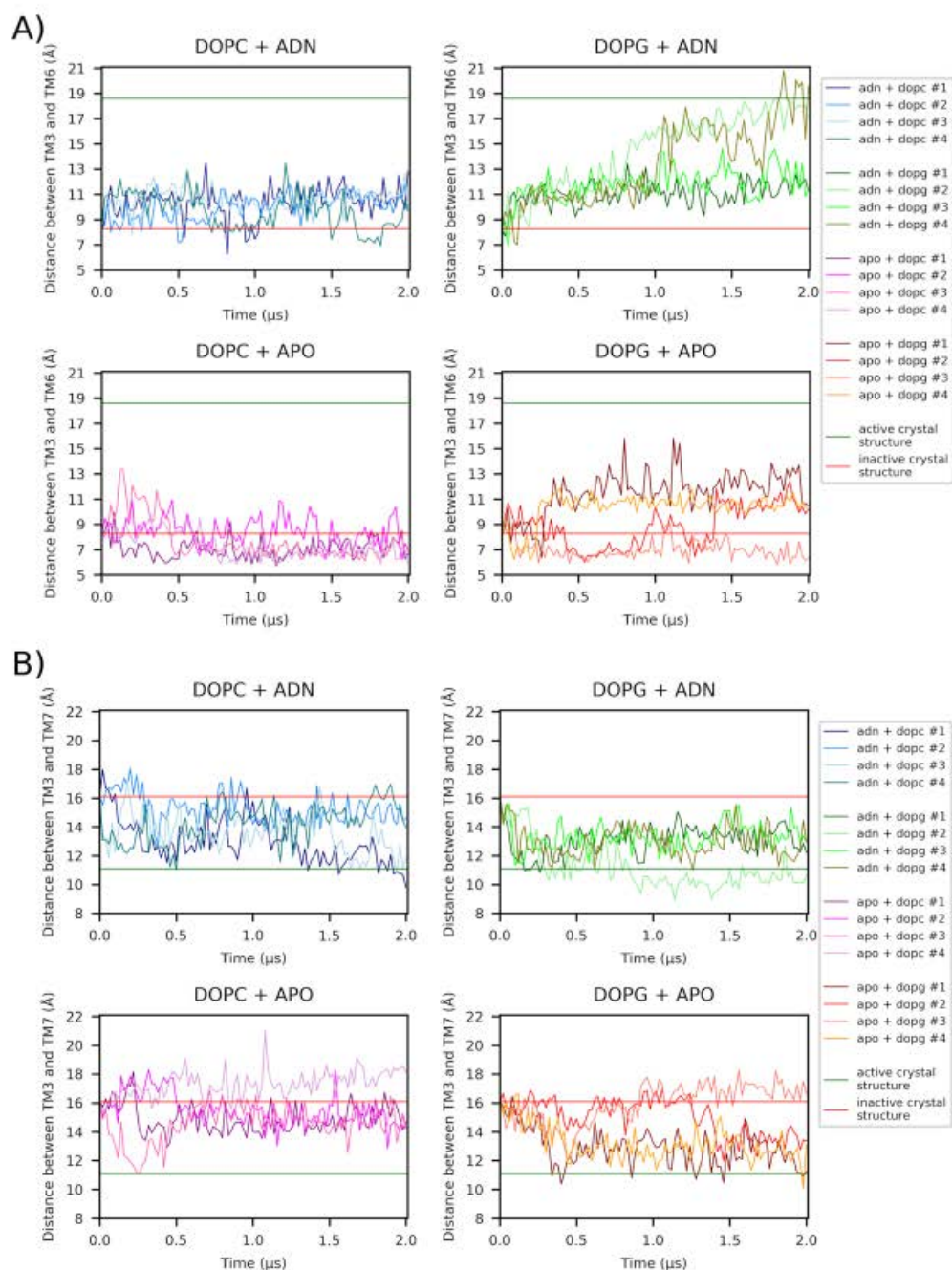
Figure 1. Examination of structural features depicting adenosine-dependent receptor activation in A2aR from 2 μs -length MD simulations. Lipid (DOPC, DOPG) and ligand (adenosine, APO) experimental conditions were considered. 4 replicas for each condition combination were run. Structures were taken every 0.02 μs. (**A**) The TM3–TM6 distance is measured between Cα atoms of R102[3.50] and E288[6.30]. (**B**) The TM3–TM7 distance is measured between Cα atoms of R102[3.50] and Y288[7.53]. Horizontal TM3–TM6 and TM3–TM7 red lines correspond to the distances between the aforementioned respective atoms for the inactive receptor (PDB entry: 4EIY)[16] whereas horizontal green lines correspond to the distances for the active receptor (PDB entry: 6GDG)[17]. ADN stands for adenosine. Figures adapted from[7].

nature research

A)

B)
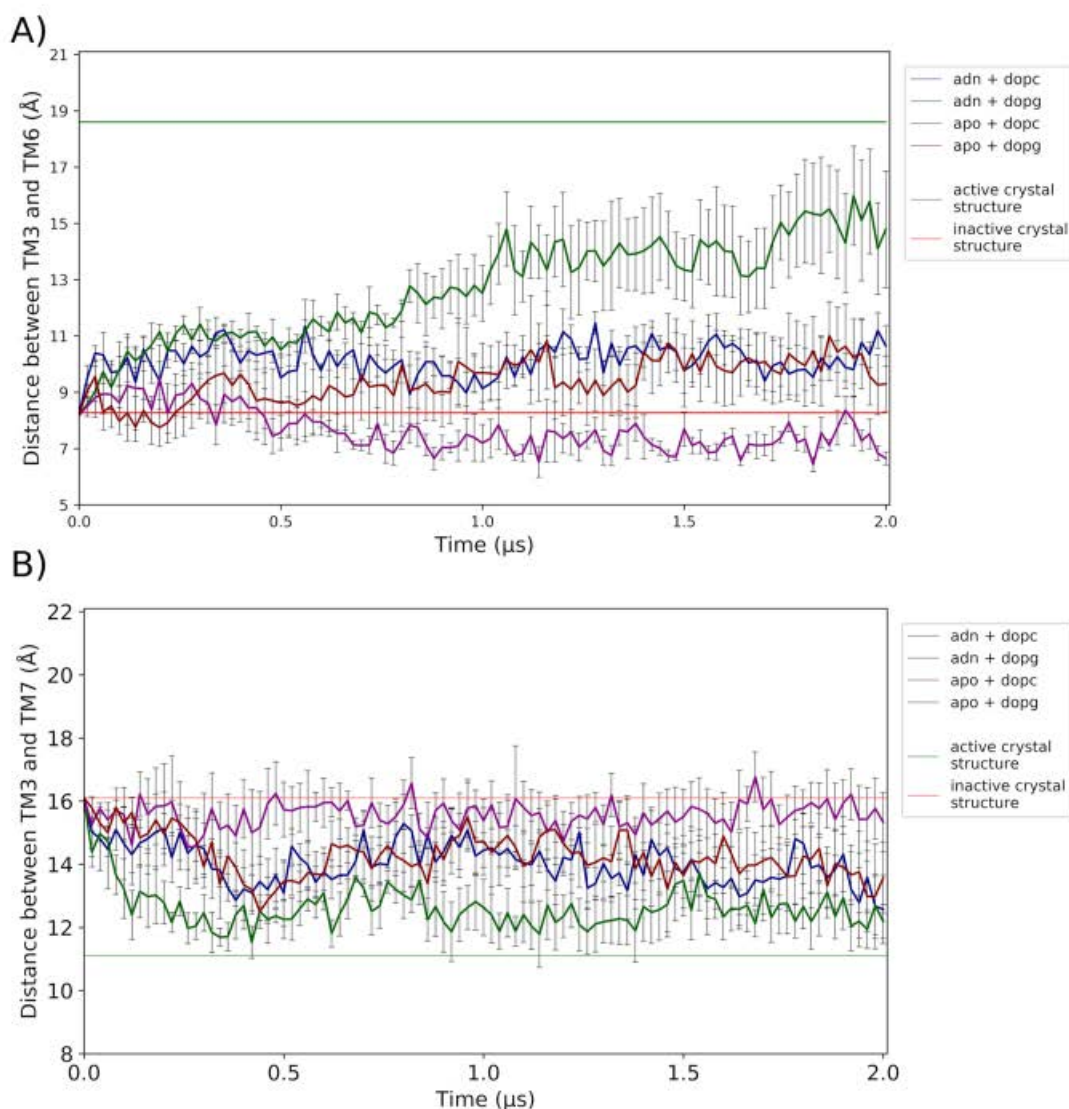
Figure 2. Descriptive statistics, mean and standard error of the mean (SEM), for the sampled 4 replicas in each of the conditions (lipid, adenosine) depicted in Fig. 1. (**A**) TM3–TM6 distance. (**B**) TM3–TM7 distance. Horizontal lines have the same definition as in in Fig. 1. ADN stands for adenosine.

more potent agonist than adenosine one would expect that the performed statistics would reflect this pharmacological feature. Table 2 displays the P values of NECA MD simulations, which can be compared with those of adenosine in Table 1. If we focus on those factors related with ligand, we see that, in the case of TM3–TM6 dependent variable, the P value for the Ligand factor is slightly lower for NECA ($P = 7.61 \times 10^{-4}$) in comparison with adenosine ($P = 7.98 \times 10^{-4}$). More important is the Time $\times$ Ligand effect: $P = 3.97 \times 10^{-14}$ for NECA and $P = 1.47 \times 10^{-7}$ for adenosine. Moreover, in the case of the TM3–TM7 dependent variable, the P values for the Ligand factor are $P = 0.0174$ and $P = 0.0201$ for NECA and adenosine, respectively, whereas for the Time $\times$ Ligand effect the P values are $P = 0.5272$ and $P = 0.9984$ for NECA and adenosine, respectively. Overall, we see that the effect of ligand factor is stronger for NECA than for adenosine in agreement with their agonist potency profiles.

As a hypothesis to be tested with further studies, it could be proposed that, by generalizing the previous results, the herein shown formalism could be applied in high throughput MD simulations of large collections of ligands. In doing so, the P values of the MD simulations could be later used as a statistical descriptor to rank agonists according to their capability to activate the receptor (at in silico level and with the inherent limitations of a computational study). Considering that each agonist is compared with the free receptor, this is a way to

	TM3–TM6	TM3–TM7
Between-trajectory effects		
Lipid	$P = 6.18 \times 10^{-3}$	$P = 0.0411$
Ligand	$P = 7.98 \times 10^{-4}$	$P = 0.0201$
Lipid × ligand	$P = 0.5669$	$P = 0.9288$
Within-trajectory effects		
Time	$P = 6.10 \times 10^{-10}$	$P = 2.11 \times 10^{-5}$
Time × lipid	$P = 5.34 \times 10^{-34}$	$P = 0.9912$
Time × ligand	$P = 1.47 \times 10^{-7}$	$P = 0.9984$
Time × lipid × ligand	$P = 0.9473$	$P = 0.2869$

Table 1. Three-factor (time, ligand, lipid)-ANOVA of receptor activation with repeated measurements on time factor. Ligand: adenosine (present/absent). Lipid: DOPC/DOPG. Statistical analysis of data depicted on Figs. 1 and 2.

approach the agonist efficacy concept, from MD simulations and within a statistical perspective. Ranked P values of a set of agonists for a particular receptor in combination with the structure of these ligands could be used as a component of following quantitative structure–activity studies. These studies could lead to new drug design. In this respect, MD simulations could provide a time-dependent framework for virtual screening purposes. This virtual screening can be made either directly through MD simulations of the chosen ligands or indirectly by ligand docking on selected receptor structures from MD simulations of apo receptors or ligand-bound receptors—the latter in the case of evaluating allosteric modulators. In this way, MD-based virtual screening can be a complement to the more classical structure-based virtual screening, which targets static crystal structures[9–11].

MD is a computational technique especially appropriate for addressing the flexibility of the target proteins, GPCRs in the present study. It seems logical that, in general, considering the flexibility of the target can increase the probability of identifying new ligands. However, whether this is really an advantage for GPCR drug discovery is a current debate. In a recent publication on the performance of virtual screening against GPCR homology models[12], in which binding site plasticity was considered by including ensembles of structures, it was shown that MD refinement resulted in moderate improvements of structural accuracy and the virtual screening performance of snapshots was either comparable to or worse than that of the raw homology models[12]. However, and from a different perspective, the methodological approach herein shown is focused on the statistical significance of structural features reflecting receptor activation. To this end, we are proposing multiple-way ANOVA for the statistical analysis of those MD simulations that are addressed to allow the distinction between agonists, neutral antagonists and inverse agonists (through statistical comparison with the MD simulations of the apo receptor). Molecular docking screening focused on specific ligand sets has been considered elsewhere[13]. In this study, a large library virtual screen against an active β2-adrenergic receptor (β2AR) crystal structure returned agonists exclusively and with a high hit rate[13]. However, it seems that, in general, structural information from active receptors is not transferrable to other receptors despite reasonable sequence identity. When the same authors used the β2AR active state as a template for the construction of a dopamine D2 receptor (DRD2) activated model, although both receptors share 42% sequence identity, virtual screening was not satisfactory: few weak agonists mixed with an inverse agonist were selected from the modeled DRD2 active state[13]. Thus, it seems plausible to hypothesize that MD simulations can potentially be an appropriate complement for virtual screening based on static structures and, interestingly, they can be especially addressed to distinguish between agonists, neutral antagonists and inverse agonists, particularly, in those cases in which the crystal active receptor state has not been determined. We must admit that the computational cost of the required MD simulations can be a limiting barrier of the methodology if is intended for high throughput screening. However, it may be accepted that, with a sustained exponential growth in computational power, long and massive MD simulations can be accessible in the near future.

Concluding remarks

To summarize, we conclude that multiple-factor ANOVA with repeated measurements on the time factor can be a useful statistical technique for the analysis of MD simulations of ligand-bound GPCRs under various experimental conditions. The proposed methodology has the benefit of including P values for assessing statistical significance of testing hypotheses, in particular agonist efficacy. In addition, resulting P values can provide a probabilistic framework for dynamic structure-based virtual screening if the limitation of the computational cost is overcome. The methodology can be extended to systems other than GPCRs by defining the appropriate dependent variables.

Methods

Three-factor (time, ligand, lipid) analysis of variance (ANOVA) is proposed for the statistical analysis of GPCR MD simulations to assess receptor activation. This method was selected because it is a confirmatory statistical technique in which a hypothesis concerning receptor activation can be tested and associated P values obtained. Either the TM6–TM3 or the TM7–TM3 distances were chosen as dependent variables because it is known that their respective increase or decrease with respect to the inactive receptor state are indicative of receptor
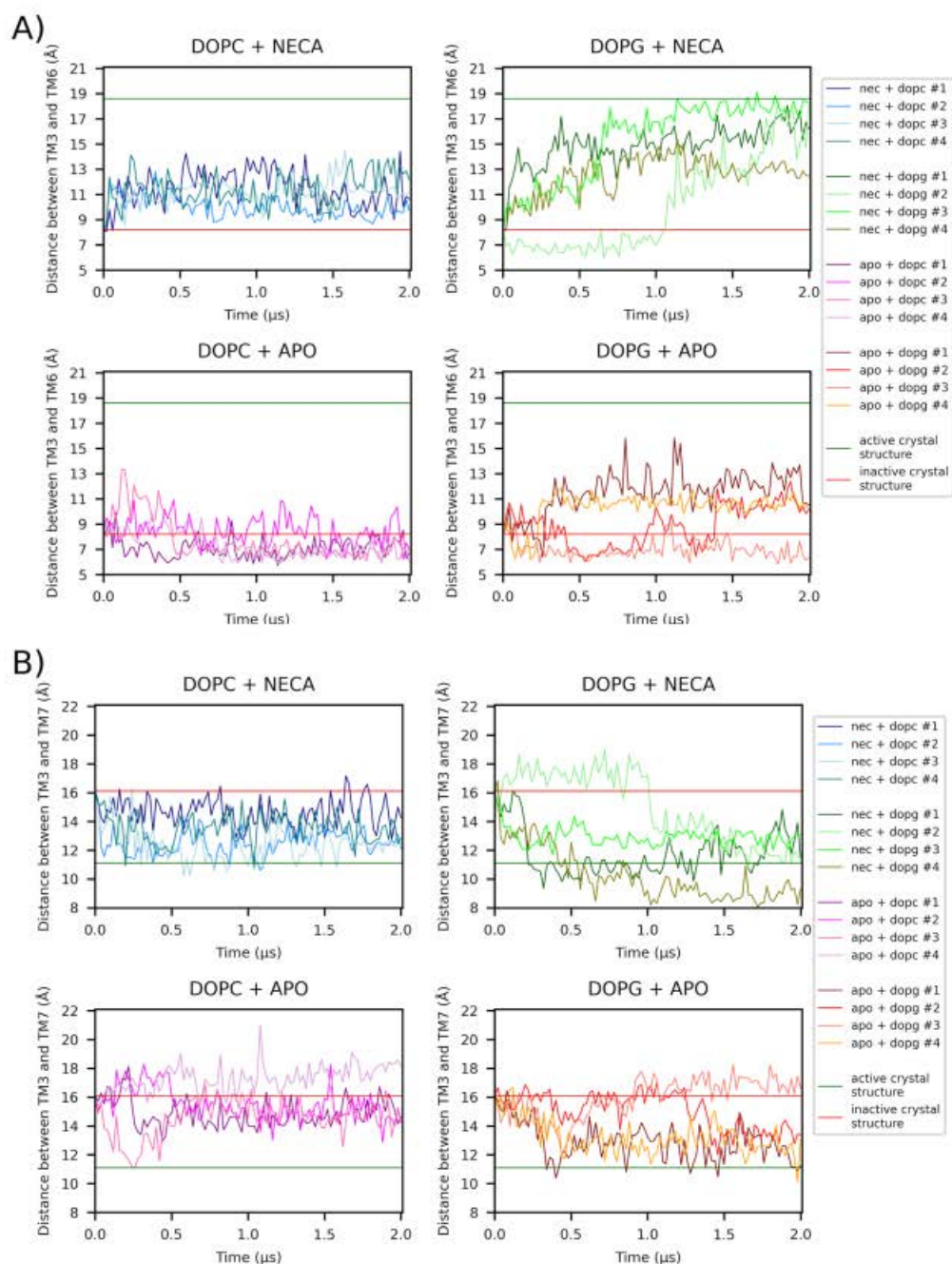
111

Figure 3. Examination of structural features depicting NECA-dependent receptor activation in A2aR from 2 μs -length MD simulations. Lipid (DOPC, DOPG) and ligand (NECA, APO) experimental conditions were considered. 4 replicas for each condition combination were run. Structures were taken every 0.02 μs. (**A**) The TM3–TM6 distance is measured between Cα atoms of R102$^{3.50}$ and E288$^{6.30}$. (**B**) The TM3–TM7 distance is measured between Cα atoms of R102$^{3.50}$ and Y288$^{7.53}$. Horizontal TM3–TM6 and TM3–TM7 red lines correspond to the distances between the aforementioned respective atoms for the inactive receptor (PDB entry: 4EIY)[16] whereas horizontal green lines correspond to the distances for the active receptor (PDB entry: 6GDG)[17]. Figures adapted from Ref [7].
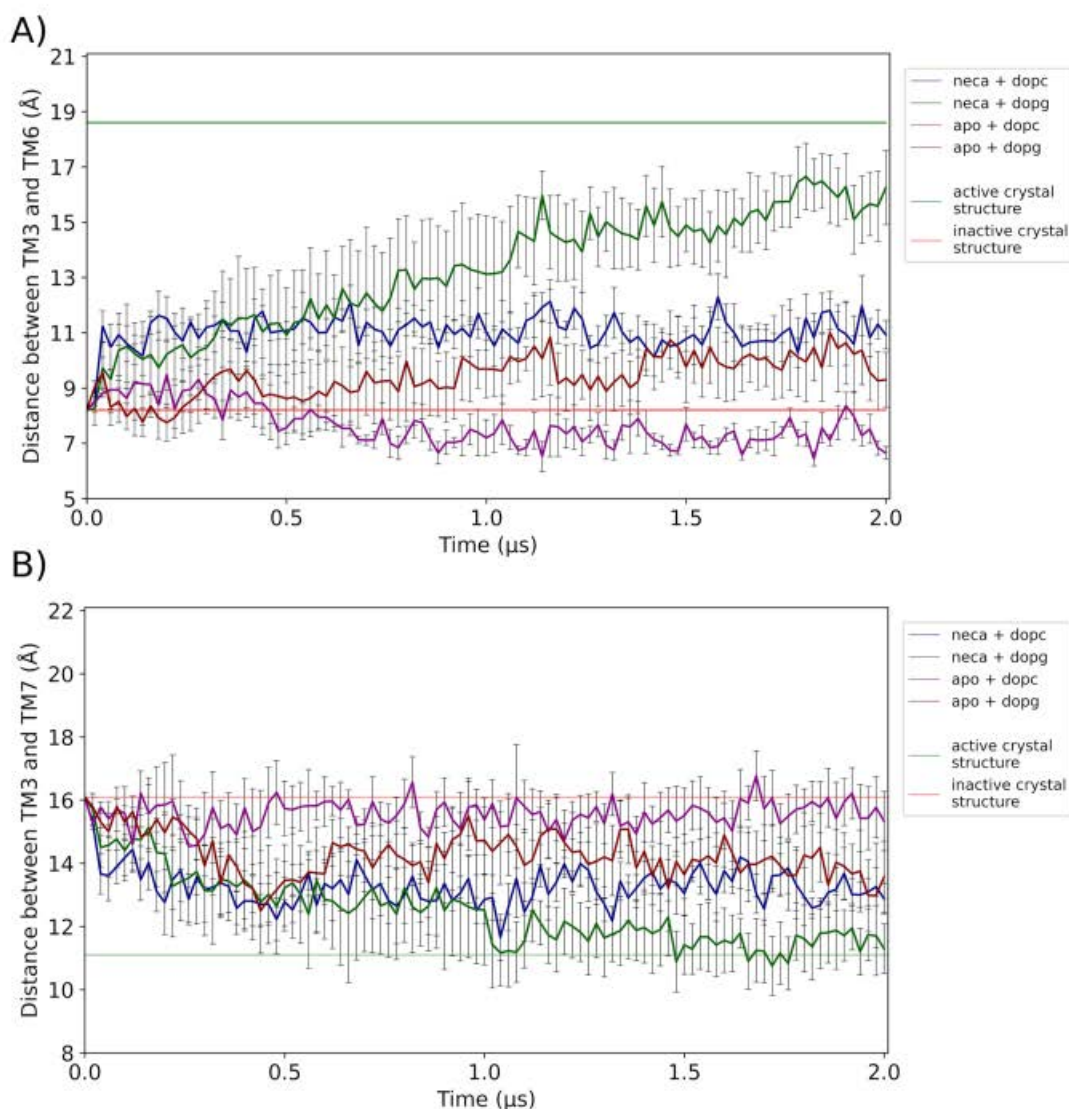
Figure 4. Descriptive statistics, mean and standard error of the mean (SEM), for the sampled 4 replicas in each of the conditions (lipid, NECA) depicted in Fig. 3. (**A**) TM3–TM6 distance. (**B**) TM3–TM7 distance. Horizontal lines have the same definition as in in Fig. 1 and 3.

activation. To allow for variability, 4 trajectories or replicas for each of the selected ligand and lipid factors were run. Each trajectory is considered as a subject or experimental unit in the statistical analysis performed. Special attention was paid to the fact that an MD simulation inherently involves time-dependent data. Thus, we have time-dependent values for TM6–TM3 and TM7–TM3 along the trajectories. The length of each of the trajectories was 2 μs. Values of each of the dependent variables were collected every 0.02 μs, totalizing 100 time-points for each replica. Thus, we have 100 values for each trajectory providing information on how TM6–TM3 and TM7–TM3 evolve along time for each combination of ligand and lipid values (see below). Time was included in the ANOVA model as a repeated-measurement factor as each trajectory is repeatedly measured along time. To evaluate the efficacy of adenosine, the Ligand factor with 2 values (adenosine present or absent) was included. Note that when analyzing the trajectories corresponding to NECA agonist the values of the Ligand factor are NECA present or absent. The lipid composition of the membrane (Lipid) was included in the ANOVA model as the third factor. Two lipid values were considered: DOPC or DOPG. This would allow to test the lipid effect on receptor activation and whether the agonist capability depends or not on the lipid environment. 24 trajectories (3 (ligand) × 2 (lipid) × 4 (replica)) were included in the analyses. The TM3–TM6 distance was measured between Cα

113

	TM3–TM6	TM3–TM7
Between-trajectory effects		
Lipid	$P = 0.0296$	$P = 0.1860$
Ligand	$P = 7.61 \times 10^{-4}$	$P = 0.0174$
Lipid × ligand	$P = 0.7809$	$P = 0.7299$
Within-trajectory effects		
Time	$P = 1.84 \times 10^{-14}$	$P = 3.55 \times 10^{-6}$
Time × lipid	$P = 5.15 \times 10^{-45}$	$P = 0.0045$
Time × ligand	$P = 3.97 \times 10^{-14}$	$P = 0.5272$
Time × lipid × ligand	$P = 0.8651$	$P = 0.5814$

Table 2. Three-factor (time, ligand, lipid)-ANOVA of receptor activation with repeated measurements on time factor. Ligand: NECA (present/absent). Lipid: DOPC/DOPG. Statistical analysis of data depicted on Figs. 3 and 4.

atoms of R102[3.50] and E288[6.30]. The TM3–TM7 distance was measured between Cα atoms of R102[3.50] and Y288[7.53] (see Ref[14] for numbering notation). In order for ANOVA to be applied some assumptions need to be satisfied: (1) the distribution of values should be normally distributed and (2) the groups should come from populations with equal variances (homogeneity of variances). The normality assumption for each group of 4 replicas was verified through the Shapiro–Wilk test for normality whereas the homogeneity of variances was tested by the F-distribution. We checked the applicability conditions at each time-point of the trajectories corresponding to adenosine system. For the TM3–TM6 dependent variable, the normality assumption was accomplished in 93% of the time points whereas the homogeneity of variances assumption was satisfied in 88% of time points. For the TM3–TM7 dependent variable, the normality assumption was accomplished in 94% of the time points whereas the homogeneity of variances assumption was satisfied in 96% of time points. Considering the broad compliance of the assumptions and the robustness of the ANOVA method, which allows its application even if the assumptions are not fully accomplished[15], we think the herein proposal of ANOVA formalism for MD simulations analysis is justified. SAS 9.4 statistical package (SAS Institute Inc., Cary, NC, USA) was used for statistical analyses. P values lower than 0.05 were considered statistically significant.

References

1. Hollingsworth, S. A. & Dror, R. O. Molecular dynamics simulation for All. *Neuron* **99**, 1129–1143. https://doi.org/10.1016/j.neuron.2018.08.011 (2018).
2. Hauser, A. S., Attwood, M. M., Rask-Andersen, M., Schioth, H. B. & Gloriam, D. E. Trends in GPCR drug discovery: new agents, targets and indications. *Nat. Rev. Drug Discov.* **16**, 829–842. https://doi.org/10.1038/nrd.2017.178 (2017).
3. Gusach, A. *et al.* Beyond structure: emerging approaches to study GPCR dynamics. *Curr. Opin. Struct. Biol.* **63**, 18–25 (2020).
4. Weis, W. I. & Kobilka, B. K. The molecular basis of G protein-coupled receptor activation. *Annu. Rev. Biochem.* **87**, 897–919. https://doi.org/10.1146/annurev-biochem-060614-033910 (2018).
5. Diaz, Ó., Dalton, J. A. R. & Giraldo, J. Artificial intelligence: a novel approach for drug discovery. *Trends Pharmacol. Sci.* **40**, 550–551. https://doi.org/10.1016/j.tips.2019.06.005 (2019).
6. Wolf, A. & Kirschner, K. N. Principal component and clustering analysis on molecular dynamics data of the ribosomal L11-23S subdomain. *J. Mol. Model.* **19**, 539–549. https://doi.org/10.1007/s00894-012-1563-4 (2013).
7. Bruzzese, A., Dalton, J. A. R. & Giraldo, J. Insights into adenosine A2A receptor activation through cooperative modulation of agonist and allosteric lipid interactions. *PLoSComput. Biol.* **16**, e1007818. https://doi.org/10.1371/journal.pcbi.1007818 (2020).
8. Zhou, B., Hall, D. A. & Giraldo, J. Can adding constitutive receptor activity redefine biased signaling quantification?. *Trends PharmacolSci* **40**, 156–160. https://doi.org/10.1016/j.tips.2019.01.002 (2019).
9. Liu, L. & Jockers, R. Structure-based virtual screening accelerates GPCR drug discovery. *Trends Pharmacol. Sci.* **41**, 381–384 (2020).
10. Lee, Y., Lazim, R., Macalino, S. J. Y. & Choi, S. Importance of protein dynamics in the structure-based drug discovery of class A G protein-coupled receptors (GPCRs). *Curr. Opin. Struct. Biol.* **55**, 147–153. https://doi.org/10.1016/j.sbi.2019.03.015 (2019).
11. Salmaso, V. & Moro, S. Bridging molecular docking to molecular dynamics in exploring ligand-protein recognition process: an overview. *Front. Pharmacol.* **9**, 923. https://doi.org/10.3389/fphar.2018.00923 (2018).
12. Jaiteh, M., Rodríguez-Espigares, I., Selent, J. & Carlsson, J. Performance of virtual screening against GPCR homology models: Impact of template selection and treatment of binding site plasticity. *PLoS. Comput. Biol.* **16**, e1007680. https://doi.org/10.1371/journal.pcbi.1007680 (2020).
13. Weiss, D. R. *et al.* Conformation guides molecular efficacy in docking screens of activated β-2 adrenergic G protein coupled receptor. *ACS Chem. Biol.* **8**, 1018–1026. https://doi.org/10.1021/cb400103f (2013).
14. Ballesteros, J. A. & Weinstein, H. Integrated methods for the construction of three-dimensional models and computational probing of structure-function relations in G protein-coupled receptors. *Methods Neurosci.* **25**, 366–428 (1995).
15. Cody, R. P. & Smith, J. K. *Applied Statistics and the SAS° Programming Language* (Prentice Hall, Pearson, 2006).
16. Liu, W. *et al.* Structural basis for allosteric regulation of GPCRs by sodium ions. *Science* **337**, 232–236 (2012).
17. García-Nafría, J., Lee, Y., Bai, X., Carpenter, B. & Tate, C. G. Cryo-EM structure of the adenosine A2A receptor coupled to an engineered heterotrimeric G protein. *Life* **7**, e35946. https://doi.org/10.7554/eLife.35946 (2018).

114

Author contributions

A.B. prepared figures. J.G. performed the statistical analyses and wrote the main manuscript text. All authors reviewed the manuscript.

Competing interests

The authors declare no competing interests.

Additional information

Correspondence and requests for materials should be addressed to J.G.

Reprints and permissions information is available at www.nature.com/reprints.

Publisher's note Springer Nature remains neutral with regard to jurisdictional claims in published maps and institutional affiliations.

9.   SUPPLEMENTARY MATERIALS

9.1.   STRUCTURAL INSIGHTS INTO POSITIVE AND NEGATIVE ALLOSTERIC REGULATION OF
A G PROTEIN-COUPLED RECEPTOR THROUGH PROTEIN-LIPID INTERACTIONS
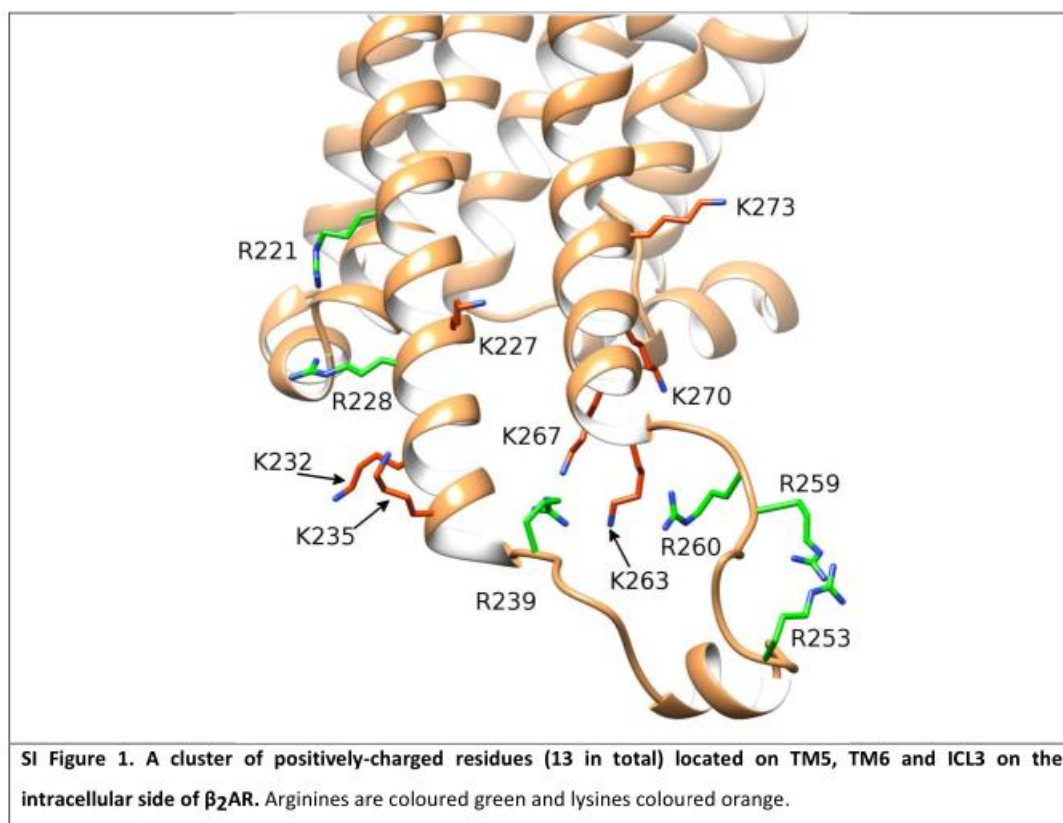
SUPPLEMENTARY INFORMATION

Structural insights into positive and negative allosteric regulation of a G protein-coupled receptor through protein-lipid interactions
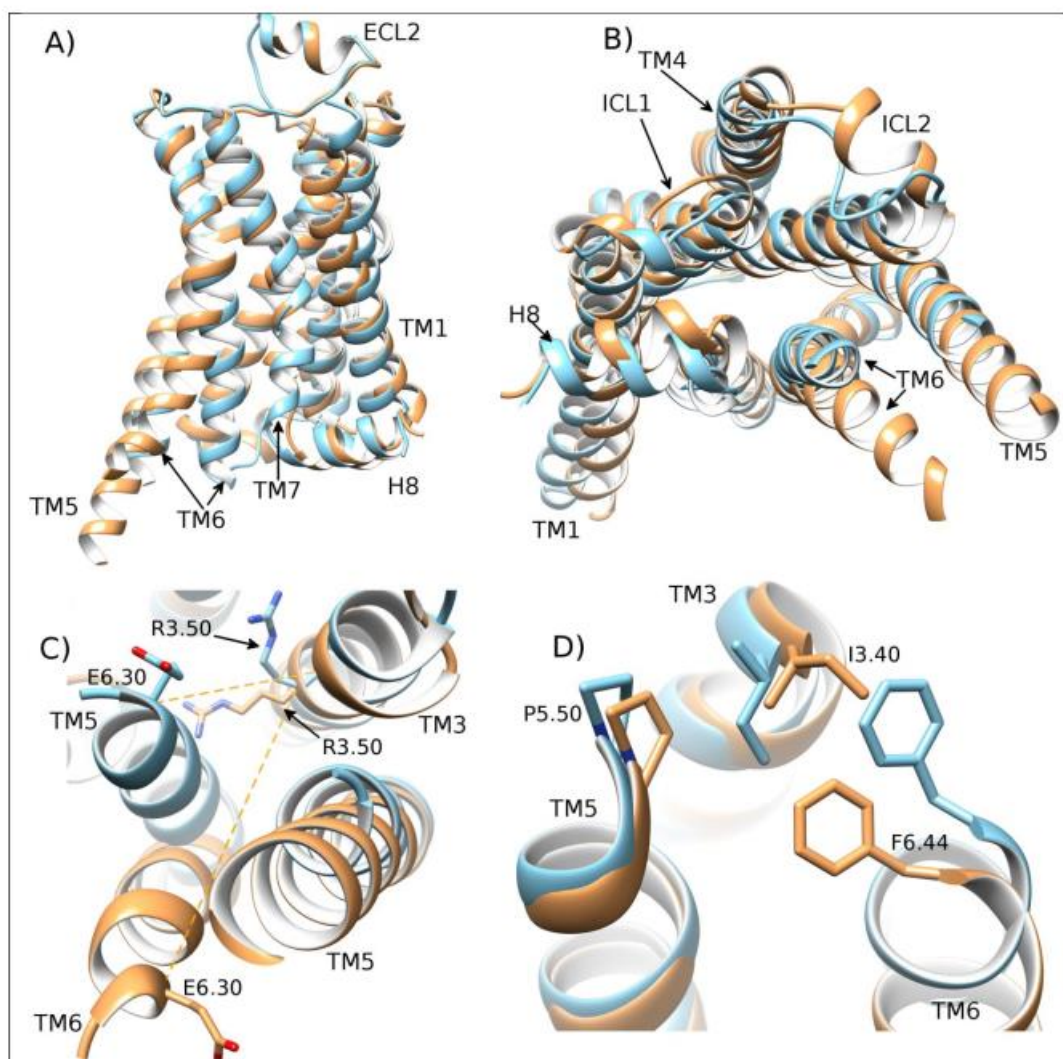
Agustin Bruzzese[a], Carles Gil[b], James A.R. Dalton[a,*], Jesús Giraldo[a,*].

[a]Laboratory of Molecular Neuropharmacology and Bioinformatics, Institut de Neurociències and Unitat de Bioestadística, Universitat Autònoma de Barcelona, Spain; Network Biomedical Research Centre on Mental Health (CIBERSAM), Spain.
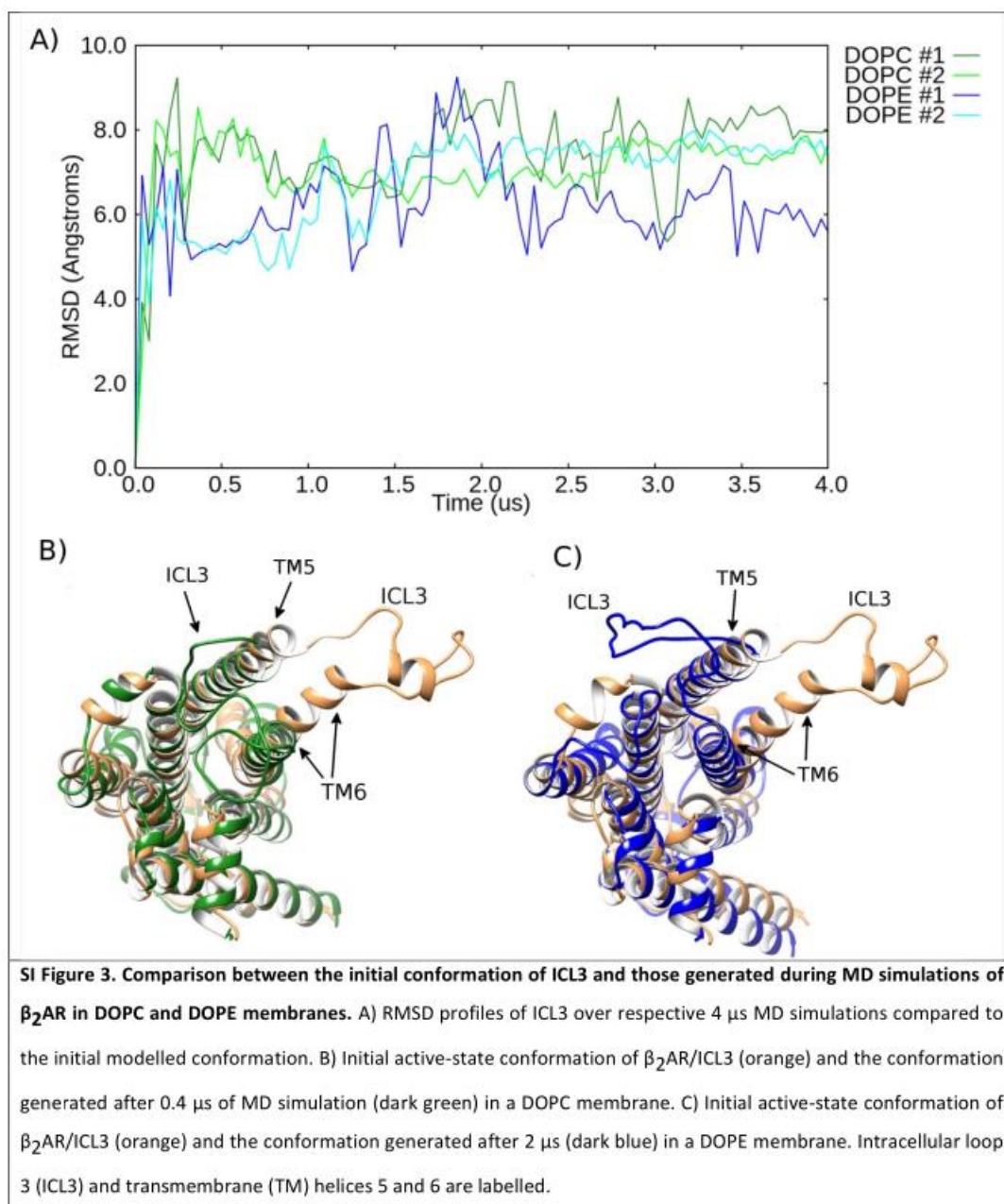
[b]Department of Biochemistry and Molecular Biology, Institut de Neurociències, Universitat Autònoma de Barcelona, Spain
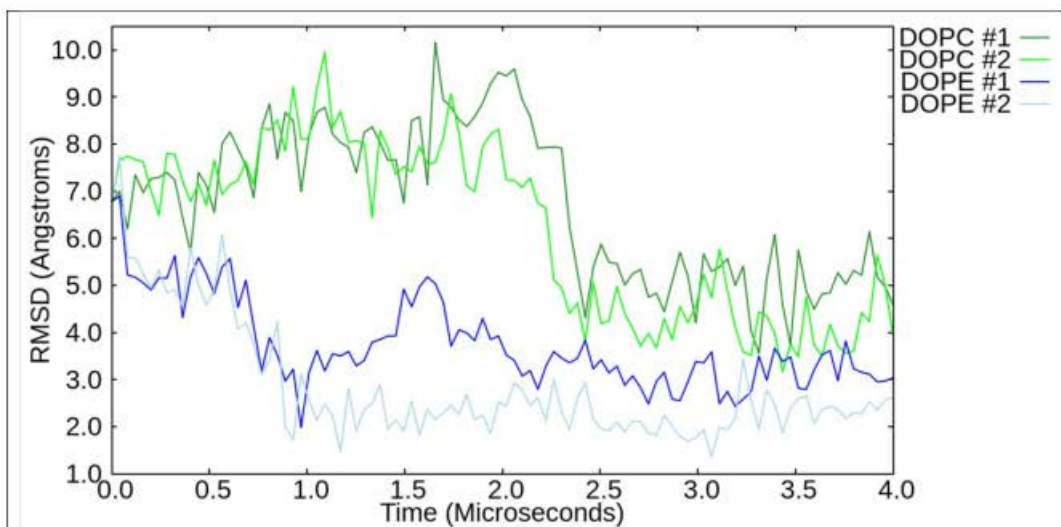
* Corresponding authors: james.dalton@uab.es and jesus.giraldo@uab.es

SI Figure 1. A cluster of positively-charged residues (13 in total) located on TM5, TM6 and ICL3 on the intracellular side of β$_2$AR. Arginines are coloured green and lysines coloured orange.

SI Figure 2. Structural comparison between β₂AR active and inactive crystal structures. A) Structural superposition of the active-state crystal structure (PDB id: 3SN6, orange) on the inactive-state crystal structure (PDB id: 2RH1, cyan). B) Intracellular view of TM6 movement between inactive and active states. C) The intracellular-side of the receptor and the distance (indicated by dashed lines) between ionic-lock residues ($R^{3.50}$ and $E^{6.30}$) in both states. D) Packing of the triad core in active and inactive crystal structures. Relevant structural features are labelled: intracellular loops (ICLs) and transmembrane (TM) helices.

SI Figure 3. Comparison between the initial conformation of ICL3 and those generated during MD simulations of β₂AR in DOPC and DOPE membranes. A) RMSD profiles of ICL3 over respective 4 μs MD simulations compared to the initial modelled conformation. B) Initial active-state conformation of β₂AR/ICL3 (orange) and the conformation generated after 0.4 μs of MD simulation (dark green) in a DOPC membrane. C) Initial active-state conformation of β₂AR/ICL3 (orange) and the conformation generated after 2 μs (dark blue) in a DOPE membrane. Intracellular loop 3 (ICL3) and transmembrane (TM) helices 5 and 6 are labelled.

SI Figure 4. Comparison of the modulation of TM6 conformation in β₂AR by different lipid membranes. RMSD profiles of conformational changes in TM6 observed during respective 4 μs MD simulations, compared to the inactive crystal structure of β₂AR (PDB id: 2RH1). The four lines constitute two MD simulations in DOPC membrane (dark green and light green) and two MD simulations in DOPE membrane (dark blue and light blue).
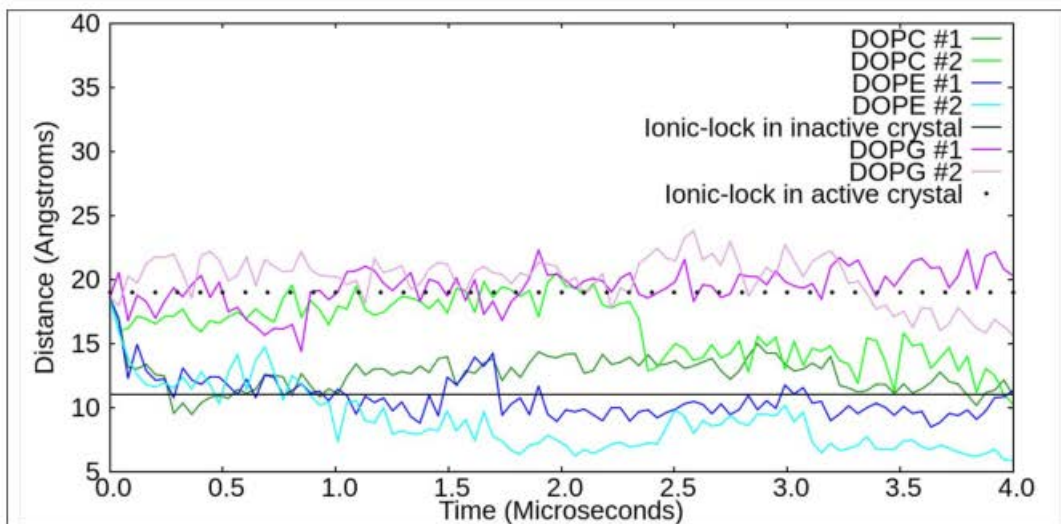

SI Figure 5. Comparison of distance between ionic-lock residues (R³·⁵⁰ and E⁶·³⁰) as a measure of deactivation or stabilization of the active state of β2AR. The six oscillating lines show ionic-lock status over respective 4 μs MD simulations of β2AR in DOPC (dark green and light green), DOPE (dark blue and light blue), and DOPG (dark magenta and light magenta) membranes. Corresponding flat-lines are included to show the observed distance in the active (dotted line, PDB id: 3SN6) and inactive (solid line, PDB id: 2RH1) β2AR crystal structures.
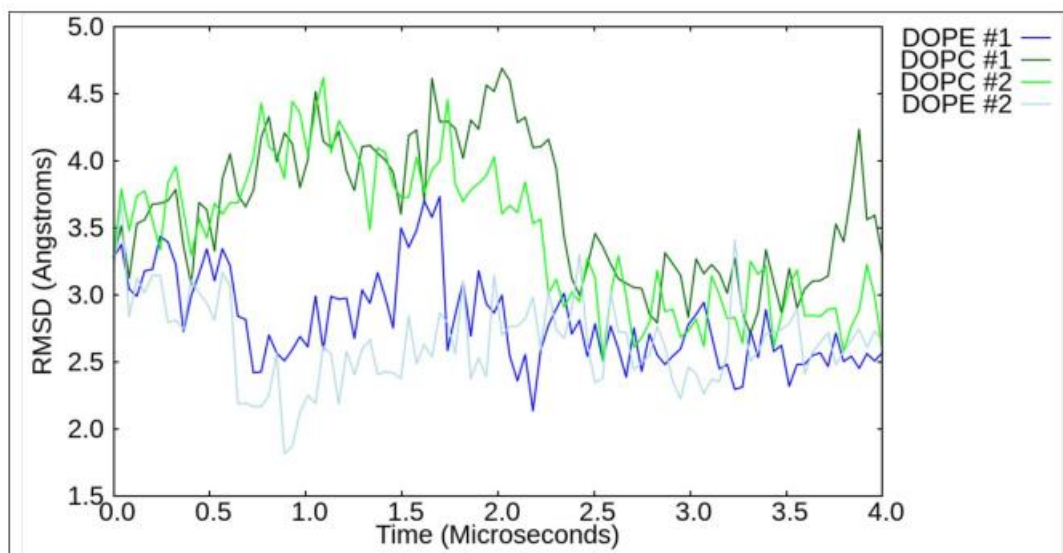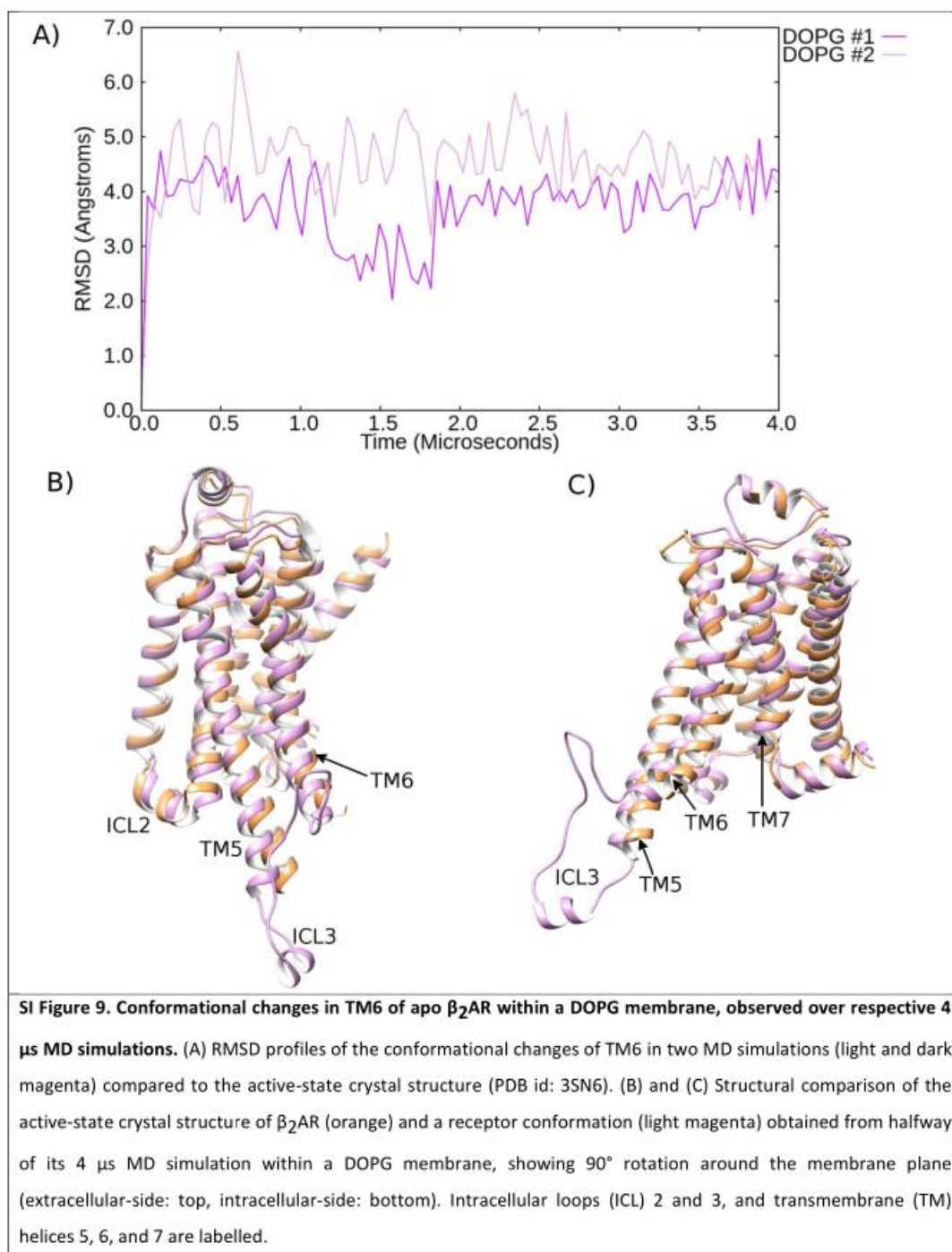
SI Figure 6. Comparison of full or partial inactivation processes of β$_2$AR in DOPE or DOPC membranes. RMSD profiles of conformational changes in helices 1-8 observed during respective 4 μs MD simulations compared to the inactive crystal structure of β$_2$AR (PDB id: 2RH1). The four lines constitute two MD simulations in DOPC membrane (dark green and light green) and two MD simulations in DOPE membrane (dark blue and light blue).
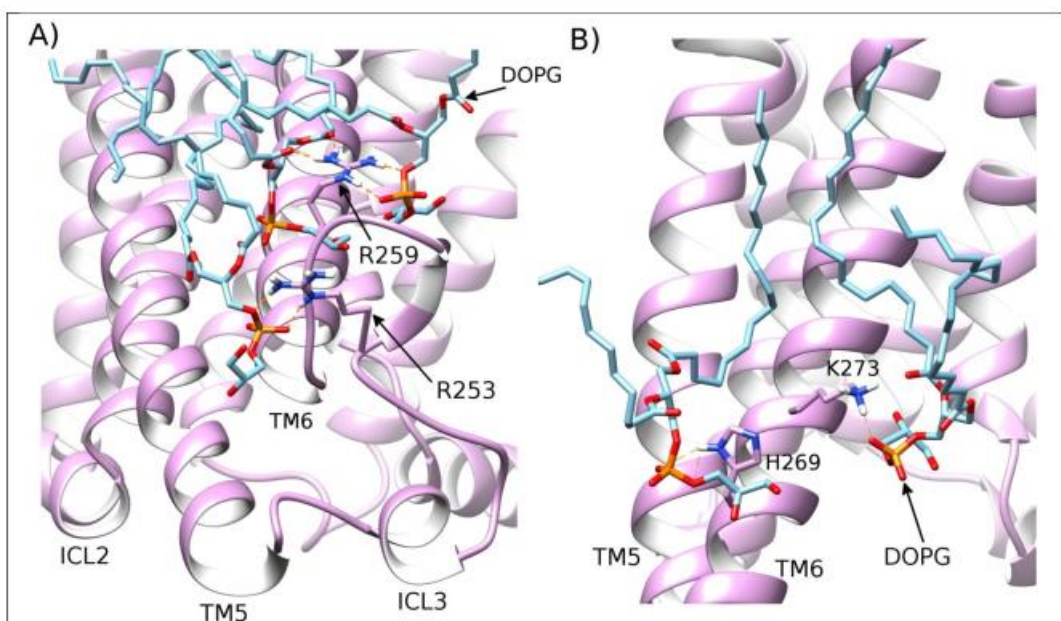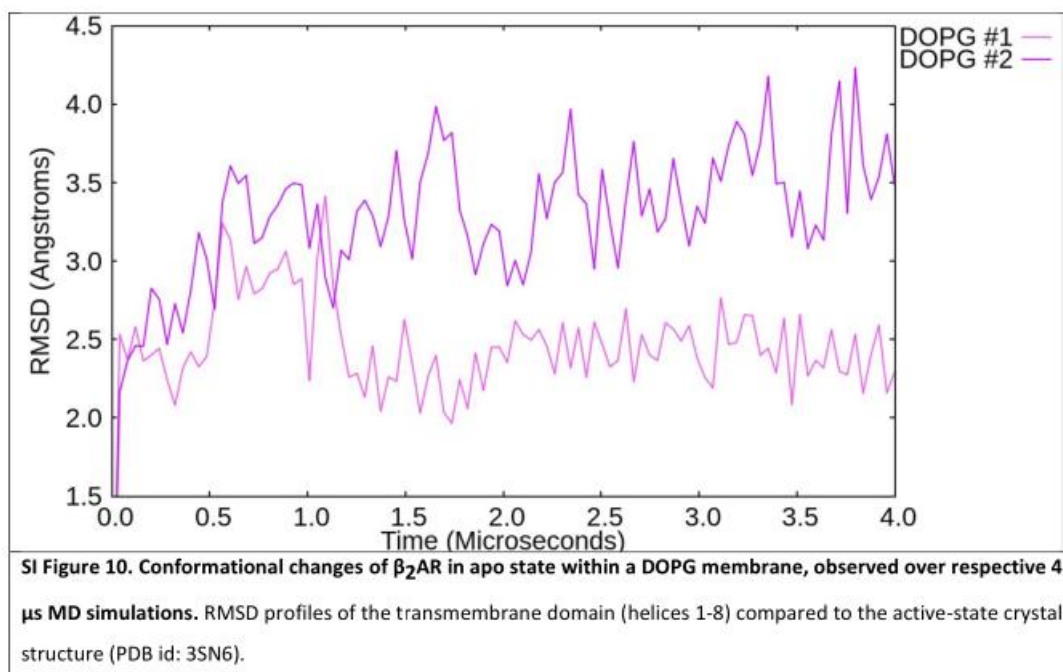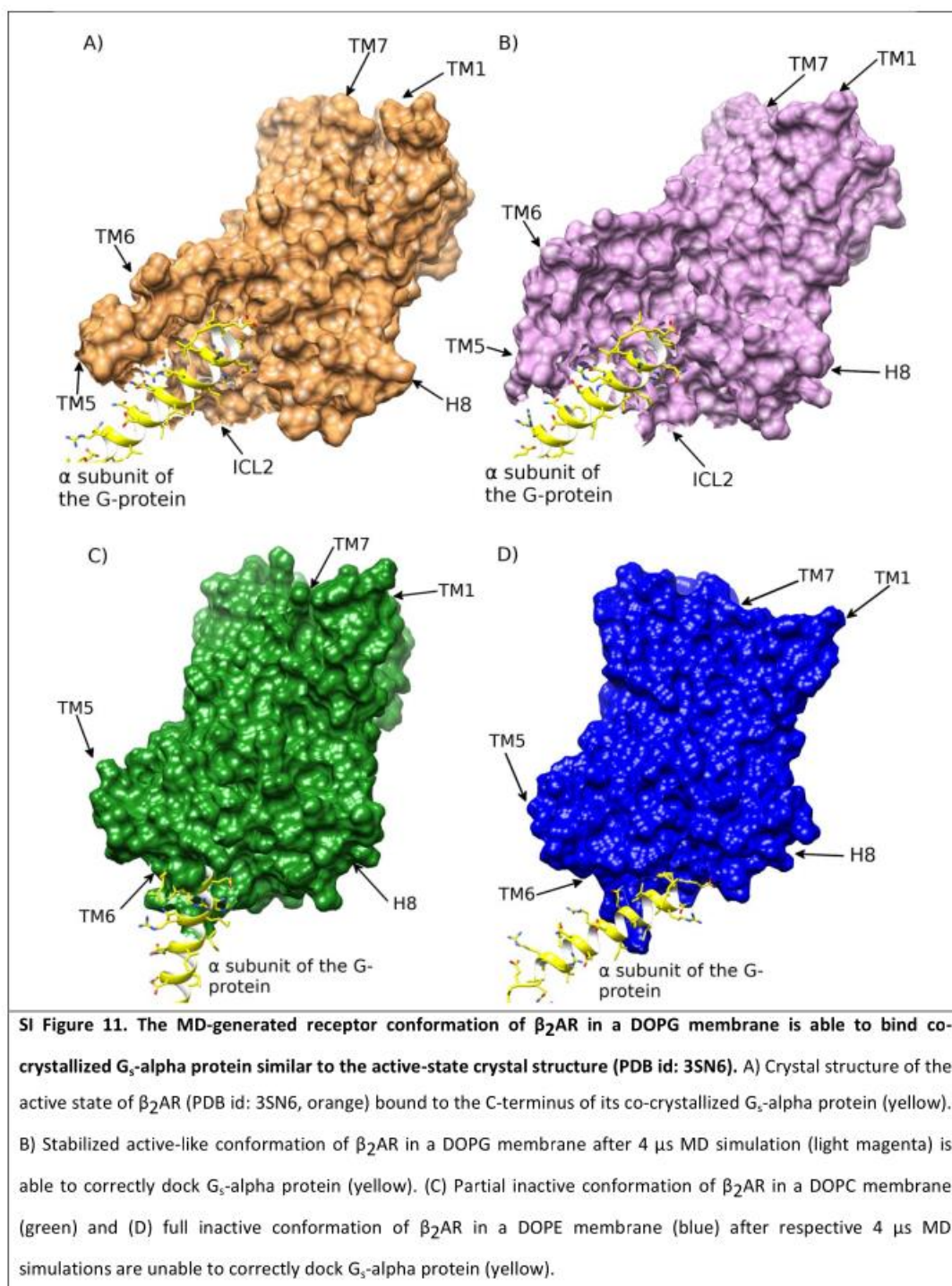
SI Figure 7. Selected protein-lipid interactions assisting the stabilization of an active-like state of β_2AR in a DOPG membrane. A) Selected allosteric interactions between positively charged residues (R253, R259) on intracellular loop 3 (ICL3) of β_2AR (light magenta) with DOPG lipids (light blue) after 4.0 µs MD simulation. B) Interactions between selected residues on TM6 (H269$^{6.31}$, K273$^{6.35}$) and phosphate groups of DOPG lipids (light blue) allow the stabilization of TM6 in an outward conformation.
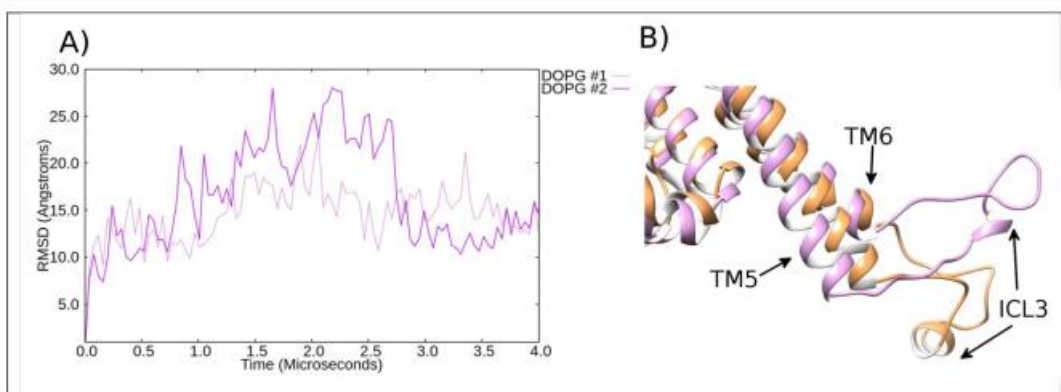
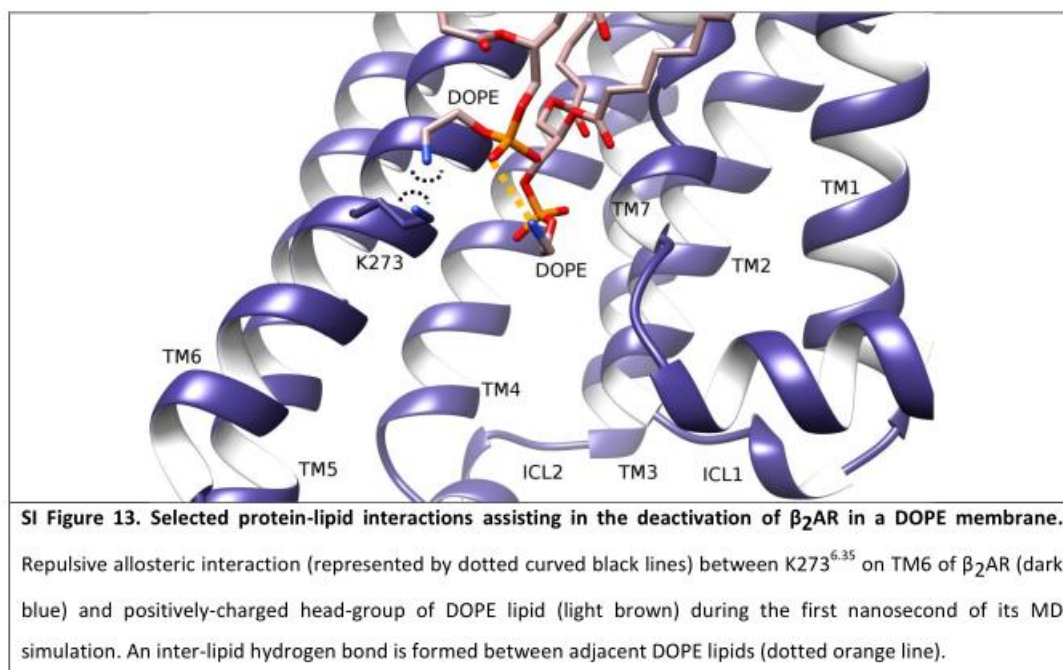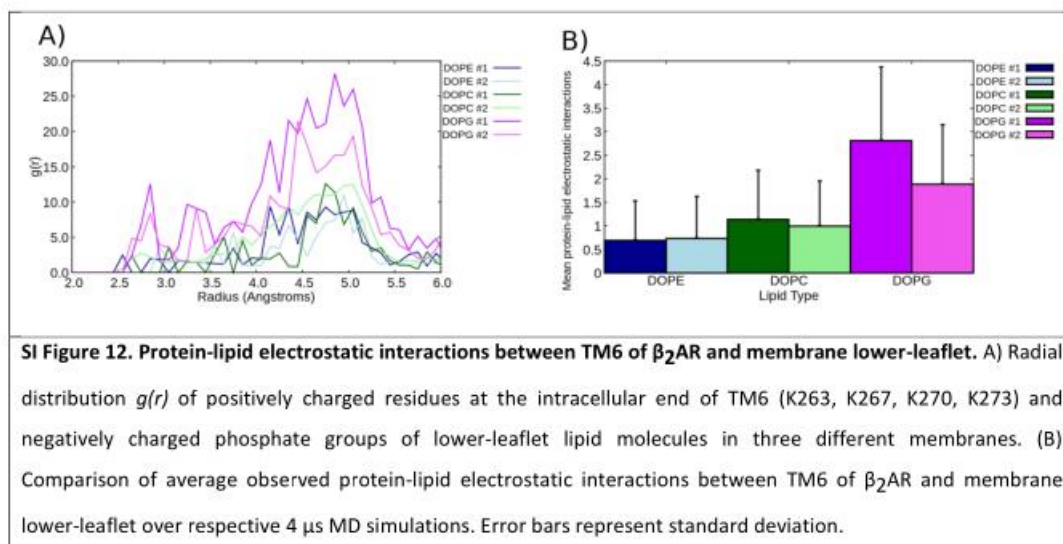**SI Figure 8. Comparison between the initial conformation of ICL3 and that generated during MD simulations of β_2AR in a DOPG membrane.** A) RMSD profiles of ICL3 observed during 4 µs MD simulations compared to the initial active-state conformation. B) Initial active-state conformation of β_2AR (orange) superimposed with the conformation of ICL3 observed after 0.1 µs (light magenta) in a DOPG membrane.

SI Figure 9. Conformational changes in TM6 of apo β$_2$AR within a DOPG membrane, observed over respective 4 µs MD simulations. (A) RMSD profiles of the conformational changes of TM6 in two MD simulations (light and dark magenta) compared to the active-state crystal structure (PDB id: 3SN6). (B) and (C) Structural comparison of the active-state crystal structure of β$_2$AR (orange) and a receptor conformation (light magenta) obtained from halfway of its 4 µs MD simulation within a DOPG membrane, showing 90° rotation around the membrane plane (extracellular-side: top, intracellular-side: bottom). Intracellular loops (ICL) 2 and 3, and transmembrane (TM) helices 5, 6, and 7 are labelled.

SI Figure 10. Conformational changes of β_2AR in apo state within a DOPG membrane, observed over respective 4 μs MD simulations. RMSD profiles of the transmembrane domain (helices 1-8) compared to the active-state crystal structure (PDB id: 3SN6).

SI Figure 11. The MD-generated receptor conformation of β₂AR in a DOPG membrane is able to bind co-crystallized Gₛ-alpha protein similar to the active-state crystal structure (PDB id: 3SN6). A) Crystal structure of the active state of β₂AR (PDB id: 3SN6, orange) bound to the C-terminus of its co-crystallized Gₛ-alpha protein (yellow). B) Stabilized active-like conformation of β₂AR in a DOPG membrane after 4 µs MD simulation (light magenta) is able to correctly dock Gₛ-alpha protein (yellow). (C) Partial inactive conformation of β₂AR in a DOPC membrane (green) and (D) full inactive conformation of β₂AR in a DOPE membrane (blue) after respective 4 µs MD simulations are unable to correctly dock Gₛ-alpha protein (yellow).

SI Figure 12. Protein-lipid electrostatic interactions between TM6 of β$_2$AR and membrane lower-leaflet. A) Radial distribution *g(r)* of positively charged residues at the intracellular end of TM6 (K263, K267, K270, K273) and negatively charged phosphate groups of lower-leaflet lipid molecules in three different membranes. (B) Comparison of average observed protein-lipid electrostatic interactions between TM6 of β$_2$AR and membrane lower-leaflet over respective 4 μs MD simulations. Error bars represent standard deviation.

SI Figure 13. Selected protein-lipid interactions assisting in the deactivation of β$_2$AR in a DOPE membrane. Repulsive allosteric interaction (represented by dotted curved black lines) between K273$^{6.35}$ on TM6 of β$_2$AR (dark blue) and positively-charged head-group of DOPE lipid (light brown) during the first nanosecond of its MD simulation. An inter-lipid hydrogen bond is formed between adjacent DOPE lipids (dotted orange line).

SI Figure 14. Conformational sampling of β₂AR in apo state within DOPC, DOPE and DOPG membranes over respective 4 μs MD simulations. Conformational change (RMSD compared to active crystal structure, PDB id: 3SN6) of TM7 motif NPXXY against distance between ionic-lock residues ($R^{3.50}$ and $E^{6.30}$). Data is extracted from 2 to 4 μs of each respective MD simulation.

Table S1. Protein conformational state measurements of β_2AR taken across respective MD simulations in three different phospholipid membranes (DOPC, DOPE, DOPG).

Measure (Å)	Time (µs)	DOPE		DOPC		DOPG	
		#1	#2	#1	#2	#1	#2
Ionic Lock Distance	0.0	18.6	18.6	18.6	18.6	18.6	18.6
	1.0	11.3	7.6	11.7	17.6	18.1	21.0
	2.0	9.2	7.4	14.1	19.2	19.1	21.5
	3.0	10.9	8.9	13.8	14.4	19.7	21.2
	4.0	11.1	5.8	11.1	10.2	20.3	16.8
RMSD Transmembrane helix 6 w/t inactive crystal	0.0	6.7	6.7	6.7	6.7	6.7	6.7
	1.0	2.8	2.7	8.2	8.3	7.7	8.3
	2.0	3.3	2.8	9.3	8.4	8.8	9.3
	3.0	3.2	1.9	4.9	4.8	8.3	8.3
	4.0	3.0	2.6	4.7	4.0	8.3	7.8
RMSD Transmembrane helix 6 w/t active crystal	0.0	0.0	0.0	0.0	0.0	0	0
	1.0	5.4	5.8	6.1	2.9	3.2	4.9
	2.0	6.5	6.2	3.7	3.2	3.4	4.5
	3.0	5.3	6.1	4.7	3.5	3.7	4.4
	4.0	5.2	6.7	4.8	4.4	4.3	4.1
RMSD Helices 1-8 w/t inactive crystal	0.0	3.3	3.3	3.3	3.3	3.3	3.3
	1.0	2.6	2.3	4.1	3.9	4.8	4.2
	2.0	2.9	2.6	4.7	3.8	4.9	4.8
	3.0	2.7	2.4	3.3	2.9	4.5	4.3
	4.0	2.5	2.7	3.4	2.8	4.4	4.1
RMSD Helices 1-8 w/t active crystal	0.0	0.0	0.0	0.0	0.0	0.0	0.0
	1.0	3.9	4.2	3.9	4.7	2.3	3.1
	2.0	4.5	5.0	3.9	4.4	2.4	3.0
	3.0	3.5	4.9	3.3	4.7	2.3	3.2
	4.0	4.8	5.0	4.3	4.4	2.3	3.5
RMSD NPxxY w/t inactive crystal	0.0	3.7	3.7	3.7	3.7	3.7	3.7
	1.0	3.2	2.9	3.2	3.0	2.8	4.2
	2.0	3.1	3.0	3.5	4.7	4.6	4.2
	3.0	2.8	3.0	3.9	3.6	4.7	4.9
	4.0	2.6	2.7	3.6	4.0	4.5	4.8
RMSD NPxxY w/t active crystal	0.0	0.0	0.0	0.0	0.0	0.0	0.0
	1.0	3.3	4.1	3.1	3.0	3.0	3.2
	2.0	3.2	3.3	3.0	2.6	2.8	3.6
	3.0	2.9	4.1	3.2	3.3	2.7	3.1
	4.0	3.0	4.2	2.8	2.2	2.4	2.8

9.2. INSIGHTS INTO ADENOSINE A2A RECEPTOR ACTIVATION THROUGH COOPERATIVE MODULATION OF AGONIST AND ALLOSTERIC LIPID INTERACTIONS
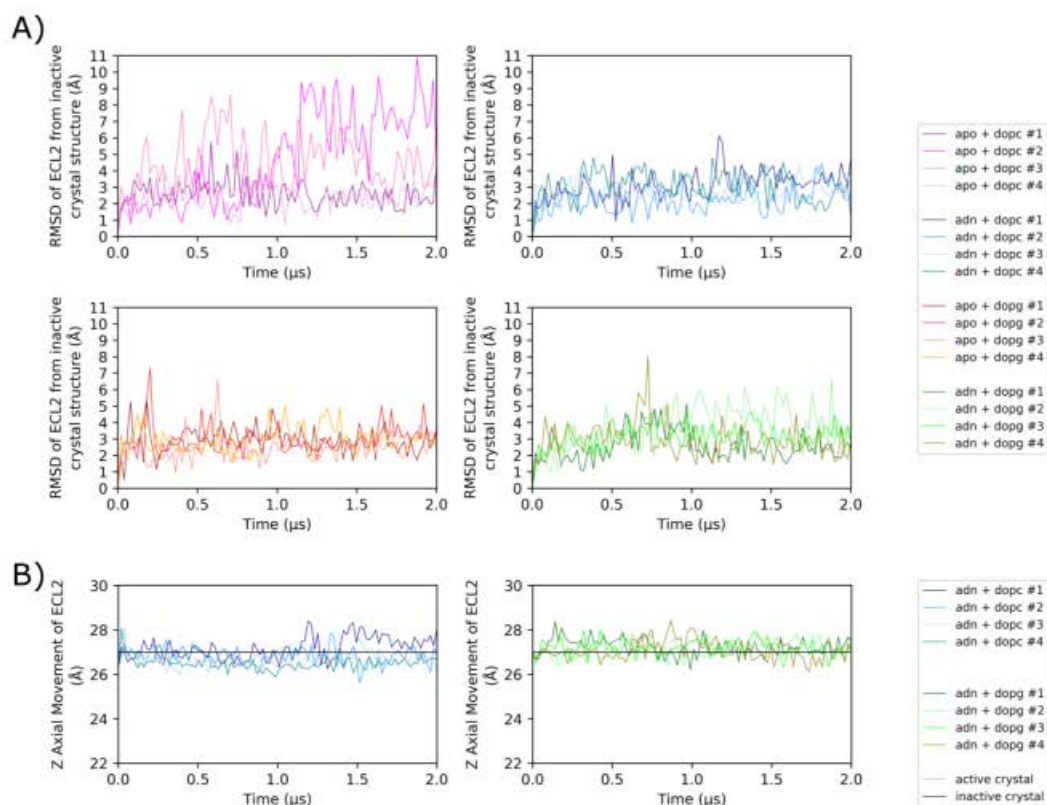
S1 Fig. Docking of NECA in the inactive crystal structure of adenosine A2a receptor (A2aR). A) Molecular structure of NECA. Comparison of B) co-crystallized NECA (lime) in agonist-bound A2aR crystal structure (PDB entry: 2YDV, light green), and C) docked NECA (magenta) in the inactive crystal structure of A2aR (PDB entry: 4EIY, pink). Selected residues participating in ligand binding are displayed. Extracellular loop (ECL) 2 and transmembrane (TM) helices 5-7 are labelled.

S2 Fig. Structural comparison between A2aR intermediate and inactive crystal structures: A) structural superposition of the intermediate adenosine-bound crystal structure (PDB entry: 2YDO, light green) on the inactive-state crystal structure (PDB entry: 4EIY, pink). B) Comparative positioning of residue $L^{3.43}$ located on TM3 and rotameric state of $W^{6.48}$ on TM6. C) Intracellular distance between residues $R^{3.50}$ and $Y^{7.53}$ on TM3 and TM7 (indicated by dashed lines) before/after receptor conformational change. D) Distance between residues $R^{3.50}$ and $Q^{5.68}$ (indicated by dashed lines). E) Partial separation of ionic-lock residues $R^{3.50}$ and $E^{6.30}$ on TM3 and TM6 (indicated by dashed lines). Relevant structural features are labelled: extracellular loops (ECL) 1, 2 and 3, and transmembrane (TM) helices 1-3, 5-7.

S3 Fig. Structural comparison between A2aR active and inactive crystal structures: A) structural superposition of the active-state crystal structure (PDB entry: 6GDG, brown) on the inactive-state crystal structure (PDB entry: 4EIY, pink). B) Proposed scheme of activation for A2aR, including rotation and upwards axial movement of TM3, outwards movement of TM5, rotation plus outward movement of TM6, and inwards movement of TM7. C) Comparative positioning of residue $L^{3.43}$ located on TM3 and rotameric state of $W^{6.48}$ on TM6. D) Intracellular conformational change of TM5 with increased separation (indicated by dashed lines) between residues $R^{3.50}$ and $Q^{5.68}$ after receptor activation. E) Intracellular comparison of distance between residues $R^{3.50}$ and $Y^{7.53}$ after receptor activation (indicated by dashed lines). F) Intracellular conformational change of TM6 and separation (indicated by dashed lines) of ionic-lock residues $R^{3.50}$ and $E^{6.30}$ after receptor activation. Relevant structural features are labelled: intracellular loop (ICL) 2, extracellular loops (ECL) 1, 2 and 3, and transmembrane (TM) helices 1-3, 5-7.

S4 Fig. Comparison of conformational change of extracellular loop 2 (ECL2) in MD simulations of A2aR. A) RMSD of ECL2 from the starting inactive A2aR crystal structure (PDB entry: 4EIY). B) Vertical movement of ECL2 along Z-axis (containing residues: G142-A173). MD simulations are performed in quadruplicate, with or without bound adenosine (ADN) in DOPC or DOPG homogeneous membranes.
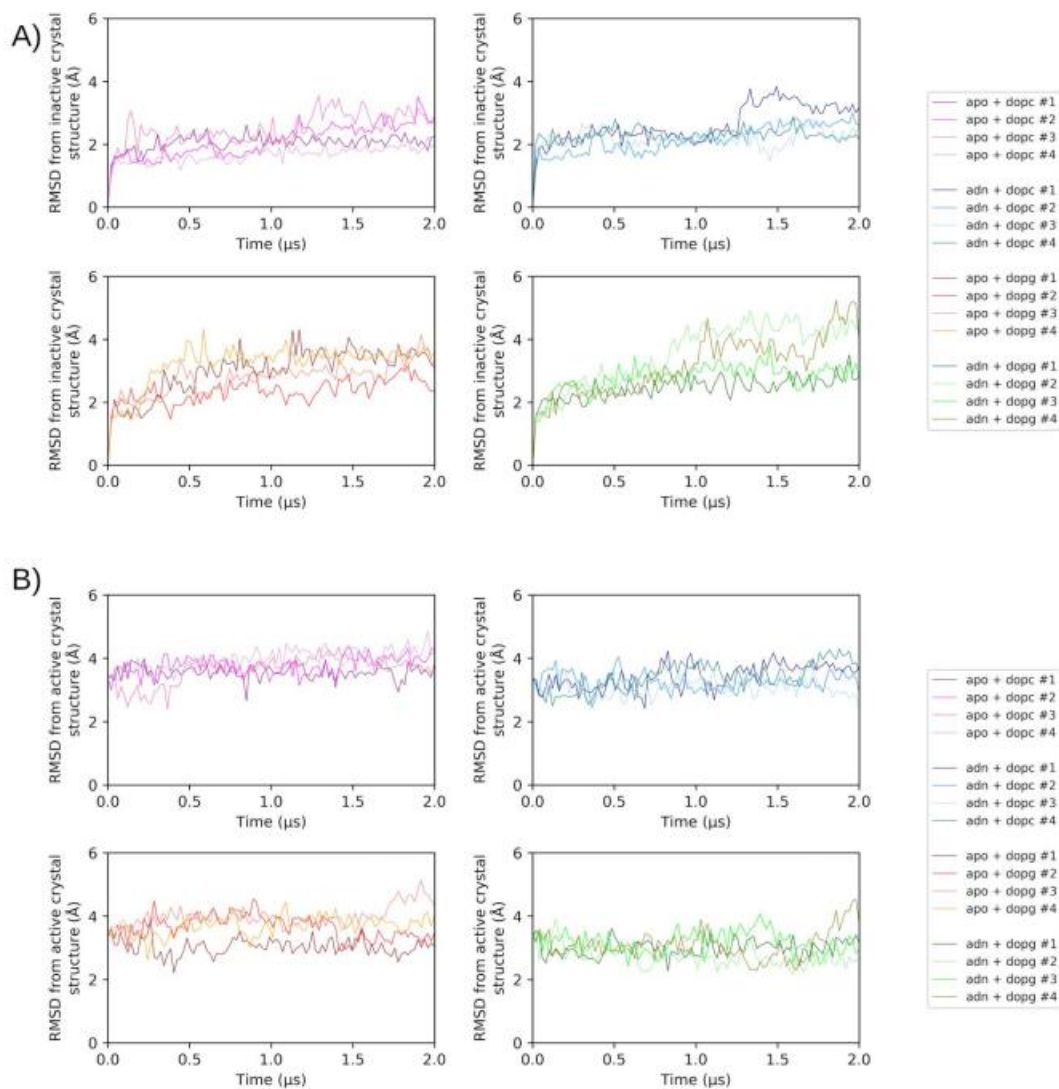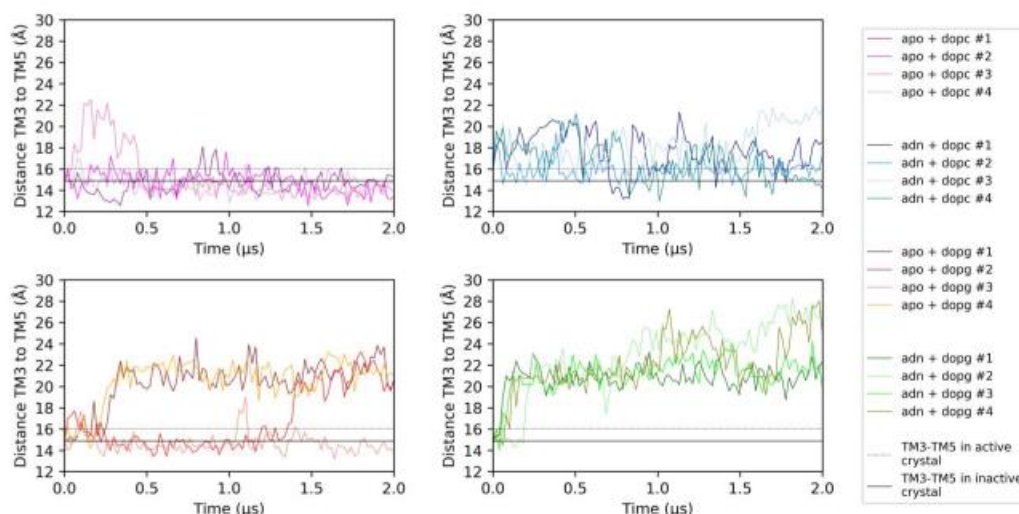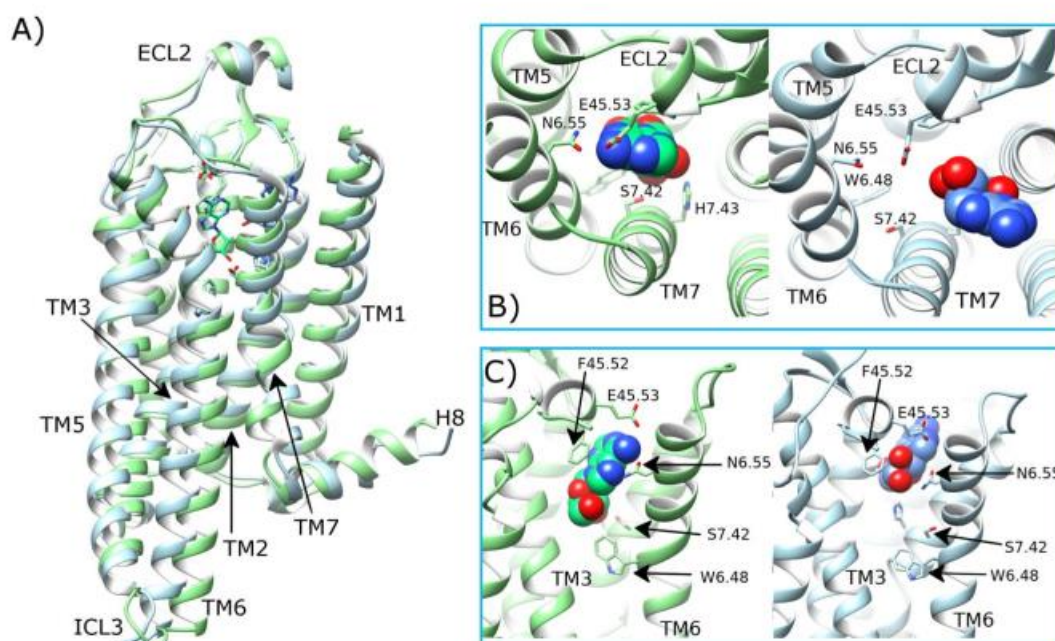
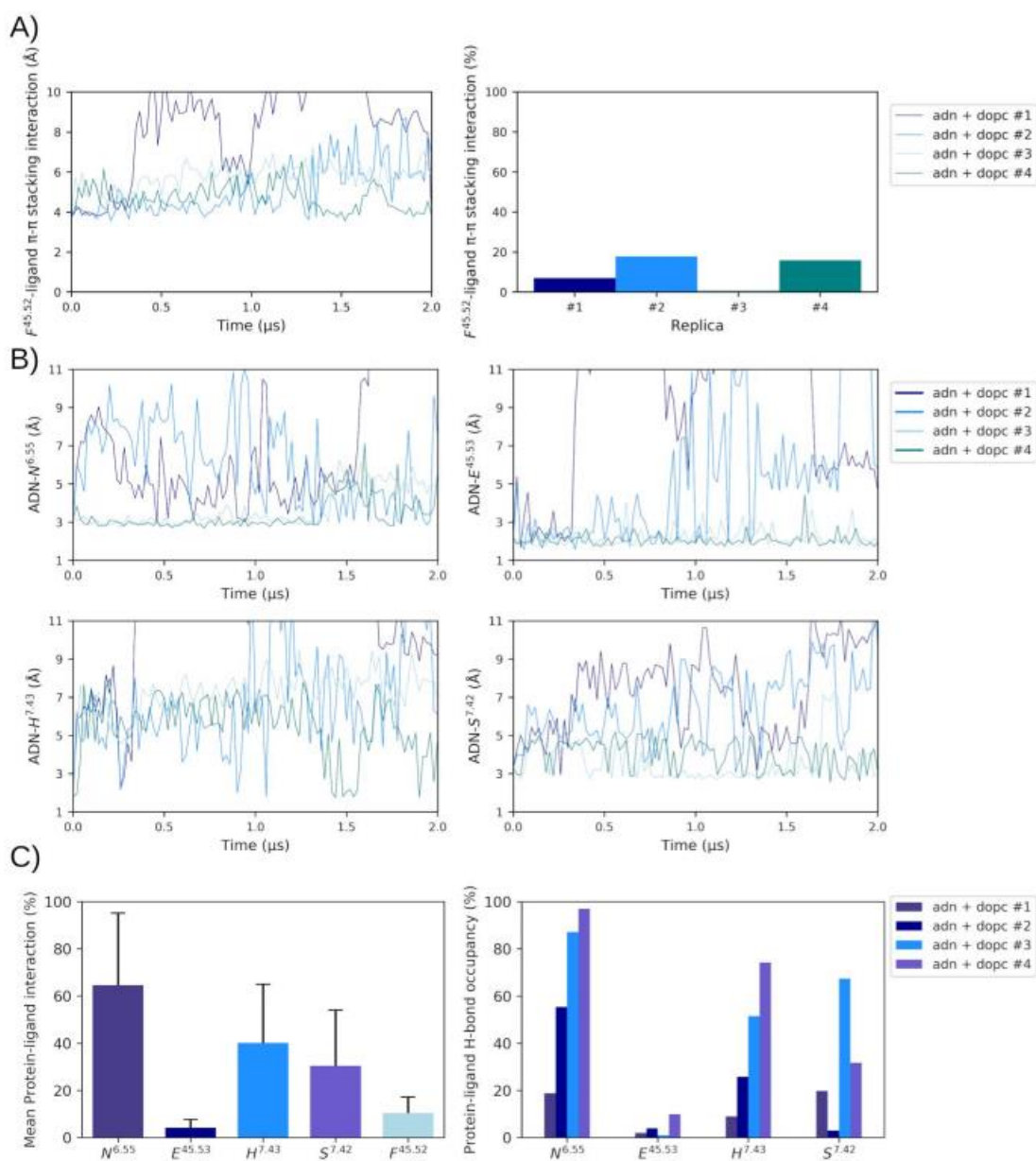**S5 Fig. Conformational change of helix bundle of A2aR in MD simulations.** A) RMSD of helices 1-7 from the inactive crystal structure (PDB entry: 4EIY) and B) with respect to the active crystal structure of A2aR (PDB entry: 6GDG). MD simulations are performed in quadruplicate, with or without bound adenosine (ADN) in DOPC or DOPG homogeneous membranes.
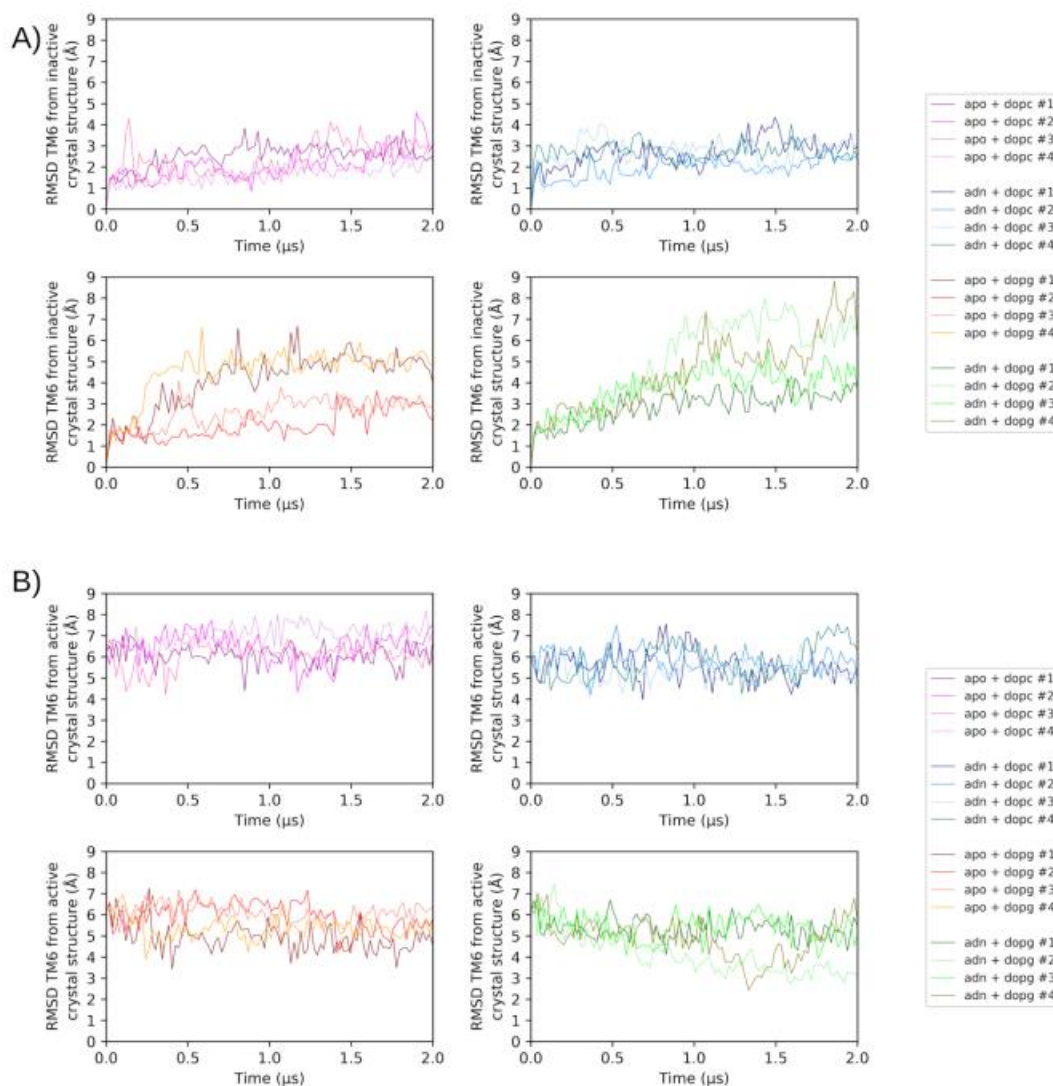
S6 Fig. TM6 conformational change of A2aR in MD simulations. A) RMSD from the starting inactive A2aR crystal structure (PDB entry: 4EIY) and B) with respect to the active A2aR crystal structure (PDB entry: 6GDG). MD simulations are performed in quadruplicate, with or without bound adenosine (ADN) and in DOPC or DOPG homogeneous membranes.
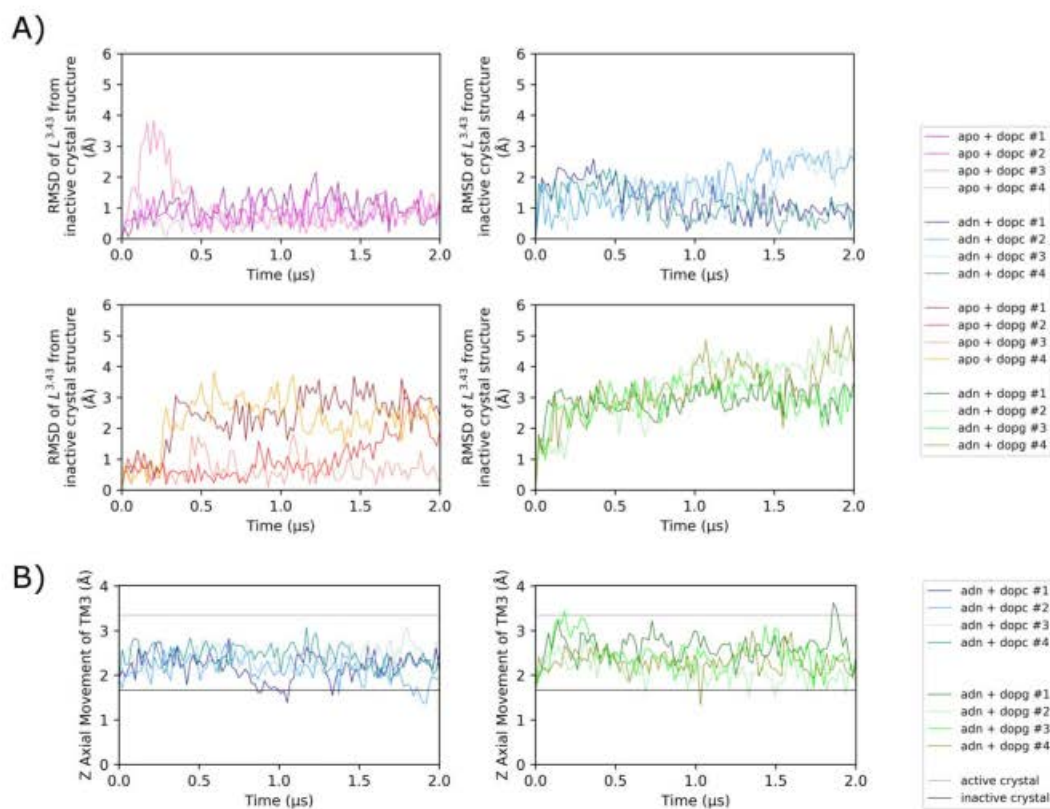
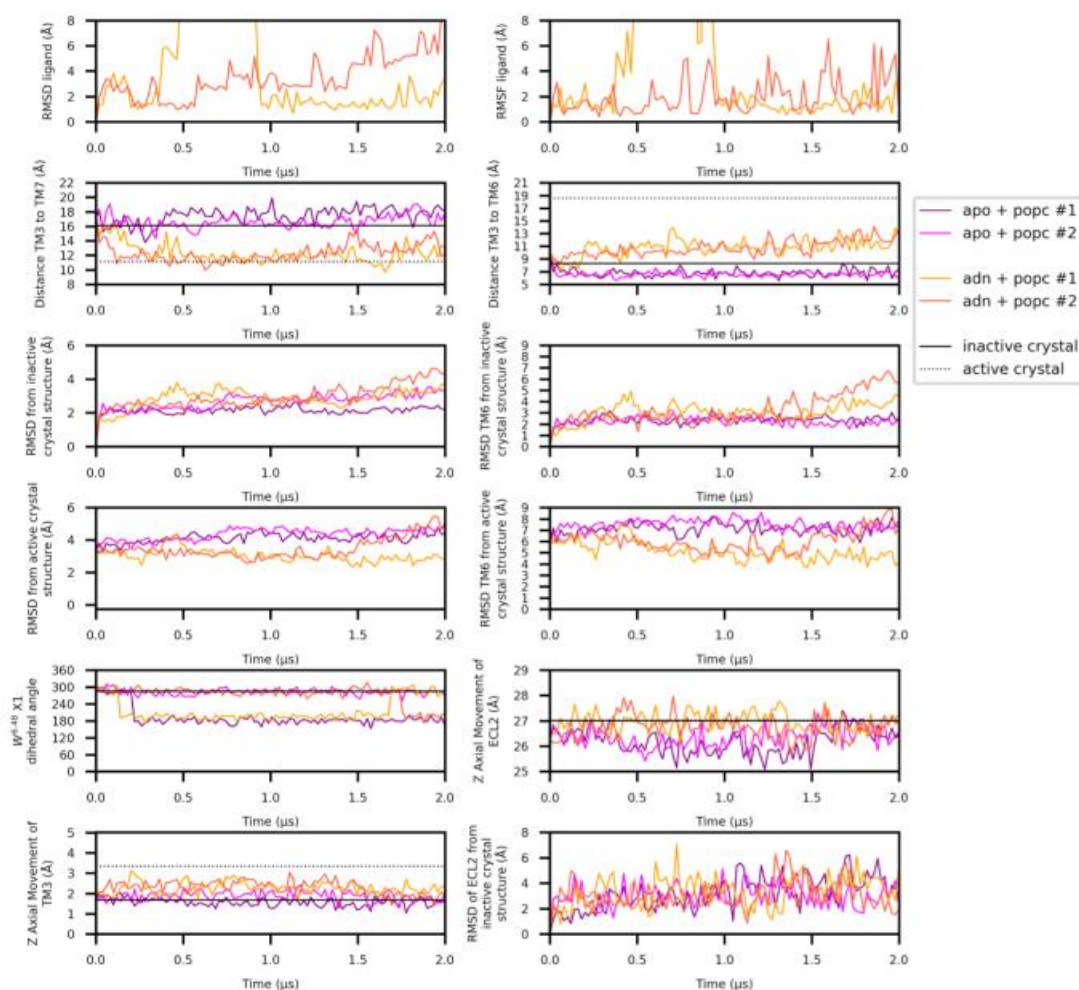**S7 Fig. Assessment of conformational change along TM3 during MD simulations of A2aR.** A) RMSD of residue L3.43 on TM3 compared to the inactive crystal structure (PDB entry: 4EIY) and B) assessment of vertical movement of TM3 along Z-axis. MD simulations are performed in quadruplicate with or without bound adenosine (ADN) and in DOPC or DOPG homogeneous membranes.

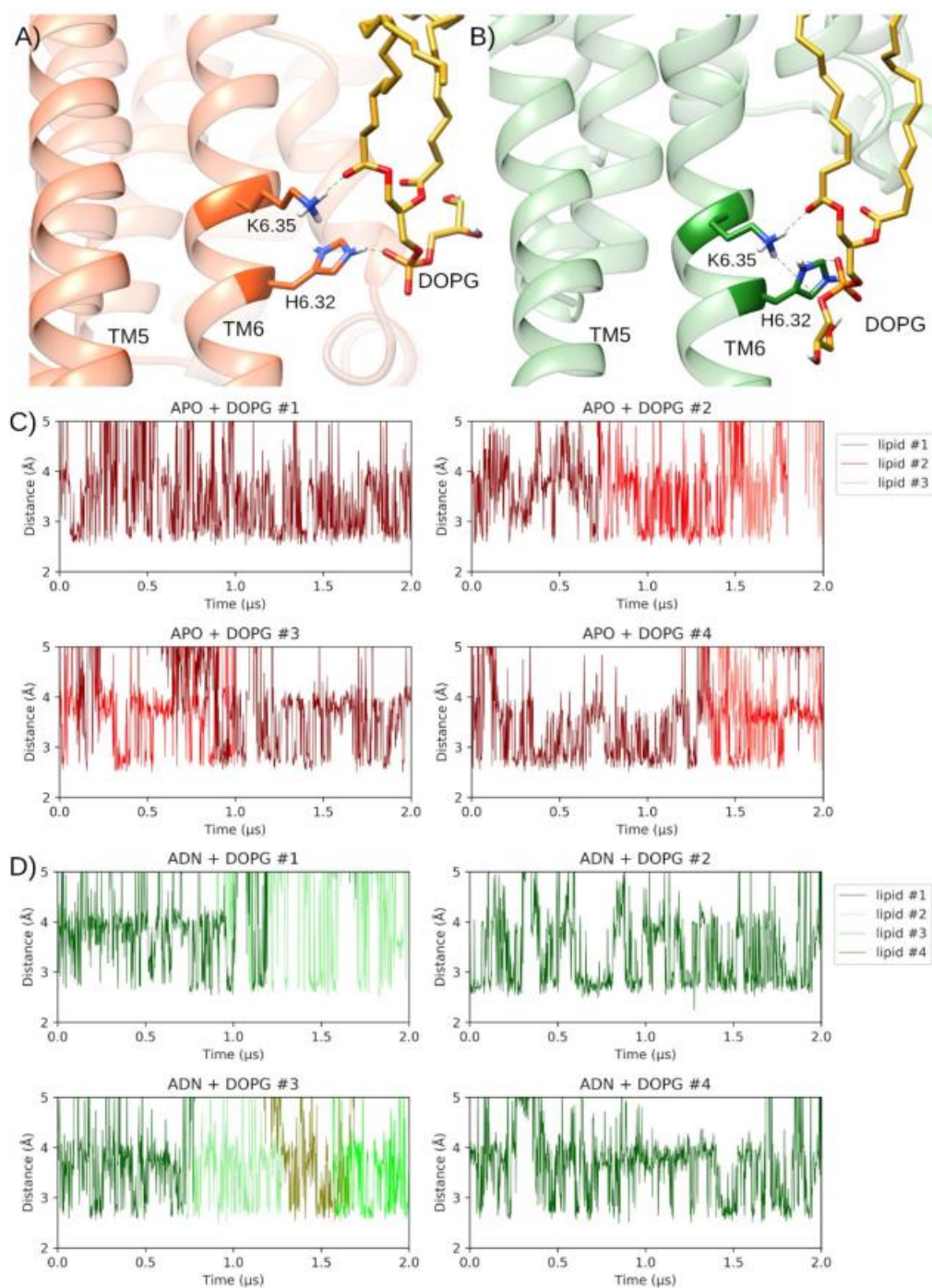**S8 Fig. Assessment of rotameric conformational change of residue W[6.48] on TM6.** A) W246[6.48] rotameric switch starting from *gauche*(-) (285°) (belonging to replica #2 from 1.7 μs in APO embedded in DOPC, in magenta) to trans (180°) during MD simulation replica #4 from 1.8 μs in DOPG with bound adenosine (in green). B) χ1 dihedral angle of residue W246[6.48] over time. MD simulations are performed in quadruplicate, with or without bound adenosine (ADN) in DOPC or DOPG homogeneous membranes.

S9 Fig. Comparison of TM3-TM5 inter-helical distance in MD simulations of A2aR. Distance between TM3-TM5 is measured between Cα atoms of R102$^{3.50}$ and Q207$^{5.68}$. MD simulations are performed in quadruplicate, with or without bound adenosine (ADN) in DOPC or DOPG homogeneous membranes.

S10 Fig. Alternative binding pose of adenosine in A2aR in DOPC membrane. A) Superposition of the intermediate crystal structure of A2aR (PDB entry: 2YDO, light green) and an MD-generated conformation achieved within a DOPC membrane bound to adenosine (in blue, belonging to replica #1 at 1.9 μs) showing B) and C) ligand atoms as spheres and selected residues making protein-ligand interactions as sticks. Intracellular loop (ICL) 3, extracellular loop (ECL) 2, and transmembrane (TM) helices 1-3 and 5-7 are labelled.
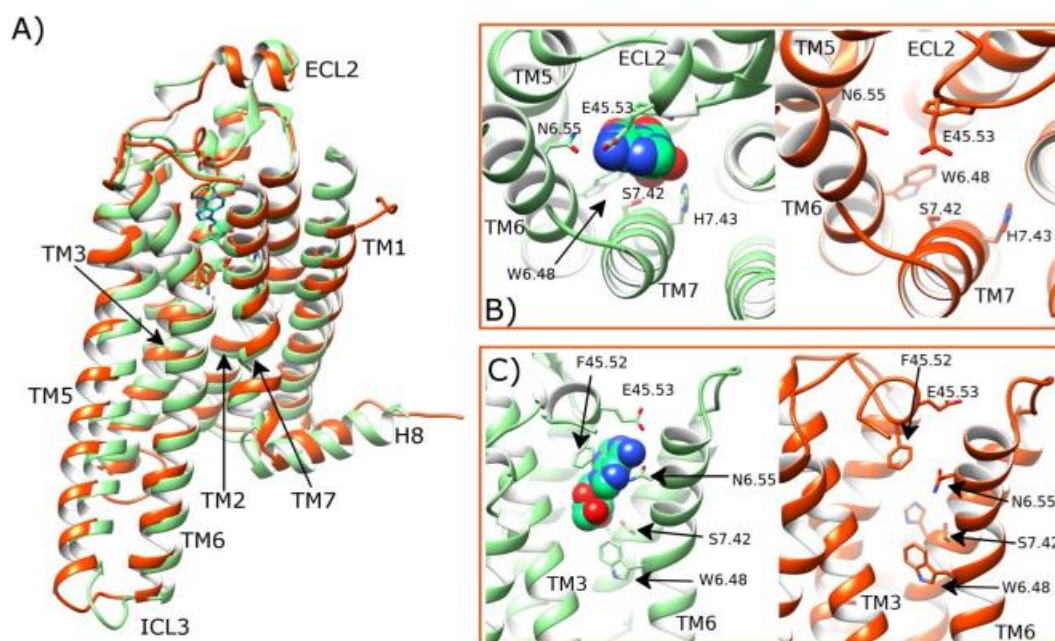
S11 Fig. Assessment of key protein-ligand interactions in MD simulations of adenosine-bound A2aR embedded in DOPC membrane. A) Left: distance of $F^{45.52}$ with respect to ribose moiety of adenosine (ADN). Right: frequency (%) of protein-ligand π-π stacking (within range of 0.0 to 4.0 Å) over 2 μs. B) Evaluation of protein-ligand H-bond distances formed by residues: $N253^{6.55}$, $E169^{45.53}$, $H278^{7.43}$, $S277^{7.42}$ (N---O or O---O). C) Mean protein-ligand interactions (%) and protein-ligand H-bond occupancies per replica (%) for selected residues.
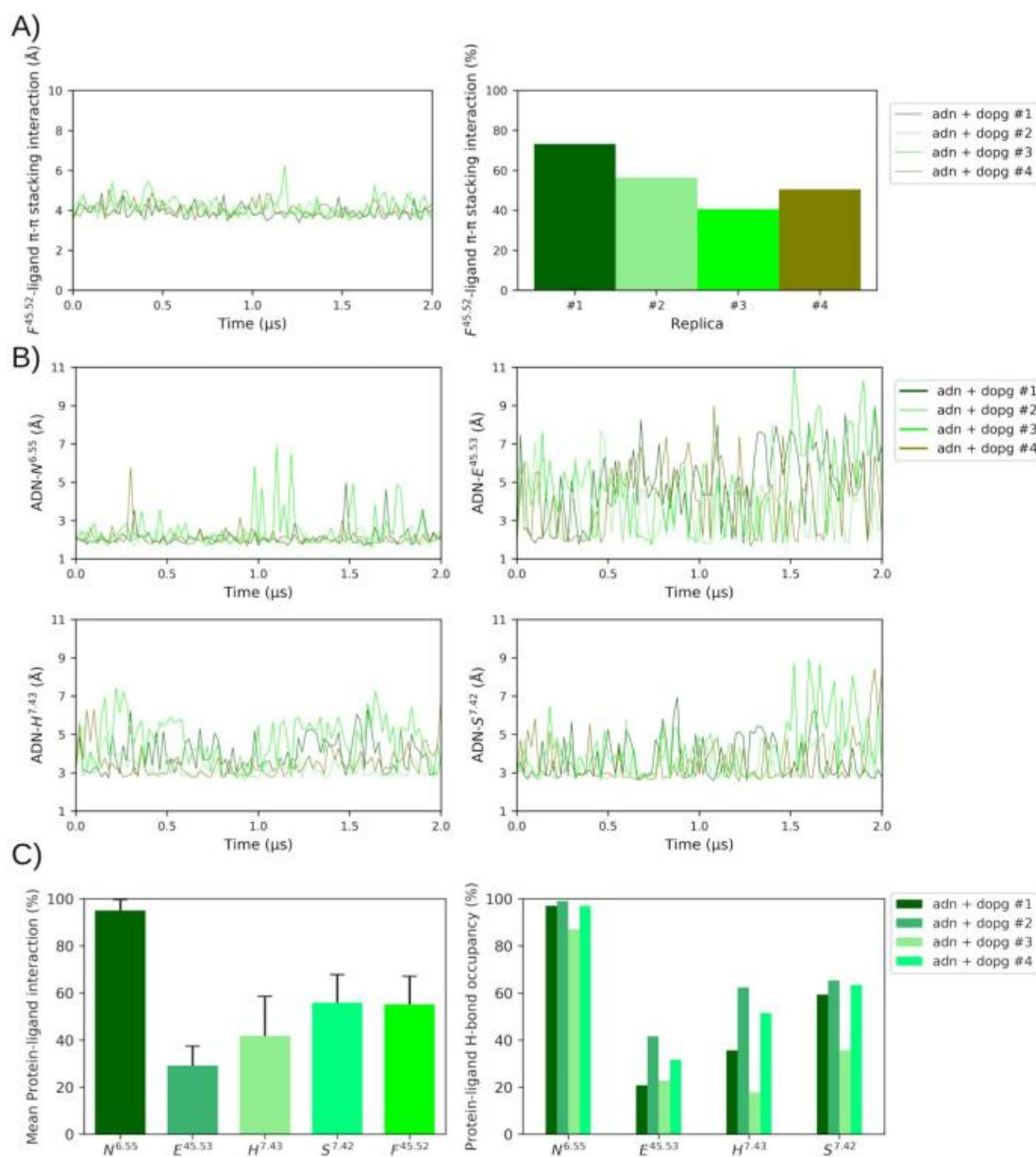
S12 Fig. MD simulation data of adenosine A2a receptor (A2aR) with or without bound adenosine (ADN) starting from the inactive receptor crystal structure (PDB id: 4EIY) in a POPC membrane. Top row: RMSD and conformational fluctuation (RMSF) of bound adenosine ligand; second row: TM3-TM7 and ionic lock (TM3-TM6) inter-helical distances; third row: RMSD of whole TMD (TMs 1-7) or only TM6; fourth row: RMSD compared to active crystal structure (PDB id: 6GDG) of whole TMD (TMs 1-7) or only TM6; fifth row: $\chi 1$ dihedral angle of W246$^{6.48}$ on TM6 starting from *gauche*(-) crystal position (285°), and vertical movement of extracellular loop 2 (ECL2); bottom row: vertical movement of TM3 and RMSD of ECL2. MD simulations are performed in duplicate in POPC homogeneous membranes.
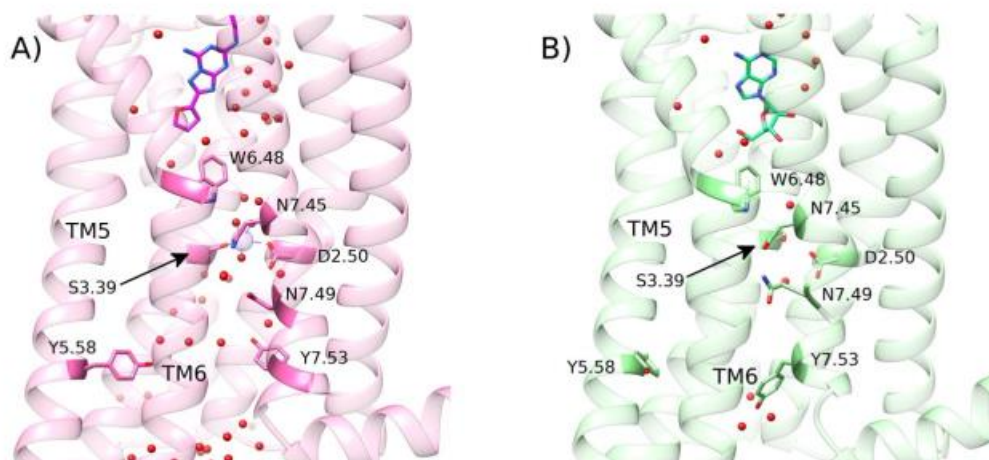
S13 Fig. Protein-lipid interaction between closest DOPG molecule and residue H230$^{6.32}$ in MD simulations of A2aR with or without bound adenosine. A) Residues H230$^{6.32}$ and K233$^{6.35}$ on TM6 of A2aR in apo state (orange) and B) A2aR with bound adenosine (green) interacting with DOPG lipid (gold). Histidine-lipid interaction distances over time in four replicas of A2aR in DOPG membrane in C) apo state and D) adenosine-bound (ADN), respectively.
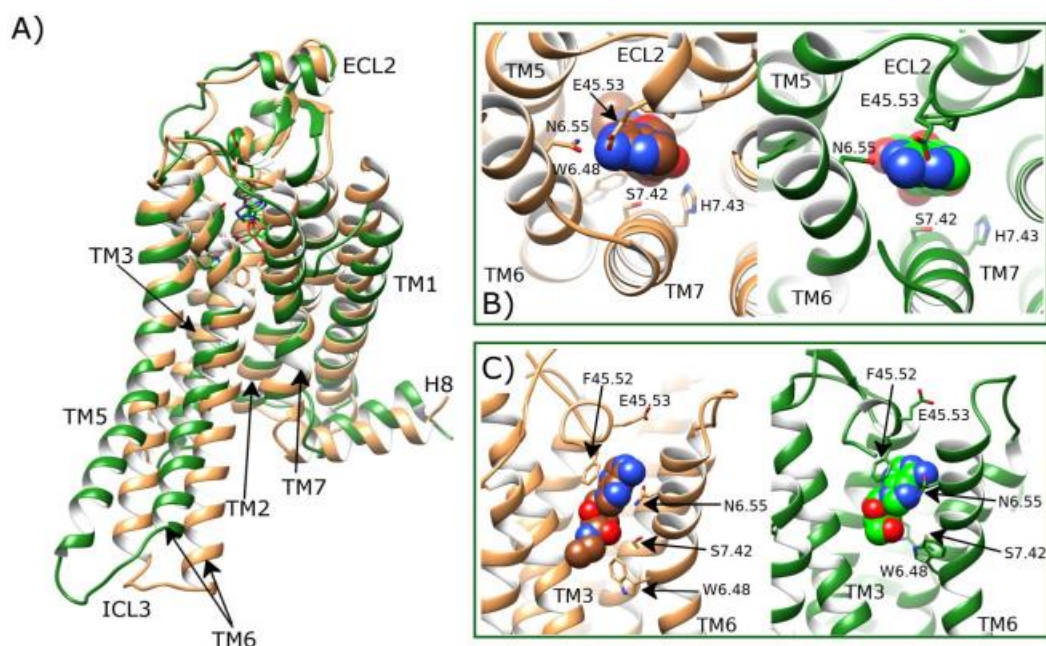
S14 Fig. Intermediate conformation of the apo state of A2aR in a DOPG membrane. A) Comparison of the intermediate crystal structure of A2aR (PDB entry: 2YDO, light green) and an MD-generated apo conformation achieved within a DOPG membrane (in red, belonging to replica #2 at 1.6 μs) showing B) and C) selected residues delineating the orthosteric pocket. Intracellular loop (ICL) 3, extracellular loop (ECL) 2, and transmembrane (TM) helices 1-3, 5-7 are labelled
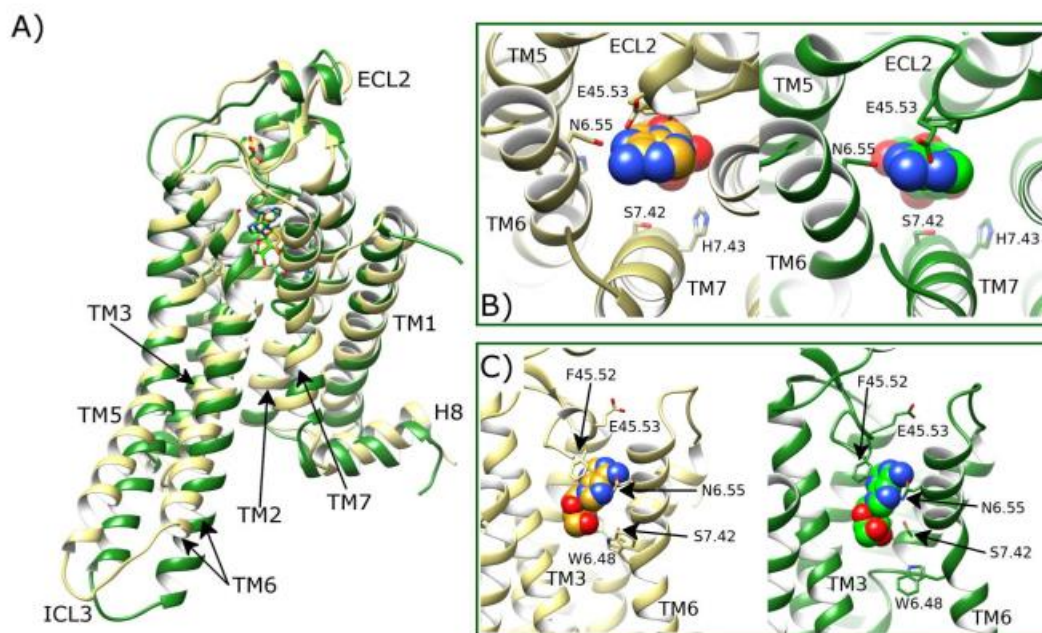
S15 Fig. Assessment of key protein-ligand interactions in MD simulations of adenosine-bound A2aR embedded in DOPG membrane. A) Left: distance of $F^{45.52}$ with respect to ribose moiety of adenosine (ADN). Right: frequency (%) of protein-ligand π-π stacking (within range of 0.0 to 4.0 Å) over 2 µs. B) Evaluation of protein-ligand H-bond distances formed by residues: $N253^{6.55}$, $E169^{45.53}$, $H278^{7.43}$, $S277^{7.42}$ (N---O or O---O). C) Mean protein-ligand interactions (%) and protein-ligand H-bond occupancies per replica (%) for selected residues.
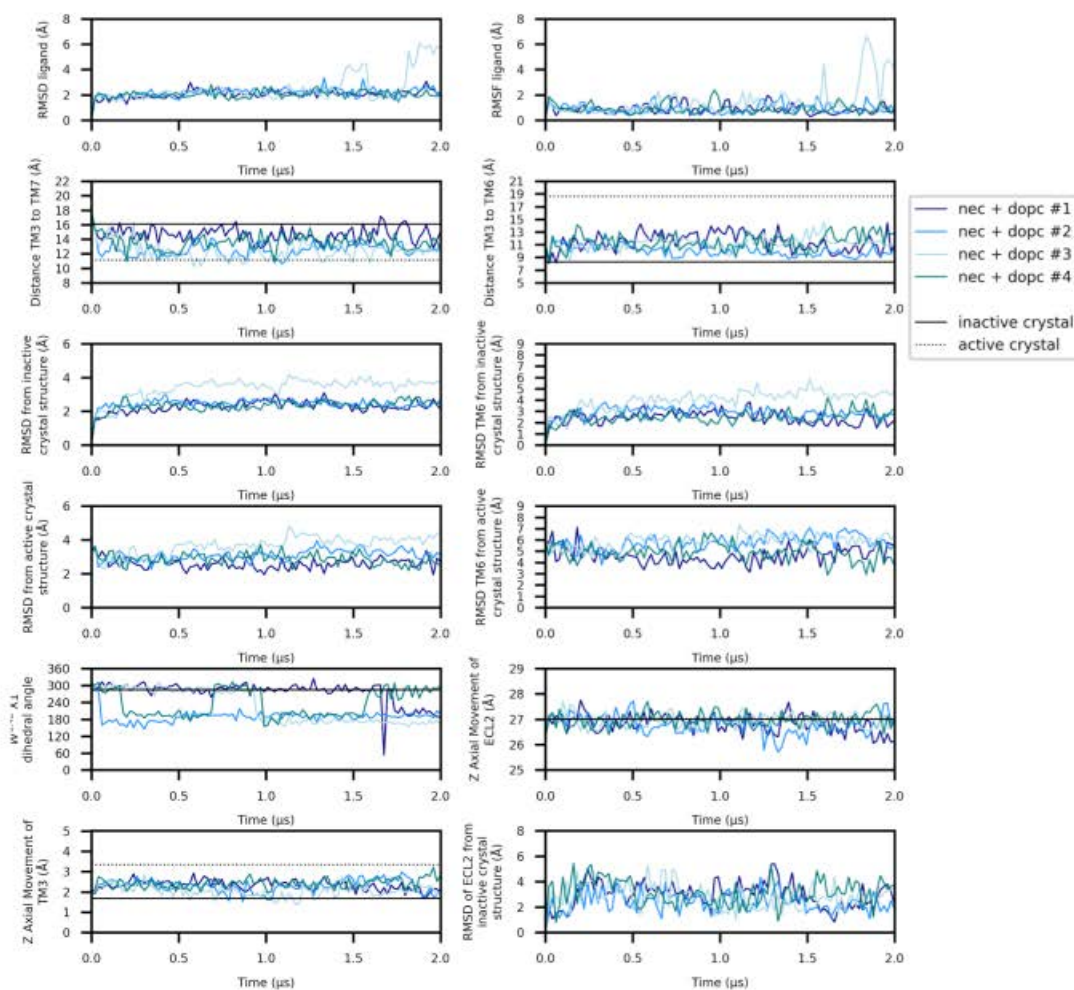
S16 Fig. State-dependent water-mediated polar network across the ZM241385-bound and adenosine-bound A2aR crystal structures. The water network retrieved from: A) the inactive crystal structure (PDB entry: 4EIY, pink) and B) the intermediate crystal structure (PDB entry: 2YDO, light green). Residues and ligands are shown as sticks and water molecules are shown as red spheres.
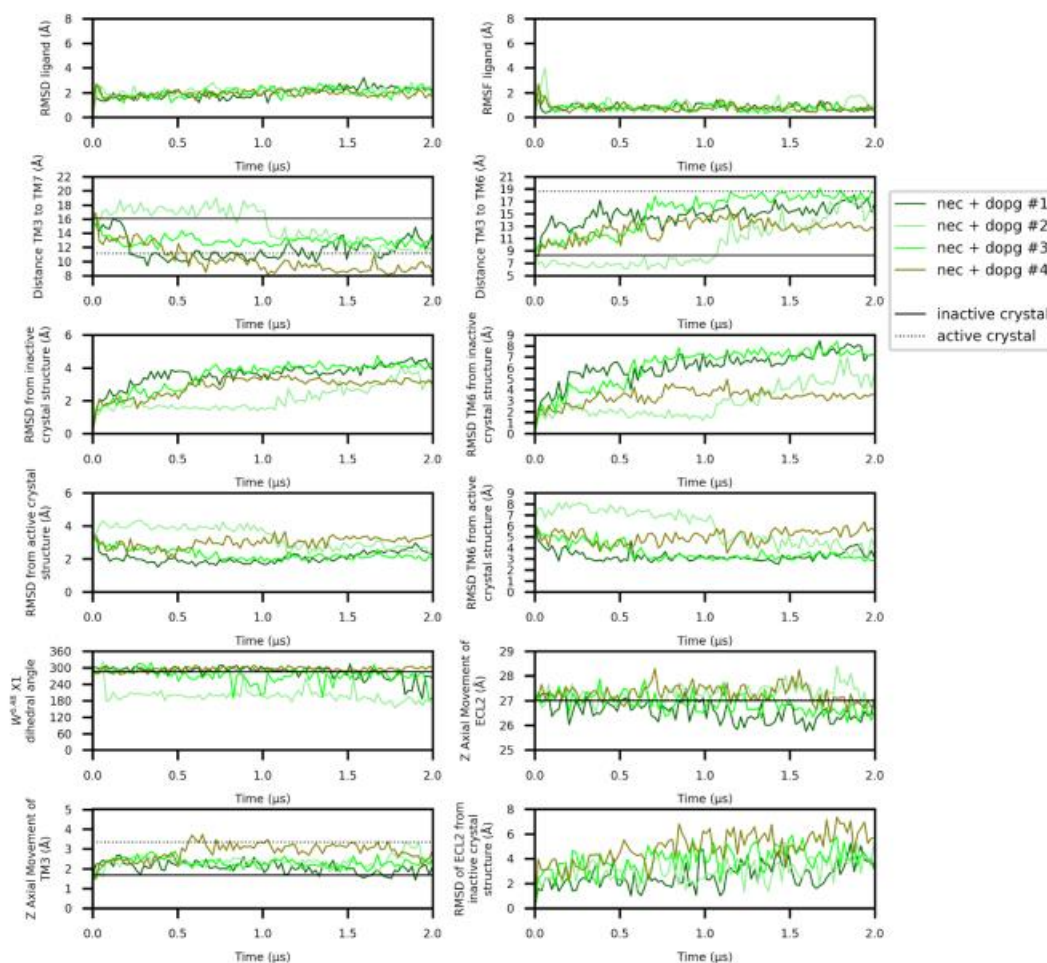

S17 Fig. Alternative active-like conformational state of A2aR generated in an MD simulation with bound adenosine in a DOPG membrane. A) Comparison of an MD-generated conformation of A2aR bound to adenosine within a DOPG membrane (in green, belonging to replica #4 at 1.8 µs) with the active crystal structure of A2aR (brown, PDB entry: 6GDG) showing B) and C) ligand atoms as spheres and residues making protein-ligand interactions as sticks. Intracellular loop (ICL) 3, extracellular loop (ECL) 2, and transmembrane (TM) helices 1-3, 5-7 are labelled.

147

S18 Fig. Comparison of two active-like receptor conformations generated in MD simulations of A2aR with bound adenosine in a DOPG membrane. A) Comparison of an MD-generated conformation of A2aR bound to adenosine within DOPG belonging to replica #2 (at 1.6 µs, green) with respect to replica #4 (at 1.8 µs, olive green) showing B) and C) ligand atoms as spheres and residues making protein-ligand interactions as sticks. Intracellular loop (ICL) 3, extracellular loop (ECL) 2, and transmembrane (TM) helices 1-3, 5-7 are labelled.
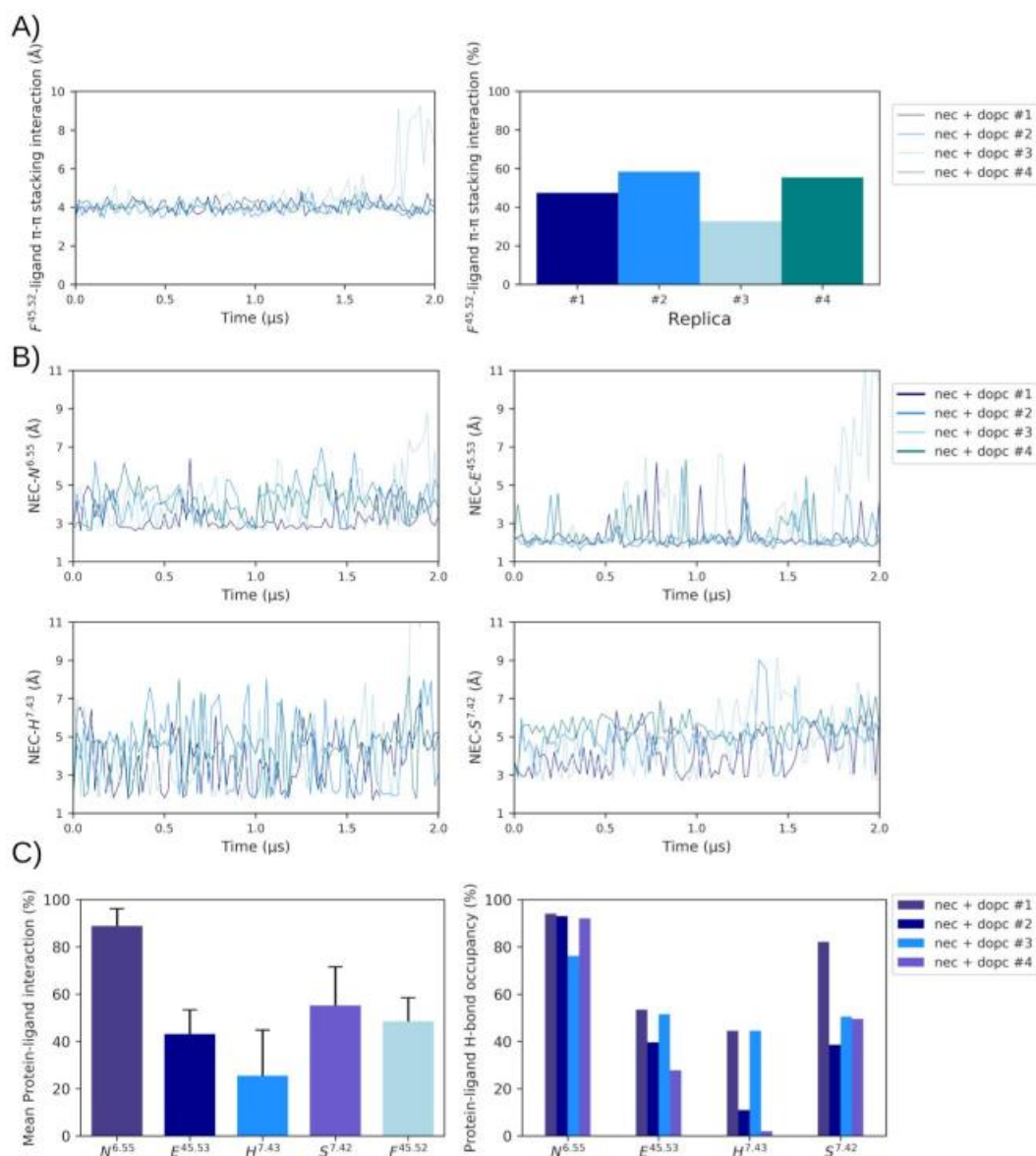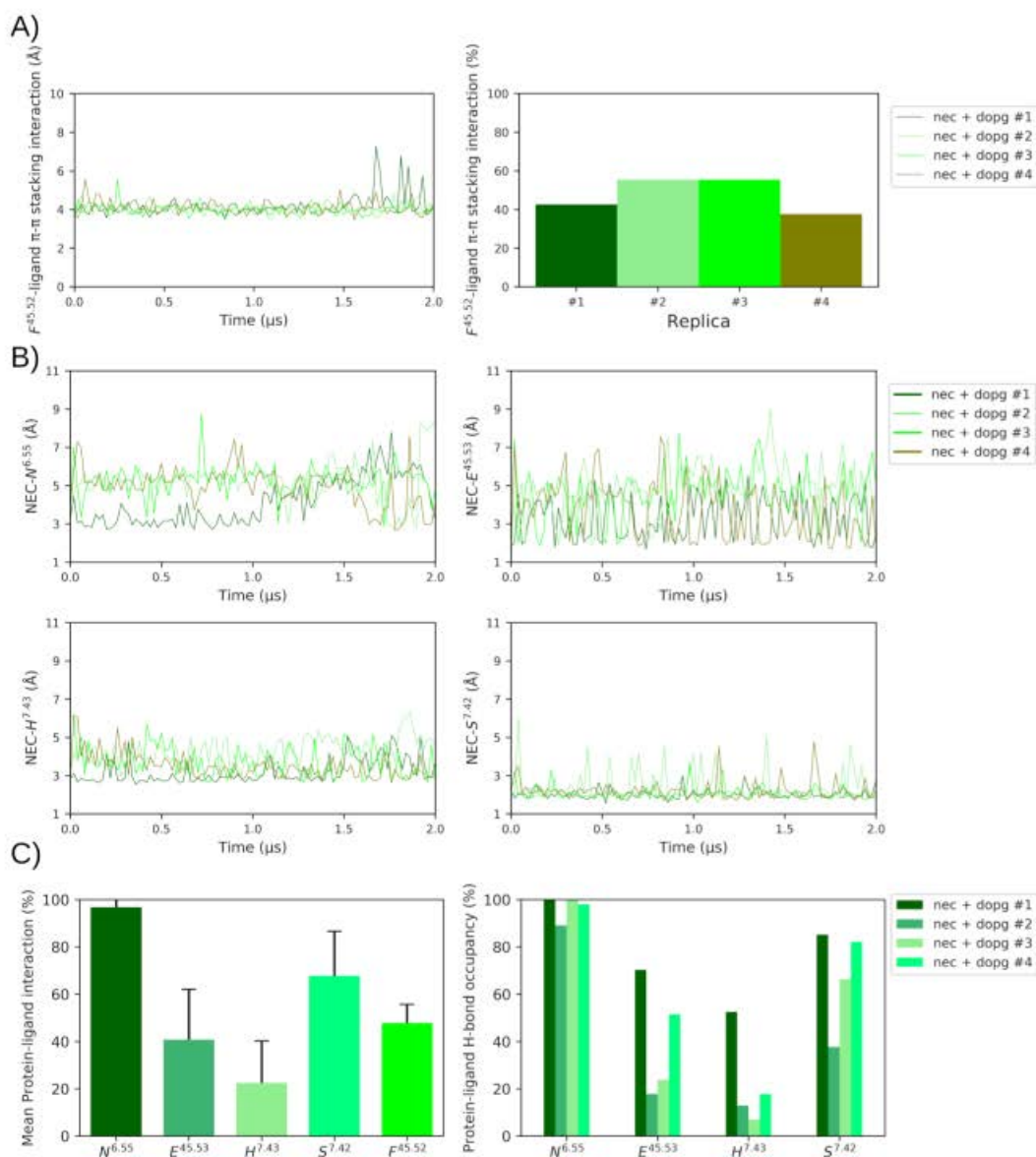
S19 Fig. MD simulation data of adenosine A2a receptor (A2aR) with bound NECA starting from the inactive receptor crystal structure (PDB id: 4EIY) in a DOPC membrane. Top row: RMSD and conformational fluctuation (RMSF) of bound NECA ligand; second row: TM3-TM7 and ionic lock (TM3-TM6) inter-helical distances; third row: RMSD of whole TMD (TMs 1-7) or only TM6; fourth row: RMSD compared to active crystal structure (PDB id: 6GDG) of whole TMD (TMs 1-7) or only TM6; fifth row: $\chi 1$ dihedral angle of W246[6.48] on TM6 starting from *gauche*(-) crystal position (285°), and vertical movement of extracellular loop 2 (ECL2); bottom row: vertical movement of TM3 and RMSD of ECL2. MD simulations are performed in quadruplicate in DOPC homogeneous membranes.
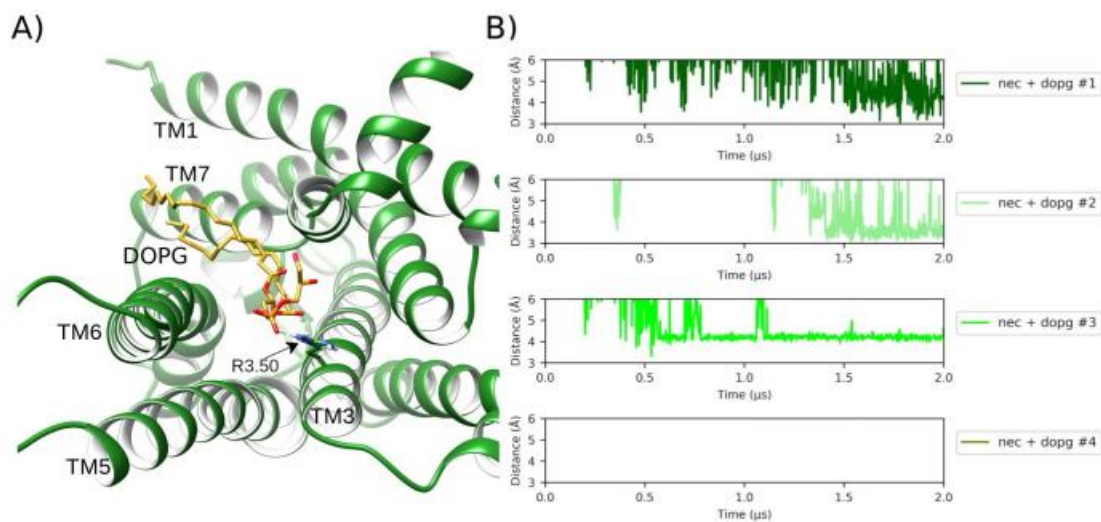
S20 Fig. MD simulation data of adenosine A2a receptor (A2aR) with bound NECA starting from the inactive receptor crystal structure (PDB id: 4EIY) in a DOPG membrane. Top row: RMSD and conformational fluctuation (RMSF) of bound NECA ligand; second row: TM3-TM7 and ionic lock (TM3-TM6) inter-helical distances; third row: RMSD of whole TMD (TMs 1-7) or only TM6; fourth row: RMSD compared to active crystal structure (PDB id: 6GDG) of whole TMD (TMs 1-7) or only TM6; fifth row: χ1 dihedral angle of W246[6.48] on TM6 starting from *gauche*(-) crystal position (285°), and vertical movement of extracellular loop 2 (ECL2); bottom row: vertical movement of TM3 and RMSD of ECL2. MD simulations are performed in quadruplicate in DOPG homogeneous membranes.

S21 Fig. Assessment of key protein-ligand interactions in MD simulations of NECA-bound A2aR embedded in DOPC membrane. A) Left: distance of $F^{45.52}$ with respect to ribose moiety of NECA. Right: frequency (%) of protein-ligand π-π stacking (within range of 0.0 to 4.0 Å) over 2 μs. B) Evaluation of protein-ligand H-bond distances formed by residues: $N253^{6.55}$, $E169^{45.53}$, $H278^{7.43}$, $S277^{7.42}$ (N---O or O---O). C) Mean protein-ligand interactions (%) and protein-ligand H-bond occupancies per replica (%) for selected residues.
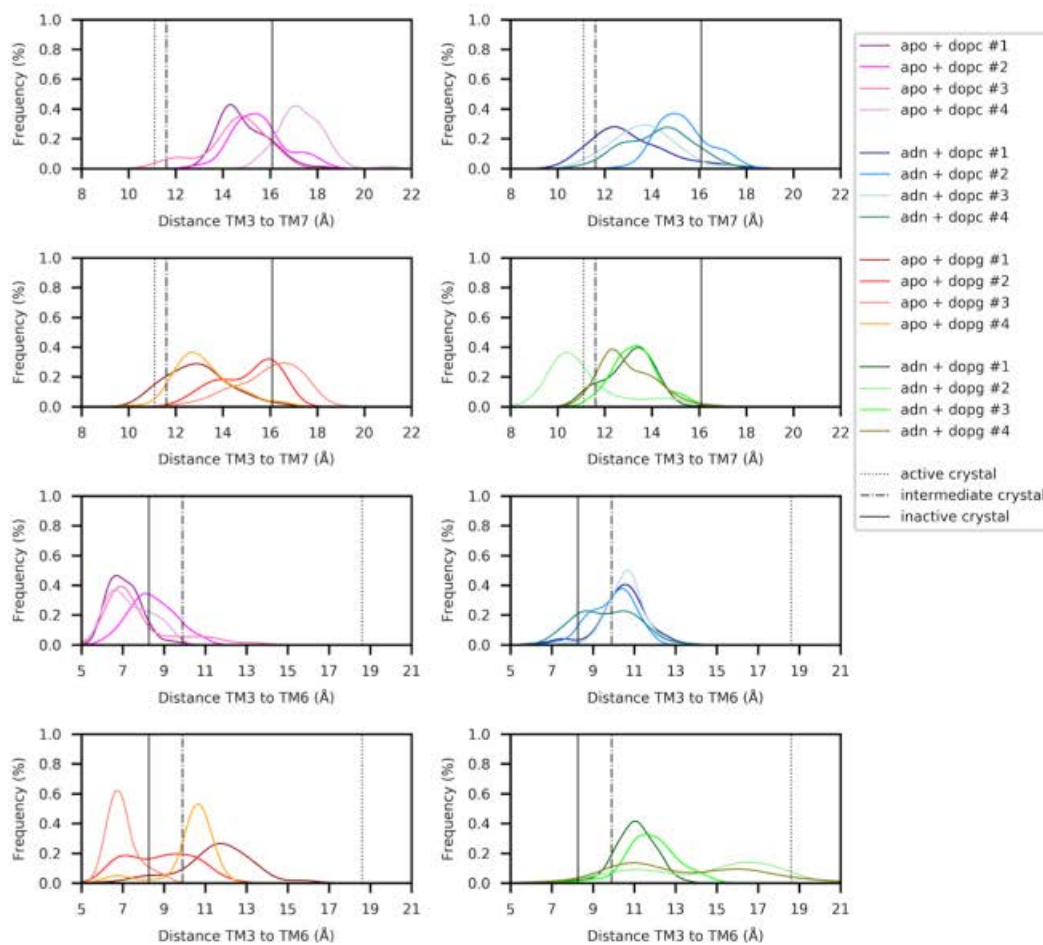
S22 Fig. Assessment of key protein-ligand interactions in MD simulations of NECA-bound A2aR embedded in DOPG membrane. A) Left: Distance of $F^{45.52}$ with respect to ribose moiety of NECA. Right: frequency (%) of protein-ligand π-π stacking (within range of 0.0 to 4.0 Å) interaction over 2 μs. B) Evaluation of protein-ligand H-bond distances formed by residues: N253$^{6.55}$, E169$^{45.53}$, H278$^{7.43}$, S277$^{7.42}$ (N---O or O---O). C) Mean protein-ligand interactions (%) and protein-ligand H-bond occupancies per replica (%) for selected residues.
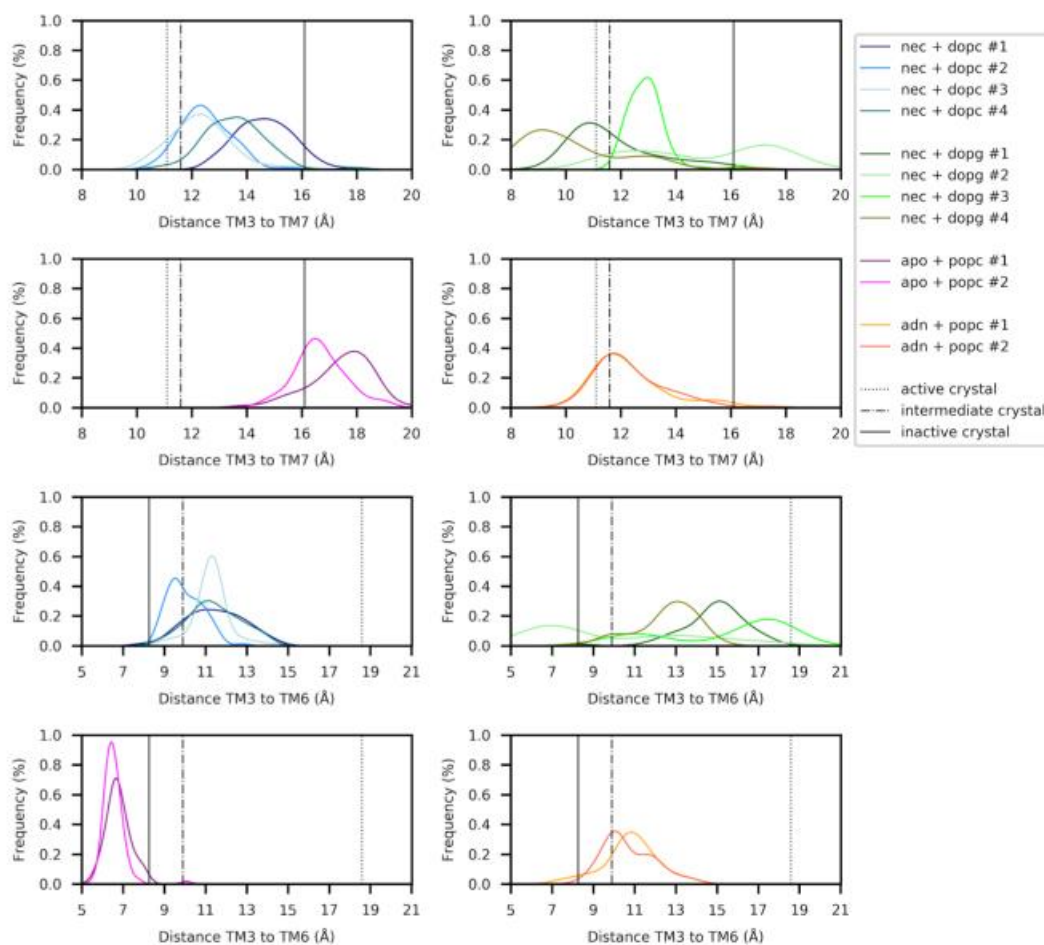
S23 Fig. Protein-lipid allosteric interaction with the ionic-lock in MD simulations of NECA-bound A2aR in DOPG membrane. A) Electrostatic interaction between ionic-lock residue R102[3.50] of A2aR (green) from an intracellular viewpoint and a DOPG lipid, which intrudes between TM6 and TM7 (snapshot belonging to replica #1 at 1.7 μs). B) Protein-lipid interaction distance over time between R102[3.50] sidechain and lipid phosphate group in four replicas of NECA-bound A2aR in DOPG membrane.

S24 Fig. Frequency distribution of receptor conformations formed during different MD simulations with and without bound adenosine in two different membranes (DOPC or DOPG) according to two different inter-helical distances. A) Population of receptor conformations according to distance between residues $R^{3.50}$ and $Y^{7.53}$ (TM3-TM7), and (B) between ionic lock residues $R^{3.50}$ and $E^{6.30}$ (TM3-TM6). Vertical black lines indicate values of inactive (PDB entry: 4EIY), intermediate (PDB entry: 2YDO) and active (PDB entry: 6GDG) crystal structures.

S25 Fig. Frequency distribution of receptor conformations (according to two inter-helical distances) formed during MD simulations with bound NECA in two different membranes (DOPC or DOPG) or with/without bound adenosine in a POPC membrane. First and second rows: population of receptor conformations according to distance between $^{R3.50}$ and $^{Y7.53}$ (TM3-TM7); third and fourth rows: according to distance between ionic lock residues $^{R3.50}$ and $E^{6.30}$ (TM3-TM6). Vertical black lines indicate values of inactive (PDB entry: 4EIY), intermediate (PDB entry: 2YDO) and active (PDB entry: 6GDG) crystal structures.

S26 Fig. Boxplots of receptor characteristics from MD simulations of adenosine A2a receptor (A2aR) in apo or with bound adenosine (ADN) or NECA in three different membranes. Top row: inter-helical distances between: residues $R^{3.50}$ and $Y^{7.53}$ (TM3-TM7), and ionic lock residues $R^{3.50}$ and $E^{6.30}$ (TM3-TM6); bottom row: vertical movements of extracellular loop 2 (ECL2) and TM3, respectively. MD simulations in DOPG or DOPC were performed in quadruplicate. MD simulations in POPC were performed in duplicate.

S1 Table. Adenosine A2a receptor crystal structures.

PDB	Conformation	Ligand	Ligand name
3EML	inactive	inverse agonist	ZM241385
3PWH	inactive	inverse agonist	ZM241385
3REY	inactive	antagonist	XAC
3RFM	inactive	antagonist	Caffeine
4EIY	inactive	inverse agonist	ZM241385
3UZA	inactive	antagonist	Compound 4g
3UZC	inactive	antagonist	Compound 4e
3VG9	inactive	inverse agonist	ZM241385
3VGA	inactive	inverse agonist	ZM241385
5IU4	inactive	inverse agonist	ZM241385
5IU7	inactive	antagonist	Compound 12c
5IU8	inactive	antagonist	Compound 12f
5IUA	inactive	antagonist	Compound 12b
5IUB	inactive	antagonist	Compound 12x
5K2A	inactive	antagonist	ZM241385
5K2B	inactive	inverse agonist	ZM241385
5K2C	inactive	inverse agonist	ZM241385
5K2D	inactive	inverse agonist	ZM241385
5JTB	inactive	inverse agonist	ZM241385
5UVI	inactive	inverse agonist	ZM241385
5MZP	inactive	antagonist	Caffeine
5MZJ	inactive	antagonist	Theophylline
5N2R	inactive	antagonist	PSB36
5NLX	inactive	inverse agonist	ZM241385
5NM2	inactive	inverse agonist	ZM241385
5NM4	inactive	inverse agonist	ZM241385
5UVI	inactive	inverse agonist	ZM241385
5VRA	inactive	inverse agonist	ZM241385
5OLG	inactive	inverse agonist	ZM241385
5OLH	inactive	antagonist	Vipadenant
5OLO	inactive	antagonist	Tozadenant
5OLV	inactive	antagonist	LUAA47070
5OLZ	inactive	antagonist	Compound 4e
5OM1	inactive	antagonist	Compound 4e
5OM4	inactive	antagonist	Compound 4e
5UIG	inactive	antagonist	J3.651.884G
6AQF	inactive	inverse agonist	ZM241385
3QAK	intermediate	agonist	UK-432097
2YDO	intermediate	agonist	Adenosine (ADN)
2YDV	intermediate	agonist	NECA
4UG2	intermediate	agonist	CGS21680
4UHR	intermediate	agonist	CGS21680
5WF5	intermediate	agonist	UK-432097
5WF6	intermediate	agonist	UK-432097
5G53	active	agonist	NECA
6GDG	active	agonist	NECA

S2 Table. Comparison of A2aR crystal structure distances. Comparison of TM3-TM6, TM3-TM5 and TM3-TM7 inter-helical distances in active, intermediate and inactive crystal states.

Distances (Å)	TM3-TM5 (R102$^{3.50}$- Q207$^{5.68}$)	TM3-TM6 (R102$^{3.50}$- E228$^{6.30}$)	TM3-TM7 (R102$^{3.50}$-Y288$^{7.53}$)
Inactive Crystal (PDB entry: 4EIY)	14.9	8.2	16.1
Intermediate Crystal (PDB entry: 2YDO)	17.6	9.9	11.6
Active Crystal (PDB entry: 6GDG)	15.7	18.6	11.1

S3 Table. Evaluation of Gαs protein docking. Comparison of best docking quality of Gα$_s$ protein into inactive, intermediate and active crystals structures, and different MD-generated conformations of A2aR achieved under different conditions and performed in quadruplicate.

Condition	Gα$_s$ docking interface score (I_sc)	RMSD of docked Gα$_s$ alpha-5 helix from active crystal structure (PDB id: 6GDG) (Å)	Time (µs)
Active crystal (PDB id: 6GDG)	-7.9	0.8	-
Intermediate crystal (PDB id: 2YDO)	-5.7	6.3	-
Inactive crystal (PDB id: 4EIY)	-3.7	8.5	-
apo + dopc #1	-4.0	7.8	1.8
apo + dopc #2	-3.3	7.2	1.1
apo + dopc #3	-3.6	7.8	1.5
apo + dopc #4	-3.3	7.3	1.2
adn + dopc #1	-4.5	6.8	1.7
adn + dopc #2	-5.3	6.4	1.2
adn + dopc #3	-4.8	5.8	1.6
adn + dopc #4	-5.8	5.8	1.3
apo + dopg #1	-6.1	4.9	1.6
apo + dopg #2	-4.4	6.8	1.4
apo + dopg #3	-3.5	8.3	1.1
apo + dopg #4	-4.3	6.2	1.8
adn + dopg #1	-5.5	3.6	1.8
adn + dopg #2	-7.7	0.8	1.6
adn + dopg #3	-4.5	3.4	1.4
adn + dopg #4	-8.4	2.3	1.8
neca + dopc #1	-4.9	6.4	1.4
neca + dopc #2	-4.1	6.3	1.2
neca + dopc #3	-5.0	5.1	1.5
neca + dopc #4	-4.5	7.4	1.6
neca + dopg #1	-7.2	1.3	1.9
neca + dopg #2	-6.4	2.4	1.8
neca + dopg #3	-7.7	1.1	1.6
neca + dopg #4	-4.3	5.3	1.3
apo + popc #1	-3.2	7.8	1.5
apo + popc #2	-3.5	7.3	1.7
adn + popc #1	-4.2	5.5	1.7
adn + popc #2	-4.8	6.6	1.5